RISING STARS IN CLINICAL MICROBIOLOGY: 2022

EDITED BY: Fangfeng Yuan, Zhanbo Zhu, Dania AlQasrawi and Rafael Franco
PUBLISHED IN: Frontiers in Cellular and Infection Microbiology

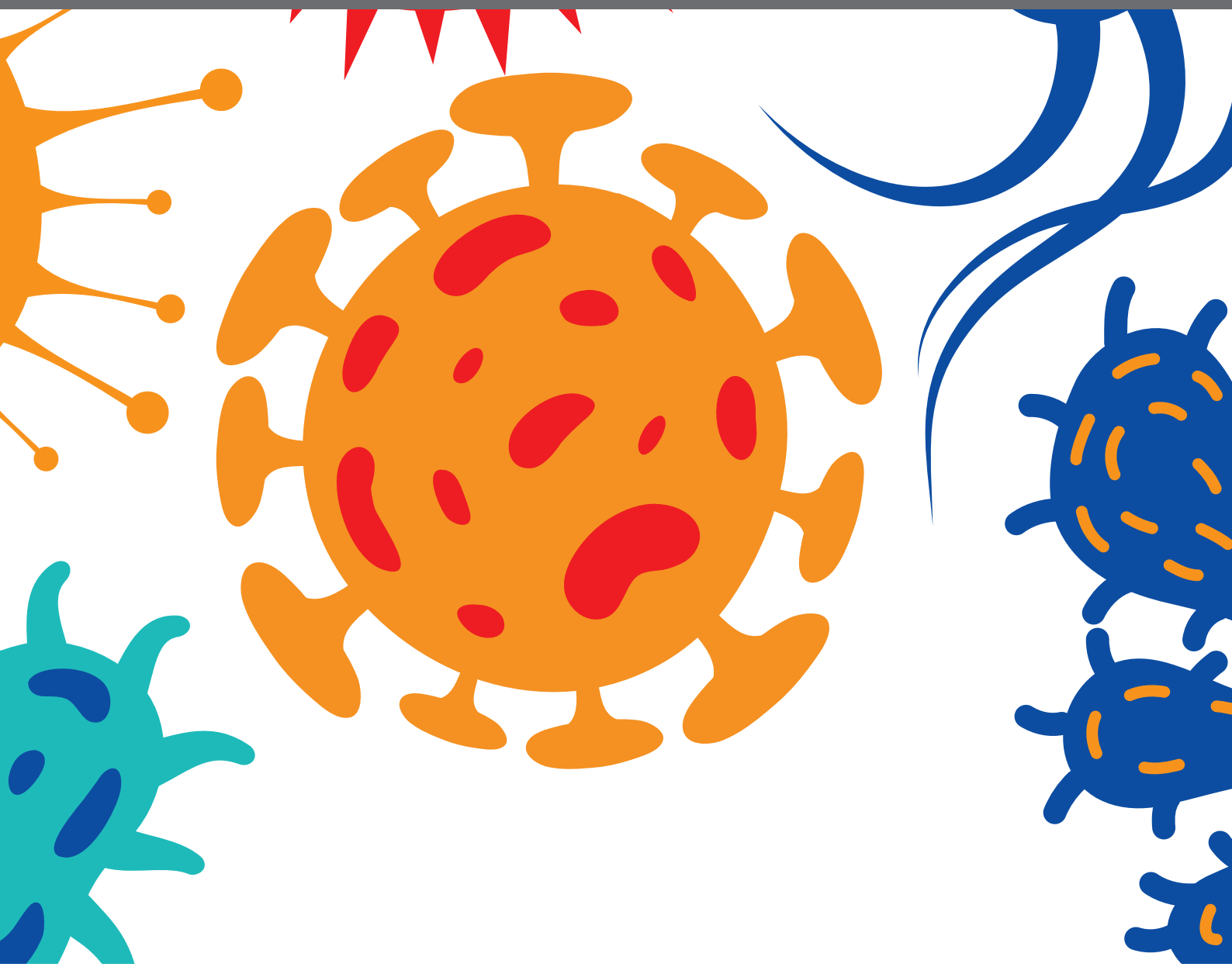

frontiers Research Topics

frontiers

ISSN 1664-8714
ISBN 978-2-83250-880-0
DOI 10.3389/978-2-83250-880-0

About Frontiers

Frontiers is more than just an open-access publisher of scholarly articles: it is a pioneering approach to the world of academia, radically improving the way scholarly research is managed. The grand vision of Frontiers is a world where all people have an equal opportunity to seek, share and generate knowledge. Frontiers provides immediate and permanent online open access to all its publications, but this alone is not enough to realize our grand goals.

Frontiers Journal Series

The Frontiers Journal Series is a multi-tier and interdisciplinary set of open-access, online journals, promising a paradigm shift from the current review, selection and dissemination processes in academic publishing. All Frontiers journals are driven by researchers for researchers; therefore, they constitute a service to the scholarly community. At the same time, the Frontiers Journal Series operates on a revolutionary invention, the tiered publishing system, initially addressing specific communities of scholars, and gradually climbing up to broader public understanding, thus serving the interests of the lay society, too.

Dedication to Quality

Each Frontiers article is a landmark of the highest quality, thanks to genuinely collaborative interactions between authors and review editors, who include some of the world's best academicians. Research must be certified by peers before entering a stream of knowledge that may eventually reach the public - and shape society; therefore, Frontiers only applies the most rigorous and unbiased reviews.
Frontiers revolutionizes research publishing by freely delivering the most outstanding research, evaluated with no bias from both the academic and social point of view. By applying the most advanced information technologies, Frontiers is catapulting scholarly publishing into a new generation.

What are Frontiers Research Topics?

Frontiers Research Topics are very popular trademarks of the Frontiers Journals Series: they are collections of at least ten articles, all centered on a particular subject. With their unique mix of varied contributions from Original Research to Review Articles, Frontiers Research Topics unify the most influential researchers, the latest key findings and historical advances in a hot research area! Find out more on how to host your own Frontiers Research Topic or contribute to one as an author by contacting the Frontiers Editorial Office: frontiersin.org/about/contact

RISING STARS IN CLINICAL MICROBIOLOGY: 2022

Topic Editors:
Fangfeng Yuan, Koch Institute for Integrative Cancer Research, Massachusetts Institute of Technology, United States
Zhanbo Zhu, Heilongjiang Bayi Agricultural University, China
Dania AlQasrawi, Mayo Clinic Florida, United States
Rafael Franco, University of Barcelona, Spain

Citation: Yuan, F., Zhu, Z., AlQasrawi, D., Franco, R., eds. (2022). Rising Stars in Clinical Microbiology: 2022. Lausanne: Frontiers Media SA.
doi: 10.3389/978-2-83250-880-0

Table of Contents

frontiers | Frontiers in Cellular and Infection Microbiology

TYPE Editorial
PUBLISHED 14 November 2022
DOI 10.3389/fcimb.2022.1066181

OPEN ACCESS

EDITED AND REVIEWED BY
Max MAURIN,
Université Grenoble Alpes,
France

*CORRESPONDENCE
Rafael Franco
rfranco123@gmail.com

SPECIALTY SECTION
This article was submitted to Clinical Microbiology, a section of the journal Frontiers in Cellular and Infection Microbiology

RECEIVED 10 October 2022
ACCEPTED 31 October 2022
PUBLISHED 14 November 2022

CITATION
Franco R (2022) Editorial: Rising stars in clinical microbiology: 2022. *Front. Cell. Infect. Microbiol.* 12:1066181. doi: 10.3389/fcimb.2022.1066181

Editorial: Rising stars in clinical microbiology: 2022

Rafael Franco[1,2,3]*

[1]CiberNed Network Center for Neurodegenerative Diseases, National Spanish Health Institute Carlos III, Madrid, Spain, [2]Molecular Neurobiology Laboratory, Department of Biochemistry and Molecular Biomedicine, Faculty of Biology, Universitat de Barcelona, Barcelona, Spain, [3]School of Chemistry, Universitat de Barcelona, Barcelona, Spain

KEYWORDS

SARS-CoV-2, microbiota, viral infection, cancer, constipation, rheumatoid arthritis, probiotics

Editorial on the Research Topic
Rising stars in clinical microbiology: 2022

The objective of this Research Topic was to highlight "rising stars" in what concerns new approaches in microbiology research that address pending issues and, more importantly, that arise in response to new challenges such as the one posed by the SARS-CoV-2 pandemic. In addition, one of the articles, through a meta-analysis, underscores the possible relationship between the gram negative bacterium *Porphyromonas gingivalis* and a common age-related disease involving alterations in the immunological response, namely rheumatoid arthritis (Li et al.). Altered immunological responses caused by age, drug use, environmental factors, etc. may be incited and/or aggravated by microorganisms. One of the most popular articles, with >1800 views as of today (October 10, 2022), is devoted to the potential of vitamin D to combat inflammation in macrophages in patients with Crohn's disease who are also infected with *Mycobacterium avium subsp. paratuberculosis* (Vaccaro et al). Another article, a review with >2,200 views, deals with the anti-cancer potential of oncolytic viruses. This review suggests that gastrointestinal tumors can be managed more effectively if immunotherapy takes into account the synergistic action of oncolytic viruses with immunoregulatory power (Li et al.).

In further confirmation of the correlation between the intestinal microbiota and disease risk and/or its impact on disease progression, the Research Topic contains multiple highly compelling studies and reviews on this subject. One of the reviews highlights the possibility that probiotics may decrease the risk of viral infection. Multiple mechanisms may be in operation, from the probiotic triggering of anti-viral immune cells to the production of antiviral metabolites and binding of these compounds to viruses to prevent cell infection. The article includes a table presenting the effects of common bacteria present in probiotic preparations in terms of preparing the human body to fight invading viral pathogens (Wang et al.). *Akkermansia muciniphila*, a commensal bacterium present in the intestine, is beneficial in the maintenance of a healthy microflora and a balanced gut immune system (see Rodrigues et al., 2022, for a review). Interestingly, Lv et al. decipher the genomic architecture of

Akkermansia species found in the human intestine, also identifying different phylogroups when comparing data obtained from Chinese and Western populations. The authors also demonstrate the presence of a strain, *A. glicaniphila GP37*, previously described only in python (Lv et al.). The relevance of a proper microbiota is highlighted in another paper, in which alteration of bile acid metabolism is observed in patients with slow transit constipation. The authors conclude that their study "*provides an in-depth understanding of the relationship between the fecal microbiota, metabolites, and intestinal dysfunction in slow transit constipation patients*" (Fan et al.).

Microbiology is a common source of novel techniques to detect infections. This calls to mind the difficulties of obtaining the virus causing hepatitis D *via* PCR. The causal factor for hepatitis D is a viroid with a high complementarity of RNA sequences, resulting in a compact structure with a high degree of complementarity: that is, with bases that form a tight double helix. This structure is so difficult to relax to allow the RNA polymerase to act in a PCR assay that it is necessary to boil the sample for 15 min to achieve success (F. Rodriguez-Frías, personal communication; see details in Schaper et al., 2010 and Homs et al., 2014). Although there are RNAs that are very fragile, that of the viroid that causes hepatitis D in fact remains undegraded under adverse conditions. In the single methodological article included in the Research Topic, a luciferase-based methodology is used to detect antibodies against swine fever virus. The method consists of immunoprecipitation and, to increase detection sensitivity, takes advantage of the high yield of Gaussia luciferase, which is obtained from *Gaussia princeps*, a marine copepod (Ding et al.,).

The Research Topic also includes an original research article and a review related to SARS-CoV-2 coronavirus infection. The review summarizes the primary mechanisms involved in severe cases of respiratory distress in patients with COVID-19. Among the novel contributions of this article is a description of the involvement of vitamin D in its role as an immunomodulator. It seems that patients who have low levels of blood vitamin D have poor prognosis; however, it is not demonstrated whether vitamin supplementation helps patients with COVID-19 (Zheng et al.). The original research article reports on the isolation and testing of chimeric virus-like particles that contain proteins coded by the SARS-CoV-2 genome. The authors prepared a plasmid that contained the sequence of the spike protein, which interacts with the virus receptor at host cells, in two forms: one intact, and another as a spike–H5N1 protein fusion, H5N1 being a protein of the avian influenza A virus. Virus-like particles containing these proteins, produced in a "*baculovirus insect cell expression system*," were found to be immunogenic in mice. These results indicate that the approach may be useful in the design of novel anti-SARS-CoV-2 vaccines (Chen et al.).

Finally, the Research Topic does not lack discussion of novel and sophisticated techniques: Dai et al. propose the popular CRISPR/Cas9 system as a method of preparing a defective form of BHV-1 bovine herpesvirus virus, which causes vulvovaginitis and rhinotracheitis in cattle. The defective virus could eventually be used to prepare a vaccine, but at present has served to demonstrate that the UL41 viral gene is important for replication. Bioinformatics approaches show value in the construction of a model of the *Fiber* protein (gene ON164651) of the CAdV-1 canine adenovirus. The model has served to predict KLGVKPTTY as the amino acid sequence that binds to the major histocompatibility complex-1 in lymphocytes, thus paving the way for the development of an epitope-based vaccine (Wang et al.).

Author contributions

The author confirms being the sole contributor of this work and has approved it for publication.

Conflict of interest

The author declares that the research was conducted in the absence of any commercial or financial relationships that could be construed as a potential conflict of interest.

Publisher's note

References

Homs, M., Giersch, K., Blasi, M., Lutgehetmann, M., Buti, M., Esteban, R., et al. (2014). Relevance of a full-length genomic RNA standard and a thermal-shock step for optimal hepatitis delta virus quantification. *J. Clin. Microbiol.* 52, 3334–3338. doi: 10.1128/JCM.00940-14

Rodrigues, V. F., Elias-Oliveira, J., Pereira, Í.S., Pereira, J. A., Barbosa, S. C., Machado, M. S. G., et al. (2022). Akkermansia muciniphila and gut immune system: A good friendship that attenuates inflammatory bowel disease, obesity, and diabetes. *Front. Immunol.* 13. doi: 10.3389/FIMMU.2022.934695

Schaper, M, Rodriguez-Frias, F, Jardi, R, Tabernero, D, Homs, M, Ruiz, G, et al. (2010) *J. Hepatol.* 52 (5), 658–664. doi: 10.1016/j.jhep.2009.10.036

frontiers | Frontiers in Cellular and Infection Microbiology

ORIGINAL RESEARCH
published: 04 April 2022
doi: 10.3389/fcimb.2022.875772

Cathelicidin Mediates an Anti-Inflammatory Role of Active Vitamin D (Calcitriol) During *M. paratuberculosis* Infection

Joseph A. Vaccaro[†], *Ahmad Qasem*[†] *and Saleh A. Naser*[*]

Division of Molecular Microbiology, Burnett School of Biomedical Sciences, College of Medicine, University of Central Florida, Orlando, FL, United States

OPEN ACCESS

Edited by:
Dania AlQasrawi,
Mayo Clinic Florida, United States

Reviewed by:
Amit Kumar Singh,
National Institute on Aging, United States
Davide Cossu,
University of Sassari, Italy

***Correspondence:**
Saleh A. Naser
saleh.naser@ucf.edu

[†]*These authors share first authorship*

Specialty section:
This article was submitted to Clinical Microbiology, a section of the journal Frontiers in Cellular and Infection Microbiology

Received: *14 February 2022*
Accepted: *07 March 2022*
Published: *04 April 2022*

Citation:
Vaccaro JA, Qasem A and Naser SA (2022) Cathelicidin Mediates an Anti-Inflammatory Role of Active Vitamin D (Calcitriol) During M. paratuberculosis Infection. Front. Cell. Infect. Microbiol. 12:875772. doi: 10.3389/fcimb.2022.875772

Vitamin D is a key regulator in calcium and phosphorus metabolism which are essential for maintaining bone health. Recent reports also showed a role for vitamin D in immune regulation which may be linked to vitamin D deficiency in autoimmune disorders including inflammatory diseases and Crohn's disease (CD). This study examines the role of vitamin D deficiency in the regulation of Cathelicidin Antimicrobial Peptide (*CAMP*) in CD-like macrophages. The latter includes macrophages infected with *Mycobacterium avium* subsp. *paratuberculosis* (MAP) isolated from CD patient. Initially, we measured cathelicidin and calcitriol in *ex vivo* plasma samples from CD patients with or without MAP infection (*N=40* per group). We also measured the expression and production of *CAMP*/LL-37, TNF-α, IL-1β, IL-10, cellular oxidative stress markers, and bacterial viability following treatment of MAP-infected macrophages with four different forms of vitamin D (D2, D3, calcifediol, and calcitriol). From these studies, we determined that LL-37 and calcitriol were significantly lower in CD samples from MAP-positive patients [155.55 ± 49.77 ng/mL and 51.48 ± 31.04 pg/mL, respectively] compared to MAP-negative patients [193.01 ± 78.95 ng/mL and 272.36 ± 94.77 pg/mL, respectively]. Moreover, calcitriol and calcifediol upregulated *CAMP* expression by nearly 5-fold and 3-fold, respectively. However, following MAP infection, only calcitriol increased *CAMP* by 3-folds. Both calcitriol and LL-37 reduced intracellular MAP viability by ~3 folds and inhibited TNF-α and IL-1β expression and production in these cells. Treating co-culture of Caco-2 monolayers and MAP-infected macrophages with LL-37 or calcitriol have shown a reduction in *NOX-1* expression and DHE signal, in addition to a higher NADPH/NADPt ratio. Notably, calcitriol's anti-inflammatory effects were lost upon *CAMP* knockdown by CAMP-siRNA transfection. Altogether, the data indicate that MAP infection and burden is significant in CD by disrupting the conversion of calcifediol to calcitriol and downregulation of *CAMP* expression leading to vitamin D deficiency.

Keywords: vitamin D, cathelicidin, calcitriol, LL-37, MAP, CAMP, paratubercolosis, Crohn's disease

INTRODUCTION

Vitamin D is a steroid hormone crucial to the efficient uptake and storage of calcium and phosphorus (Christakos et al., 2016). Most vitamin D are endogenously synthesized in humans using exposure to ultraviolet radiation, which converts 7-dehydrocholesterol to an isomer of the pro-vitamin D_3; it then undergoes hydroxylation in the liver *via* the enzyme CYP27A1 to yield calcifediol or 25(OH)D_3 (El-Sharkawy and Malki, 2020). Calcifediol makes up the majority of circulating vitamin D but displays minimal hormonal activity (Chang and Lee, 2019). When blood calcium or phosphate levels are low, the parathyroid gland detects the decline and releases parathyroid hormone (PTH) (Chang and Lee, 2019). PTH acts upon the kidneys to stimulate the hydroxylation of 25(OH)D_3 to 1,25(OH)$_2D_3$, or calcitriol, using the enzyme CYP27B1 (Chang and Lee, 2019; El-Sharkawy and Malki, 2020). Interestingly, this enzyme can also be found in extra-renal tissues, including macrophages, where it regulates various intracellular events (Adams et al., 2014). Calcitriol, the active form of vitamin D, is then carried through the circulation to tissues across the body (Christakos et al., 2016). As a fat-soluble hormone, it is capable of binding to the ubiquitously expressed vitamin D receptor (VDR), which heterodimerizes with the retinoid X receptor (RXR), then translocates to the nucleus, where it begins stimulating transcription of its target genes (Christakos et al., 2016).

Among the genes enhanced by the VDR/RXR complex is *CAMP*, encoding Cathelicidin Antimicrobial Peptide (Carlberg, 2019). The active form of cathelicidin is LL-37, which is a 37 residue-long peptide produced by macrophages in response to inflammation (Vandamme et al., 2012). Like the defensin family, cathelicidin displays potent bactericidal and anti-inflammatory effects, through disruption of microbial membranes and conveying anti-inflammatory signals to immune cells (Vandamme et al., 2012). Cathelicidin has shown notable beneficial effects even on persistent, long-term infections like tuberculosis and those found in inflammatory bowel disease (IBD) (Liu et al., 2006; Liu et al., 2007; Tabatabaeizadeh et al., 2018; Alqasrawi et al., 2020; Alqasrawi et al., 2021). Its broad-spectrum effect on immunity makes cathelicidin a potential link between vitamin D and resistance to pathogens, even pathogens that are comparatively understudied; however, its dependence on vitamin D signaling exposes cathelicidin to disruption when calcitriol is restricted (Liu et al., 2007; Carlberg, 2019). Under ordinary circumstances, Toll-like receptors (TLRs) stimulation enhances transcription of the VDR and CYP27B1 in macrophages (Liu et al., 2006). This signal allows the macrophage to enhance vitamin D-mediated cathelicidin production even without high circulating calcitriol (Liu et al., 2006; Liu et al., 2007). However, previous work has shown that *Mycobacterium tuberculosis* (Mtb) lipoprotein LprE inhibits CYP27B1 and VDR upregulation, reducing cathelicidin production and enhancing bacterial survival (Padhi et al., 2019). This mechanism partially explains the persistence of tuberculosis within alveolar macrophages, and related bacteria might share a similar mechanism (Padhi et al., 2019).

Mycobacterium avium subsp. *paratuberculosis* (MAP) is known to cause Johne's disease in ruminants, resulting in intestinal damage and chronic wasting (Rathnaiah et al., 2017). Furthermore, in some genetically susceptible patients, MAP infection causes Crohn's disease (CD), an inflammatory bowel disease (IBD) characterized by asymmetrical, segmental, transmural inflammation with a relapsing-remitting pattern (Greenstein, 2003; Naser et al., 2004; Behr and Kapur, 2008; Rathnaiah et al., 2017). Similar to Mtb, MAP can infect macrophages and evade immune system clearance to establish a persistent infection, which warranted the necessity of using antibiotics for MAP eradication among infected CD patients (Perencevich and Burakoff, 2006; Arsenault et al., 2014; Qasem et al., 2016; Davis et al., 2017). Therefore, we were intrigued to find out if MAP shares Mtb's method of evading immune detection by interfering with vitamin D signaling, which could be responsible for interference with *CAMP* expression and subsequent dysregulation of the intestinal microbiota in CD.

Additionally, therapeutic interventions of inactive vitamin D for IBD, which have so far shown mixed results for CD overall, might prove ineffective in MAP-infected patients and effective for MAP-uninfected patients. As such, it is necessary to determine whether MAP survival depends on interference with macrophage conversion of inactive calcifediol to active calcitriol, thereby inhibiting cathelicidin production and bacterial clearance. The objective of this study is to examine the effect of various forms of vitamin D and exogenous cathelicidin treatment on MAP infection and burden and subsequent macrophage-mediated inflammatory response. Our study clearly outlines a novel immunoevasive mechanism of MAP infection and reveals the importance of vitamin D signaling in eradicating infection in CD.

Abbreviations: ANOVA, Analysis of variance; CAMP, Cathelicidin Antimicrobial Peptide; CD, Crohn's disease; cDNA, complementary DNA; CI, Confidence interval; CYP27A1, Cytochrome P450 Family 27 Subfamily A Member 1; CYP27B1, Cytochrome P450 Family 27 Subfamily B Member 1; DHE, Dihydroethidium; DAPI, 4′,6-diamidino-2-phenylindole; ELISA, Enzyme-linked immunosorbent assay; EMEM, Eagle's Minimum Essential Medium; GAPDH, Glyceraldehyde-3-phosphate dehydrogenase; IBD, Inflammatory Bowel Disease; IL-1β, Interleukin 1-beta; IL-10, Interleukin 10; LPS, Lipopolysaccharide; MAP, *Mycobacterium avium* subsp. *tuberculosis*; Mtb, *Mycobacterium tuberculosis;* NADP, Nicotinamide adenine dinucleotide phosphate; NOX-1, Nitric oxide synthase; PMA, Phorbol 12-myristate 13-acetate; PTH, Parathyroid hormone; RA, Rheumatoid arthritis; RT-qPCR, Reverse transcription quantitative real-time PCR; RXR, Retinoid X receptor; siRNA, Short interfering RNA; TLR, Toll-like receptor; TNF-α, Tumor necrosis factor alpha; VDR, Vitamin D receptor.

MATERIALS AND METHODS

Measurement of Plasma Calcitriol and Cathelicidin in Clinical Samples

Plasma from peripheral blood samples (4.0 mL K_2-EDTA tube) was collected from 100 CD patients (CDAI ≥220 and ≤450). The status of MAP infection was subsequently determined *via IS900* PCR as described earlier (Qasem et al., 2019), and then we randomly selected 40 MAP positive and 40 MAP negative CD patients for this study. We then used the Human Cathelicidin Antimicrobial Peptide ELISA Kit (MyBioSource, San Diego, CA) and the Calcitriol ELISA Kit (MyBioSource, San Diego, CA) to determine the plasma

levels of cathelicidin and calcitriol, respectively. This study was approved by the University of Central Florida Institutional Review Board # STUDY00003468. All samples were de-identified before handling.

Infection and Treatment of Monocyte-Derived Macrophages

The THP-1 cell line (ATCC TIB-202) was cultured in RPMI-1640 medium (ATCC 30-2001) with 10% fetal bovine serum (FBS; Sigma Life Science, St. Louis, MO). The cells were maintained in a humidified 5% CO_2 incubator at 37°C and grown to confluency in cell culture flasks. A total of 1.0 mL of cell suspension was transferred to 12-well tissue culture plates with $1x10^5$ cells per well. They were then differentiated into monocyte-derived macrophages using 50 ng/mL phorbol 12-myristate 13-acetate (PMA; Sigma Life Science, St. Louis, MO) followed by 48 hours of incubation at 37°C. Next, monocyte-derived macrophages were treated with 5 μg/mL lipopolysaccharide (LPS) or infected with clinical MAP UCF4 ($1x10^7$ CFU/mL), followed by 24 hours of incubation at the same conditions. When the macrophages were infected or stimulated with LPS, they also were dosed with 50 ng/mL vitamin D2, vitamin D3, calcifediol, or calcitriol, all purchased from Sigma Aldrich (St. Louis, MO), or 30 μg/mL LL-37 (Tocris Bioscience, Bristol, UK).

Measurement of *CAMP, NOX-1, TNF-α, IL-1β*, and *IL-10* Expression in Treated Macrophages and Caco-2 Monolayers

RNA was isolated from each 1.0 mL sample of monocyte-derived macrophages following 24 hours of treatment with vitamin D or cathelicidin or from Caco-2 cells following 24 hours of co-culture with infected or treated macrophages. RNA was then reverse-transcribed to cDNA, then gene expression was measured using specific primers for *GAPDH, CAMP, TNF-α, IL-1β*, and *IL-10* obtained from Bio-rad (Hercules, CA) followed by quantitative reverse transcription PCR (RT-qPCR) analysis. RNA was extracted using the RNeasy ® Mini Kit (Qiagen, Hilden, Germany) according to manufacturer protocols. RNA concentrations were measured using NanoDrop (OD at 260 nm). Next, cDNA was synthesized from 1000 ng of each RNA sample using 5.8 μL master mix made from the High Capacity cDNA Reverse Transcription Kit (Applied Biosystems, Waltham, MA) and then topped up to a total volume of 20 μL with RNase-free water, according to manufacturer protocols. A thermal cycler (MyGene Series Peltier Thermal Cycler) was used to perform the reactions for 5 min at 25°C, 20 min at 46°C, and 1 min at 95°C. The cDNA samples were stored at -20°C or used immediately for RT-qPCR analysis. For each sample, 5 μL of cDNA was mixed with 10 μL of Fast SYBR Green Master Mix (ThermoFisher Scientific, Waltham, MA), 1 μL primer mix, and 4 μL of DEPC-treated water. Samples were added in triplicate to a 96-well microamp RT-PCR reaction plate, and the experiment was run using 7500 Fast Real-Time PCR System (Applied Biosystems, Waltham, MA). Deleted: repeated sentence. GAPDH was the control used to obtain baseline CT readings. Relative mRNA expression levels were calculated using the equation (2^(- ΔΔCT).

Measurement of LL-37, TNF-α, IL-1β, and IL-10 Protein Level in Treated Macrophages

Following 24 hours of infection and treatment with vitamin D forms or LL-37, monocyte-derived macrophages were pelleted by centrifugation at 2,500 rpm for 5 min at 4°C. The supernatants were saved, and TNF-α, IL-1β, and IL-10 protein levels were determined using the Ella automated immunoassay system (ProteinSimple, Santa Clara, CA). The Human Cathelicidin Antimicrobial Peptide ELISA Kit (MyBioSource, San Diego, CA) was used to determine LL-37 levels following manufacturer's instructions.

Measurement of MAP Viability in MGIT Culture

We inoculated 1 mL BACTEC™ MGIT™ ParaTB medium (BD Diagnostics, Sparks, MD) with 10^7 CFU/mL MAP strain UCF4 as described earlier (Qasem and Naser, 2018). The media was then treated with LL-37 (Tocris Bioscience, Bristol, UK) and Halt™ Protease Inhibitor Cocktail (Thermo Scientific, Rockford, IL). The same amount of protease inhibitor cocktail and LL-37 was added to the media every 3 days to maintain a consistent concentration. Bacterial growth expressed in CFU/mL was quantified daily using the BACTEC™ MGIT™ 320 for 20 consecutive days. The medium contains a molecule which fluoresces in the presence of actively respiring mycobacteria, permitting automatic quantification of growth as described previously (Qasem et al., 2016).

Measurement of MAP Viability in Infected Macrophages

We cultured THP-1 macrophages in 2 mL media as described previously. Following 24 hours of MAP infection and vitamin D/LL-37 treatment, the cultures were treated with 350 μL lysis buffer (Qiagen, Hilden, Germany) and incubated at room temperature for 15 minutes. Subsequently, 700 μL of each sample were transferred to a respective 1.5 mL microcentrifuge tube, and all samples were centrifuged for 1 minute at 8,000 rcf. The pellet was resuspended by gently vortexing, and 100 μL of each sample was mixed with 100 μL BacTiter-Glo Microbial Cell Viability Assay (Promega, Madison, WI) in a 96 well opaque-sided plate. Samples were incubated at room temperature on a shaker for 5 minutes, and luminescence was recorded using the GloMax Navigator system GM-2000 (Promega, Madison, WI). Bacterial viability was analyzed from the generated luminescence.

Measurement of Calcitriol Production in Treated Macrophages

Following 24 hours of infection with MAP and treatment with 50 ng/mL calcifediol, THP-1 monocyte-derived macrophages were pelleted by centrifugation at 2,500 rpm for 5 min at 4°C. The supernatants were saved, and calcitriol levels were determined using the Calcitriol ELISA Kit (MyBioSource, San Diego, CA).

Knockdown of CAMP by siRNA Transfection

5 nmol of Silencer™ Pre-Designed siRNA (siRNA ID: 14402, ThermoFisher, Waltham, MA) specific to *CAMP* were diluted

first in 50 uL nuclease-free H_2O. 3.3 µL of this stock were mixed with 30 µL Optimem media (Gibco, Waltham, MA) and further diluted in an additional 450 µL Optimem. 27 µL Lipofectamine reagent (Invitrogen, Carlsbad, CA) was then mixed with 450 µL Optimem and the resulting mixture was added to the 459 µL of diluted siRNA mix. 300 µL of the resulting transfection master mix was added to every 2 mL of media containing target cells, or 15 µL into 100 µL of a 96 well plate.

Co-Culturing THP-1 Macrophages With Caco-2 Monolayers

The effects of calcitriol and cathelicidin on macrophage-mediated oxidative stress were examined in a human enterocyte-like cell line (Caco-2 ATCC HTB-37). Cells were routinely cultured in ATCC-formulated Eagle's Minimum Essential Medium (EMEM) supplemented with 20% FBS (ATCC, Manassas, VA) and maintained at 37°C in a humidified 5% CO_2 incubator. Cells were grown in 12-well plates or microscope slides at a density of 3×10^5 cells per well until confluency and differentiation were reached in 21 days. On day 14, THP-1 macrophages were plated separately in co-culture wells. They were differentiated, infected with MAP, and treated with vitamin D within these wells as previously described. 24 hours following the infection, the co-culture wells were transferred to the 12-well plates containing Caco-2 cells to permit the free exchange of cytokines and other paracrine signals.

Visualizing Caco-2 Oxidative Stress *via* DHE Fluorescence Staining Assay

DHE fluorescence staining was performed on Caco-2 monolayers following 24 hours of co-culture with MAP-infected macrophages. First, monolayers were washed twice with cold PBS and then fixed with 4% paraformaldehyde (PFA) for 15 min. Monolayers were then washed twice with cold PBS and treated with 1 µM DHE stain (Sigma Aldrich, St. Louis, MO) for 25 min. Next, 60 µL VECTASHIELD Antifade Mounting Medium containing 4′,6-diamidino-2-phenylindole (DAPI; Vector Laboratories, Burlingame, CA) was used to co-stain nuclei. Slides were examined under Amscope IN480TC-FL-MF603 Fluorescence Microscope, where red staining indicates oxidative stress and blue staining represents nuclei. Captured images were analyzed by measuring average integrated density using NIH Image J 1.39o software, which was also used to generate merged images as we described earlier (Qasem et al., 2021).

Measurement of Nicotinamide Adenine Dinucleotide Phosphate (NADPH)

Following 24 hours of co-culture with infected and treated macrophages, Caco-2 cells were lysed, and their levels of NADPH and total NADP were measured using the NADP/NADPH Assay Kit (Abcam, Cambridge, UK) according to manufacturer protocols. Briefly, the cell lysates were halved, with one half heated for 30 min to degrade the oxidized NADP+ while leaving the NADPH untouched. Each lysate was then mixed with the kit developer in triplicate on a 96 well plate and left to incubate in the dark for 24 hours. NADP was then quantified for each well, with the heated lysate measuring the reduced NADPH as a fraction of total NADP.

Statistical Analysis

GraphPad Prism V.7.02 (GraphPad, La Jolla, CA, USA) was used for analyzing data statistics. The Kolmogorov–Smirnov normality test was used to test normal distribution for all values. Two-way analysis of variance (ANOVA) was used to assess significance among experiments, which was followed by Bonferroni correction test. Data are expressed as average ± SD of the mean, and the difference between treated samples vs. controls was considered statistically significant at a level of P-value < 0.05 and 95% confidence interval (CI). All experiments were performed in triplicates.

RESULTS

Cathelicidin and Calcitriol Are Reduced in MAP-Infected CD Patients

We measured cathelicidin and calcitriol levels in 80 clinical plasma samples, 40 of which were MAP negative, 40 of which were MAP positive. We observed statistically significant reductions in plasma cathelicidin (**Figure 1A**) and plasma calcitriol (**Figure 1B**). Cathelicidin in MAP-positive patients measures 155.55 ± 49.77 ng/mL, increasing to 193.01 ± 78.95 ng/mL in MAP-negative patients. The shift in calcitriol levels was more dramatic than cathelicidin; the average calcitriol for MAP-positive patients was 51.48 ± 31.04 pg/mL, but 272.36 ± 94.77 pg/mL. This trend lends preliminary support to the hypothesis that MAP infection alters calcifediol hydroxylation.

Calcitriol Enhances *CAMP* Expression and Cathelicidin Production in THP-1 Macrophages

We next examined whether THP-1 macrophages respond to treatment with all forms of vitamin D or only calcitriol and calcifediol. Treatment with vitamin D2 and D3 did not significantly enhance *CAMP* expression compared with the control. Calcifediol treatment enhanced *CAMP* expression in uninfected cells by a factor of 3.29 ± 0.15, and calcitriol enhanced expression by a factor of 5.24 ± 0.08 (**Figure 2A**). The effect of calcitriol increased in a dose-dependent manner. Treatment with 25 ng/mL calcitriol enhanced expression by only 2.79 ± 0.07 fold, and 100 ng/mL yielded a 6.37 ± 0.07-fold change (**Figure 2B**). These phenomena change after MAP infection; MAP-infected cells had no significant *CAMP* enhancement upon treatment with calcifediol. However, calcitriol is still effective at increasing *CAMP* expression during MAP infection, increasing *CAMP* mRNA by a factor of 2.52 ± 0.23 (**Figure 2C**). These trends were later validated by ELISA, confirming that expression corresponds with LL-37 production (**Figure 3**).

Calcitriol and LL-37 Significantly Reduce the Pro-Inflammatory Milieu Elicited by MAP-Infected Macrophages

To examine calcitriol's effect on MAP-induced inflammation, we infected THP-1 macrophages with MAP and treated them with different forms of vitamin D. Calcitriol was the only form of vitamin D which significantly reduced TNF-α and IL-1β

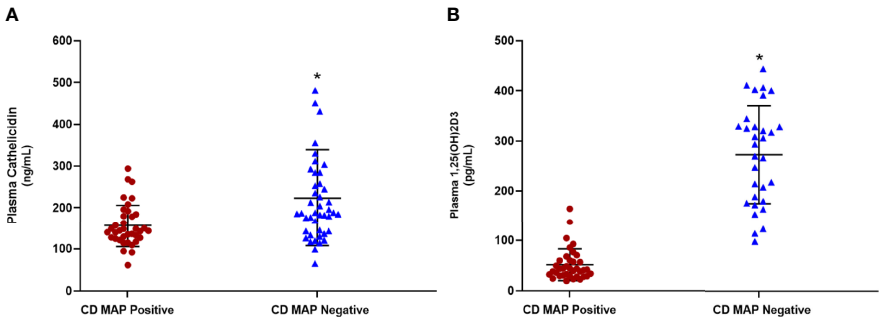

FIGURE 1 | Levels of cathelicidin **(A)** and calcitriol (1,25(OH)2D3) **(B)** in clinical plasma samples obtained from MAP-positive CD and MAP-negative CD patients (N= 40 per group), were determined by the Human Cathelicidin Antimicrobial Peptide ELISA Kit (MyBioSource, San Diego, CA) and the Calcitriol ELISA Kit (MyBioSource, San Diego, CA). *Indicates P-value of less than 0.05.

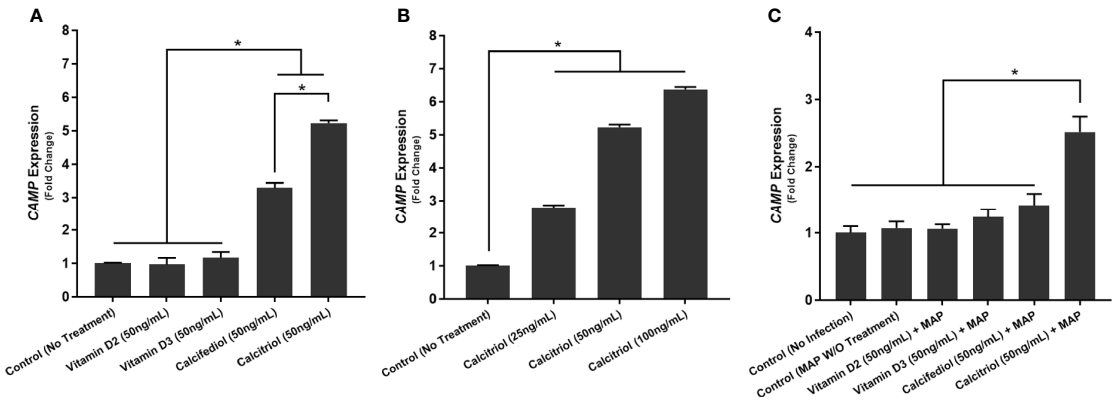

FIGURE 2 | Effect of different forms of vitamin D **(A)** and different concentrations of calcitriol **(B)** on CAMP expression in the presence of MAP infection **(C)**. Relative expression was quantified using RT-qPCR. *Indicates P-value of less than 0.05.

expression (**Figures 4A, B**) and production (**Table 1**) compared to the untreated, infected cells. Furthermore, calcitriol treatment partially rescued IL-10 expression (**Figure 4C**) and production (**Table 1**) in infected macrophages.

We observed similar effects with LL-37 treatment. MAP-infected macrophages showed a sharp decrease in TNF-α expression upon LL-37 treatment, a 5.27 ± 0.23-fold increase reduced to 2.61 ± 0.08 after treatment (**Figure 5A**). IL-1β showed a similar decrease with LL-37, a 4.12 ± 0.16-fold change reduced to 2.13 ± 0.13-fold (**Figure 5B**). IL-10, by contrast, increased in expression upon LL-37 treatment from 1.94 ± 0.11-fold to 3.85 ± 0.17-fold (**Figure 5C**). These trends were then verified by measuring cytokine production levels. TNF-α was secreted into the supernatant at concentrations of 173.12 ± 4.73 pg/mL upon MAP infection, but LL-37 treatment reduced it to 89.43 ± 4.96 pg/mL. Likewise, IL-1β secretion dropped from 163.87 ± 5.72 pg/mL to 82.23 ± 4.39 pg/mL and IL-10 secretion increased from 69.18 ± 3.69 pg/mL to 102.31 ± 4.11 pg/mL (**Table 2**). Interestingly, LPS-stimulated macrophages also decreased pro-inflammatory cytokine expression and increased IL-10 expression upon LL-37 treatment (**Figures 5D–F**). These results were verified by measuring cytokine production levels (**Table 2**). As such, LL-37 not only functions by clearing bacteria but can serve as an anti-inflammatory signal.

LL-37 Reduces MAP Viability in Both Bacterial Culture and Macrophages

To verify that LL-37 reduces extracellular MAP viability, we inoculated five MGIT tubes with MAP and cultured them over the course of 20 days with differing concentrations of LL-37. We observed a concentration-dependent bacteriostatic effect of LL-37, by reducing both rate of growth and maximum bacterial load. At 50 ug/mL, MAP culture required an additional 3 days to reach the stationary phase, and bacterial load at stationary phase was far lower than the untreated culture (**Figure 6**).

Additionally, we tested the effects of multiple vitamin D forms and LL-37 on bacterial viability in MAP-infected macrophages. There was no significant change upon treatment with the inactive forms of vitamin D. However, both LL-37 treatment and calcitriol treatment substantially reduced MAP viability from 2.92 ± 0.45*10^4 CFU/mL to 1.07 ± 0.41*10^4 CFU/mL and 1.24 ± 0.52*10^4 CFU/mL, respectively (**Figure 7**).

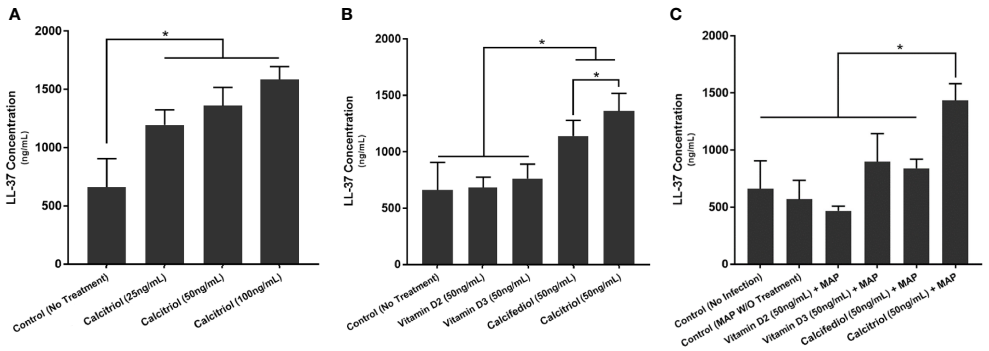

FIGURE 3 | Effects of different forms of vitamin D **(A)** and different concentrations of calcitriol **(B)** on LL-37 production in the presence of MAP infection **(C)**. Cytokine concentration was quantified using the Ella system (ProteinSimple). *Indicates P-value of less than 0.05.

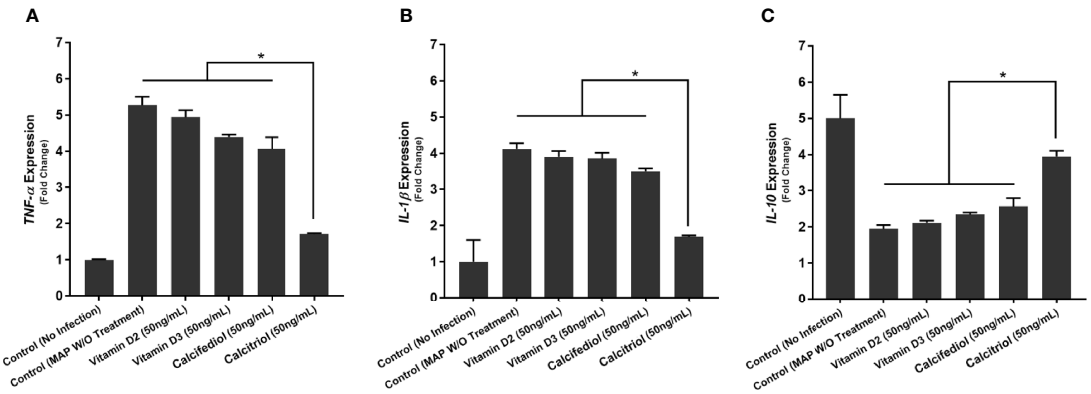

FIGURE 4 | Effects of Vitamin D Treatment on the expression of TNF-α **(A)**, IL-1β **(B)**, and IL-10 **(C)** in MAP-infected macrophages. Relative expression was quantified using RT-qPCR. *Indicates P-value of less than 0.05.

TABLE 1 | Effect of Vitamin D treatment on cytokine production in MAP-infected macrophages.

Infection and Treatment	TNF-α ± SD (pg/mL)	IL-1β ± SD (pg/mL)	IL-10 ± SD (pg/mL)
Control (no infection)	60.52 ± 1.75	56.13 ± 1.81	125.65 ± 6.11
Control (MAP W/O Treatment)	173.12 ± 4.73	163.87 ± 5.72	69.18 ± 3.97
MAP + Vitamin D2	157.84 ± 3.14	145.37 ± 6.17	73.14 ± 3.69
MAP + Vitamin D3	151.11 ± 5.44	140.61 ± 5.74	76.95 ± 5.26
MAP + 25(OH)D	136.21 ± 2.48	127.54 ± 3.84	82.12 ± 2.55
MAP + 1,25(OH)2D3	81.66 ± 2.79*	74.39 ± 3.72*	105.28 ± 4.58*

Indicates P-value of less than 0.05.

Knockdown of CAMP Eliminates the Anti-Inflammatory Effect of Calcitriol During MAP Infection

We treated two groups of macrophages with 50 ng/mL calcifediol and infected one group with MAP. Following 24 hours of infection, we collected the supernatant and measured calcitriol level. The uninfected macrophages yielded 72.98 ± 2.86 pg/mL calcitriol, while infected macrophages produced only 16.64 ± 9.23 pg/mL (**Figure 8A**). As such, the data indicate that MAP interferes with the conversion of calcifediol to calcitriol.

Furthermore, we transfected THP-1 macrophages with CAMP-siRNA to inhibit cathelicidin translation while leaving other VDR-controlled genes unaffected (**Figure 8B**). We analyzed cytokine expression (**Figure 9**) and production (**Table 3**) in cells where *CAMP* was knocked down and calcitriol was present in the medium. *CAMP*-knockdown macrophages treated with calcitriol showed no significant reduction compared with untreated macrophages in TNF-α, IL-1β and IL-10 expression had no significant rescue. Accordingly, we conclude that during MAP infection, cathelicidin is necessary for calcitriol to mediate its anti-inflammatory effects.

Calcitriol and Cathelicidin Reduce Macrophage-Mediated Oxidative Stress on Co-Cultured Caco-2 Monolayers

To examine the tissue damage effect of MAP-infected macrophages on co-cultured Caco-2 monolayers, we used three methods to assess oxidative stress levels. First, co-cultured Caco-2 monolayers were

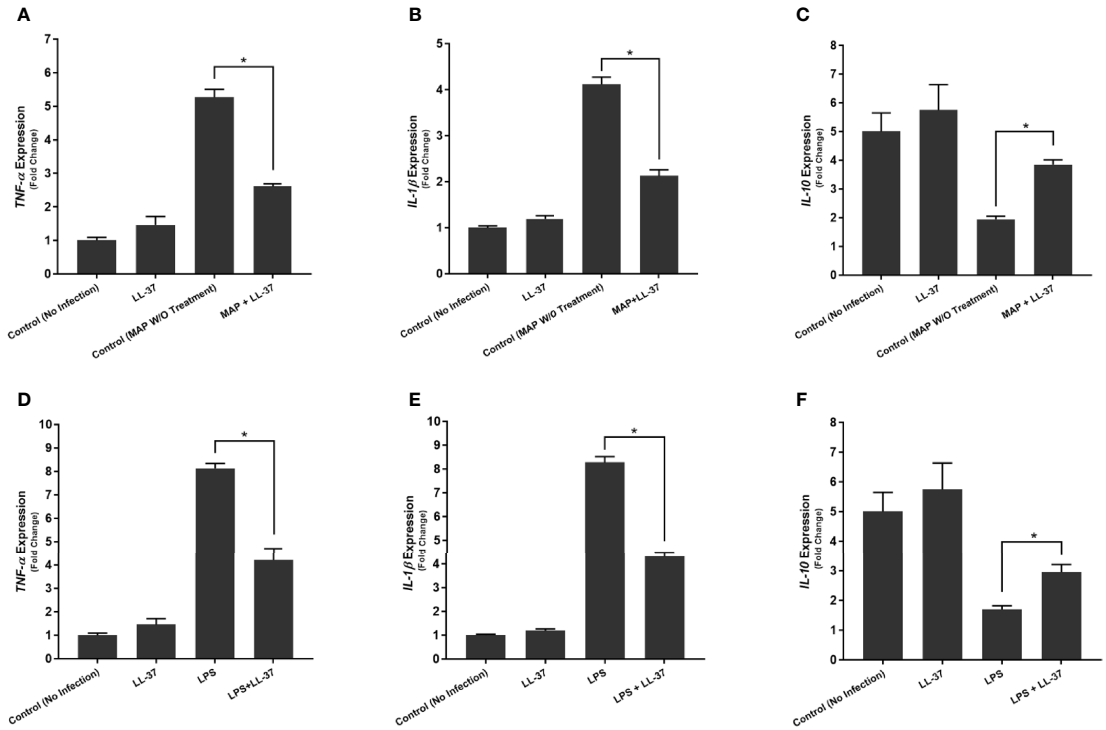

FIGURE 5 | Effects of LL-37 treatment on the expression of TNF-α **(A, D)**, IL-1β **(B, E)**, and IL-10 **(C, F)** in MAP-infected **(A–C)** and LPS-stimulated **(D–F)** macrophages. Relative expression was quantified using RT-qPCR. *Indicates P-value of less than 0.05.

TABLE 2 | Effects of LL-37 treatment on cytokine production in MAP-infected and LPS-stimulated macrophages.

Infection and Treatment	TNF-α ± SD (pg/mL)	IL-1β ± SD (pg/mL)	IL-10 ± SD (pg/mL)
Control (No Infection)	60.52 ± 1.75	56.13 ± 1.81	125.65 ± 6.11
LL-37	64.12 ± 2.83	61.42 ± 3.94	129.37 ± 3.82
Control (MAP W/O Treatment)	173.12 ± 4.73	163.87 ± 5.72	69.18 ± 3.69
MAP + LL-37	89.43 ± 4.96*	82.23 ± 4.39*	102.31 ± 4.11*
LPS Treatment	194.21 ± 3.51	183.04 ± 2.48	51.23 ± 1.56
LPS + LL-37	95.75 ± 2.64*	94.71 ± 1.75*	96.14 ± 6.41*

Indicates P-value of less than 0.05.

stained with DHE, imaged, and the red DHE stain was quantified using imageJ software (**Figure 10A**). Untreated MAP infection in co-cultured macrophages raised oxidative stress in the monolayer 14.78 ± 0.71 fold compared with the control. Treatment with LL-37 or calcitriol reduced oxidative stress to 1.74 ± 1.22 fold and 2.78 ± 1.00 fold, respectively (**Figure 10B**).

We verified these results with analysis of *NOX-1* expression and NADPH/NADP assay in co-cultured Caco-2 monolayers. Expression of *NOX-1* was 5.09 ± 0.09 fold higher when the co-cultured macrophages went untreated, but calcitriol treatment reduced it to 2.03 ± 0.14 fold, and LL-37 reduced *NOX-1* expression to 2.51 ± 0.16 (**Figure 11A**). MAP infection in co-cultured macrophages caused a decline in NADPH/NADPt ratio to 44.51 ± 3.81%, indicating that a highly oxidative intracellular environment was present. Treating MAP-infected macrophages with LL-37 or calcitriol rescued NADPH to 63.12 ± 2.63% and 73.44 ± 1.17% of total NADP, respectively (**Figure 11B**).

DISCUSSION

Vitamin D deficiency is widespread in CD patients (Chatu et al., 2013; White, 2018). A recent meta-analysis found an inverse relationship between circulating vitamin D and CD severity (Sadeghian et al., 2016). Similarly, low vitamin D levels are inversely correlated with the likelihood of later surgical intervention in these patients (Ananthakrishnan et al., 2013). From a therapeutic standpoint, vitamin D supplementation has shown promise in reducing disease activity and inflammatory biomarkers (Guzman-Prado et al., 2020). However, little is known about how vitamin D is metabolized in patients with inflammatory bowel disease.

Vitamin D activation is necessary to mediate transcriptional changes (Christakos et al., 2016). It has been reported that vitamin D can directly inhibit the growth of bacteria following exposure to high doses, but the mechanism is unclear (Greenstein et al., 2012). Subversion of the antibacterial response is a classical and potent way for mycobacteria to evade the host immune response and establish persistent infection (Arsenault et al., 2014; Liu et al., 2017). Therefore, understanding how MAP alters the function of the macrophages in CD is crucial to explain why it is challenging

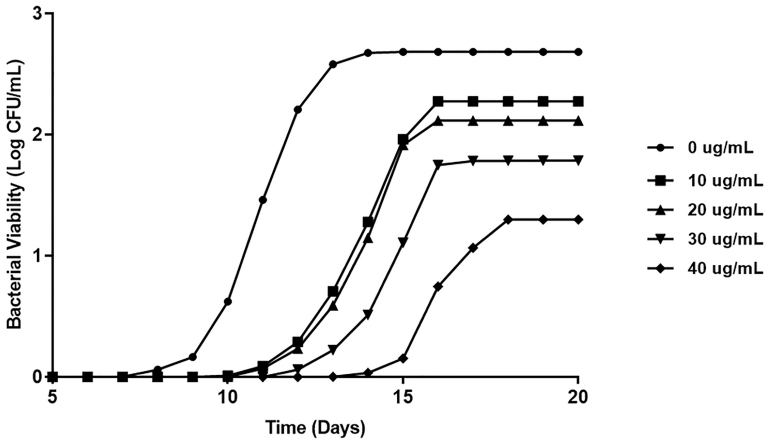

FIGURE 6 | Direct effect of LL-37 treatment on MAP viability in MGIT culture. BD Bactec MGIT™ Para-TB medium (Becton Dickinson, Sparks, Maryland, USA) system was used to determine the *in vitro* inhibitory effect of LL-37 on MAP over 20 days. Bacterial viability was calculated using fluorescence quenching technology and by the BACTEC™ MGIT™ 320.

to eradicate the infection in these patients. It is worth noting that Mtb possesses a host of mechanisms that assist in its survival within alveolar macrophages, many of which involve preventing phagolysosome fusion and halting apoptotic signals (Pecora et al., 2006; Jo, 2013). Interestingly, calcitriol has been shown to upregulate autophagy *via* cathelicidin, which leads to phagolysosome fusion and destruction of phagocytosed bacteria (Yuk et al., 2009; Shin et al., 2010). Similarly, a substantial body of work in cattle establishes MAP's adept evasion of the bovine immune system (Arsenault et al., 2014).

Previous work has shown that Mtb possesses at least one protein that subverts the vitamin D signaling pathway in macrophages, altering the antibacterial response (Padhi et al., 2019). Here, we present evidence that MAP is similarly capable of affecting vitamin D activation. Our analysis of clinical samples has shown that calcitriol and cathelicidin are both reduced in MAP-positive CD patients compared with MAP-negative CD patients. Moreover, we demonstrated that both calcifediol and calcitriol induce expression and production of cathelicidin in uninfected macrophages, but MAP infection alters calcifediol's

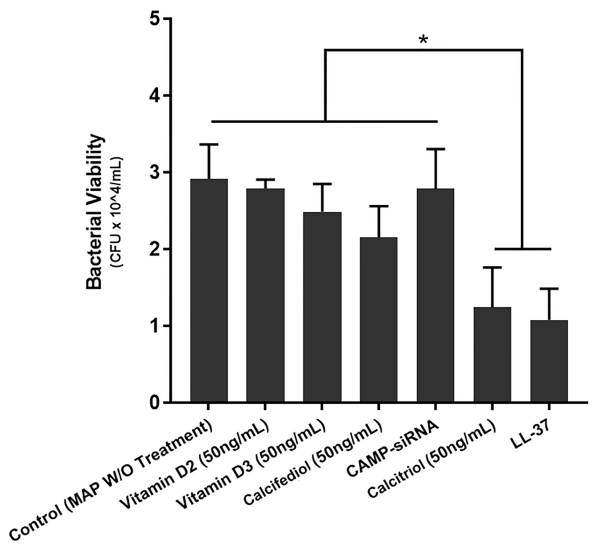

FIGURE 7 | Effects of various vitamin D forms and LL-37 on intracellular MAP Viability in infected macrophages following 24 hours of treatment. Luminescence signal was detected using the GloMax Navigator system (Promega, GM-2000), and bacterial viability was analyzed from the generated luminescence. *Indicates P-value of less than 0.05.

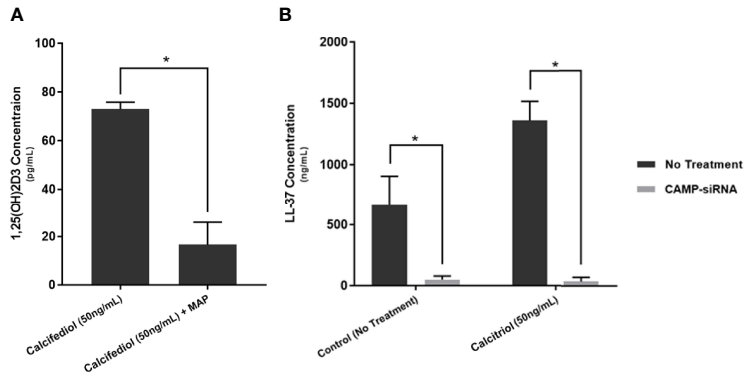

FIGURE 8 | Calcitriol concentration following 24 of treating MAP-infected macrophages with 50 ng/mL of calcifediol **(A)**, and verification of successful cathelicidin knockdown by CAMP-siRNA **(B)**. Values were determined by Calcitriol ELISA Kit (MyBioSource, San Diego, CA) and the Human Cathelicidin Antimicrobial Peptide ELISA Kit (MyBioSource, San Diego, CA). *Indicates P-value of less than 0.05.

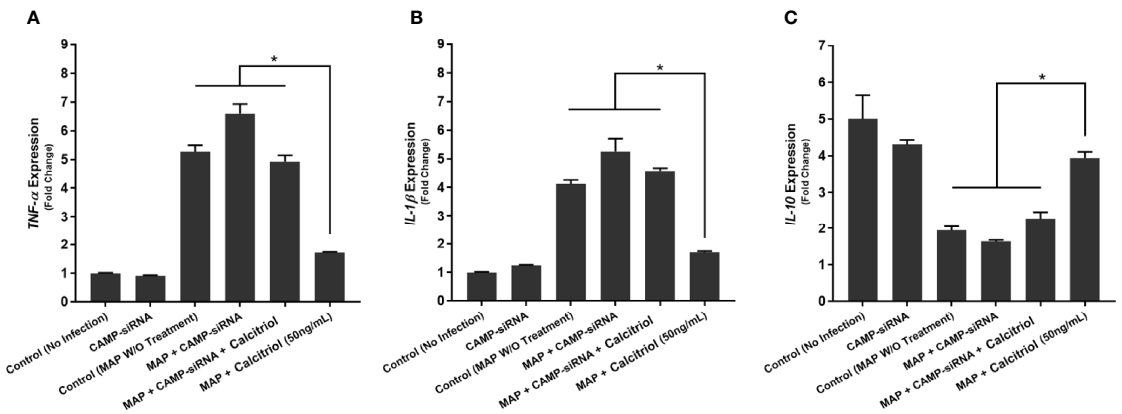

FIGURE 9 | Effects of CAMP-siRNA transfection on the expression of TNF-α **(A)**, IL-1β **(B)**, and IL-10 **(C)** in MAP-infected macrophages. *Indicates P-value of less than 0.05.

TABLE 3 | Effect of CAMP-siRNA transfection on cytokine production in MAP-infected macrophages.

Infection and Treatment	TNF-α ± SD (pg/mL)	IL-1β ± SD (pg/mL)	IL-10 ± SD (pg/mL)
Control (No Infection)	60.52 ± 1.75	56.13 ± 1.81	125.65 ± 6.11
CAMP-siRNA	69.07 ± 3.65	61.91 ± 2.63	120.46 ± 3.97
Control (MAP W/O Treatment)	173.12 ± 4.73	163.87 ± 5.72	69.18 ± 3.69
MAP + CAMP-siRNA	182.67 ± 3.18	173.75 ± 4.57	75.62 ± 5.26
MAP + CAMP-siRNA + 1,25 (OH)2D3	144.18 ± 4.03	132.86 ± 5.76	80.19 ± 2.55
MAP + 1,25(OH)2D3	81.66 ± 2.79*	74.39 ± 3.72*	105.28 ± 4.58*

*Indicates P-value of less than 0.05.

inductive capacity. First, calcitriol treatment reduces pro-inflammatory cytokine expression and restores IL-10 production in MAP-infected macrophages. In addition, LL-37 treatment displayed similar effects to calcitriol, and we verified that LL-37 has potent anti-microbial effects against MAP in both bacterial culture and infected macrophages. Consequently, *CAMP* knockdown removes the beneficial effects of calcitriol and cathelicidin on MAP infection, which validated the role of LL-37 as a mediator of calcitriol's anti-inflammatory signal in macrophages. Finally, we show that the anti-inflammatory effect of calcitriol and cathelicidin reduces MAP-induced oxidative stress in Caco-2 cells co-cultured with infected macrophages.

These findings strongly suggest that MAP and Mtb share a homologous mechanism that interferes with vitamin D signaling, which justifies further study on how MAP uniquely leads to CD pathogenesis. Additionally, our data highlight cathelicidin's key role in mediating vitamin D's anti-inflammatory properties and indicate that MAP substantially improves its viability by disrupting vitamin D signaling (**Figure 12**). Likewise, the inductive effect of cathelicidin on co-cultured epithelial cells suggests that this effect may correspond with reduced oxidative stress in intestinal tissue.

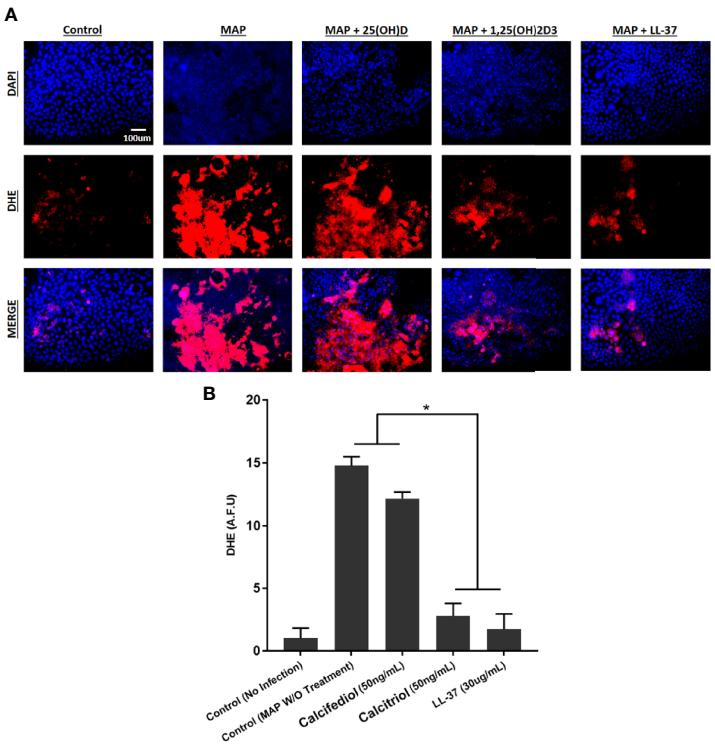

FIGURE 10 | **(A)** The impact of calcitriol and LL-37 treatment on oxidative stress measured by co-cultured Caco-2 monolayers. Total nuclei are stained with DAPI in blue. DHE positive cells are stained in red, and merged cells are presented in pink. **(B)** Quantitative corrected DHE fluorescence integrated density from control and treated groups. *Indicates P-value of less than 0.05.

Further studies may determine if MAP suppresses calcitriol production in the same way as Mtb *via* a lipoprotein-mediated disruption of TLR2 signaling (Padhi et al., 2019). However, the lack of a comprehensive genomic map of any MAP strain may hamper the bioinformatics approach to examine homology between the two species. Nevertheless, impeded stimulation of this pathway would be compelling evidence of a homologous protein and could then direct protein isolation and purification studies.

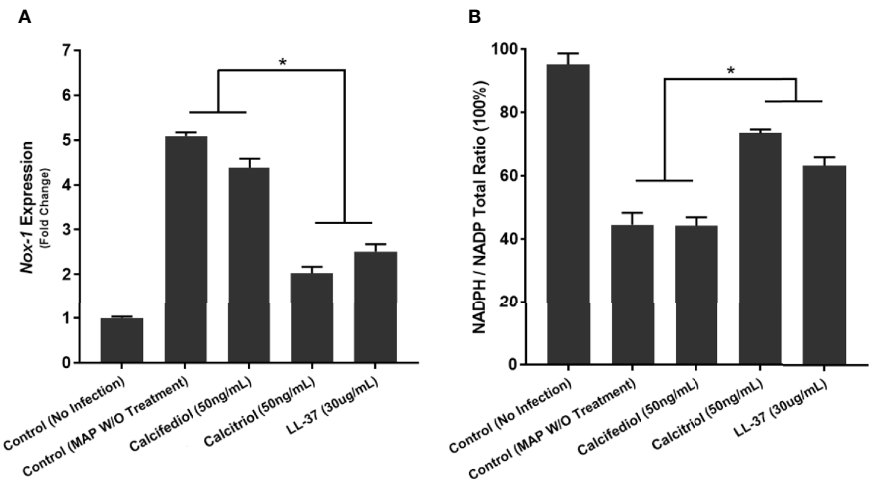

FIGURE 11 | Quantitative Analysis of Oxidative Stress levels in Caco-2 Cells Co-Cultured with MAP-infected Macrophages following 24 hours of calcitriol or LL-37 treatment. Expression of *NOX-1* was quantified as fold change in comparison to Caco-2 cells co-cultured with uninfected macrophages **(A)**. Ratio of NADPH to NADP in lysate of Caco-2 cells expressed as a percentage **(B)** was measured using the NADP/NADPH Assay Kit (Abcam, Cambridge, UK). *Indicates P-value of less than 0.05.

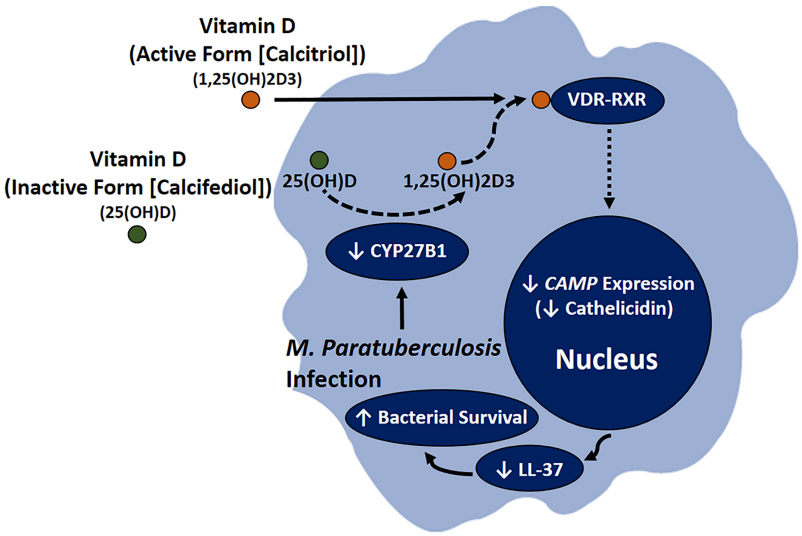

FIGURE 12 | Role of MAP infection in CD pathogenesis through downregulating the conversion of calcifediol to calcitriol, resulting in lower *CAMP* expression, which leads to reduction in LL-37 production and increased bacterial viability in infected macrophages.

Outside the context of immunity, vitamin D is a crucial signal for maintaining bone homeostasis (Christakos et al., 2016). Since IBD patients are at increased risk of osteoporosis and other skeletal abnormalities, an investigation into the mechanism by which IBD disrupts bone homeostasis is warranted (Andreassen et al., 1997). Previous work in our laboratory has identified distinct changes in undercarboxylated osteocalcin, activated osteocalcin, and serum calcium levels in MAP-infected bovines and CD patients (Naser et al., 2018). We have further noted a correlation between osteoporosis markers in the blood of rheumatoid arthritis (RA) patients, polymorphisms in the TNF-α gene and those of its receptor, and MAP infection (Naser et al., 2019). The findings of this study are highly suggestive of a novel mechanism by which MAP might interfere with bone homeostasis. An aberrant, prolonged inflammatory response paired with impaired vitamin D activation may account for MAP's deleterious effect on CD and RA patients, where its presence would represent a subgroup at particular risk of osteoporosis. Consequently, testing for MAP DNA in RA and CD patients may prove valuable for clinicians.

From a therapeutic standpoint, MAP suppression of vitamin D activation suggests that the active form of vitamin D supplementation may prove more effective in MAP-infected CD patients since most of vitamin D commercial supplements are inactive (Christakos et al., 2016). This suggestion has some precedent in clinical trials with Mtb; despite vitamin D deficiency being a risk factor for tuberculosis, a course of supplementation with inactive vitamin D in Mongolian children had no significant impact on Mtb infection rates (Ganmaa et al., 2020). Furthermore, the fact that cathelicidin supplementation mirrors the effects of calcitriol on macrophage-mediated inflammation and enterocyte oxidative stress suggests that LL-37 could be a therapeutic option for the suppression of CD inflammatory symptoms. Accordingly, further studies of this phenomenon and vitamin D's effect on CD patients are warranted.

DATA AVAILABILITY STATEMENT

The original contributions presented in the study are included in the article/supplementary material. Further inquiries can be directed to the corresponding author.

ETHICS STATEMENT

The studies involving human participants were reviewed and approved by University of Central Florida Institutional Review Board # STUDY00003468. The patients/participants provided their written informed consent to participate in this study.

AUTHOR CONTRIBUTIONS

Conceptualization, AQ, JV, and SN. Formal analysis, JV and AQ. Funding acquisition, SN. Methodology, AQ, JV, and SN. Supervision, SN. Writing - original draft, JV. Writing - review and editing, AQ and SN. All authors have read and agreed to the submitted version of the manuscript.

FUNDING

This study was supported in part by the Florida legislative grant.

ACKNOWLEDGMENTS

A special thanks to all our fellow lab members for their wisdom and helpful feedback.

REFERENCES

Adams, J. S., Rafison, B., Witzel, S., Reyes, R. E., Shieh, A., Chun, R., et al. (2014). Regulation of the Extrarenal CYP27B1-Hydroxylase. *J. Steroid Biochem. Mol. Biol.* 144 Pt A, 22–27. doi: 10.1016/j.jsbmb.2013.12.009

Alqasrawi, D., Naser, E., and Naser, S. A. (2021). Nicotine Increases Macrophage Survival Through α7nachr/NF-κb Pathway in Mycobacterium Avium Paratuberculosis Infection. *Microorganisms* 9. doi: 10.3390/microorganisms9051086

Alqasrawi, D., Qasem, A., and Naser, S. A. (2020). Divergent Effect of Cigarette Smoke on Innate Immunity in Inflammatory Bowel Disease: A Nicotine-Infection Interaction. *Int. J. Mol. Sci.* 21. doi: 10.3390/ijms21165801

Ananthakrishnan, A. N., Cagan, A., Gainer, V. S., Cai, T., Cheng, S.-C., Savova, G., et al. (2013). Normalization of Plasma 25-Hydroxy Vitamin D Is Associated With Reduced Risk of Surgery in Crohn's Disease. *Inflamm. Bowel Dis.* 19, 1921–1927. doi: 10.1097/MIB.0b013e3182902ad9

Andreassen, H., Rungby, J., Dahlerup, J. F., and Mosekilde, L. (1997). Inflammatory Bowel Disease and Osteoporosis. *Scand. J. Gastroenterol.* 32, 1247–1255. doi: 10.3109/00365529709028155

Arsenault, R. J., Maattanen, P., Daigle, J., Potter, A., Griebel, P., and Napper, S. (2014). From Mouth to Macrophage: Mechanisms of Innate Immune Subversion by Mycobacterium Avium Subsp. Paratuberculosis. *Vet. Res.* 45, 54. doi: 10.1186/1297-9716-45-54

Behr, M. A., and Kapur, V. (2008). The Evidence for Mycobacterium Paratuberculosis in Crohn's Disease. *Curr. Opin. Gastroenterol.* 24, 17–21. doi: 10.1097/MOG.0b013e3282f1dcc4

Carlberg, C. (2019). Vitamin D Signaling in the Context of Innate Immunity: Focus on Human Monocytes. *Front. Immunol.* 10, 2211. doi: 10.3389/fimmu.2019.02211

Chang, S. W., and Lee, H. C. (2019). Vitamin D and Health - The Missing Vitamin in Humans. *Pediatr. Neonatol.* 60, 237–244. doi: 10.1016/j.pedneo.2019.04.007

Chatu, S., Chhaya, V., Holmes, R., Neild, P., Kang, J. Y., Pollok, R. C., et al. (2013). Factors Associated With Vitamin D Deficiency in a Multicultural Inflammatory Bowel Disease Cohort. *Frontline Gastroenterol.* 4, 51–56. doi: 10.1136/flgastro-2012-100231

Christakos, S., Dhawan, P., Verstuyf, A., Verlinden, L., and Carmeliet, G. (2016). Vitamin D: Metabolism, Molecular Mechanism of Action, and Pleiotropic Effects. *Physiol. Rev.* 96, 365–408. doi: 10.1152/physrev.00014.2015

Davis, W. C., Kuenstner, J. T., and Singh, S. V. (2017). Resolution of Crohn's (Johne's) Disease With Antibiotics: What Are the Next Steps? *Expert Rev. Gastroenterol. Hepatol.* 11, 393–396. doi: 10.1080/17474124.2017.1300529

El-Sharkawy, A., and Malki, A. (2020). Vitamin D Signaling in Inflammation and Cancer: Molecular Mechanisms and Therapeutic Implications. *Molecules* 25. doi: 10.3390/molecules25143219

Ganmaa, D., Uyanga, B., Zhou, X., Gantsetseg, G., Delgerekh, B., Enkhmaa, D., et al. (2020). Vitamin D Supplements for Prevention of Tuberculosis Infection and Disease. *New Engl. J. Med.* 383, 359–368. doi: 10.1056/NEJMoa1915176

Greenstein, R. J. (2003). Is Crohn's Disease Caused by a Mycobacterium? Comparisons With Leprosy, Tuberculosis, and Johne's Disease. *Lancet Infect. Dis.* 3, 507–514. doi: 10.1016/S1473-3099(03)00724-2

Greenstein, R. J., Su, L., and Brown, S. T. (2012). Vitamins A & D Inhibit the Growth of Mycobacteria in Radiometric Culture. *PloS One* 7, e29631. doi: 10.1371/journal.pone.0029631

Guzman-Prado, Y., Samson, O., Segal, J. P., Limdi, J. K., and Hayee, B. (2020). Vitamin D Therapy in Adults With Inflammatory Bowel Disease: A Systematic Review and Meta-Analysis. *Inflamm. Bowel Dis.* 26, 1819–1830. doi: 10.1093/ibd/izaa087

Jo, E.-K. (2013). Autophagy as an Innate Defense Against Mycobacteria. *Pathog. Dis.* 67, 108–118. doi: 10.1111/2049-632X.12023

Liu, C. H., Liu, H., and Ge, B. (2017). Innate Immunity in Tuberculosis: Host Defense vs Pathogen Evasion. *Cell Mol. Immunol.* 14, 963–975. doi: 10.1038/cmi.2017.88

Liu, P. T., Stenger, S., Li, H., Wenzel, L., Tan, B. H., Krutzik, S. R., et al. (2006). Toll-Like Receptor Triggering of a Vitamin D-Mediated Human Antimicrobial Response. *Science* 311, 1770–1773. doi: 10.1126/science.1123933

Liu, P. T., Stenger, S., Tang, D. H., and Modlin, R. L. (2007). Cutting Edge: Vitamin D-Mediated Human Antimicrobial Activity Against Mycobacterium Tuberculosis Is Dependent on the Induction of Cathelicidin. *J. Immunol.* 179, 2060–2063. doi: 10.4049/jimmunol.179.4.2060

Naser, S. A., Ghobrial, G., Romero, C., and Valentine, J. F. (2004). Culture of Mycobacterium Avium Subspecies Paratuberculosis From the Blood of Patients With Crohn's Disease. *Lancet* 364, 1039–1044. doi: 10.1016/S0140-6736(04)17058-X

Naser, A., Odeh, A. K., Sharp, R. C., Qasem, A., Beg, S., and Naser, S. A. (2019). Polymorphisms in TNF Receptor Superfamily 1b (TNFRSF1B:rs3397) Are Linked to Mycobacterium Avium Paratuberculosis Infection and Osteoporosis in Rheumatoid Arthritis. *Microorganisms* 7. doi: 10.3390/microorganisms7120646

Naser, A., Qasem, A., and Naser, S. A. (2018). Mycobacterial Infection Influences Bone Biomarker Levels in Patients With Crohn's Disease. *Can. J. Physiol. Pharmacol.* 96, 662–667. doi: 10.1139/cjpp-2017-0700

Padhi, A., Pattnaik, K., Biswas, M., Jagadeb, M., Behera, A., and Sonawane, A. (2019). Mycobacterium Tuberculosis LprE Suppresses TLR2-Dependent Cathelicidin and Autophagy Expression to Enhance Bacterial Survival in Macrophages. *J. Immunol.* 203, 2665–2678. doi: 10.4049/jimmunol.1801301

Pecora, N. D., Gehring, A. J., Canaday, D. H., Boom, W. H., and Harding, C. V. (2006). Mycobacterium Tuberculosis LprA Is a Lipoprotein Agonist of TLR2 That Regulates Innate Immunity and APC Function. *J. Immunol.* 177, 422–429. doi: 10.4049/jimmunol.177.1.422

Perencevich, M., and Burakoff, R. (2006). Use of Antibiotics in the Treatment of Inflammatory Bowel Disease. *Inflamm. Bowel Dis.* 12, 651–664. doi: 10.1097/01.MIB.0000225330.38119.c7

Qasem, A., and Naser, S. A. (2018). Tnfα Inhibitors Exacerbate Mycobacterium Paratuberculosis Infection in Tissue Culture: A Rationale for Poor Response of Patients With Crohn's Disease to Current Approved Therapy. *BMJ Open Gastroenterol.* 5, e000216. doi: 10.1136/bmjgast-2018-000216

Qasem, A., Naser, A. E., and Naser, S. A. (2021). Enteropathogenic Infections Modulate Intestinal Serotonin Transporter (SERT) Function by Activating Toll-Like Receptor 2 (TLR-2) in Crohn's Disease. *Sci. Rep.* 11, 22624. doi: 10.1038/s41598-021-02050-3

Qasem, A., Ramesh, S., and Naser, S. A. (2019). Genetic Polymorphisms in Tumour Necrosis Factor Receptors (TNFRSF1A/1B) Illustrate Differential Treatment Response to Tnfα Inhibitors in Patients With Crohn's Disease. *BMJ Open Gastroenterol.* 6, e000246. doi: 10.1136/bmjgast-2018-000246

Qasem, A., Safavikhasraghi, M., and Naser, S. A. (2016). A Single Capsule Formulation of RHB-104 Demonstrates Higher Anti-Microbial Growth Potency for Effective Treatment of Crohn's Disease Associated With Mycobacterium Avium Subspecies Paratuberculosis. *Gut Pathog.* 8, 45. doi: 10.1186/s13099-016-0127-z

Rathnaiah, G., Zinniel, D. K., Bannantine, J. P., Stabel, J. R., Gröhn, Y. T., Collins, M. T., et al. (2017). Pathogenesis, Molecular Genetics, and Genomics of Mycobacterium Avium Subsp. Paratuberculosis, the Etiologic Agent of Johne's Disease. *Front. Vet. Sci.* 4, 187. doi: 10.3389/fvets.2017.00187

Sadeghian, M., Saneei, P., Siassi, F., and Esmaillzadeh, A. (2016). Vitamin D Status in Relation to Crohn's Disease: Meta-Analysis of Observational Studies. *Nutrition* 32, 505–514. doi: 10.1016/j.nut.2015.11.008

Shin, D.-M., Yuk, J.-M., Lee, H.-M., Lee, S.-H., Son, J. W., Harding, C. V., et al. (2010). Mycobacterial Lipoprotein Activates Autophagy *via* TLR2/1/CD14 and a Functional Vitamin D Receptor Signalling. *Cell. Microbiol.* 12, 1648–1665. doi: 10.1111/j.1462-5822.2010.01497.x

Tabatabaeizadeh, S.-A., Tafazoli, N., Ferns, G. A., Avan, A., and Ghayour-Mobarhan, M. (2018). Vitamin D, the Gut Microbiome and Inflammatory Bowel Disease. *J. Res. Med. Sci.: Off. J. Isfahan Univ. Med. Sci.* 23, 75–75. doi: 10.4103/jrms.JRMS_606_17

Vandamme, D., Landuyt, B., Luyten, W., and Schoofs, L. (2012). A Comprehensive Summary of LL-37, the Factotum Human Cathelicidin Peptide. *Cell. Immunol.* 280, 22–35. doi: 10.1016/j.cellimm.2012.11.009

White, J. H. (2018). Vitamin D Deficiency and the Pathogenesis of Crohn's Disease. *J. Steroid Biochem. Mol. Biol.* 175, 23–28. doi: 10.1016/j.jsbmb.2016.12.015

Yuk, J.-M., Shin, D.-M., Lee, H.-M., Yang, C.-S., Jin, H. S., Kim, K.-K., et al. (2009). Vitamin D3 Induces Autophagy in Human Monocytes/Macrophages *via* Cathelicidin. *Cell Host Microbe* 6, 231–243. doi: 10.1016/j.chom.2009.08.004

Conflict of Interest: The authors declare that the research was conducted in the absence of any commercial or financial relationships that could be construed as a potential conflict of interest.

this article, or claim that may be made by its manufacturer, is not guaranteed or endorsed by the publisher.

frontiers | Frontiers in Cellular and Infection Microbiology

REVIEW
published: 03 June 2022
doi: 10.3389/fcimb.2022.921534

Oncolytic Viruses: Immunotherapy Drugs for Gastrointestinal Malignant Tumors

Qingbo Li[1†], Patrick Kwabena Oduro[2†], Rui Guo[3,4†], Ruiqiao Li[2], Ling Leng[2], Xianbin Kong[1], Qilong Wang[2*] and Long Yang[3,4*]*

[1] College of Traditional Chinese Medicine, Tianjin University of Traditional Chinese Medicine, Tianjin, China, [2] Research Institute of Traditional Chinese Medicine, Tianjin University of Traditional Chinese Medicine & State Key Laboratory of Component-Based Chinese Medicine, Ministry of Education, Tianjin, China, [3] Research Center for Infectious Diseases, Tianjin University of Traditional Chinese Medicine, Tianjin, China, [4] School of Integrative Medicine, Tianjin University of Traditional Chinese Medicine, Tianjin, China

OPEN ACCESS

Edited by:
Zhanbo Zhu,
Heilongjiang Bayi Agricultural University, China

Reviewed by:
Chang Li,
Chinese Academy of Agricultural Sciences (CAAS), China
Jianfeng Dai,
Soochow University, China

***Correspondence:**
Xianbin Kong
kongxianbinvip@163.com
Qilong Wang
wangqilong_00@tjutcm.edu.cn
Long Yang
long.yang@tjutcm.edu.cn

[†]These authors have contributed equally to this work and share first authorship

Specialty section:
This article was submitted to Clinical Microbiology, a section of the journal Frontiers in Cellular and Infection Microbiology

Received: *16 April 2022*
Accepted: *09 May 2022*
Published: *03 June 2022*

Citation:
Li Q, Oduro PK, Guo R, Li R, Leng L, Kong X, Wang Q and Yang L (2022) Oncolytic Viruses: Immunotherapy Drugs for Gastrointestinal Malignant Tumors. Front. Cell. Infect. Microbiol. 12:921534. doi: 10.3389/fcimb.2022.921534

Oncolytic virus therapy has advanced rapidly in recent years. Natural or transgenic viruses can target tumor cells and inhibit tumor growth and metastasis in various ways without interfering with normal cell and tissue function. Oncolytic viruses have a high level of specificity and are relatively safe. Malignant tumors in the digestive system continue to have a high incidence and mortality rate. Although existing treatment methods have achieved some curative effects, they still require further improvement due to side effects and a lack of specificity. Many studies have shown that oncolytic viruses can kill various tumor cells, including malignant tumors in the digestive system. This review discusses how oncolytic virus therapy improves malignant tumors in the digestive system from the point-of-view of basic and clinical studies. Also, the oncolytic virus anti-tumor mechanisms underpinning the therapeutic potential of oncolytic viruses are expounded. In all, we argue that oncolytic viruses might eventually provide therapeutic solutions to malignant tumors in the digestive system.

Keywords: oncolytic virus, digestive system, immunotherapy, cancer, tumor

1 INTRODUCTION

Gastrointestinal malignancies' mortality rate remains high, with gastric and colorectal tumors among the top five cancers with high incidence rates worldwide (Sung et al., 2021). For decades, a growing list of different treatment options to control gastrointestinal cancers has been emerging. The main treatment choices are chemotherapy, radiotherapy, radiofrequency ablation, and surgical resection. However, these treatment options have a number of drawbacks, including severe side effects, inability to complete resection, and resistance to long-term use of drugs. This shows that effective treatments with profound tumor-carnage properties and low adverse and side effects are needed.

Oncolytic viruses are usually natural or modified viruses that target and kill tumor cells. These viruses regulate key intracellular processes and anti-viral responses such as apoptosis, inflammation, angiogenesis, and the cell cycle (Chen et al., 2021). Also, oncolytic viruses can enhance the host's anti-tumor immunity through multiple mechanisms (Ramelyte et al., 2021). The ability of oncolytic

viruses to regulate the above-stated intracellular processes and anti-viral events, as well as their capacity to be transformed to express tumor-destructive factors, makes them an effective anti-tumor agent of great clinical potential. In addition, compared to other anti-tumor agents, oncolytic viruses generally have outstanding characteristics, such as being non-pathogenic, having a relatively good safety profile, and the ability to be engineered to destroy tumor cells but not healthy cells, as well as the ability to deliver therapeutic payloads and produce immune-boosting molecules specific to the tumor cells they infect (Lawler et al., 2017). Because of these unique features, oncolytic virotherapy–generally defined as a treatment option that uses oncolytic viruses to kill cancer cells–has emerged as a promising therapeutic approach to treat cancers, including malignant tumors of the digestive system (Cook and Chauhan, 2020).

On the therapeutic front, critical breakthrough lenses that have emerged are the need to optimize oncolytic virotherapy to modulate the tumor immune microenvironment and combine oncolytic virotherapy with other immunotherapies or anticancer treatment options to derive maximal clinical benefit. Therefore, this mini-review provides a comprehensive overview of the development and application of oncolytic virus immunotherapy alone and/or in combination with other therapies to treat malignant tumors of the digestive system. We also discuss preclinical and clinical studies supporting oncolytic viruses' role in gastrointestinal malignant tumor therapy and detail the unique therapeutic mechanisms modulated by oncolytic viruses against cancers.

2 ANTI-TUMOR MECHANISM OF ONCOLYTIC VIRUS

2.1 Direct Oncolysis

When an oncolytic virus infects and replicates in tumor cells, it affects the synthesis of nucleic acid and protein in cells and damages organelles such as lysosomes, endoplasmic reticulum, and mitochondria, leading to alterations in cell function and, finally, killing tumor cells (**Figure 1**). For example, the recombinant Newcastle disease virus R2B-GFP virus causes the loss of mitochondrial membrane permeability in 4T1 and B16-F10 cells, resulting in cell death (Ramamurthy et al., 2021). The M1 virus kills cancer cells by inducing endoplasmic reticulum stress-mediated apoptosis (Lin et al., 2014). In addition, the capsid protein of an oncolytic virus can also play a direct role in oncolysis (Yang et al., 2021). Engineered A4 virus carrying the TRAIL gene expresses TRAIL protein on the viral surface by linking to the Leu zipper of capsid protein IX (Wang et al., 2016), which can bind to its receptor TRAILR1 (also known as DR4) or TRAILR2 (also known as DR5) to specifically induce apoptosis in cancer cells (Johnstone et al., 2008).

2.2 Inhibition of Intra-Tumor Angiogenesis

Angiogenesis plays an important role in tumor growth and development (Lugano et al., 2020). Many studies have shown that an oncolytic virus can effectively inhibit tumor angiogenesis and limit the supply of oxygen and nutrients to tumor cells. As a result, tumor cells are eliminated (Gholami et al., 2016), while at the same time, tumor cell proliferation is prevented (Qian and Pezzella, 2018).

Tumor angiogenesis can be influenced by oncogene-mediated protein expression and cellular stress factors such as hypoxia, low pH, nutrient deficiency, or reactive oxygen species induction (Al-Ostoot et al., 2021). An oncolytic virus can play an anti-angiogenesis role in many ways (Angarita et al., 2013) (**Figure 2**): (1) Direct infection of tumor vascular cells leads to the lysis of vascular endothelial cells; (2) Induce virus-mediated immune response, resulting in cell aggregation and reduced tumor blood flow; (3) Express viral proteins with anti-angiogenesis properties or inhibit the synthesis of angiogenesis promoting factors.

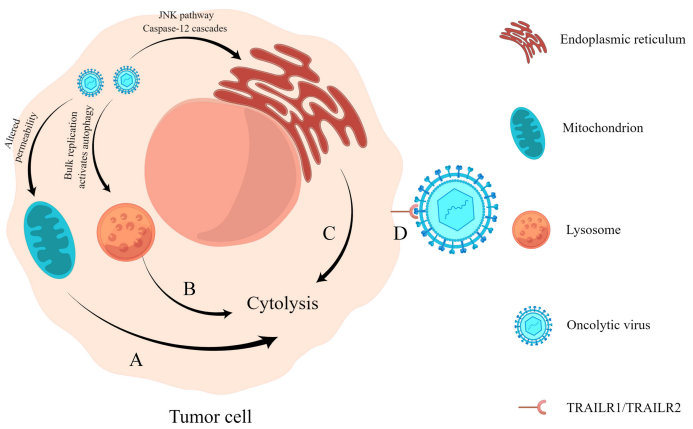

FIGURE 1 | Direct oncolysis. **(A)** Oncolytic virus acts on the mitochondria of tumor cells, resulting in the loss of mitochondrial permeability, resulting in abnormal cell metabolism and death. **(B)** Oncolytic viruses replicate abundantly and cause lysosomes to become damaged, triggering cell lysis (Yang et al., 2021). **(C)** Oncolytic virus infection causes endoplasmic reticulum stress response and cell lysis by activating the JNK pathway and caspase-12 cascades. **(D)** Virus surface capsid protein binds to TRAILR1 or TRAILR2 and causes apoptosis through the molecular mechanism of trail-mediated apoptosis.

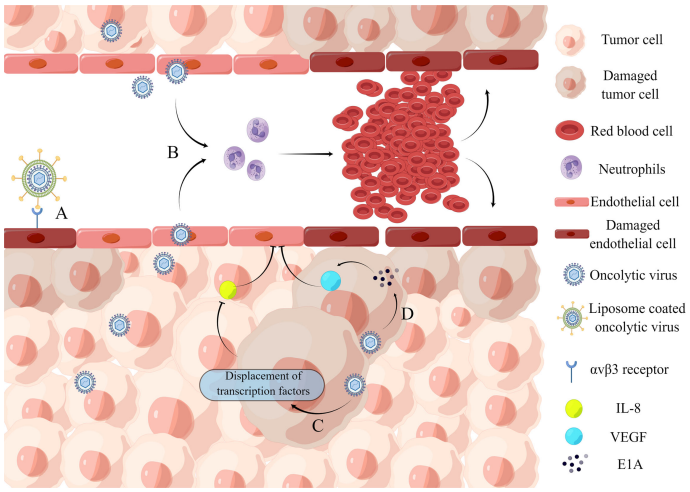

FIGURE 2 | Inhibition of intra-tumor angiogenesis. **(A)** Binding of iRGD liposome-encapsulated oncolytic virus to αvβ3 receptor directly induces lysis of HUVECs. **(B)** Oncolytic virus infection causes the recruitment of a large number of neutrophils and the formation of microthrombosis, resulting in the loss of blood perfusion and the increase of tumor cell apoptosis caused by ischemia. **(C)** Oncolytic virus dl922-947 treatment reduces IL-8 production in ATC cell lines by displacing the transcription factor NF-κB p65 from the IL8 promoter, thereby inhibiting tumor angiogenesis. **(D)** Adenovirus can express E1A protein, which can downregulate VEGF by interacting with angiogenic proteins, thereby affecting neointima in the tumor microenvironment and ultimately achieving tumor lysis.

A recent study demonstrates the ability of an oncolytic virus to lyse vascular endothelial cells. The iNDV3α-LP binds to tumor neovascularization *in-vivo* and promotes endothelial cell lysis (Wang et al., 2022). And the effect on blood flow is mainly through the recruitment of neutrophils. VSV infection of tumors causes massive neutrophil infiltration, resulting in loss of perfusion due to ischemia, which leads to increased apoptosis of tumor cells (Breitbach et al., 2007). When cancer progresses, the concentration of anti-angiogenic factors decreases. Endothelial cell growth and migration are stimulated by vascular endothelial growth factor (VEGF), epidermal growth factor (EGF), fibroblast growth factor (FGF), and interleukin-8 (IL-8) (Jośko et al., 2000). For example, an oncolytic adenovirus impairs IL-8-induced angiogenesis in pancreatic cancer (Passaro et al., 2016). Furthermore, several oncolytic herpesviruses are engineered to produce angiostatin, which has anti-angiogenic properties in a range of tumor models (Ye et al., 2006; Nair et al., 2021). However, some oncolytic viruses, such as herpesvirus C-REV, enhance tumor angiogenesis rather than inhibit it (Aghi et al., 2007; Kurozumi et al., 2008; Sahin et al., 2012). Therefore, caution should be exercised concerning their use in oncolytic virotherapy. However, combining pro-angiogenic oncolytic viruses with anti-angiogenic strategies can improve their efficacy.

2.3 Regulation of Anti-Tumor Immunity

The expression of immunosuppressive cytokines in tumor cells and tumor immune microenvironment is linked to the inactivation of effector immune cells and even recruitment of immunosuppressive cells, resulting in the body's inability to clear tumor cells in this immunosuppressive state (Borsig, 2018; Axelrod et al., 2019). Therefore, changing the suppressed state of the tumor immune microenvironment has an essential role in clearing tumor cells. Oncolytic viruses can alter the cytokine milieu and enhance immune cell maturation and activation, restoring and increasing the body's function in tumor cell clearance (Raja et al., 2018; Galon and Bruni, 2019) **(Figure 3)**.

An oncolytic virus can play an anti-tumor role by reversing the immune silencing state of the tumor immune microenvironment. For example, OHSV2 can effectively reduce the levels of bone marrow-derived suppressor cells (MDSCs) and regulatory T cells (Tregs) in the spleen, thus achieving reversal of the immunosuppressed state (Zhang et al., 2020). In addition,

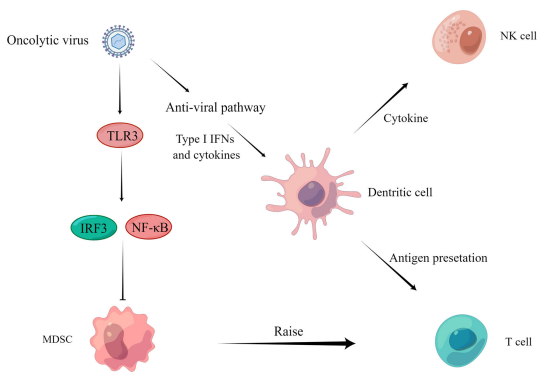

FIGURE 3 | Regulation of anti-tumor immunity. On the one hand, the virus activates IRF3 or NF-κB through the TLR3 pathway and inhibits the proliferation of MDSCs (Katayama et al., 2018) to recruit T cells to play an immune role. On the other hand, the virus activates the anti-viral pathway, induces the production of type I IFN and other cytokines, acts on DCs, NK cells, and T cells through cytokine and antigen presentation, and finally activates the body's immune response and kills tumor cells.

treatment of homozygous mice bearing 4T1 TNBC tumors with G47Δ-mIL12 was able to reduce MDSCs, leading to CD8 T cell-dependent inhibition of 4T1 tumor growth, inhibition of tumor angiogenesis, and prevention of lung metastasis, while increasing intra-tumor CD8 T cell infiltration, with local and systemic anti-cancer effects (Ghouse et al., 2020).

Tumor killing is aided by natural killer cells (NK), CD8 T cells, and dendritic cells (DC). Oncolytic viruses have been proven in numerous investigations to activate or recruit these immune cells to have an anti-tumor effect. The levels of NK cells, CD8 T cells, and DC increased dramatically after OHSV2 treatment (Ghouse et al., 2020). This treatment response was equated to being the mechanism by which OHSV2 exerts its oncolytic activity. In addition, oncolytic herpes simplex virus (T-VEC) can recruit tumor antigen-specific CD8 T cells and induce anti-inflammatory gene characteristics in injected and non-injected tumors (Ye et al., 2018). Furthermore, Newcastle disease virus (NDV) infection stimulates type I interferon (IFN) production *via* other tumor-infiltrating immune cells (García-Romero et al., 2020), as well as type I IFN signaling for antigen presentation, DC maturation, memory cytotoxic T lymphocyte activation and survival, NK cell activation, and neutrophil recruitment (Zitvogel et al., 2015; Parker et al., 2016). Engineered lysing virus and Semliki Forest Virus (SFV) infections that express a programmed death ligand-1 (PD-L1) inhibitor, as well as a granulocyte-macrophage colony-stimulating factor (GM-CSF), have been shown to activate antigen-specific T cell (Ma et al., 2020; Wang et al., 2020).

Oncolytic virus therapy can establish long-term anti-tumor immunity in immune regulation and prevent tumor recurrence. For example, the M1 virus can destroy the immune tolerance of the tumor immune microenvironment, change the immunosuppressive state, trigger an effective CD8 T cell-dependent treatment effect, and establish long-term anti-tumor immune memory in a tumor model with poor immunogenicity (Liu et al., 2020). A study of the oncolytic vaccinia virus also illustrates this mechanism. The use of tumor-selective oncolytic vaccinia viruses encoding interleukin-7 (IL-7) and interleukin-12 (IL-12) can make mice with complete tumor regression resist the re-attack by the same tumor cells (Nakao et al., 2020).

3 ONCOLYTIC VIRUS IMMUNOTHERAPY IN GASTROINTESTINAL MALIGNANT TUMORS

3.1 Oncolytic Virus (Including Transgenic) Monotherapy

In this new era of innovative medicine, oncolytic viruses have become a promising primary treatment essential to fighting cancer. Various natural viruses have been found to have an effective oncolytic effect throughout many years of research. Natural viruses, on the other hand, have low specificity and pathogenicity, so researchers have been continuously optimizing them through transgenic technology to enhance their tumor specificity and selectivity. This section aims to focus on the latest advances in clinical applications of various oncolytic virus immunotherapies in the treatment of malignant tumors of the digestive system, especially when coupled with other cancer treatment strategies (**Table 1**).

3.1.1 Colorectal Cancer (CRC)

Coxsackievirus is a single-stranded RNA virus that belongs to the small ribonucleic acid family of human enteroviruses (Simmonds et al., 2020), among which coxsackievirus B3 (CVB3) has much great potential in the fight against colorectal cancer. However, wild-type (WT) CVB3 treatment leads to cardiac and pancreatic damage (Deng et al., 2019; Jia et al., 2019; Hazini et al., 2021b). As a result, strategies to improve its safety while also improving its therapeutic efficacy are required. First, one way is to select from numerous strains preferentially. Also, PD uses N- and 6-O-sulfonated acetylated heparin sulfate (HS) to enter host cells. It infects colorectal cancer cell lines with the highest efficiency *in-vitro* when compared to Nancy and 31-1-93 (Zautner et al., 2003). In addition to the good safety profile, *in-vivo*, PD application in a mouse colorectal cancer transplant tumor model showed significant tumor growth inhibition (Hazini et al., 2018). Second, another effective strategy is targeting the damage produced by CVB3 in the pancreas with transgenic modification of coxsackieviruses. For instance, researchers inserted miR-375TS into CVB3's 3′UTR, a multi-protein coding sequence of CVB3, that reduced viral infection of pancreatic cells while maintaining CVB3's tumor lytic function in an *in-vitro* experiment (Pryshliak et al., 2020). Of course, viral toxicity to the heart is non-negligible. In this case, combining the basal pancreas-specific expression of miR-375 with the heart-specific expression of miR-TS would enhance CVB3 virus effectiveness in preventing virus replication in the pancreas and heart while retaining the anti-tumor effect. This strategy further improves the specificity of CVB3 in animal experiments (Hazini et al., 2021b). It is worth noting that coxsackieviruses' safety is tightly linked to the virus's route of administration, and a recent study indicated that intratumoral injection of recombinant CVB3 variant PD-H caused no side effects. In immunocompetent mice, however, intraperitoneal administration resulted in weak pancreatitis and myocarditis (Hazini et al., 2021a).

In addition to CVB3, the herpes simplex virus (HSV) has shown tumor lysis potential. In 2015, the U.S. Food and Drug Administration (FDA) approved genetically modified T-VEC to treat advanced melanoma patients (Guo et al., 2019). In recent years, the herpes simplex virus has demonstrated therapeutic potential against various tumors (Hamada and Yura, 2020; Mondal et al., 2020; Bernstock et al., 2021). For example, HSV-2 expressing GM-CSF showed potent anti-tumor effects in multiple CRC cell lines and mouse CRC models, as well as the ability to modulate the immune response to enhance the therapeutic effect further. According to a recent animal study, HSV-2 expressing GM-CSF-induced immune response was effective against metastatic tumors, resulting in lasting anti-tumor effects and efficient prevention of tumor recurrence (Zhang W. et al., 2021). Furthermore,

TABLE 1 | Oncolytic virus (including transgenic) monotherapy.

Type of cancer	Virus	Virus name	Route of virus administration	Effect	Reference
Colorectal cancer	CV	PD	Intratumoral injection.	Strongly inhibit tumor growth	(Hazini et al., 2018)
		PD-H	Intratumoral injection	Strongly inhibit tumor growth	(Hazini et al., 2021a)
		CVB3-375TS (3+)	Intratumoral injection	Reduced toxicity to pancreas	(Pryshliak et al., 2020)
		H3N-375TS	Intratumoral injection	Significantly slow down tumor growth	(Hazini et al., 2021b)
		H3N-375/1TS	Intratumoral injection	Significantly slow down tumor growth	(Hazini et al., 2021b)
	HSV	oHSV2	Intratumoral injection	Significantly slow down tumor growth	(Ying et al., 2017)
		oHSV2	Intratumoral injection	Effectively kill primary tumors and attack distal and metastatic tumors	(Zhang W. et al., 2021)
	VSV	ΔM51 mutant	Cell experiment	Significant cytotoxicity	(Gray et al., 2019)
	VV	VVLΔTKΔN1L-mIL-21	Intratumoral injection	Reduced toxicity to pancreas	(Wang et al., 2021)
Liver cancer	ARV	ARV-PB1	Cell experiment	Replicate normal and induce intense cytopathy	(Kozak et al., 2017)
	Influenza A virus	M1	i.v.	Reduced toxicity to pancreas	(Ying et al., 2017)
	AdV	Ad-VT	Intratumoral injection	Reduced toxicity to pancreas	(Tian et al., 2020)
	CV	NOV	Intratumoral injection	Reduced toxicity to pancreas	(Jeong and Yoo, 2020)
		CVV	i.p.	Effectively reduce cancer cell metastasis	(Yoo et al., 2017)
	Chimeric virus	rVSV-NDV	I.v.	Reduced toxicity to pancreas	(Abdullahi et al., 2018)
Pancreatic cancer	AdV	Ad5/3-E2F-d24-vIL2	Intratumoral injection	Significantly prolonged survival	(Quixabeira et al., 2021)
		LOAd703	i.p.	Significantly slow down tumor growth	(Eriksson et al., 2017)
		OBP-702	Intratumoral injection	Significantly inhibit the growth and invasion of cancer cells	(Koujima et al., 2020)
	OV	CF33-hNIS-antiPDL1	i.v.	Reduced toxicity to pancreas	(Woo et al., 2020)
	VSV	VSV-p53OV	Cell experiment	Normal replication and stable inheritance	(Steinhauer et al., 1992)
Gastric cancer	HSV	T-SOCS3	Cell experiment	Significant cytotoxicity	(Matsumura et al., 2021)
		G47Δ	Intratumoral injection /i.v.	Reduced toxicity to pancreas	(Sugawara et al., 2020)
	AdV	Ad-Surp-mK5/Ad-Surp-MnSOD 296	unknown	Reduced toxicity to pancreas	(Liu et al., 2022)
Oesophageal cancer	HSV	G47Δ	Intratumoral injection	Reduced toxicity to pancreas	(Yajima et al., 2021)

vesicular stomatitis virus (VSV) and its ΔM51 mutant exhibited a destructive effect on SW480 colorectal cancer cells in an *in-vitro* cellular study (Gray et al., 2019). VVLΔTKΔN1L-mIL-21, a novel lysing virus-containing IL-21, effectively induced adaptive T-cell responses that eliminated primary tumors and prevented tumor recurrence in an animal study (Wang et al., 2021). These studies, taken together, provide new viral options for the treatment of colorectal cancer. Aside from the anti-tumor effects, genetic modification of the virus can help us determine the appropriate dose for treatment. In complete and EEV forms, the recombinant virus CF33Fluc, which was obtained by substituting the thymidine kinase gene with firefly luciferase (Fluc), is more effective than the parental virus in another animal study. Real-time non-invasive imaging of viral replication can be used to assess viral replication in real-time (Warner et al., 2019).

3.1.2 Liver Cancer

Hepatitis C virus (HCV) infection is common in people with liver cancer, and IFN is frequently used to treat it. As a result, treating liver cancer patients with an oncolytic virus will present two challenges: the first is determining whether the oncolytic virus can play a role in HCV-infected cells, and the second is determining whether interferon can inhibit the replication of the oncolytic virus. Researchers have recently looked into the two issues mentioned above. Studies have shown that avian reovirus ARV-PB1 can kill various liver cancer cell lines *in-vitro* (Kozak et al., 2017). In liver cancer cell lines infected with HCV, ARV-PB1 can still replicate normally and play a typical role in tumor lysis. Another study discovered that IFNα could activate IFN stimulating genes (ISGs), inhibit M1 virus replication, and prevent cell apoptosis. Thus, IFN treatment antagonizes the M1 virus's oncolytic action. Other anti-hepatitis drugs, such as

direct anti-viral small molecule drugs (DAA) and ribavirin (RBV) for chronic hepatitis C, do not inhibit M1's oncolytic activity. As a result, the patient's conditions must be evaluated before beginning IFNα and M1 virus combined therapy in patients with hepatocellular carcinoma complicated by hepatitis B virus or hepatitis B virus infection. When the expression of ISGs is abundant in the tumors of patients with liver cancer, coadministration of IFNα with M1 virus is not recommended. The standard chemical-based anti-hepatitis regimens should be selected in this case (Ying et al., 2017).

Various recombinant viruses have better tumor specificity, less toxicity to normal cells, and can inhibit tumors from metastasizing. In a tumor-bearing nude mouse model assay, the dual cancer-specific anti-tumor recombinant adenovirus Ad-apoptin-hTERTp-E1a (Ad-VT) showed tumor-specific replication and specific tumor-killing. In addition, in hepatocellular carcinoma QGY-7703 cells, it effectively inhibited tumor growth and promoted apoptosis (Tian et al., 2020). The NOV, which was obtained by inserting TRAIL and Ang1 into the engineered VV, also had anti-tumor effects *via* the apoptotic pathway in CRC homologous mouse models (Jeong and Yoo, 2020). The treatment of mice with *in-situ* hepatocellular carcinoma with the novel hybrid virus rVSV-NDV significantly prolonged the mice's survival time. In addition, it had a reduced cytotoxic effect on healthy hepatocytes and neurons while retaining its benefits (Abdullahi et al., 2018). Furthermore, more than half of hepatocellular carcinoma patients develop metastases (Yoo et al., 2017), and oncolytic viruses have shown promise in the treatment of metastatic liver cancer. For instance, in an animal model of metastatic liver cancer established with a high CD44-expressing Sk-Hep-1 cell line, CVV, an engineered poxvirus produced by repeated selective replication in cancer tissue and deletion of the viral thymidine kinase gene, attenuates cell migration. Therefore, they reverse the metastasis of highly metastatic Sk-Hep-1 cells by inducing low CD44 to reduce the expression of EMT markers. This study provides a new avenue for treating metastatic liver cancer (Yoo et al., 2017).

3.1.3 Pancreatic Cancer (PC)

Pancreatic cancer has an extremely poor prognosis. Due to its aggressive nature, pancreatic cancer has a 5-year survival rate of less than 10% (Mcguigan et al., 2018), and only 15% of patients are suitable for surgical resection treatment, with the majority of patients progressing to locally advanced stages or developing into metastatic disease (Strobel et al., 2019). Adenovirus and orthopoxvirus effectively suppress tumor metastasis and prolong the survival rate. An animal study has shown that recombinant adenovirus Ad5/3-E2F-d24-vIL2 can counteract immunosuppression and coordinate lymphocyte-mediated immunity (Quixabeira et al., 2021). Adenovirus also aids oncolysis by modulating several signaling pathways, including the CD40, 4-1BB, and ERK signaling pathways. One adenovirus, LOAd703, that carries trimers CD40L and 4-1BBL can initiate and regulate multiple signaling pathways, kill cancer cells, and affect the immune microenvironment (Eriksson et al., 2017). Another recombinant adenovirus, OBP-702, can effectively inhibit the migration of pancreatic ductal adenocarcinoma (PDAC) cells induced by neurosecretory factors by suppressing extracellular regulated protein kinase (ERK) signal transduction in a preclinical, experimental study (Koujima et al., 2020). The application of orthopoxvirus shows that the route of administration impacts oncolytic viruses' therapeutic effects. An artificially designed immunolytic agent, CF33-hNIS-antiPDL1, had a better curative effect when administered intraperitoneally than intravenous. Early IP treatment has been shown in animal studies to significantly reduce tumor burden, delay disease development, and increase the likelihood of survival (Woo et al., 2020).

VSV is also one of the oncolytic viruses used in pancreatic cancer therapy. However, pancreatic ductal adenocarcinoma cells have a wide range of sensitivity and tolerance to VSV-based oncolytic viruses like VCV-ΔM51 (Felt and Grdzelishvili, 2017). A novel VSV (called VSV-p53OV) derived from the original VSV-p53wt and VSV-p53-CC inhibited PDAC cells from multiplying. However, like other RNA viruses, VSV lacks the proofreading function of the virally encoded RNA-dependent RNA polymerase (RdRp) and is prone to gene mutation [65]. Thus, the genetic stability of the advantageous transgenic fragments carried by VSV is essential. Surprisingly, after 33 generations of virus passages, all viruses retained the original virus-carried p53 (p53wt or p53-CC) and red fluorescent protein (RFP) sequences without any mutations in the transgenic fragment in a basic research study (Seegers et al., 2020).

3.1.4 Gastric Cancer

The herpes simplex virus is the most frequently studied in gastric cancer investigations. However, not all gastric cancer cell lines will respond to the herpes simplex virus transformation. MKN1 is resistant to OHSV expressing platelet lectin-1 (TSP-1) (Tsuji et al., 2013). For MKN1, researchers have developed a new herpes simplex virus called T-SOCS3 that expresses cell signal transduction inhibitor 3 (SOCS-3). In MKN1 cells with low SOCS3 expression after T-01 infection, T-SOCS3 showed a more efficient oncolytic effect in a basic research (Matsumura et al., 2021). In addition, the fourth-generation oncolytic herpes simplex virus (T-hTERT) containing the ICP6 gene, which is regulated by the hTERT promoter, was more toxic to MKN1 cells in an *in-vitro* cellular study (Kato et al., 2021). These studies provide a new strategy for treating drug-resistant gastric cancer cell lines.

Due to the lack of reliable screening strategies and apparent specific clinical manifestations, many patients with gastric cancer present in advanced stages (Smyth et al., 2020). Gastric cancer has a 5-year survival rate of 25-30% (Tirino et al., 2018) and is the third leading cause of cancer-related mortality (Seidlitz et al., 2021). Even in the late stages of gastric cancer, the third-generation herpes simplex virus type 1 (HSV-1) G47Δ can replicate in gastric cancer cell lines, including sclerosing gastric cancer cell lines, and induce cytopathic effects. In addition, G47Δ significantly inhibited tumor growth in an *in-vivo* subcutaneous tumor model, and when administered intratumorally, G47Δ demonstrated good anti-tumor effects regardless of the dose regimen. In a peritoneal dissemination model, intraperitoneal

injection of G47Δ also showed significant effectiveness, probably because G47Δ could rapidly penetrate disseminated tumors and selectively replicate therein without the need to inject the virus into each tumor node (Sugawara et al., 2020).

Development of oncolytic adenoviruses to tackle gastric malignancies remain a hot research topic in cancer therapeutics. Rigvir® was the first non-genetically modified gastric cancer virotherapy agent to be approved (Alberts et al., 2016). However, Rigvir®'s therapeutic scope is not limited to gastric cancer only. For instance, *in-vitro* experiments–*in-vivo* confirmation is lacking–have shown an inhibitory effect on the viability of multiple tumor cells of human origin, including pancreatic cancer cells (Tilgase et al., 2018). A recent *in-vitro* experiment found that the combination of adenoviruses carrying mK5 and MnSOD genes showed stronger cytotoxicity than a single virus therapy. In addition, no significant differences in body weight were found between the combination treatment mice and the normal mice, demonstrating that this unique combination therapy is plausibly safe (Liu et al., 2022). This strategy of combining two viruses differs from the traditional combination therapies, and it points to a new direction for oncolytic viral research.

3.1.5 Esophageal Cancer

The third-generation oncolytic herpes simplex virus type 1 (HSV-1) g47d might be used to treat a variety of human malignancies, including esophageal cancer (Wang et al., 2014; Wang et al., 2015; Sugawara et al., 2020; Uchihashi et al., 2021). G47d administered intratumorally has been found to have an effective oncolytic effect on subcutaneous and *in-situ* EC tumors in mice. Furthermore, g47d was safe when given orally and intraesophageally in high doses (Yajima et al., 2021). In a tumor-bearing animal model, VSV reduces the development of a variety of cancers when administered intratumorally or intravenously (Felt and Grdzelishvili, 2017), indicating that it might be used to treat esophageal cancer. Although the mechanism by which VSV induces autophagy activity *via* MPS remains unknown, a study found that VSV has oncolytic activity in the esophageal cancer cell line KYSE-30, suggesting that M51R mutant matrix protein (M51R mMP) may promote oncolysis (Douzandegan et al., 2019).

3.2 Oncolytic Virus Combined With Chemotherapy

Chemotherapy is one of the most commonly used treatments for cancer. On the other hand, long-term chemotherapy use causes drug resistance, which is accompanied by increasingly severe side effects (Phillips and Mousa, 2022), such as hepatotoxicity and nephrotoxicity, which cause a slew of issues and lower the patient's quality of life. In recent years, oncolytic viruses paired with chemotherapy have demonstrated many benefits, including reduced toxicity, increased specificity, and improved chemotherapy's curative efficacy **(Table 2)**.

3.3 Colorectal Cancer

One of the most pressing issues in oncolytic viral treatment for colorectal cancer is overcoming chemotherapeutic drug resistance. Although oxaliplatin is one of the first-line chemotherapy drugs for stage III and IV colorectal cancer, patients who are resistant to it have a poor prognosis. Coxsackievirus A11 (CVA11) has a potential oncolytic effect on the sensitivity of the caco-2 cell line to oxaliplatin treatment. However, it has little effect on the oxaliplatin-resistant cell line WiDr. Moreover, the oncolytic activity of CVA11 is enhanced after oxaliplatin pretreatment, but the combination treatment's cytotoxicity is stronger than either oxaliplatin or CVA11 monotherapy (Wang et al., 2018). It is not by chance that oxaliplatin combined with an oncolytic virus has such a positive impact. Combining lonidamine with the M1 virus shows a synergistic anti-tumor effect. In a mouse colorectal cancer model, lonidamine enhanced the infection and tumor-killing effects of the M1 virus by inhibiting myeloproliferative proto-oncogene (MYC), which not only reveals that lonidamine is a potential synergist of the M1 virus but also implies that MYC deficiency is a potential selective biomarker of M1 virus oncolytic efficacy (Cai et al., 2020). However, it is worth noting that targeted therapeutic combinations do not always improve outcomes. A clinical trial, for example, found that combining

TABLE 2 | Oncolytic viruses combined with chemotherapy.

Type of cancer	Virus	Virus name	Chemotherapeutic drug	Route of virus administration	Effect	Reference
Colorectal cancer	CV	A11	Oxaliplatin	Intratumoral injection	Significantly enhance the efficacy of monotherapy	(Wang et al., 2018)
	Influenza A virus	M1	Lonidamine	i.v.	Infection and tumor killing effect of M1 virus	(Cai et al., 2020)
Liver cancer	NDV	NDV	Fludarabine	i.p.	Synergistic inhibition of tumor growth	(Meng et al., 2019)
		NDV	5-FU	i.p.	Synergistic inhibition of tumor growth	(Assayaghi et al., 2019)
Pancreatic cancer	VV	VV-ING4	Gemcitabine	Intratumoral injection	Synergistic inhibition of tumor growth	(Wu et al., 2017)
	HSV	HF10	Erlotinib, Gemcitabine	Intratumoral injection	Safe treatment for locally advanced pancreatic cancer	(Hirooka et al., 2018)
	ARV	Pelareorep	Gemcitabine	i.v.	Improve the expected survival rate of chemotherapy alone	(Mahalingam et al., 2018)
		Pelareorep	5-FU, Irinotecan, Irinotecan	i.v.	Synergistic inhibition of tumor growth	(Mahalingam et al., 2020)

lysing euthero virus (Reolysin ™) with standard first-line chemotherapy resulted in a shorter progression-free survival than chemotherapy drugs alone (Jonker et al., 2018).

3.3.1 Liver Cancer

Newcastle disease virus (NDV) mediates innate and adaptive immunity, resulting in a cross-activated anti-tumor immune response (Schwaiger et al., 2017). In addition, its therapeutic effects are associated with CD8 T cells, NK cells, and type I IFNs, but not with CD4 lymphocytes (Zamarin et al., 2014; Ricca et al., 2018). Recent studies have discovered that combining NDV with chemotherapeutic drugs can increase NK cell infiltration and improve anti-tumor effects. Fludarabine, a chemotherapeutic agent for chronic myeloid leukemia, promotes viral replication by targeting signal transducers and activator of transcription 1 (STAT1). This response promotes tumor catabolism and increases ubiquitin proteasomal degradation by accelerating phosphorylated cell signaling with transcriptional activator 3 (p-STAT3) and indoleamine 2,3-dioxygenase-1 (IDO1). Through the mechanisms described above, NDV-mediated viral immunotherapy enhances NK cell infiltration and reduces the number of MDSCs in the tumor immune microenvironment (Meng et al., 2019). NDV has also been demonstrated to improve the anti-tumor action of the chemotherapeutic drug 5-fluorouracil (5-FU) by increasing apoptosis induction. The combination of NDV and 5-FU showed stronger anti-tumor effects than either treatment with NDV or 5-FU alone in an animal study (Assayaghi et al., 2019).

3.3.2 Pancreatic Cancer

Gemcitabine is one of the first-line chemotherapeutic agents for pancreatic cancer. However, due to its increased drug resistance and reduced therapeutic effect, new approaches are needed to improve the efficacy of gemcitabine. Thus, combining gemcitabine with oncolytic viruses may have great anti-tumor therapeutic potential. For example, studies have shown that when gemcitabine (0.01 or 0.05 mM) is combined with oncolytic adenovirus YDC002, the anti-cancer outcomes in pancreatic cancer are better than with a single treatment. This indicates that oncolytic virus YDC002 can make highly resistant pancreatic cancer cells more sensitive to gemcitabine. Besides, it has been found that YDC002 can effectively destroy the extracellular matrix and enhance gemcitabine-induced apoptosis. The safety of gemcitabine and YDC002 combination treatment has been shown to be negligible. Even when compared to gemcitabine or YDC002 alone, this combination therapy treatment did not apparently affect body weight and liver function (Jung et al., 2017).

In addition, gemcitabine can penetrate cancerous cells effectively, and when used in conjunction with other drugs or treatment strategies, beneficial synergistic effects are often reported (Wu et al., 2017). The efficacy and safety of gemcitabine, when combined with other therapies against pancreatic cancer, have also been proven in several clinical studies. For example, a phase I clinical trial found that combining Erlotinib and gemcitabine with direct injection of herpes simplex virus mutant HF10 under ultrasound endoscopic guidance had a stronger anti-tumor effect and that all experimental doses (1×10^6, 3×10^6, or 1×10^7pfu/day×4 times) during dose escalation showed good safety and efficacy (Hirooka et al., 2018). Furthermore, in a phase II clinical trial investigating the role of pelareorep in combination with gemcitabine for advanced pancreatic cancer (the median OS of patients receiving this combination was 10.2 months), the 1- and 2-year survival rates were 45% and 24%, respectively, which were significantly higher than the expected survival rates with gemcitabine therapy alone. This was similar to the efficacy obtained with FOLFIRINOX in the same experimental setting. Pelareorep plus gemcitabine, on the other hand, demonstrated a better safety profile than FOLFIRINOX therapy and could be used as an adjunct to gemcitabine monotherapy (Mahalingam et al., 2018). In a phase Ib clinical study, the combination of pelareorep and pembrolizumab with chemotherapy (5-FU, gemcitabine, or irinotecan) had no significant toxicity despite the desirable efficacy (Mahalingam et al., 2020).

3.3.3 Gastric Cancer

A dual therapy of intraperitoneal injection of green fluorescent protein (GFP)-expressing attenuated adenovirus (OBP-401) plus paclitaxel (PTX) has been demonstrated to successfully suppress peritoneal metastasis of gastric cancer in an *in-situ* xenograft model. Synergistically, OBP-401 and PTX can inhibit the viability of human gastric cancer cells, and PTX enhances OBP-401's anti-tumor effects by boosting viral replication in cancer cells. However, further research into the combined therapy's clinical efficacy and tolerance is required (Ishikawa et al., 2020).

3.4 Oncolytic Virus Combined With Targeted Therapy

Targeted therapy is one of the most successful ways to treat tumors by inhibiting tumor cell growth or inducing apoptosis by acting on specific cell receptors, signaling, and other channels that promote tumor growth and survival, neovascularization, and cell cycle regulation. However, targeted therapy also has drawbacks, such as drug resistance and side effects, and the use of oncolytic viruses in combination with targeted therapy has improved the therapeutic effect **(Table 3)**.

3.4.1 Colorectal Cancer

EGFR signaling is important for apoptosis, angiogenesis, cell proliferation, migration, and invasion. Cetuximab can enhance the anti-tumor activity of the herpes simplex virus canerpaturev (C-REV) by promoting viral distribution and inhibiting angiogenesis while not interfering with the viral replication process. It is noteworthy that injection of C-REV prior to cetuximab REV has no additive effect on tumor growth compared to C-REV alone in a preclinical study. Therefore, the order of application should be carefully considered (Wu et al., 2019). In addition to cetuximab, the combination therapy of propranolol and oncolytic viruses has been shown to enhance anti-angiogenic effects. Also, propranolol and T1012 combined

TABLE 3 | Oncolytic viruses combined with targeted therapy.

Type of cancer	Virus	Virus name	Targeted drug	Route of virus administration	Effect	Reference
Colorectal cancer	HSV	CRV	Cetuximab	Intratumoral injection	Synergistic antitumor effect	(Wu et al., 2019)
		T1012G	Propranolol	Intratumoral injection	Synergistic antitumor effect	(Hu et al., 2021a)
		T3855	Trametinib	Intratumoral injection	Synergistic antitumor effect	(Zhou et al., 2021)
	VV	VVL15	PI3K inhibition	i.v.	Synergistic antitumor effect	(Ferguson et al., 2020)
Liver cancer	NDV	NDV	DCA	i.p./i.v.	Synergistic antitumor effect	(Meng et al., 2020)
Pancreatic cancer	VSV	VSV-S	Anti-PD-1 antibody	Intratumoral injection	Synergistic antitumor effect	(Tang et al., 2022)
	AdV	Delta-24-RGD	PS targeted antibody	Intratumoral injection	Synergistic antitumor effect	(Dai et al., 2017)
Gastric cancer	HSV	T1012G	Propranolol	Intratumoral injection	Synergistic antitumor effect	(Hu et al., 2021b)

therapy promoted vascular endothelial growth factor secretion inhibition. However, this combined treatment does not promote viral replication compared to that of cetuximab in an animal study (Hu et al., 2021a).

Furthermore, dysregulation of the mitogen-activated protein kinase (MAPK) signaling cascades occurs frequently in several melanomas. Because of this, the RAS/RAF/MEK/ERK pathway is one of the most studied pathways in cancer biology for the reason that this pathway's upregulated signaling activity promotes cell proliferation, metastasis, angiogenesis, and others (Degirmenci et al., 2020; Guo et al., 2020). It has been shown that the MEK inhibitor (MEKi) trametinib in combination with OHSV was able to completely eradicate tumors in a CT26 (KRAS-G12D) mouse model. Also, treatment with MEKi promoted OHSV replication in BRAF wt/KRAS mutated tumor cells *in-vitro* (Zhou et al., 2021). In addition to this pathway, IC87114, a selective inhibitor targeting phosphatidylinositol trihydroxyl kinase (PI3K), significantly promoted viral delivery to tumors (Ferguson et al., 2020).

3.4.2 Liver Cancer

The Newcastle disease virus may be useful in the treatment of hepatocellular carcinoma. Unfortunately, due to lactate accumulation, STAT3 activation, IDO1 upregulation, and increased MDSCs infiltration, the Newcastle disease virus causes immunosuppression. The pyruvate dehydrogenase kinase (PDK) inhibitor dichloroacetate (DCA), on the other hand, improves T cell anti-tumor activity by reducing lactate-mediated immunosuppression (Ohashi et al., 2013). This shows that DCA and the Newcastle disease virus can be combined to overcome individual shortfalls. A study report involving DCA and Newcastle disease virus combination treatment against hepatocellular carcinoma indicates that the PDK inhibitor DCA significantly reduced lactate release, STAT3 activation, IDO1 upregulation, and MDSC infiltration in Newcastle disease virus-treated hepatocellular carcinoma. In addition, the presence of DCA boosted Newcastle disease virus replication in hepatocellular carcinoma, implying that DCA improved the anti-tumor immune response to Newcastle disease virus, culminating in the prolonged survival time of tumor-bearing mice (Meng et al., 2020).

3.4.3 Pancreatic Cancer

The programmed death-1 (PD-1) receptor participates in a key pathway of tumor immune escape. Targeted PD-1 immune checkpoint treatment has been approved to treat patients with certain types of malignancies (Tsuruta et al., 2022). In a recent animal study, VSV-S therapy was shown to eliminate tumors in some cases wholly, and it had even better efficacy when combined with anti-PD-1 therapy (Tang et al., 2022).

Phosphatidylserine (PS)-targeted antibodies have shown good efficacy in pancreatic cancer studies and can increase the therapeutic effects of oncolytic viruses against tumors (Digumarti et al., 2014; Chalasani et al., 2015; Freimark et al., 2016). In a mouse PDAC model, elta-24-RGD promotes PS receptor exposure in infected cells, allowing for the application of both elta-24-RGD viral therapy and PS-targeted antibodies in hepatic metastatic pancreatic cancer cells lines. PS-targeting antibodies in combination with elta-24-RGD demonstrated a stronger tumor effect than treatment alone (Dai et al., 2017).

3.4.4 Gastric Cancer

Propranolol coupled with T1012G has a synergistic lethal effect on human and mouse colorectal cancer cells, and also, propranolol has a comparable effect on gastric cancer. Propranolol was discovered to improve the anti-tumor efficacy of viral T1012G in gastric cancer cells by modulating STAT3-PKR-dependent anti-viral responses, which were maintained with type I IFN application, and that β-adrenergic receptor inhibition may provide optimal survival conditions for oncolytic viruses by enhancing intracellular viral replication (Hu et al., 2021b).

3.5 Oncolytic Virus Combined With Physical Therapy

3.5.1 Liver Cancer

Radiofrequency ablation (RFA) is the most effective local treatment for early-stage hepatocellular carcinoma. However, it is prone to recurrence when treating medium-to-large tumors. G47Δ, a triple-mutated third-generation oncolytic HSV-1, can enhance RFA efficacy by inducing systemic and specific immunity. The sequential use of G47Δ, RFA, and ICI can further improve the anti-tumor effect (Yamada et al., 2020). Radiofrequency ablation also has a facilitative effect on oncolytic viral therapy. When high doses of T-VEC are injected intratumorally under the guidance of ultrasound and optical imaging techniques, radiofrequency ablation enhances the therapeutic effect of the G47Δ oncolytic virus in a preclinical

study. This dual application opens up a new path for treating larger hepatocellular carcinomas locally, while local injection of the virus reduces the viral therapy's systemic toxicity (Song et al., 2019).

3.5.2 Pancreatic Cancer

Nano blade is a novel tumor ablation technique with the benefits of protecting blood vessels and avoiding heat sink effects. Still, inhomogeneous electric field size is common due to the non-standard distribution of electrode needles or the large size of tumors, therefore, tumors are frequently not wholly resected with nano blade (Kingham et al., 2012). This disadvantage can be avoided by combining it with the use of an oncolytic virus. In a recent study, researchers discovered that combining nano blade and M1 virus inhibited tumor proliferation and significantly prolonged the survival time of *in-situ* immunologically active mouse PC models. On the other hand, the nano blade improves the efficiency of M1 tumor lysis because the extracellular matrix physically limits M1 viruses and immune cells from the vicinity of tumor cells, and the nano blade reduces this impediment by inducing electroporation and T cell immune activation. Thus, the two complement each other and improve tumor treatment (Sun et al., 2021).

3.6 Other Combination Therapy With Oncolytic Virus

In addition to the four combination therapy modalities mentioned above, numerous combined treatment strategies have shown promising efficacy in experimental and clinical studies.

In pancreatic cancer, oncolytic viruses paired with chemotherapy have shown promising results, and triple therapy combined with radiotherapy has further boosted therapeutic efficacy. Among multiple combinations of treatment strategies, animals treated with triple combination therapy had the best anti-tumor effect and survival, with one animal experiencing total tumor remission. Although there was no statistically significant difference between the triple combination therapy group and the OAd-hamIFN + radiotherapy group, the significant efficacy of OAd-hamIFN combined with radiotherapy may lead to a reduction in chemotherapy drug dosage. It could be a lifesaver for patients who are unable to tolerate existing chemotherapy treatments (Salzwedel et al., 2018). Through transgenic technology, some success has been made in combating VSV resistance. VSV was combined with ruxolitinib, polybrene, or DEAE-dextran as a new triple therapy to promote VSV attachment and replication and overcome VSV resistance (Felt et al., 2017).

4 CONCLUSIONS AND CHALLENGES

With the development of research on oncolytic virus therapy against malignant tumors of the digestive system, the application of oncolytic viruses in clinical treatment shows remarkable potential. Combined with traditional therapies, oncolytic viruses can have a better anti-tumor effect and show many advantages. First, transgenic oncolytic viruses can assist with the clinical diagnosis of cancers and the detection of disseminated tumor cells. Second, an oncolytic virus and its combination therapy can act on the tumor site more accurately and with stronger specificity. Third, the combination of oncolytic virus therapy and ablation technology improves the limitations of tumor ablation. Fourth, the combination of oncolytic viruses and existing chemotherapeutic drugs can improve the curative effect and reduce the side effects of tumor treatment. Lastly, the application of an oncolytic virus provides a new way to treat unresectable tumors, especially malignant tumors in the special anatomical position of the pancreas.

However, the best route of administration of an oncolytic virus needs to be further studied. At present, there are three main methods: intratumoral injection, intravenous injection, and intraperitoneal injection. Different methods have their own advantages and disadvantages. The intratumoral injection can avoid blood dilution and accurately reach the tumor location, but the limited activation of the systemic immune response weakens tumor cells scattered in other locations. Intravenous injection can be widely used throughout the body and is more convenient, particularly for clinical management (Bommareddy et al., 2018), but its wide range of action does not mean that it can act on target organs, and the effect is greatly reduced (Ferguson et al., 2012). Intraperitoneal injection for tumors in the digestive system seems to achieve more ideal results due to its special anatomical location (Kulu et al., 2009).

In addition, oncolytic viruses and their combination therapies present certain risks. Because of the human anti-viral response, fatigue, fever, chills, leukopenia, and hypotension may occur at the time of oncolytic virotherapy (Andtbacka et al., 2015; Ribas et al., 2016; Gao et al., 2021; Zhang B. et al., 2021), and these adverse effects, although not seriously detrimental to patient health, require the vigilance of researchers and maybe more serious in frail patients. However, oncolytic viral therapy has also caused such serious adverse reactions as grade 3 autoimmune hepatitis, grade 3 aseptic meningitis, and grade 4 pneumonia (Ribas et al., 2017). The treatment strategy should be changed promptly when adverse reactogens are identified. Moreover, the sequential order of combination therapy may affect the treatment efficacy (Wu et al., 2019), and investigators can unfold more research on this aspect. Also, due to the genetic variability of the virus and the imperfect manufacturing and preparation processes, there may be potential risks in the application, and many studies have not yet entered clinical trials. Its clinical efficacy and safety need to be further evaluated.

Therefore, to solve the above problems, we should further explore the drug delivery route of the virus, select the most effective and safe way, optimize the virus preparation process, ensure the stability of the virus, speed up the experimental

progress, conduct more extensive and in-depth research, and bring good news to tumor patients as soon as possible.

AUTHOR CONTRIBUTIONS

QL, PO, and RG: writing, editing, and visualization. RL and LL: reviewing and editing. XK and QW: conceptualization and supervision. LY: supervision. All authors contributed to the article and approved the submitted version.

FUNDING

This study was supported by the Scientific research project of Tianjin Education Commission (2021KJ134), Science and Technology Program of Tianjin (21ZYJDJC00070).

ACKNOWLEDGMENTS

The figures were drawn by Figdraw (www.figdraw.com).

REFERENCES

Abdullahi, S., Jäkel, M., Behrend, S. J., Steiger, K., Topping, G., Krabbe, T., et al. (2018). A Novel Chimeric Oncolytic Virus Vector for Improved Safety and Efficacy as a Platform for the Treatment of Hepatocellular Carcinoma. *J. Virol.* 92, e01386–18. doi: 10.1128/JVI.01386-18

Aghi, M., Rabkin, S. D., and Martuza, R. L. (2007). Angiogenic Response Caused by Oncolytic Herpes Simplex Virus-Induced Reduced Thrombospondin Expression can be Prevented by Specific Viral Mutations or by Administering a Thrombospondin-Derived Peptide. *Cancer Res.* 67, 440–444. doi: 10.1158/0008-5472.CAN-06-3145

Alberts, P., Olmane, E., Brokāne, L., Krastiņa, Z., Romanovska, M., Kupčs, K., et al. (2016). Long-Term Treatment With the Oncolytic ECHO-7 Virus Rigvir of a Melanoma Stage IV M1c Patient, a Small Cell Lung Cancer Stage IIIA Patient, and a Histiocytic Sarcoma Stage IV Patient-Three Case Reports. *Apmis* 124, 896–904. doi: 10.1111/apm.12576

Al-Ostoot, F. H., Salah, S., Khamees, H. A., and Khanum, S. A. (2021). Tumor Angiogenesis: Current Challenges and Therapeutic Opportunities. *Cancer Treat Res. Commun.* 28, 100422. doi: 10.1016/j.ctarc.2021.100422

Andtbacka, R. H., Kaufman, H. L., Collichio, F., Amatruda, T., Senzer, N., Chesney, J., et al. (2015). Talimogene Laherparepvec Improves Durable Response Rate in Patients With Advanced Melanoma. *J. Clin. Oncol.* 33, 2780–2788. doi: 10.1200/JCO.2014.58.3377

Angarita, F. A., Acuna, S. A., Ottolino-Perry, K., Zerhouni, S., and Mccart, J. A. (2013). Mounting a Strategic Offense: Fighting Tumor Vasculature With Oncolytic Viruses. *Trends Mol. Med.* 19, 378–392. doi: 10.1016/j.molmed.2013.02.008

Assayaghi, R. M., Alabsi, A. M., Swethadri, G., and Ali, A. M. (2019). Liver Pathology in Rats Treated With Newcastle Disease Virus Strains AF2240 and V4-UPM. *Asian Pac. J. Cancer Prev.* 20, 3071–3075. doi: 10.31557/APJCP.2019.20.10.3071

Axelrod, M. L., Cook, R. S., Johnson, D. B., and Balko, J. M. (2019). Biological Consequences of MHC-II Expression by Tumor Cells in Cancer. *Clin. Cancer Res.* 25, 2392–2402. doi: 10.1158/1078-0432.CCR-18-3200

Bernstock, J. D., Hoffman, S. E., Chen, J. A., Gupta, S., Kappel, A. D., Smith, T. R., et al. (2021). The Current Landscape of Oncolytic Herpes Simplex Viruses as Novel Therapies for Brain Malignancies. *Viruses* 13, 1158. doi: 10.3390/v13061158

Bommareddy, P. K., Shettigar, M., and Kaufman, H. L. (2018). Integrating Oncolytic Viruses in Combination Cancer Immunotherapy. *Nat. Rev. Immunol.* 18, 498–513. doi: 10.1038/s41577-018-0014-6

Borsig, L. (2018). Selectins in Cancer Immunity. *Glycobiology* 28, 648–655. doi: 10.1093/glycob/cwx105

Breitbach, C. J., Paterson, J. M., Lemay, C. G., Falls, T. J., Mcguire, A., Parato, K. A., et al. (2007). Targeted Inflammation During Oncolytic Virus Therapy Severely Compromises Tumor Blood Flow. *Mol. Ther.* 15, 1686–1693. doi: 10.1038/sj.mt.6300215

Cai, J., Zhu, W., Lin, Y., Hu, J., Liu, X., Xu, W., et al. (2020). Lonidamine Potentiates the Oncolytic Efficiency of M1 Virus Independent of Hexokinase 2 But *via* Inhibition of Antiviral Immunity. *Cancer Cell Int.* 20, 532. doi: 10.1186/s12935-020-01598-w

Chalasani, P., Marron, M., Roe, D., Clarke, K., Iannone, M., Livingston, R. B., et al. (2015). A Phase I Clinical Trial of Bavituximab and Paclitaxel in Patients With HER2 Negative Metastatic Breast Cancer. *Cancer Med.* 4, 1051–1059. doi: 10.1002/cam4.447

Chen, D., Wang, R., Long, M., Li, W., Xiao, B., Deng, H., et al. (2021). Identification of *In Vitro* and *In Vivo* Oncolytic Effect in Colorectal Cancer Cells by Orf Virus Strain NA1/11. *Oncol. Rep.* 45, 535–546. doi: 10.3892/or.2020.7885

Cook, M., and Chauhan, A. (2020). Clinical Application of Oncolytic Viruses: A Systematic Review. *Int. J. Mol. Sci.* 21, 7505. doi: 10.3390/ijms21207505

Dai, B., Roife, D., Kang, Y., Gumin, J., Rios Perez, M. V., Li, X., et al. (2017). Preclinical Evaluation of Sequential Combination of Oncolytic Adenovirus Delta-24-RGD and Phosphatidylserine-Targeting Antibody in Pancreatic Ductal Adenocarcinoma. *Mol. Cancer Ther.* 16, 662–670. doi: 10.1158/1535-7163.MCT-16-0526

Degirmenci, U., Wang, M., and Hu, J. (2020). Targeting Aberrant RAS/RAF/MEK/ERK Signaling for Cancer Therapy. *Cells* 9, 198. doi: 10.3390/cells9010198

Deng, H., Liu, H., De Silva, T., Xue, Y., Mohamud, Y., Ng, C. S., et al. (2019). Coxsackievirus Type B3 Is a Potent Oncolytic Virus Against KRAS-Mutant Lung Adenocarcinoma. *Mol. Ther. Oncol.* 14, 266–278. doi: 10.1016/j.omto.2019.07.003

Digumarti, R., Bapsy, P. P., Suresh, A. V., Bhattacharyya, G. S., Dasappa, L., Shan, J. S., et al. (2014). Bavituximab Plus Paclitaxel and Carboplatin for the Treatment of Advanced non-Small-Cell Lung Cancer. *Lung Cancer* 86, 231–236. doi: 10.1016/j.lungcan.2014.08.010

Douzandegan, Y., Tahamtan, A., Gray, Z., Nikoo, H. R., Tabarraei, A., and Moradi, A. (2019). Cell Death Mechanisms in Esophageal Squamous Cell Carcinoma Induced by Vesicular Stomatitis Virus Matrix Protein. *Osong Public Health Res. Perspect.* 10, 246–252. doi: 10.24171/j.phrp.2019.10.4.08

Eriksson, E., Milenova, I., Wenthe, J., Ståhle, M., Leja-Jarblad, J., Ullenhag, G., et al. (2017). Shaping the Tumor Stroma and Sparking Immune Activation by CD40 and 4-1BB Signaling Induced by an Armed Oncolytic Virus. *Clin. Cancer Res.* 23, 5846–5857. doi: 10.1158/1078-0432.CCR-17-0285

Felt, S. A., Droby, G. N., and Grdzelishvili, V. Z. (2017). Ruxolitinib and Polycation Combination Treatment Overcomes Multiple Mechanisms of Resistance of Pancreatic Cancer Cells to Oncolytic Vesicular Stomatitis Virus. *J. Virol.* 91, e00461–17. doi: 10.1128/JVI.00461-17

Felt, S. A., and Grdzelishvili, V. Z. (2017). Recent Advances in Vesicular Stomatitis Virus-Based Oncolytic Virotherapy: A 5-Year Update. *J. Gen. Virol.* 98, 2895–2911. doi: 10.1099/jgv.0.000980

Ferguson, M. S., Chard Dunmall, L. S., Gangeswaran, R., Marelli, G., Tysome, J. R., Burns, E., et al. (2020). Transient Inhibition of PI3Kδ Enhances the Therapeutic Effect of Intravenous Delivery of Oncolytic Vaccinia Virus. *Mol. Ther.* 28, 1263–1275. doi: 10.1016/j.ymthe.2020.02.017

Ferguson, M. S., Lemoine, N. R., and Wang, Y. (2012). Systemic Delivery of Oncolytic Viruses: Hopes and Hurdles. *Adv. Virol.* 2012, 805629. doi: 10.1155/2012/805629

Freimark, B. D., Gong, J., Ye, D., Gray, M. J., Nguyen, V., Yin, S., et al. (2016). Antibody-Mediated Phosphatidylserine Blockade Enhances the Antitumor Responses to CTLA-4 and PD-1 Antibodies in Melanoma. *Cancer Immunol. Res.* 4, 531–540. doi: 10.1158/2326-6066.CIR-15-0250

Galon, J., and Bruni, D. (2019). Approaches to Treat Immune Hot, Altered and Cold Tumours With Combination Immunotherapies. *Nat. Rev. Drug Discovery*

18, 197–218. doi: 10.1038/s41573-018-0007-y

Gao, P., Ding, G., and Wang, L. (2021). The Efficacy and Safety of Oncolytic Viruses in the Treatment of Intermediate to Advanced Solid Tumors: A Systematic Review and Meta-Analysis. *Transl. Cancer Res.* 10, 4290–4302. doi: 10.21037/tcr-21-905

García-Romero, N., Palacín-Aliana, I., Esteban-Rubio, S., Madurga, R., Rius-Rocabert, S., Carrión-Navarro, J., et al. (2020). Newcastle Disease Virus (NDV) Oncolytic Activity in Human Glioma Tumors Is Dependent on CDKN2A-Type I IFN Gene Cluster Codeletion. *Cells* 9, 1405. doi: 10.3390/cells9061405

Gholami, S., Marano, A., Chen, N. G., Aguilar, R. J., Frentzen, A., Chen, C. H., et al. (2016). Erratum to: A Novel Vaccinia Virus With Dual Oncolytic and Anti-Angiogenic Therapeutic Effects Against Triple-Negative Breast Cancer. *Breast Cancer Res. Treat* 156, 607–608. doi: 10.1007/s10549-016-3767-2

Ghouse, S. M., Nguyen, H. M., Bommareddy, P. K., Guz-Montgomery, K., and Saha, D. (2020). Oncolytic Herpes Simplex Virus Encoding IL12 Controls Triple-Negative Breast Cancer Growth and Metastasis. *Front. Oncol.* 10, 384. doi: 10.3389/fonc.2020.00384

Gray, Z., Tabarraei, A., Moradi, A., and Kalani, M. R. (2019). M51R and Delta-M51 Matrix Protein of the Vesicular Stomatitis Virus Induce Apoptosis in Colorectal Cancer Cells. *Mol. Biol. Rep.* 46, 3371–3379. doi: 10.1007/s11033-019-04799-3

Guo, Z. S., Lu, B., Guo, Z., Giehl, E., Feist, M., Dai, E., et al. (2019). Vaccinia Virus-Mediated Cancer Immunotherapy: Cancer Vaccines and Oncolytics. *J. Immunother. Cancer* 7, 6. doi: 10.1186/s40425-018-0495-7

Guo, Y. J., Pan, W. W., Liu, S. B., Shen, Z. F., Xu, Y., and Hu, L. L. (2020). ERK/MAPK Signalling Pathway and Tumorigenesis. *Exp. Ther. Med.* 19, 1997–2007. doi: 10.3892/etm.2020.8454

Hamada, M., and Yura, Y. (2020). Efficient Delivery and Replication of Oncolytic Virus for Successful Treatment of Head and Neck Cancer. *Int. J. Mol. Sci.* 21, 7073. doi: 10.3390/ijms21197073

Hazini, A., Dieringer, B., Klingel, K., Pryshliak, M., Geisler, A., Kobelt, D., et al. (2021a). Application Route and Immune Status of the Host Determine Safety and Oncolytic Activity of Oncolytic Coxsackievirus B3 Variant PD-H. *Viruses* 13, 1918. doi: 10.3390/v13101918

Hazini, A., Dieringer, B., Pryshliak, M., Knoch, K. P., Heimann, L., Tolksdorf, B., et al. (2021b). miR-375- and miR-1-Regulated Coxsackievirus B3 Has No Pancreas and Heart Toxicity But Strong Antitumor Efficiency in Colorectal Carcinomas. *Hum. Gene Ther.* 32, 216–230. doi: 10.1089/hum.2020.228

Hazini, A., Pryshliak, M., Brückner, V., Klingel, K., Sauter, M., Pinkert, S., et al. (2018). Heparan Sulfate Binding Coxsackievirus B3 Strain PD: A Novel Avirulent Oncolytic Agent Against Human Colorectal Carcinoma. *Hum. Gene Ther.* 29, 1301–1314. doi: 10.1089/hum.2018.036

Hirooka, Y., Kasuya, H., Ishikawa, T., Kawashima, H., Ohno, E., Villalobos, I. B., et al. (2018). A Phase I Clinical Trial of EUS-Guided Intratumoral Injection of the Oncolytic Virus, HF10 for Unresectable Locally Advanced Pancreatic Cancer. *BMC Cancer* 18, 596. doi: 10.1186/s12885-018-4453-z

Hu, J., Chen, C., Lu, R., Zhang, Y., Wang, Y., Hu, Q., et al. (2021a). β-Adrenergic Receptor Inhibitor and Oncolytic Herpesvirus Combination Therapy Shows Enhanced Antitumoral and Antiangiogenic Effects on Colorectal Cancer. *Front. Pharmacol.* 12, 735278. doi: 10.3389/fphar.2021.735278

Hu, J., Lu, R., Zhang, Y., Li, W., Hu, Q., Chen, C., et al. (2021b). β-Adrenergic Receptor Inhibition Enhances Oncolytic Herpes Virus Propagation Through STAT3 Activation in Gastric Cancer. *Cell Biosci.* 11, 174. doi: 10.1186/s13578-021-00687-1

Ishikawa, W., Kikuchi, S., Ogawa, T., Tabuchi, M., Tazawa, H., Kuroda, S., et al. (2020). Boosting Replication and Penetration of Oncolytic Adenovirus by Paclitaxel Eradicate Peritoneal Metastasis of Gastric Cancer. *Mol. Ther. Oncol.* 18, 262–271. doi: 10.1016/j.omto.2020.06.021

Jeong, S. N., and Yoo, S. Y. (2020). Novel Oncolytic Virus Armed With Cancer Suicide Gene and Normal Vasculogenic Gene for Improved Anti-Tumor Activity. *Cancers (Basel)* 12, 1070. doi: 10.3390/cancers12051070

Jia, Y., Miyamoto, S., Soda, Y., Takishima, Y., Sagara, M., Liao, J., et al. (2019). Extremely Low Organ Toxicity and Strong Antitumor Activity of miR-34-Regulated Oncolytic Coxsackievirus B3. *Mol. Ther. Oncol.* 12, 246–258. doi: 10.1016/j.omto.2019.01.003

Jośko, J., Gwóźdź, B., Jedrzejowska-Szypułka, H., and Hendryk, S. (2000). Vascular Endothelial Growth Factor (VEGF) and its Effect on Angiogenesis. *Med. Sci. Monit.* 6, 1047–1052. doi: 10.1007/978-3-319-28140-7_58

Johnstone, R. W., Frew, A. J., and Smyth, M. J. (2008). The TRAIL Apoptotic Pathway in Cancer Onset, Progression and Therapy. *Nat. Rev. Cancer* 8, 782–798. doi: 10.1038/nrc2465

Jonker, D. J., Tang, P. A., Kennecke, H., Welch, S. A., Cripps, M. C., Asmis, T., et al. (2018). A Randomized Phase II Study of FOLFOX6/Bevacizumab With or Without Pelareorep in Patients With Metastatic Colorectal Cancer: IND.210, a Canadian Cancer Trials Group Trial. *Clin. Colorectal Cancer* 17, 231–239.e237. doi: 10.1016/j.clcc.2018.03.001

Jung, K. H., Choi, I. K., Lee, H. S., Yan, H. H., Son, M. K., Ahn, H. M., et al. (2017). Oncolytic Adenovirus Expressing Relaxin (YDC002) Enhances Therapeutic Efficacy of Gemcitabine Against Pancreatic Cancer. *Cancer Lett.* 396, 155–166. doi: 10.1016/j.canlet.2017.03.009

Katayama, Y., Tachibana, M., Kurisu, N., Oya, Y., Terasawa, Y., Goda, H., et al. (2018). Oncolytic Reovirus Inhibits Immunosuppressive Activity of Myeloid-Derived Suppressor Cells in a TLR3-Dependent Manner. *J. Immunol.* 200, 2987–2999. doi: 10.4049/jimmunol.1700435

Kato, T., Nakamori, M., Matsumura, S., Nakamura, M., Ojima, T., Fukuhara, H., et al. (2021). Oncolytic Virotherapy With Human Telomerase Reverse Transcriptase Promoter Regulation Enhances Cytotoxic Effects Against Gastric Cancer. *Oncol. Lett.* 21, 490. doi: 10.3892/ol.2021.12751

Kingham, T. P., Karkar, A. M., D'angelica, M. I., Allen, P. J., Dematteo, R. P., Getrajdman, G. I., et al. (2012). Ablation of Perivascular Hepatic Malignant Tumors With Irreversible Electroporation. *J. Am. Coll. Surg.* 215, 379–387. doi: 10.1016/j.jamcollsurg.2012.04.029

Koujima, T., Tazawa, H., Ieda, T., Araki, H., Fushimi, T., Shoji, R., et al. (2020). Oncolytic Virus-Mediated Targeting of the ERK Signaling Pathway Inhibits Invasive Propensity in Human Pancreatic Cancer. *Mol. Ther. Oncol.* 17, 107–117. doi: 10.1016/j.omto.2020.03.016

Kozak, R. A., Hattin, L., Biondi, M. J., Corredor, J. C., Walsh, S., Xue-Zhong, M., et al. (2017). Replication and Oncolytic Activity of an Avian Orthoreovirus in Human Hepatocellular Carcinoma Cells. *Viruses* 9, 90. doi: 10.3390/v9040090

Kulu, Y., Dorfman, J. D., Kuruppu, D., Fuchs, B. C., Goodwin, J. M., Fujii, T., et al. (2009). Comparison of Intravenous Versus Intraperitoneal Administration of Oncolytic Herpes Simplex Virus 1 for Peritoneal Carcinomatosis in Mice. *Cancer Gene Ther.* 16, 291–297. doi: 10.1038/cgt.2008.83

Kurozumi, K., Hardcastle, J., Thakur, R., Shroll, J., Nowicki, M., Otsuki, A., et al. (2008). Oncolytic HSV-1 Infection of Tumors Induces Angiogenesis and Upregulates CYR61. *Mol. Ther.* 16, 1382–1391. doi: 10.1038/mt.2008.112

Lawler, S. E., Speranza, M. C., Cho, C. F., and Chiocca, E. A. (2017). Oncolytic Viruses in Cancer Treatment: A Review. *JAMA Oncol.* 3, 841–849. doi: 10.1001/jamaoncol.2016.2064

Lin, Y., Zhang, H., Liang, J., Li, K., Zhu, W., Fu, L., et al. (2014). Identification and Characterization of Alphavirus M1 as a Selective Oncolytic Virus Targeting ZAP-Defective Human Cancers. *Proc. Natl. Acad. Sci. U.S.A.* 111, E4504–E4512. doi: 10.1073/pnas.1408759111

Liu, Y., Cai, J., Liu, W., Lin, Y., Guo, L., Liu, X., et al. (2020). Intravenous Injection of the Oncolytic Virus M1 Awakens Antitumor T Cells and Overcomes Resistance to Checkpoint Blockade. *Cell Death Dis.* 11, 1062. doi: 10.1038/s41419-020-03285-0

Liu, S. S., Hu, J. Q., Gu, J. F., Ni, A. M., Tang, W. H., and Liu, X. Y. (2022). Combined Oncolytic Adenovirus Carrying MnSOD and Mk5 Genes Both Regulated by Survivin Promoter has a Synergistic Inhibitory Effect on Gastric Cancer. *Neoplasma* 69, 36–48. doi: 10.4149/neo_2021_210508N624

Lugano, R., Ramachandran, M., and Dimberg, A. (2020). Tumor Angiogenesis: Causes, Consequences, Challenges and Opportunities. *Cell Mol. Life Sci.* 77, 1745–1770. doi: 10.1007/s00018-019-03351-7

Mahalingam, D., Goel, S., Aparo, S., Patel Arora, S., Noronha, N., Tran, H., et al. (2018). A Phase II Study of Pelareorep (REOLYSIN(®)) in Combination With Gemcitabine for Patients With Advanced Pancreatic Adenocarcinoma. *Cancers (Basel)* 10, 160. doi: 10.3390/cancers10060160

Mahalingam, D., Wilkinson, G. A., Eng, K. H., Fields, P., Raber, P., Moseley, J. L., et al. (2020). Pembrolizumab in Combination With the Oncolytic Virus Pelareorep and Chemotherapy in Patients With Advanced Pancreatic Adenocarcinoma: A Phase Ib Study. *Clin. Cancer Res.* 26, 71–81. doi: 10.1158/1078-0432.CCR-19-2078

Ma, J., Ramachandran, M., Jin, C., Quijano-Rubio, C., Martikainen, M., Yu, D., et al. (2020). Characterization of Virus-Mediated Immunogenic Cancer Cell Death and the Consequences for Oncolytic Virus-Based Immunotherapy of Cancer. *Cell Death Dis.* 11, 48. doi: 10.1038/s41419-020-2236-3

Matsumura, S., Nakamori, M., Tsuji, T., Kato, T., Nakamura, M., Ojima, T., et al. (2021). Oncolytic Virotherapy With SOCS3 Enhances Viral Replicative Potency and Oncolysis for Gastric Cancer. *Oncotarget* 12, 344–354. doi: 10.18632/oncotarget.27873

Mcguigan, A., Kelly, P., Turkington, R. C., Jones, C., Coleman, H. G., and Mccain, R. S. (2018). Pancreatic Cancer: A Review of Clinical Diagnosis, Epidemiology, Treatment and Outcomes. *World J. Gastroenterol.* 24, 4846–4861. doi: 10.3748/wjg.v24.i43.4846

Meng, G., Fei, Z., Fang, M., Li, B., Chen, A., Xu, C., et al. (2019). Fludarabine as an Adjuvant Improves Newcastle Disease Virus-Mediated Antitumor Immunity in Hepatocellular Carcinoma. *Mol. Ther. Oncol.* 13, 22–34. doi: 10.1016/j.omto.2019.03.004

Meng, G., Li, B., Chen, A., Zheng, M., Xu, T., Zhang, H., et al. (2020). Targeting Aerobic Glycolysis by Dichloroacetate Improves Newcastle Disease Virus-Mediated Viro-Immunotherapy in Hepatocellular Carcinoma. *Br. J. Cancer* 122, 111–120. doi: 10.1038/s41416-019-0639-7

Mondal, M., Guo, J., He, P., and Zhou, D. (2020). Recent Advances of Oncolytic Virus in Cancer Therapy. *Hum. Vaccin Immunother.* 16, 2389–2402. doi: 10.1080/21645515.2020.1723363

Nair, M., Bolyard, C., Lee, T. J., Kaur, B., and Yoo, J. Y. (2021). Therapeutic Application of Brain-Specific Angiogenesis Inhibitor 1 for Cancer Therapy. *Cancers (Basel)* 13, 3562. doi: 10.3390/cancers13143562

Nakao, S., Arai, Y., Tasaki, M., Yamashita, M., Murakami, R., Kawase, T., et al. (2020). Intratumoral Expression of IL-7 and IL-12 Using an Oncolytic Virus Increases Systemic Sensitivity to Immune Checkpoint Blockade. *Sci. Transl. Med.* 12, eaax7992. doi: 10.1126/scitranslmed.aax7992

Ohashi, T., Akazawa, T., Aoki, M., Kuze, B., Mizuta, K., Ito, Y., et al. (2013). Dichloroacetate Improves Immune Dysfunction Caused by Tumor-Secreted Lactic Acid and Increases Antitumor Immunoreactivity. *Int. J. Cancer* 133, 1107–1118. doi: 10.1002/ijc.28114

Parker, B. S., Rautela, J., and Hertzog, P. J. (2016). Antitumour Actions of Interferons: Implications for Cancer Therapy. *Nat. Rev. Cancer* 16, 131–144. doi: 10.1038/nrc.2016.14

Passaro, C., Borriello, F., Vastolo, V., Di Somma, S., Scamardella, E., Gigantino, V., et al. (2016). The Oncolytic Virus Dl922-947 Reduces IL-8/CXCL8 and MCP-1/CCL2 Expression and Impairs Angiogenesis and Macrophage Infiltration in Anaplastic Thyroid Carcinoma. *Oncotarget* 7, 1500–1515. doi: 10.18632/oncotarget.6430

Phillips, M. C., and Mousa, S. A. (2022) Clinical Application of Nano-Targeting for Enhancing Chemotherapeutic Efficacy and Safety in Cancer Management *Nanomed. (Lond).* 17, 405–21 doi: 10.2217/nnm-2021-0361

Pryshliak, M., Hazini, A., Knoch, K., Dieringer, B., Tolksdorf, B., Solimena, M., et al. (2020). MiR-375-Mediated Suppression of Engineered Coxsackievirus B3 in Pancreatic Cells. *FEBS Lett.* 594, 763–775. doi: 10.1002/1873-3468.13647

Qian, C. N., and Pezzella, F. (2018). Tumor Vasculature: A Sally Port for Inhibiting Cancer Cell Spreading. *Cancer Commun. (Lond).* 38, 52. doi: 10.1186/s40880-018-0322-z

Quixabeira, D. C. A., Zafar, S., Santos, J. M., Cervera-Carrascon, V., Havunen, R., Kudling, T. V., et al. (2021). Oncolytic Adenovirus Coding for a Variant Interleukin 2 (vIL-2) Cytokine Re-Programs the Tumor Microenvironment and Confers Enhanced Tumor Control. *Front. Immunol.* 12, 674400. doi: 10.3389/fimmu.2021.674400

Raja, J., Ludwig, J. M., Gettinger, S. N., Schalper, K. A., and Kim, H. S. (2018). Oncolytic Virus Immunotherapy: Future Prospects for Oncology. *J. Immunother. Cancer* 6, 140. doi: 10.1186/s40425-018-0458-z

Ramamurthy, N., Pathak, D. C., D'silva, A. L., Batheja, R., Mariappan, A. K., Vakharia, V. N., et al. (2021). Evaluation of the Oncolytic Property of Recombinant Newcastle Disease Virus Strain R2B in 4T1 and B16-F10 Cells *in-Vitro*. *Res. Vet. Sci.* 139, 159–165. doi: 10.1016/j.rvsc.2021.07.028

Ramelyte, E., Tastanova, A., Balázs, Z., Ignatova, D., Turko, P., Menzel, U., et al. (2021). Oncolytic Virotherapy-Mediated Anti-Tumor Response: A Single-Cell Perspective. *Cancer Cell* 39, 394–406.e394. doi: 10.1016/j.ccell.2020.12.022

Ribas, A., Dummer, R., Puzanov, I., Vanderwalde, A., Andtbacka, R. H. I., Michielin, O., et al. (2017). Oncolytic Virotherapy Promotes Intratumoral T Cell Infiltration and Improves Anti-PD-1 Immunotherapy. *Cell* 170, 1109–1119.e1110. doi: 10.1016/j.cell.2017.08.027

Ribas, A., Hamid, O., Daud, A., Hodi, F. S., Wolchok, J. D., Kefford, R., et al. (2016). Association of Pembrolizumab With Tumor Response and Survival Among Patients With Advanced Melanoma. *Jama* 315, 1600–1609. doi: 10.1001/jama.2016.4059

Ricca, J. M., Oseledchyk, A., Walther, T., Liu, C., Mangarin, L., Merghoub, T., et al. (2018). Pre-Existing Immunity to Oncolytic Virus Potentiates Its Immunotherapeutic Efficacy. *Mol. Ther.* 26, 1008–1019. doi: 10.1016/j.ymthe.2018.01.019

Sahin, T. T., Kasuya, H., Nomura, N., Shikano, T., Yamamura, K., Gewen, T., et al. (2012). Impact of Novel Oncolytic Virus HF10 on Cellular Components of the Tumor Microenviroment in Patients With Recurrent Breast Cancer. *Cancer Gene Ther.* 19, 229–237. doi: 10.1038/cgt.2011.80

Salzwedel, A. O., Han, J., Larocca, C. J., Shanley, R., Yamamoto, M., and Davydova, J. (2018). Combination of Interferon-Expressing Oncolytic Adenovirus With Chemotherapy and Radiation is Highly Synergistic in Hamster Model of Pancreatic Cancer. *Oncotarget* 9, 18041–18052. doi: 10.18632/oncotarget.24710

Schwaiger, T., Knittler, M. R., Grund, C., Roemer-Oberdoerfer, A., Kapp, J. F., Lerch, M. M., et al. (2017). Newcastle Disease Virus Mediates Pancreatic Tumor Rejection *via* NK Cell Activation and Prevents Cancer Relapse by Prompting Adaptive Immunity. *Int. J. Cancer* 141, 2505–2516. doi: 10.1002/ijc.31026

Seegers, S. L., Frasier, C., Greene, S., Nesmelova, I. V., and Grdzelishvili, V. Z. (2020). Experimental Evolution Generates Novel Oncolytic Vesicular Stomatitis Viruses With Improved Replication in Virus-Resistant Pancreatic Cancer Cells. *J. Virol.* 94, e01643–19. doi: 10.1128/JVI.01643-19

Seidlitz, T., Koo, B. K., and Stange, D. E. (2021). Gastric Organoids-an *In Vitro* Model System for the Study of Gastric Development and Road to Personalized Medicine. *Cell Death Differ.* 28, 68–83. doi: 10.1038/s41418-020-00662-2

Simmonds, P., Gorbalenya, A. E., Harvala, H., Hovi, T., Knowles, N. J., Lindberg, A. M., et al. (2020). Recommendations for the Nomenclature of Enteroviruses and Rhinoviruses. *Arch. Virol.* 165, 793–797. doi: 10.1007/s00705-019-04520-6

Smyth, E. C., Nilsson, M., Grabsch, H. I., Van Grieken, N. C., and Lordick, F. (2020). Gastric Cancer. *Lancet* 396, 635–648. doi: 10.1016/S0140-6736(20)31288-5

Song, J., Zhang, F., Ji, J., Chen, M., Li, Q., Weng, Q., et al. (2019). Orthotopic Hepatocellular Carcinoma: Molecular Imaging-Monitored Intratumoral Hyperthermia-Enhanced Direct Oncolytic Virotherapy. *Int. J. Hyperthermia* 36, 344–350. doi: 10.1080/02656736.2019.1569731

Steinhauer, D. A., Domingo, E., and Holland, J. J. (1992). Lack of evidence for proofreading mechanisms associated with an RNA virus polymerase. *Gene* 122, 281–288.

Strobel, O., Neoptolemos, J., Jäger, D., and Büchler, M. W. (2019). Optimizing the Outcomes of Pancreatic Cancer Surgery. *Nat. Rev. Clin. Oncol.* 16, 11–26. doi: 10.1038/s41571-018-0112-1

Sugawara, K., Iwai, M., Yajima, S., Tanaka, M., Yanagihara, K., Seto, Y., et al. (2020). Efficacy of a Third-Generation Oncolytic Herpes Virus G47Δ in Advanced Stage Models of Human Gastric Cancer. *Mol. Ther. Oncol.* 17, 205–215. doi: 10.1016/j.omto.2020.03.022

Sung, H., Ferlay, J., Siegel, R. L., Laversanne, M., Soerjomataram, I., Jemal, A., et al. (2021). Global Cancer Statistics 2020: GLOBOCAN Estimates of Incidence and Mortality Worldwide for 36 Cancers in 185 Countries. *CA Cancer J. Clin.* 71, 209–249. doi: 10.3322/caac.21660

Sun, S., Liu, Y., He, C., Hu, W., Liu, W., Huang, X., et al. (2021). Combining NanoKnife With M1 Oncolytic Virus Enhances Anticancer Activity in Pancreatic Cancer. *Cancer Lett.* 502, 9–24. doi: 10.1016/j.canlet.2020.12.018

Tang, S., Shi, L., Luker, B. T., Mickler, C., Suresh, B., Lesinski, G. B., et al. (2022). Modulation of the Tumor Microenvironment by Armed Vesicular Stomatitis Virus in a Syngeneic Pancreatic Cancer Model. *Virol. J.* 19, 32. doi: 10.1186/s12985-022-01757-7

Tian, Y., Yao, W., He, D., Xu, Y., Li, Y., Zhu, Y., et al. (2020). A Dual Cancer-Specific Recombinant Adenovirus Suppresses the Growth of Liver Cancer Cells *In Vivo* and *In Vitro*. *Anticancer Drugs* 31, 110–122. doi: 10.1097/CAD.0000000000000854

Tilgase, A., Patetko, L., Blāķe, I., Ramata-Stunda, A., Borodušķis, M., and Alberts, P. (2018). Effect of the Oncolytic ECHO-7 Virus Rigvir® on the Viability of Cell

Lines of Human Origin *In Vitro*. *J. Cancer* 9, 1033–1049. doi: 10.7150/jca.23242

Tirino, G., Pompella, L., Petrillo, A., Laterza, M. M., Pappalardo, A., Caterino, M., et al. (2018). What's New in Gastric Cancer: The Therapeutic Implications of Molecular Classifications and Future Perspectives. *Int. J. Mol. Sci.* 19, 2659. doi: 10.3390/ijms19092659

Tsuji, T., Nakamori, M., Iwahashi, M., Nakamura, M., Ojima, T., Iida, T., et al. (2013). An Armed Oncolytic Herpes Simplex Virus Expressing Thrombospondin-1 has an Enhanced *In Vivo* Antitumor Effect Against Human Gastric Cancer. *Int. J. Cancer* 132, 485–494. doi: 10.1002/ijc.27681

Tsuruta, A., Shiiba, Y., Matsunaga, N., Fujimoto, M., Yoshida, Y., Koyanagi, S., et al. (2022). Diurnal Expression of PD-1 on Tumor-Associated Macrophages Underlies the Dosing Time-Dependent Anti-Tumor Effects of the PD-1/PD-L1 Inhibitor BMS-1 in B16/BL6 Melanoma-Bearing Mice. *Mol. Cancer Res* molcanres MCR-21-0786-E.2021. doi: 10.1158/1541-7786.MCR-21-0786

Uchihashi, T., Nakahara, H., Fukuhara, H., Iwai, M., Ito, H., Sugauchi, A., et al. (2021). Oncolytic Herpes Virus G47Δ Injected Into Tongue Cancer Swiftly Traffics in Lymphatics and Suppresses Metastasis. *Mol. Ther. Oncol.* 22, 388–398. doi: 10.1016/j.omto.2021.06.008

Wang, J. Y., Chen, H., Dai, S. Z., Huang, F. Y., Lin, Y. Y., Wang, C. C., et al. (2022). Immunotherapy Combining Tumor and Endothelium Cell Lysis With Immune Enforcement by Recombinant MIP-3α Newcastle Disease Virus in a Vessel-Targeting Liposome Enhances Antitumor Immunity. *J. Immunother. Cancer* 10, e003950. doi: 10.1136/jitc-2021-003950

Wang, G., Kang, X., Chen, K. S., Jehng, T., Jones, L., Chen, J., et al. (2020). An Engineered Oncolytic Virus Expressing PD-L1 Inhibitors Activates Tumor Neoantigen-Specific T Cell Responses. *Nat. Commun.* 11, 1–14. doi: 10.1038/s41467-020-15229-5

Wang, B., Ogata, H., Takishima, Y., Miyamoto, S., Inoue, H., Kuroda, M., et al. (2018).). A Novel Combination Therapy for Human Oxaliplatin-Resistant Colorectal Cancer Using Oxaliplatin and Coxsackievirus A11. *Anticancer Res.* 38, 6121–6126. doi: 10.21873/anticanres.12963

Wang, N., Wang, J., Zhang, Z., Cao, H., Yan, W., Chu, Y., et al. (2021). A Novel Vaccinia Virus Enhances Anti-Tumor Efficacy and Promotes a Long-Term Anti-Tumor Response in a Murine Model of Colorectal Cancer. *Mol. Ther. Oncol.* 20, 71–81. doi: 10.1016/j.omto.2020.11.002

Wang, J. N., Xu, L. H., Zeng, W. G., Hu, P., Rabkin, S. D., and Liu, R. R. (2015). Treatment of Human Thyroid Carcinoma Cells With the G47delta Oncolytic Herpes Simplex Virus. *Asian Pac. J. Cancer Prev.* 16, 1241–1245. doi: 10.7314/APJCP.2015.16.3.1241

Wang, J., Xu, L., Zeng, W., Hu, P., Zeng, M., Rabkin, S. D., et al. (2014). Treatment of Human Hepatocellular Carcinoma by the Oncolytic Herpes Simplex Virus G47delta. *Cancer Cell Int.* 14, 83. doi: 10.1186/s12935-014-0083-y

Wang, Z., Yu, B., Wang, B., Yan, J., Feng, X., Wang, Z., et al. (2016). A Novel Capsid-Modified Oncolytic Recombinant Adenovirus Type 5 for Tumor-Targeting Gene Therapy by Intravenous Route. *Oncotarget* 7, 47287–47301. doi: 10.18632/oncotarget.10075

Warner, S. G., Kim, S. I., Chaurasiya, S., O'leary, M. P., Lu, J., Sivanandam, V., et al. (2019). A Novel Chimeric Poxvirus Encoding hNIS Is Tumor-Tropic, Imageable, and Synergistic With Radioiodine to Sustain Colon Cancer Regression. *Mol. Ther. Oncol.* 13, 82–92. doi: 10.1016/j.omto.2019.04.001

Woo, Y., Zhang, Z., Yang, A., Chaurasiya, S., Park, A. K., Lu, J., et al. (2020). Novel Chimeric Immuno-Oncolytic Virus CF33-hNIS-Antipdl1 for the Treatment of Pancreatic Cancer. *J. Am. Coll. Surg.* 230, 709–717. doi: 10.1016/j.jamcollsurg.2019.12.027

Wu, Z., Ichinose, T., Naoe, Y., Matsumura, S., Villalobos, I. B., Eissa, I. R., et al. (2019). Combination of Cetuximab and Oncolytic Virus Canerpaturev Synergistically Inhibits Human Colorectal Cancer Growth. *Mol. Ther. Oncol.* 13, 107–115. doi: 10.1016/j.omto.2019.04.004

Wu, Y., Mou, X., Wang, S., Liu, X. E., and Sun, X. (2017). ING4 Expressing Oncolytic Vaccinia Virus Promotes Anti-Tumor Efficiency and Synergizes With Gemcitabine in Pancreatic Cancer. *Oncotarget* 8, 82728–82739. doi: 10.18632/oncotarget.21095

Yajima, S., Sugawara, K., Iwai, M., Tanaka, M., Seto, Y., and Todo, T. (2021). Efficacy and Safety of a Third-Generation Oncolytic Herpes Virus G47Δ in Models of Human Esophageal Carcinoma. *Mol. Ther. Oncol.* 23, 402–411. doi: 10.1016/j.omto.2021.10.012

Yamada, T., Tateishi, R., Iwai, M., Koike, K., and Todo, T. (2020). Neoadjuvant Use of Oncolytic Herpes Virus G47Δ Enhances the Antitumor Efficacy of Radiofrequency Ablation. *Mol. Ther. Oncol.* 18, 535–545. doi: 10.1016/j.omto.2020.08.010

Yang, L., Gu, X., Yu, J., Ge, S., and Fan, X. (2021). Oncolytic Virotherapy: From Bench to Bedside. *Front. Cell Dev. Biol.* 9, 790150. doi: 10.3389/fcell.2021.790150

Ye, T., Jiang, K., Wei, L., Barr, M. P., Xu, Q., Zhang, G., et al. (2018). Oncolytic Newcastle Disease Virus Induces Autophagy-Dependent Immunogenic Cell Death in Lung Cancer Cells. *Am. J. Cancer Res.* 8, 1514–1527.

Ye, Z., Wang, X., Hao, S., Zhong, J., Xiang, J., and Yang, J. (2006). Oncolytic Adenovirus-Mediated E1A Gene Therapy Induces Tumor-Cell Apoptosis and Reduces Tumor Angiogenesis Leading to Inhibition of Hepatocellular Carcinoma Growth in Animal Model. *Cancer Biother. Radiopharm.* 21, 225–234. doi: 10.1089/cbr.2006.21.225

Ying, L., Cheng, H., Xiong, X. W., Yuan, L., Peng, Z. H., Wen, Z. W., et al. (2017). Interferon Alpha Antagonizes the Anti-Hepatoma Activity of the Oncolytic Virus M1 by Stimulating Anti-Viral Immunity. *Oncotarget* 8, 24694–24705. doi: 10.18632/oncotarget.15788

Yoo, S. Y., Jeong, S. N., Kang, D. H., and Heo, J. (2017). Evolutionary Cancer-Favoring Engineered Vaccinia Virus for Metastatic Hepatocellular Carcinoma. *Oncotarget* 8, 71489–71499. doi: 10.18632/oncotarget.17288

Zamarin, D., Holmgaard, R. B., Subudhi, S. K., Park, J. S., Mansour, M., Palese, P., et al. (2014). Localized Oncolytic Virotherapy Overcomes Systemic Tumor Resistance to Immune Checkpoint Blockade Immunotherapy. *Sci. Transl. Med.* 6, 226ra232. doi: 10.1126/scitranslmed.3008095

Zautner, A. E., Körner, U., Henke, A., Badorff, C., and Schmidtke, M. (2003). Heparan Sulfates and Coxsackievirus-Adenovirus Receptor: Each One Mediates Coxsackievirus B3 PD Infection. *J. Virol.* 77, 10071–10077. doi: 10.1128/JVI.77.18.10071-10077.2003

Zhang, B., Huang, J., Tang, J., Hu, S., Luo, S., Luo, Z., et al. (2021). Intratumoral OH2, an Oncolytic Herpes Simplex Virus 2, in Patients With Advanced Solid Tumors: A Multicenter, Phase I/II Clinical Trial. *J. Immunother. Cancer* 9, e002224 doi: 10.1136/jitc-2020-002224

Zhang, W., Hu, X., Liang, J., Zhu, Y., Zeng, B., Feng, L., et al. (2020). Ohsv2 Can Target Murine Colon Carcinoma by Altering the Immune Status of the Tumor Microenvironment and Inducing Antitumor Immunity. *Mol. Ther. Oncol.* 16, 158–171. doi: 10.1016/j.omto.2019.12.012

Zhang, W., Zeng, B., Hu, X., Zou, L., Liang, J., Song, Y., et al. (2021). Oncolytic Herpes Simplex Virus Type 2 Can Effectively Inhibit Colorectal Cancer Liver Metastasis by Modulating the Immune Status in the Tumor Microenvironment and Inducing Specific Antitumor Immunity. *Hum. Gene Ther.* 32, 203–215. doi: 10.1089/hum.2020.239

Zhou, X., Zhao, J., Zhang, J. V., Wu, Y., Wang, L., Chen, X., et al. (2021). Enhancing Therapeutic Efficacy of Oncolytic Herpes Simplex Virus With MEK Inhibitor Trametinib in Some BRAF or KRAS-Mutated Colorectal or Lung Carcinoma Models. *Viruses* 13, 1758. doi: 10.3390/v13091758

Zitvogel, L., Galluzzi, L., Kepp, O., Smyth, M. J., and Kroemer, G. (2015). Type I Interferons in Anticancer Immunity. *Nat. Rev. Immunol.* 15, 405–414. doi: 10.1038/nri3845

Conflict of Interest: The authors declare that the research was conducted in the absence of any commercial or financial relationships that could be construed as a potential conflict of interest.

frontiers | Frontiers in Cellular and Infection Microbiology

REVIEW
published: 06 June 2022
doi: 10.3389/fcimb.2022.928050

Antiviral Effects and Underlying Mechanisms of Probiotics as Promising Antivirals

Yanjin Wang, Assad Moon, Jingshan Huang, Yuan Sun and Hua-Ji Qiu**

State Key Laboratory of Veterinary Biotechnology, Harbin Veterinary Research Institute, Chinese Academy of Agricultural Sciences, Harbin, China

Probiotics exert a variety of beneficial effects, including maintaining homeostasis and the balance of intestinal microorganisms, activating the immune system, and regulating immune responses. Due to the beneficial effects of probiotics, a wide range of probiotics have been developed as probiotic agents for animal and human health. Viral diseases cause serious economic losses to the livestock every year and remain a great challenge for animals. Moreover, strategies for the prevention and control of viral diseases are limited. Viruses enter the host through the skin and mucosal surface, in which are colonized by hundreds of millions of microorganisms. The antiviral effects of probiotics have been proved, including modulation of chemical, microbial, physical, and immune barriers through various probiotics, probiotic metabolites, and host signaling pathways. It is of great significance yet far from enough to elucidate the antiviral mechanisms of probiotics. The major interest of this review is to discuss the antiviral effects and underlying mechanisms of probiotics and to provide targets for the development of novel antivirals.

Keywords: probiotics, viral infections, antiviral effects, antiviral mechanisms, novel antivirals

OPEN ACCESS

Edited by:
Zhanbo Zhu,
Heilongjiang Bayi Agricultural University, China

Reviewed by:
Kangcheng Pan,
Sichuan Agricultural University, China
Yonggang Qu,
Shihezi University, China

****Correspondence:***
Hua-Ji Qiu
qiuhuaji@caas.cn
Yuan Sun
sunyuan@caas.cn

Specialty section:
This article was submitted to Clinical Microbiology, a section of the journal Frontiers in Cellular and Infection Microbiology

Received: *25 April 2022*
Accepted: *10 May 2022*
Published: *06 June 2022*

Citation:
Wang Y, Moon A, Huang J, Sun Y and Qiu H-J (2022) Antiviral Effects and Underlying Mechanisms of Probiotics as Promising Antivirals. Front. Cell. Infect. Microbiol. 12:928050. doi: 10.3389/fcimb.2022.928050

INTRODUCTION

Humans and animals are colonized by hundreds of millions of microorganisms, which are far more than the number of host cells, and some argue that the number of microorganisms is comparable to host cells (Egert and Simmering, 2016). A vast majority of these microorganisms coinhabit within the gastrointestinal tract (Sender et al., 2016; Heintz-Buschart and Wilmes, 2018; Mishra et al., 2021). Probiotics are essential to maintain the balance of intestinal microorganisms. The Food and Agriculture Organization (FAO) and the World Health Organization (WHO) define probiotics as probiotics are live microorganisms, which when administered in adequate amounts confer health benefits on the host (WHO/FAO, 2002; Drago et al., 2010; Kahouli et al., 2013). Probiotics are known for their beneficial effects, mainly including maintaining the balance of intestinal microorganisms, activating the immune system, and regulating immune response (Hao et al., 2015; Gasbarrini et al., 2016; Kim et al., 2019). Due to their beneficial effects, a variety of probiotics have been widely used for promoting animal and human health in recent years (Kim et al., 2019; Teame et al., 2020; Rad et al., 2021). Several species of probiotics and their effects as probiotic agents have been evaluated. *Lactobacillus*, *Bifidobacterium*, and yeast are widely used (Al-Ghazzewi and Tester, 2016; Wieers et al., 2020; Di Pierro and Pane, 2021; Giannakou et al., 2021).

Viral diseases remain a great challenge for humans and animals (VanderWaal and Deen, 2018). Although vaccination is the most important option to prevent viral infections, differences between evolving epidemics and vaccines available make vaccination less effective. Moreover, there are no available vaccines for emerging or re-emerging viruses. Viruses enter the host through the skin and mucosal surface, where large numbers of microorganisms are colonized (Schmidt et al., 2018; Lunjani et al., 2019; Xu and Li, 2019; Peixoto et al., 2021). Probiotics are critical for the host to inhibit incoming pathogen infections (Lloyd-Price et al., 2016; Piewngam et al., 2018). A large body of literature has shown that probiotics have antiviral effects (Pradhan et al., 2021; Salaris et al., 2021). In the present review, we summarized and discussed the mechanisms of antiviral effects of probiotics, which opens up new perspectives on the use of antiviral strategies, provides new targets for the research and development of antivirals, and helps to provide a clearer background for probiotics-based antivirals.

PROBIOTICS CONTRIBUTE TO THE CHEMICAL BARRIER TO EXERT ANTIVIRAL EFFECTS

The chemical barrier is the first barrier that pathogenic microorganisms encounter after they invade the intestine. Pathogens must break through the chemical barrier before they get access to the epithelium. Probiotics utilize carbohydrates in the host to produce various metabolites, including antimicrobial peptides (AMPs), hydrogen peroxide (H_2O_2), lactic acid, short-chain fatty acids (SCFAs), and extracellular vesicles (EV) (Knezevic et al., 2005; Gosmann et al., 2017; Vieira et al., 2017; Tyssen et al., 2018; Nahui et al., 2019). It has been revealed that the metabolites released by probiotics display important protective activities to inhibit viral infections. These metabolites form a micro-environment that is not conducive to viral reproduction (**Figure 1A**).

AMPs are known as short, positively charged, and amphipathic peptides with a broad scope of antimicrobial activity against bacteria, viruses, fungi, and protozoa (Boparai and Sharma, 2020; Bosch and Zasloff, 2021). In recent years, AMPs have attracted interests due to their therapeutic potential. Bacteriocins are the AMPs derived from bacteria (Fry, 2018). While the antibacterial effects of bacteriocins are somewhat deciphered, their antiviral effects remain to be further studied. Enterocin B produced by *Enterococcus* was shown to inhibit the cytopathic effects of influenza virus (H1N1 and H3N2) in Madin-Darby canine kidney cells (Ermolenko et al., 2019). Presumably, bacteriocins could lead to the aggregation of viral particles, block viral particles through binding to the host cell receptors or inhibiting key steps in the viral replication cycle (Wachsman et al., 2003). Bacteriocins are structurally diverse with similar antiviral mechanisms.

The probiotics that play protective roles in the vaginal mucosa are dominated by the *Lactobacillus* genus. Numerous studies have demonstrated that metabolites released by *Lactobacillus* have antiviral effects on human immunodeficiency virus (HIV). H_2O_2, one of the metabolites produced by *L. acidophilus*, is toxic to many viruses, including HIV. It is reported that the prevalence of H_2O_2-producing *Lactobacilli* was lower in HIV-positive compared with HIV-negative women (Knezevic et al., 2005).

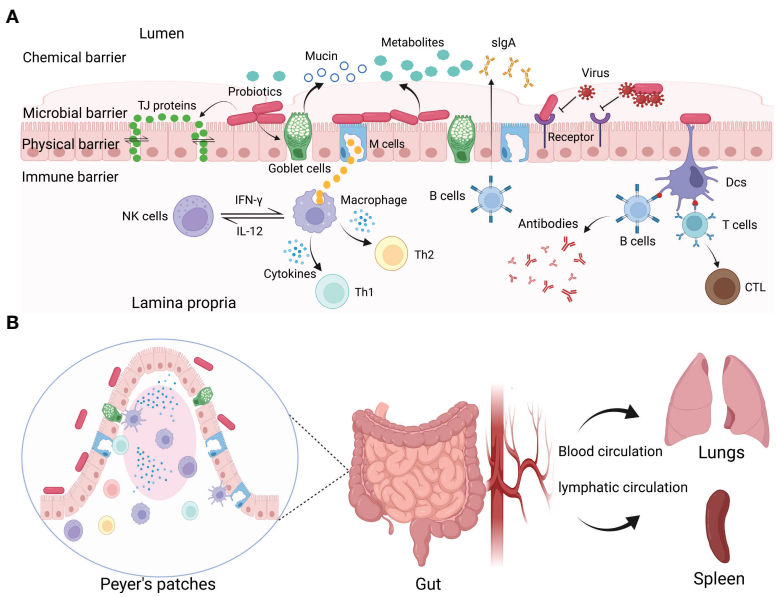

FIGURE 1 | The interactions between probiotics and viruses. **(A)** Probiotics exert protective effects on viral infections by constituting or modulating chemical, microbial, physical, and immune barriers. Probiotics can produce antiviral metabolites, block virus invasion by binding with viruses or competing for the entry receptors, regulating the tight junctions of IECs, and modulating mucosal immune responses. **(B)** Probiotics modulate systemic immune responses.

Another study showed that H_2O_2 can inhibit HIV replication in CEM (a human T-lymphoblastic cell line) cells (Klebanoff and Coombs, 1991). The H_2O_2-producing probiotics present in the vagina of healthy women have been suggested as some bacteria that maintain health. Disruption of HIV by the probiotics is caused by the toxicity of H_2O_2. Notably, there are significant differences in H_2O_2 production among different *Lactobacilli* strains, and the same strain may not even produce H_2O_2 by changing the culture conditions.

Previous studies on the antiviral effects of lactobacillus-based probiotics have focused on H_2O_2, but recent studies have shown that lactic acid is a major antiviral factor produced by *Lactobacilli* in the vaginal mucosa (O'Hanlon et al., 2011; Liu et al., 2021). Lactic acid, a final product of carbohydrates, is an important metabolite of *Lactobacillus* with anti-HIV activity (Gosmann et al., 2017; Nahui et al., 2017; Tyssen et al., 2018). The mechanism of anti-HIV effects of lactic acid-producing bacteria is likely multifactorial. First of all, lactic acid may bind to the viruses and affect the function of the virus, thereby restricting the viruses from invading host cells. Secondly, lactic acid may disrupt the viral envelope and lyse the virions of enveloped viruses (Tachedjian et al., 2017). Besides HIV, lactic acid also has a significant inhibitory effect on herpes simplex virus (HSV) (Conti et al., 2009). It has been confirmed that lactic acid successfully interferes with viral replication in cells and that both the virucidal activity and the inhibition of replication were correlated to acidic pH values.

Microorganisms in the colon produce SCFAs by using dietary carbohydrates as substrates, primarily acetate, propionate, and butyrate, as final products (Wong et al., 2006). The ability to produce SCFAs by both *Lactobacilli* and *Bifidobacteria* is highlighted (LeBlanc et al., 2017). Probiotics have been reported to regulate butyrate metabolism resulting in an enhancement of host resistance to influenza virus infection. The correlation analysis revealed that the butyrate was negatively related to viral loading (Lu et al., 2021). SCFAs produced by probiotics are also potential regulatory effectors of epithelial proliferation in the gut (Wang et al., 2018). In addition, SCFAs can not only act on the gut but also transport to distant sites through blood circulation as a chemical signal for communication. For example, the abundance of SCFAs-producing bacteria and serum SCFA levels increased in respiratory syncytial virus (RSV)-infected mice after administration of a probiotic mixture (LeBlanc et al., 2017). Likewise, similar findings have been reported on antiviral responses induced by commensal microbiota (Antunes et al., 2019).

Lactobacillus can produce extracellular vehicles (EVs), along with other bacterial and mammalian cells, which are essential for the communication between bacteria and cells. It has been proved that *L. crispatus* BC3 and *L. gasseri* BC12 protected human cervicovaginal and tonsillar tissues from HIV-1 infection *in vitro* by producing EVs (Nahui et al., 2019). EVs inhibit HIV-1 infection by reducing HIV-1 entry/attachment to target cells. In addition, probiotics can refine the barrier function by promoting goblet cells to secrete mucin to form a mucin layer above the intestinal epithelium, protecting the mucosa from virus attachment (Engevik et al., 2019; Lorella et al., 2020). For instance, probiotics mixture VSL#3 induced mucin expression in colonic epithelial cells and prompted goblet cells to secrete mucin against pathogen attachment (Caballero-Franco et al., 2007). Relevant studies have confirmed that probiotics can secrete extracellular proteins, weaken the adhesion of pathogens, and protect the intestinal cells (Liu et al., 2020). Viruses are intracellular pathogens that require the host machinery to replicate. These metabolites exert antiviral effects by preventing the viruses from attaching to host cells or directly killing the viruses, which is a broad-spectrum antiviral mechanism. In summary, probiotics enhance the chemical barrier to maintain host health by producing antiviral metabolites or stimulating goblet cells to produce mucin.

PROBIOTICS CONSTITUTE THE MICROBIAL BARRIER TO EXERT ANTIVIRAL EFFECTS

Besides producing some antiviral metabolites, probiotics can also inhibit viruses directly by interacting with viruses or competing for the cellular receptors to inhibit virus entry into host cells (**Figure 1A**) (Lievin-Le and Servin, 2014).

Several studies have revealed that probiotics can inhibit the infection of vesicular stomatitis virus (VSV) *in vitro*. It was suggested that pre-incubation of cell monolayers with probiotics, or probiotics with VSV can decrease VSV titer (Botic et al., 2007). A possible mechanism of inhibiting VSV replication is that probiotics compete with the virus for cell binding and interference with virus attachment or entry. Another possible mechanism is that probiotics can trap VSV specifically or nonspecifically. The above are two possible mechanisms by which probiotics inhibit VSV infection, and more mechanisms remain to be elucidated. *B. subtilisis* is one of the probiotics with excellent antiviral and immune regulation properties. The current study proved that *B. subtilisis* OKB105 inhibited the entry of transmissible gastroenteritis virus (TGEV) into the intestinal porcine epithelial cell line (IPEC-J2) by competing for the entry receptors (Wang et al., 2013). Another study revealed that *Enterococcus faecium* NCIMB 10415 was efficient to inhibit swine influenza virus (SIV) infection by the direct interaction between the SIV and probiotics (Wang et al., 2013). Published literature analysis indicated that the antiviral effects of probiotics are strain-dependent. Besides, the probiotics also limit pathogen access to nutrient resources. Furthermore, studies have revealed that the mucosal immune system of germ-free mice is immature due to the lack of microorganism colonization of their mucosal surfaces (Shen et al., 2014). The colonization of microorganisms also promotes the maturation of the host mucosal immune system. The microbial barrier constituted by probiotics is very important to inhibit viral infections and provides an insight into the development of novel antiviral strategies in the future.

PROBIOTICS STRENGTHEN THE PHYSICAL BARRIER TO EXERT ANTIVIRAL EFFECTS

The physical barrier is composed of epidermides and mucosae (Karst, 2016). Probiotics form a defensive barrier against the invasion of viruses by enhancing the tight junctions (TJs) between intestinal epithelial cells (IECs) (**Figure 1A**).

TJs are an important form of intercellular connection and the most important structure of the mucosal barrier (Otani and Furuse, 2020). IECs are interconnected by the TJ proteins, which are the membrane protein complex with defensive functions formed between epithelial cells and endothelial cells (Gunzel and Fromm, 2012). Different species of probiotics have been reported to protect the host from viral infections by regulating the production of the TJ proteins (Kanmani and Kim, 2019; Lorella et al., 2020). *Lactiplantibacillus* (*Lp.*) *plantarum*, *Weissella cibaria*, or *Latilactobacillus* (*Ll.*) *sakei* could protect IECs from viral infections by maintaining the activity of TJ proteins. The TJ proteins between epidermal cells are necessary to maintain the integrity of the mucosal barrier. An intact mucosal barrier can prevent pathogens or antigenic elements of pathogens from entering the lamina propria of the gut. Disruption of the epithelial barrier caused by the TJ proteins deficiency will lead to microorganism translocation to the mucosal surface, disrupting microbial homeostasis. Furthermore, it has been confirmed that *Bifidobacterium* (*Bf.*) *breve* treatment promoted the proliferation of small intestine epithelial in mice (Ishizuka et al., 2009). The proliferation of small intestinal epithelial cells promotes the production of new cells and the shedding of necrotic cells. The physical barrier created by the epithelial cells constantly renews itself and enhances the ability of the mucosa physical barrier to resist pathogens. Moreover, probiotics modulated the trans-epithelial electrical resistance and epithelial permeability (Krishnan et al., 2016). The balance of the intestinal microbial environment is necessary for humans and animals to maintain homeostasis. In summary, probiotics can inhibit viral infections by maintaining intestinal permeability and mucosal barrier integrity.

PROBIOTICS MODULATE THE IMMUNE BARRIER TO EXERT ANTIVIRAL EFFECTS

One of the most beneficial effects of probiotics is to modulate the immune response (Shida and Nanno, 2008; Azad et al., 2018). The immune barrier is the last line of the host to inhibit viral infections, consisting of mucosal and systemic immune responses (**Figures 1A, B**) (Ashraf and Shah, 2014; La Fata et al., 2018).

Mucosal Immune Responses

Generally, there are large numbers of lymphoid tissues and immune cells in the gastrointestinal tract than in the rest of the body combined. The mucosal immune system (MIS), also known as mucosa-associated lymphoid tissues (MALTs), is mainly composed of immune tissues, cells, and molecules. The mucosa is directly connected to the external environment and involved in complex immune responses (Pelaseyed et al., 2014). Various immune cells are engaged in innate immune response. Natural killer (NK) cells are pivotal members of innate immunity that play key roles in recognizing and killing target cells and regulating immune responses. Activation and proliferation of NK cells can limit viral replication effectively. It has been reported that *Lp. plantarum* 06CC2 reduces HSV-1 virus yields in the brain of mice (Matsusaki et al., 2016). *Lp. plantarum* 06CC2 enhanced immunomodulatory activity by increasing the mRNA expression of IL-12 and IFN-γ in Peyer's patches (PPs). IL-12 and IFN-γ can activate NK cells and macrophages effectively. Macrophages and NK cells cooperate with each other for virus clearance.

Pattern recognition receptors (PRRs) have extensive interactions between microorganisms and hosts. PRRs are specialized molecules that host cells recognize pathogens. At present, PRRs mainly include Toll-like receptors (TLRs), nucleotide-binding oligomerization domain (NOD)-like receptors (NLRs), retinoic acid-inducible-like receptors (RLRs), C-type lectin receptors (CLRs), absent in melanoma 2 (AIM2)-like receptors (ALRs) and cyclic GMP-AMP synthase (CGAs). Members of the TLRs can identify a wide range of pathogens, such as bacteria, viruses, and fungi. It has been demonstrated that *Lacticaseibacillus rhamnosus* GG (LGG) is therapeutically effective on diarrhea induced by rotavirus (RV) infection by the TLR3 signaling pathway (Aoki-Yoshida et al., 2016). *Ligilactobacillus (Lg.) salivarius* FFIG35 and FFIG58 also displayed antiviral effects by activating the TLR3 signaling pathway (Indo et al., 2021). TLR3 mainly recognizes nucleic acids in endosomes. Activation of TLR3 increases the expression of type I IFNs. In addition to activating TLR3, probiotics can also activate other PRRs. For example, *L. acidophilus* could enhance the antiviral effects by inducing the expression of virus immune defense genes in dendritic cells (DCs) in mice (Weiss et al., 2010). The expression of immune defense genes induced by viruses was dependent on the activation of the TLR2 pathway. In addition, *Lp. plantarum* could inhibit pneumovirus (PMV) infection in mice *via* the NLR (NOD2) and TLR (TLR2) pathways (Rice et al., 2016). Both NOD2 and TLR2 mediate the important innate immune response to inhibit viral infections. Several studies have shown that the probiotic mixtures also have immunomodulatory activity. The probiotics mixture (*L. helveticus* R0052, *Bifidobacterium* R0033, and *Bifidobacterium* R0071) had a major impact on downregulating the expression of proinflammatory cytokines, such as IL-6, IL-8, and IL-1β (Macpherson et al., 2014). The major effects include the upregulated expression of TLR3, mitogen-activated protein kinase, and factor-kappa B (NF-κB) expression. Furthermore, *Lp. plantarum*, *W. cibaria*, and *Ll. sakei* could modulate innate antiviral immune responses induced by poly(I:C) in IECs by activating the TLRs and NF-κB pathways (Kanmani and Kim, 2019). The NF-κB signaling pathway is associated with the production of proinflammatory cytokines. During viral

infections, activating the NF-κB signaling pathway can increase the production of proinflammatory cytokines and regulate the function of immune cells.

IFNs are important mediators of antiviral immunity and regulation of immune system homeostasis (Stefan et al., 2020). *Lc. rhamnosus* CRL1505 has been reported to inhibit viral infections by inducing type I IFNs in intestinal antigen-presenting cells (APCs) (Villena et al., 2014). *Lc. paracasei* DG can also significantly induce the expression of type I IFNs, which can limit the viral replication and assembly (Ishizuka et al., 2016). Besides, *Lp. plantarum* Lp-1 has been shown to exert an anti-TGEV effect on IPEC-J2 cells by inducing large amounts of IFN-β in the early stage and activating the JAK-STAT1 pathway in the late stage, and the activated JAK-STAT1 pathway increases the transcription and expression of some antiviral proteins (Wang et al., 2019).

Efficient clearance of viruses depends on the orchestration of innate and adaptive immune responses. Accumulating evidence showed that probiotics can protect the host from viral infections by stimulating an adaptive immune response. *Limosilactobacillus* (*Lm.*) *reuteri* significantly reduced the viral loads of PCV2 in feces, ileum, and mesenteric lymph nodes (MLNs) and increased the immunoglobulin A (IgA) in the ileum (Karaffova et al., 2017). IgA, the main component of the mucosal immune system, is widely distributed in the mucosal secretions of host mucosal tissues, which can inhibit viral attachment to epithelial cells, slow down viral replication, and play important roles in the immune barrier. Increasing evidence has shown that not only live probiotics but also heat-killed probiotics have immunomodulatory effects. For example, heat-killed *Lc. casei* DK128 has broad protection against IFV infection by intranasal treatment by inducing virus-specific antibodies (Jung et al., 2017). Secretory IgA can bind to the virus specifically and the antibody-captured virus can be destroyed by phagocytes.

Systemic Immune Responses

Probiotics colonized on mucosal surfaces also have distal protective activity against viral infections (**Figure 1B**). It has been confirmed that *Lm. reuteri* has antiviral effects by regulating local mucosal immunity (Karaffova et al., 2017). A recent study has shown that *Lm. reuteri* can also protect the mice from viral infections by regulating the systemic immune responses (Mudronova et al., 2018). Furthermore, orally administrated *Lc. rhamnosus* LA68 induces the expression of some cytokines in the spleen or blood and activates Th1-type immune response (Dimitrijevic et al., 2014). Probiotics or their metabolites can activate immune cells to move distal locations to mediate antiviral responses, or by stimulating immune cells to release cytokines that act distally through blood and lymphatic circulation.

Bifidobacterium, one of the main members of intestinal microorganisms, has immunomodulatory activity. *Bf. longum* improved clinical symptoms and reduced mortality in mice after being inoculated intranasally with IFV. The *Bf. longum* MM-2 enhanced NK cell activity in the lungs and spleen and increased the expression of cytokines (IFN-γ, IL-2, IL-12, and IL-18) (Kawahara et al., 2015). *E. faecalis* CECT7121 induced strong activation of DCs and secretion of high levels of inflammatory cytokines (IL-12, IL-6, TNF-α, and IL-10) (Molina et al., 2015). These cytokines are essential for antiviral innate immune response. IL-10 is a well-established inflammatory and immunosuppressive factor, which can regulate immune responses. Due to viral infections, the increase of IL-10 expression can reduce the damage to the host caused by inflammation. DCs are the sentinel cells in the immune system, acting as APCs. They are also the bridge between innate immunity and adaptive immunity and can activate T and B cells directly or migrate to the mesenteric lymph nodes. Besides, orally administrated *Lp. plantarum* conferred protective activities to IFV by producing high levels of IL-12 and IFN-γ in the lungs (Takeda et al., 2011; Park et al., 2013). IL-12 is a key regulatory molecule of innate immunity and adaptive immunity.

IFNs are mediators of innate immunity and play key roles in resisting viral infections. It is reported that double-stranded RNAs produced by lactic acid bacteria (LABs) triggered DCs to produce IFN-β (Kawashima et al., 2018). *Lc. lactis* JCM5805 regulated immune response to IFV in humans by increasing the expression of IFN-α and ISGs (Sugimura et al., 2015). In addition, oral administration of heat-killed *Lp. plantarum* had a protective activity on H1N1 influenza virus infection in mice (Maeda et al., 2009). The beneficial effects of heat-killed *Lp. plantarum* was mediated by inducing host cells to produce type I IFNs. The probiotic mixture can also protect the host from RSV infection by stimulating AM to produce IFNs (Ji et al., 2021). Activation of the IFN signaling pathway increases the expression of ISGs, the major antiviral effectors of IFNs. A growing number of studies have shown that ISGs target different stages of viral replication to inhibit viral infections. It has been reported that *B. velezensis* can reduce the pigeon circovirus (PiCV) viral load significantly in the feces and spleen of pigeons by upregulating Mx1 and signal transducers and activators of transcription 1 (STAT1) genes (Tsai et al., 2021). Myxovirus resistance 1 (*Mx1*), one of ISGs, can block the early transcription of its nucleic acid after the virus invades the cell (Zurcher et al., 1992). Orally administrated *Lc. rhamnosus* can improve the resistance to RSV infection by producing type I IFNs and ISGs (including *IFNAR1, Mx2, OAS1, OAS2*, *RNase L*, and *IFITM3*) (Garcia-Castillo et al., 2020). These molecules enhanced the ability to inhibit RSV infection in mice. *L. gasseri* SBT2055 also has prophylactic potential to prevent RSV infection by upregulating the expression of IFNs and ISGs (Eguchi et al., 2019). Moreover, a candidate protein SRCAP of *L. gasseri* SBT2055 with RSV antiviral activity was identified. But the exact function of SRCAP protein to inhibit RSV replication needs to be further determined. Furthermore, *L. gasseri* SBT2055 can also protect mice from IFV infection by increasing the expression of the *Mx1* and *Oas1a* genes, which are critical for reducing virus titer in the lungs

(Nakayama et al., 2014). Upregulated ISGs can inhibit IFV infection effectively.

Moreover, heat-killed *E. faecalis* protected mice suppress influenza virus and enterovirus infections (Chen et al., 2017). The protective activity of *E. faecalis* is associated with the activation of the MCP-1/CCR2 pathway, which might act as a key mediator in the improved antiviral immune response. The expression level of MCP-1 was negatively correlated with virus load.

It is well known that the efficient elimination of viruses relies on adaptive immunity. The mice treated with *Bf. bifidum* produced antibodies, IL-4, IL-12, and IFN-γ, and protected from the challenge with H1N1 influenza virus (Mahooti et al., 2019). IL-4 can induce Th2 immune responses, while IFN-γ modulates Th1 immune responses. The balance between Th1 and Th2 is important for the homeostasis of the host immune system. Oral administration of *Lp. plantarum* (YU) induced sIgA and neutralizing antibodies in bronchoalveolar lavage fluids and suppressed viral proliferation in the lungs (Kawashima et al., 2011). Moreover, oral administration of *Lc. rhamnosus* M21 increased the survival of mice after IFV challenge and sIgA and Th1 cytokines (IL-2 and IFN-γ) were significantly increased (Song et al., 2016). Therefore, the resistance of mice to IFV infection is attributed to the cellular immune responses activated by *Lc. rhamnosus* M21.

CONCLUSIONS AND PERSPECTIVES

The world is now facing a multitude of novel infectious diseases. Among them, viral diseases are particularly serious. Currently, WHO has stated that severe coronavirus disease 2019 (COVID-19) is a pandemic challenge to humanity. Vaccination is an important tool to inhibit viral infections. But there is a lag in vaccine development for novel viruses and some antiviral drugs also have some adverse reactions. The development of novel antiviral strategies is imminent. The role of probiotics in human and animal health has been an interesting topic in recent years. Probiotics have been proved to exert antiviral effects, representing safe alternative prophylactics for viral diseases in the future (Stavropoulou and Bezirtzoglou, 2020; Sundararaman et al., 2020). However, only a few probiotics have been investigated for their antiviral effects, and the clinical data are still insufficient. At present, the antiviral effects of probiotics were mainly carried out *in vitro* or in mouse models, which needs to be validated in the natural host of the virus. More animal models remain to be established. Accumulating evidence has indicated that the antiviral effects of probiotics are correlated with the routes of administration. The usual delivery route for probiotics is oral administration. But recent studies have shown that probiotics administered intranasally or sublingually can also reduce viral loads and improve the survival of animals. Intranasal and sublingual routes may be alternatives to oral administration. The dosage of probiotics will also affect the antiviral effects. The same probiotics strain in different doses can induce different immune responses. An excessive dose of probiotics may increase the risk of immunosuppression. Thus, we should pay more attention to the species, dosages, and routes of administration of probiotics when using probiotics-based antiviral agents. In addition, more clinical studies should be conducted to reveal which probiotics or their combinations would be the most effective ones for specific viruses.

Homeostasis of the immune system helps the host against viral infections. It has been proved that probiotics can activate not only local immune response but also systemic immune response to viral infections. The exact mechanisms remain

TABLE 1 | Antiviral effects and underlying mechanisms of various probiotics.

Probiotics	Tested virus	Models	Mechanisms	References
Bf. longum MM-2	H1N1	Mouse	Enhancing NK cells activities; Increasing the expression of cytokines (IFN-γ, IL-2, IL-12, and IL-18).	Kawahara et al., 2015
Lp. plantarum 06CC2	H1N1	Mouse	Increasing the expression of cytokines (IL-12 and IFN-γ).	Takeda et al., 2011
Heat-killed *Lc casei* DK128	H3N2	Mouse	Increasing the number of AM; Inducing virus-specific antibodies; Reducing the expression of proinflammatory cytokines.	Jung et al., 2017
Bf. bifidum	H1N1	Mouse	Inducing virus-specific antibodies; Increasing the expression of cytokines (IL-4 and IFN-γ); Enhancing lymphocyte proliferative responses.	Mahooti et al., 2019
E. faecium NCIMB 10415	SIV	3D4/21 and MDBK cell	Direct interaction with viruses.	Wang et al., 2013
B. clausii	RV	Caco-2 cells	Increasing the expression of mucin 5AC and TJ proteins.	Lorella et al., 2020
L. rhamnosus GG (LGG)	RV	Mouse	Activating the TLR3 pathway.	Aoki-Yoshida et al., 2016
Lg. salivarius FFIG35 and FFIG58	RV	PIEs	Activating the TLR3 pathway.	Indo et al., 2021

(Continued)

TABLE 1 | Continued

Probiotics	Tested virus	Models	Mechanisms	References
Bf. MCC12 and MCC1274	RV	PIEs	Activating the NF-κB signaling pathway; Increasing the expression of IFN-β; Increasing the expression of ISGs.	Ishizuka et al., 2016
Lactobacillus acidophilus (LB^+)	HIV	CEM cells	Producing H_2O_2.	Klebanoff and Coombs, 1991
L. crispatus BC3 and *L. gasseri* BC12	HIV	$CD4^+$ T cell lines, MT-4 and Jurkat; Human cervix, vaginal and tonsillar tissues *in vitro*.	Reducing virus entry/attachment to target cells.	Nahui et al., 2019
B. subtilisis OKB105	TGEV	IPEC-J2 cells	Competing with entry receptors.	Wang et al., 2013
Lp. plantarum Lp-1	TGEV	IPEC-J2 cells	Increasing the expression of IFN-β; Activating the JAK-STAT1 pathway.	Wang et al., 2019
Ll. reuteri	PCV2	Mouse	Increasing the expression of cytokines (chemokines, IFN-γ, and IgA).	Karaffova et al., 2017
Ll. reuteri	PCV2	Mouse	Increasing the percentage of $CD8^+$ and $CD49b^+CD8^-$ cells; Increasing the expression of cytokines (RANTES, GM-CSF, IFN-γ, and IgA).	Mudronova et al., 2018
B. velezensis	PiCV	Pigeon	Increasing the expression of cytokines (IFN-γ, Mx1, STAT1, TLR2, and TLR4).	Tsai et al., 2021
Lc. rhamnosus CRL1505	RSV	Mouse	Increasing the expression of cytokines (IFN-α, IFN-β, IFN-γ, and ISGs).	Villena et al., 2014
L. gasseri SBT2055	RSV	Mouse	Increasing the expression of ISGs.	Eguchi et al., 2019
Probiotic mixture (*L. rhamnosus* GG, *Escherichia coli* Nissle 1917 and VSL#3)	RSV	Mouse	Increasing the expression of IFNs; Restoring of gut microbiota balance.	Krishnan et al., 2016
Lp. plantarum	PMV	Mouse	Activating the NOD2 and TLR2 pathways.	Rice et al., 2016

unverified. Though the antiviral mechanism of probiotics has been partially uncovered, including probiotic components or metabolites and corresponding host PRRs contributing to the antiviral effects as shown in **Table 1**, it is necessary to understand the antiviral effects of probiotics in more details and more extensive and accurate investigations are demanded to clarify the mechanisms underlying the antiviral effects of probiotics using novel molecular tools and technologies. Understanding the antiviral immunity of humans and animals in the context of probiotics is conducive to the development of new antiviral strategies. The antiviral effects of various probiotics will become an interesting area of future research.

AUTHOR CONTRIBUTIONS

YW wrote the manuscript. AM, JH, YS and H-JQ revised this manuscript. All authors contributed to the article and approved the submitted version.

FUNDING

This study was supported by the National Key R&D Program of China (Grant no. 2021YFD1801403).

REFERENCES

Al-Ghazzewi, F. H., and Tester, R. F. (2016). Biotherapeutic Agents and Vaginal Health. *J. Appl. Microbiol.* 121, 18–27. doi: 10.1111/jam.13054

Antunes, K. H., Fachi, J. L., de Paula, R., Da, S. E., Pral, L. P., Dos, S. A., et al. (2019). Microbiota-Derived Acetate Protects Against Respiratory Syncytial Virus Infection Through a GPR43-Type 1 Interferon Response. *Nat. Commun.* 10, 3273. doi: 10.1038/s41467-019-11152-6

Aoki-Yoshida, A., Saito, S., Fukiya, S., Aoki, R., Takayama, Y., Suzuki, C., et al. (2016). *Lactobacillus rhamnosus* GG Increases Toll-Like Receptor 3 Gene Expression in Murine Small Intestine *Ex Vivo* and *In Vivo*. *Benef. Microbes* 7, 421–429. doi: 10.3920/BM2015.0169

Ashraf, R., and Shah, N. P. (2014). Immune System Stimulation by Probiotic Microorganisms. *Crit. Rev. Food Sci.* 54, 938–956. doi: 10.1080/10408398.2011.619671

Azad, M., Sarker, M., and Wan, D. (2018). Immunomodulatory Effects of Probiotics on Cytokine Profiles. *Biomed. Res. Int.* 2018, 8063647. doi: 10.1155/2018/8063647

Boparai, J. K., and Sharma, P. K. (2020). Mini Review on Antimicrobial Peptides, Sources, Mechanism and Recent Applications. *Protein Pept. Lett.* 27, 4–16. doi: 10.2174/0929866526666190822165812

Bosch, T., and Zasloff, M. (2021). Antimicrobial Peptides or How Our Ancestors Learned to Control the Microbiome. *mBio* 12, e0184721. doi: 10.1128/mBio.01847-21

Botic, T., Klingberg, T. D., Weingartl, H., and Cencic, A. (2007). A Novel Eukaryotic Cell Culture Model to Study Antiviral Activity of Potential Probiotic Bacteria. *Int. J. Food Microbiol.* 115, 227–234. doi: 10.1016/j.ijfoodmicro.2006.10.044

Caballero-Franco, C., Keller, K., De Simone, C., and Chadee, K. (2007). The VSL3 Probiotic Formula Induces Mucin Gene Expression and Secretion in Colonic

Epithelial Cells. *Am. J. Physiol. Gastrointest. Liver Physiol.* 292, G315–G322. doi: 10.1152/ajpgi.00265.2006

Chen, M. F., Weng, K. F., Huang, S. Y., Liu, Y. C., Tseng, S. N., Ojcius, D. M., et al. (2017). Pretreatment with a Heat-Killed Probiotic Modulates Monocyte Chemoattractant Protein-1 and Reduces the Pathogenicity of Influenza and Enterovirus 71 Infections. *Mucosal Immunol.* 10, 215–227. doi: 10.1038/mi.2016.31

Conti, C., Malacrino, C., and Mastromarino, P. (2009). Inhibition of Herpes Simplex Virus Type 2 by Vaginal Lactobacilli. *J. Physiol. Pharmacol.* 6, 19–26. doi: 10.1016/j.jcma.2017.07.010

Dimitrijevic, R., Ivanovic, N., Mathiesen, G., Petrusic, V., Zivkovic, I., Djordjevic, B., et al. (2014). Effects of *Lactobacillus rhamnosus* LA68 on the Immune System of C57BL/6 Mice upon Oral Administration. *J. Dairy Res.* 81, 202–207. doi: 10.1017/S0022029914000028

Di Pierro, F., and Pane, M. (2021). *Bifidobacterium Longum* W11: Uniqueness and Individual or Combined Clinical Use in Association with Rifaximin. *Clin. Nutr. Espen.* 42, 15–21. doi: 10.1016/j.clnesp.2020.12.025

Drago, L., Rodighiero, V., Celeste, T., Rovetto, L., and De Vecchi, E. (2010). Microbiological Evaluation of Commercial Probiotic Products Available in the USA in 2009. *J. Chemother.* 22, 373–377. doi: 10.1179/joc.2010.22.6.373

Egert, M., and Simmering, R. (2016). The Microbiota of the Human Skin. *Adv. Exp. Med. Biol.* 902, 61–81. doi: 10.1007/978-3-319-31248-4_5

Eguchi, K., Fujitani, N., Nakagawa, H., and Miyazaki, T. (2019). Prevention of Respiratory Syncytial Virus Infection With Probiotic Lactic Acid Bacterium *Lactobacillus gasseri* SBT2055. *Sci. Rep.* 9, 4812. doi: 10.1038/s41598-019-39602-7

Engevik, M. A., Luk, B., Chang-Graham, A. L., Hall, A., Herrmann, B., Ruan, W., et al. (2019). *Bifidobacterium dentium* Fortifies the Intestinal Mucus Layer *via* Autophagy and Calcium Signaling Pathways. *mBio* 10. doi: 10.1128/mBio.01087-19

Ermolenko, E. I., Desheva, Y. A., Kolobov, A. A., Kotyleva, M. P., Sychev, I. A., and Suvorov, A. N. (2019). Anti-Influenza Activity of Enterocin B *in vitro* and Protective Effect of Bacteriocinogenic Enterococcal Probiotic Strain on Influenza Infection in Mouse Model. *Probiotics Antimicrob. Proteins* 11, 705–712. doi: 10.1007/s12602-018-9457-0

Food and Agriculture Organization of the United Nations/World Health Organization (FAO/WHO) (2002). *Guidelines for the Evaluation of Probiotics in Food* (London, Ontario, Canada: Joint FAO/WHO Working Group on Drafting Guidelines for the Evaluation of Probiotics in Food).

Fry, D. E. (2018). Antimicrobial Peptides. *Surg. Infect.* 19, 804–811. doi: 10.1089/sur.2018.194

Garcia-Castillo, V., Tomokiyo, M., Raya, T. F., Islam, M. A., Takahashi, H., Kitazawa, H., et al. (2020). Alveolar Macrophages are Key Players in the Modulation of the Respiratory Antiviral Immunity Induced by Orally Administered *Lacticaseibacillus Rhamnosus* CRL1505. *Front. Immunol.* 11. doi: 10.3389/fimmu.2020.568636

Gasbarrini, G., Bonvicini, F., and Gramenzi, A. (2016). Probiotics History. *J. Clin. Gastroenterol.* 2, 13–15. doi: 10.1097/MCG.0000000000000697

Giannakou, K., Visinoni, F., Zhang, P., Nathoo, N., Jones, P., Cotterrell, M., et al. (2021). Biotechnological Exploitation of *Saccharomyces Jurei* and its Hybrids in Craft Beer Fermentation Uncovers New Aroma Combinations. *Food Microbiol.* 100, 103838. doi: 10.1016/j.fm.2021.103838

Gosmann, C., Anahtar, M. N., Handley, S. A., Farcasanu, M., Abu-Ali, G., Bowman, B. A., et al. (2017). Lactobacillus-Deficient Cervicovaginal Bacterial Communities are Associated with Increased HIV Acquisition in Young South African Women. *Immunity* 46, 29–37. doi: 10.1016/j.immuni.2016.12.013

Gunzel, D., and Fromm, M. (2012). Claudins and Other Tight Junction Proteins. *Compr. Physiol.* 2, 1819–1852. doi: 10.1002/cphy.c110045

Hao, Q., Dong, B. R., and Wu, T. (2015). Probiotics for Preventing Acute Upper Respiratory Tract Infections. *Cochrane Database Syst. Rev.* 2, 6895. doi: 10.1002/14651858

Heintz-Buschart, A., and Wilmes, P. (2018). Human Gut Microbiome: Function Matters. *Trends Microbiol.* 26, 563–574. doi: 10.1016/j.tim.2017.11.002

Indo, Y., Kitahara, S., Tomokiyo, M., Araki, S., Islam, M. A., Zhou, B., et al. (2021). *Ligilactobacillus salivarius* Strains Isolated from the Porcine Gut Modulate Innate Immune Responses in Epithelial Cells and Improve Protection against Intestinal Viral-Bacterial Superinfection. *Front. Immunol.* 12. doi: 10.3389/fimmu.2021.652923

Ishizuka, S., Iwama, A., Dinoto, A., Suksomcheep, A., Maeta, K., Kasai, T., et al. (2009). Synbiotic Promotion of Epithelial Proliferation by Orally Ingested Encapsulated *Bifidobacterium breve* and Raffinose in the Small Intestine of Rats. *Mol. Nutr. Food Res.* 53, S62–S67. doi: 10.1002/mnfr.200800041

Ishizuka, T., Kanmani, P., Kobayashi, H., Miyazaki, A., Soma, J., Suda, Y., et al. (2016). Immunobiotic *Bifidobacteria* Strains Modulate Rotavirus Immune Response in Porcine Intestinal Epitheliocytes *via* Pattern Recognition Receptor Signaling. *PLoS One* 11, e0152416. doi: 10.1371/journal.pone.0152416

Ji, J. J., Sun, Q. M., Nie, D. Y., Wang, Q., Zhang, H., Qin, F. F., et al. (2021). Probiotics Protect Against RSV Infection by Modulating the Microbiota-Alveolar-Macrophage Axis. *Acta Pharmacol. Sin.* 42, 1630–1641. doi: 10.1038/s41401-020-00573-5

Jung, Y. J., Lee, Y. T., Ngo, V. L., Cho, Y. H., Ko, E. J., Hong, S. M., et al. (2017). Heat-Killed *Lactobacillus casei* Confers Broad Protection against Influenza A Virus Primary Infection and Develops Heterosubtypic Immunity Against Future Secondary Infection. *Sci. Rep.* 7, 17360. doi: 10.1038/s41598-017-17487-8

Kahouli, I., Tomaro-Duchesneau, C., and Prakash, S. (2013). Probiotics in Colorectal Cancer (CRC) with Emphasis on Mechanisms of Action and Current Perspectives. *J. Med. Microbiol.* 62, 1107–1123. doi: 10.1099/jmm.0.048975-0

Kanmani, P., and Kim, H. (2019). Immunobiotic Strains Modulate Toll-Like Receptor 3 Agonist Induced Innate Antiviral Immune Response in Human Intestinal Epithelial Cells by Modulating IFN Regulatory Factor 3 and NF-κB Signaling. *Front. Immunol.* 101536. doi: 10.3389/fimmu.2019.01536

Karaffova, V., Csank, T., Mudronova, D., Kiraly, J., Revajova, V., Gancarcikova, S., et al. (2017). Influence of *Lactobacillus reuteri* L26 Biocenol^{TM} on Immune Response Against Porcine Circovirus Type 2 Infection in Germ-Free Mice. *Benef. Microbes* 8, 367–378. doi: 10.3920/BM2016.0114

Karst, S. M. (2016). The Influence of Commensal Bacteria on Infection with Enteric Viruses. *Nat. Rev. Microbiol.* 14, 197–204. doi: 10.1038/nrmicro.2015.25

Kawahara, T., Takahashi, T., Oishi, K., Tanaka, H., Masuda, M., Takahashi, S., et al. (2015). Consecutive Oral Administration of *Bifidobacterium longum* MM-2 Improves the Defense System against Influenza Virus Infection by Enhancing Natural Killer Cell Activity in a Murine Model. *Microbiol. Immunol.* 59, 1–12. doi: 10.1111/1348-0421.12210

Kawashima, T., Hayashi, K., Kosaka, A., Kawashima, M., Igarashi, T., Tsutsui, H., et al. (2011). *Lactobacillus plantarum* Strain YU from Fermented Foods Activates Th1 and Protective Immune Responses. *Int. Immunopharmacol.* 11, 2017–2024. doi: 10.1016/j.intimp.2011.08.013

Kawashima, T., Ikari, N., Watanabe, Y., Kubota, Y., Yoshio, S., Kanto, T., et al. (2018). Double-Stranded RNA Derived from Lactic Acid Bacteria Augments Th1 Immunity *via* Interferon-Beta from Human Dendritic Cells. *Front. Immunol.* 9. doi: 10.3389/fimmu.2018.00027

Kim, S. K., Guevarra, R. B., Kim, Y. T., Kwon, J., Kim, H., Cho, J. H., et al. (2019). Role of Probiotics in Human Gut Microbiome-Associated Diseases. *J. Microbiol. Biotechnol.* 29, 1335–1340. doi: 10.4014/jmb.1906.06064

Klebanoff, S. J., and Coombs, R. W. (1991). Viricidal Effect of *Lactobacillus Acidophilus* on Human Immunodeficiency Virus Type 1: Possible Role in Heterosexual Transmission. *J. Exp. Med.* 174, 289–292. doi: 10.1084/jem.174.1.289

Knezevic, A., Stepanovic, S., Cupic, M., Jevtovic, D., Ranin, J., and Jovanovic, T. (2005). Reduced Quantity and Hydrogen-Peroxide Production of Vaginal Lactobacilli in HIV Positive Women. *Biomed. Pharmacother.* 59, 521–533. doi: 10.1016/j.biopha.2005.06.010

Krishnan, M., Penrose, H. M., Shah, N. N., Marchelletta, R. R., and McCole, D. F. (2016). VSL3 Probiotic Stimulates T-Cell Protein Tyrosine Phosphatase-Mediated Recovery of IFN-Gamma-Induced Intestinal Epithelial Barrier Defects. *Inflamm. Bowel Dis.* 22, 2811–2823. doi: 10.1097/MIB.0000000000000954

La Fata, G., Weber, P., and Mohajeri, M. H. (2018). Probiotics and the Gut Immune System: Indirect Regulation. *Probiotics Antimicrob. Proteins* 10, 11–21. doi: 10.1007/s12602-017-9322-6

LeBlanc, J. G., Chain, F., Martin, R., Bermudez-Humaran, L. G., Courau, S., and Langella, P. (2017). Beneficial Effects on Host Energy Metabolism of Short-

Chain Fatty Acids and Vitamins Produced by Commensal and Probiotic Bacteria. *Microb. Cell Fact.* 16, 79. doi: 10.1186/s12934-017-0691-z

Lievin-Le, M. V., and Servin, A. L. (2014). Anti-Infective Activities of Lactobacillus Strains in the Human Intestinal Microbiota: From Probiotics to Gastrointestinal Anti-Infectious Biotherapeutic Agents. *Clin. Microbiol. Rev.* 27, 167–199. doi: 10.1128/CMR.00080-13

Liu, Z., Xu, C., Tian, R., Wang, W., Ma, J., Gu, L., et al. (2021). Screening Beneficial Bacteriostatic Lactic Acid Bacteria in the Intestine and Studies of Bacteriostatic Substances. *J. Zhejiang Univ. Sci. B* 22, 533–547. doi: 10.1631/jzus.B2000602

Liu, Q., Yu, Z., Tian, F., Zhao, J., Zhang, H., Zhai, Q., et al. (2020). Surface Components and Metabolites of Probiotics for Regulation of Intestinal Epithelial Barrier. *Microb. Cell Fact.* 19, 23. doi: 10.1186/s12934-020-1289-4

Lloyd-Price, J., Abu-Ali, G., and Huttenhower, C. (2016). The Healthy Human Microbiome. *Genome Med.* 8, 51. doi: 10.1186/s13073-016-0307-y

Lorella, P., Lorella, T., Cristina, B., Laura, P., Carla, D., Lucio, P., et al. (2020). Protective Action of *Bacillus Clausii* Probiotic Strains in an *In Vitro* Model of Rotavirus Infection. *Sci. Rep.* 10, 12636. doi: 10.1038/s41598-020-69533-7

Lu, W., Fang, Z., Liu, X., Li, L., Zhang, P., Zhao, J., et al. (2021). The Potential Role of Probiotics in Protection against Influenza a Virus Infection in Mice. *Foods* 10, 902. doi: 10.3390/foods10040902

Lunjani, N., Hlela, C., and O'Mahony, L. (2019). Microbiome and Skin Biology. *Curr. Opin. Allergy Clin. Immunol.* 19, 328–333. doi: 10.1097/ACI.0000000000000542

Macpherson, C., Audy, J., Mathieu, O., and Tompkins, T. A. (2014). Multistrain Probiotic Modulation of Intestinal Epithelial Cells' Immune Response to a Double-Stranded RNA Ligand, Poly(I.C). *Appl. Environ. Microbiol.* 80, 1692–1700. doi: 10.1128/AEM.03411-13

Maeda, N., Nakamura, R., Hirose, Y., Murosaki, S., Yamamoto, Y., Kase, T., et al. (2009). Oral Administration of Heat-Killed *Lactobacillus plantarum* L-137 Enhances Protection against Influenza Virus Infection by Stimulation of Type I Interferon Production in Mice. *Int. Immunopharmacol.* 9, 1122–1125. doi: 10.1016/j.intimp.2009.04.015

Mahooti, M., Abdolalipour, E., Salehzadeh, A., Mohebbi, S. R., Gorji, A., and Ghaemi, A. (2019). Immunomodulatory and Prophylactic Effects of *Bifidobacterium bifidum* Probiotic Strain on Influenza Infection in Mice. *World J. Microbiol. Biotechnol.* 35, 91. doi: 10.1007/s11274-019-2667-0

Matsusaki, T., Takeda, S., Takeshita, M., Arima, Y., Tsend-Ayush, C., Oyunsuren, T., et al. (2016). Augmentation of T Helper Type 1 Immune Response through Intestinal Immunity in Murine Cutaneous Herpes Simplex Virus Type 1 Infection by Probiotic *Lactobacillus plantarum* Strain 06CC2. *Int. Immunopharmacol.* 39, 320–327. doi: 10.1016/j.intimp.2016.08.001

Mishra, A., Lai, G. C., Yao, L. J., Aung, T. T., Shental, N., Rotter-Maskowitz, A., et al. (2021). Microbial Exposure during Early Human Development Primes Fetal Immune Cells. *Cell* 184, 3394–3409. doi: 10.1016/j.cell.2021.04.039

Molina, M. A., Diaz, A. M., Hesse, C., Ginter, W., Gentilini, M. V., Nunez, G. G., et al. (2015). Immunostimulatory Effects Triggered by *Enterococcus faecalis* CECT7121 Probiotic Strain Involve Activation of Dendritic Cells and Interferon-Gamma Production. *PLoS One* 10, e0127262. doi: 10.1371/journal.pone.0127262

Mudronova, D., Karaffova, V., Csank, T., Kiraly, J., Revajova, V., Gancarcikova, S., et al. (2018). Systemic Immune Response of Gnotobiotic Mice Infected with Porcine Circovirus Type 2 After Administration of *Lactobacillus reuteri* L26 Biocenol. *Benef. Microbes* 9, 951–961. doi: 10.3920/BM2017.0147

Nahui, P. R., Vanpouille, C., Laghi, L., Parolin, C., Melikov, K., Backlund, P., et al. (2019). Extracellular Vesicles from Symbiotic Vaginal Lactobacilli Inhibit HIV-1 Infection of Human Tissues. *Nat. Commun.* 10, 5656. doi: 10.1038/s41467-019-13468-9

Nahui, P. R., Zicari, S., Vanpouille, C., Vitali, B., and Margolis, L. (2017). Vaginal Lactobacillus Inhibits HIV-1 Replication in Human Tissues *Ex Vivo*. *Front. Microbiol.* 8. doi: 10.3389/fmicb.2017.00906

Nakayama, Y., Moriya, T., Sakai, F., Ikeda, N., Shiozaki, T., Hosoya, T., et al. (2014). Oral Administration of *Lactobacillus gasseri* SBT2055 is Effective for Preventing Influenza in Mice. *Sci. Rep.* 4, 4638. doi: 10.1038/srep04638

O'Hanlon, D. E., Moench, T. R., and Cone, R. A. (2011). In Vaginal Fluid, Bacteria Associated with Bacterial Vaginosis can be Suppressed with Lactic Acid But Not Hydrogen Peroxide. *BMC Infect. Dis.* 11, 200. doi: 10.1186/1471-2334-11-200

Otani, T., and Furuse, M. (2020). Tight Junction Structure and Function Revisited. *Trends Cell Biol.* 30, 805–817. doi: 10.1016/j.tcb.2020.08.004

Park, M. K., Ngo, V., Kwon, Y. M., Lee, Y. T., Yoo, S., Cho, Y. H., et al. (2013). *Lactobacillus plantarum* DK119 as a Probiotic Confers Protection against Influenza Virus by Modulating Innate Immunity. *PLoS One* 8, e75368. doi: 10.1371/journal.pone.0075368

Peixoto, R. S., Harkins, D. M., and Nelson, K. E. (2021). Advances in Microbiome Research for Animal Health. *Annu. Rev. Anim. Biosci.* 9, 289–311. doi: 10.1146/annurev-animal-091020-075907

Pelaseyed, T., Bergstrom, J. H., Gustafsson, J. K., Ermund, A., Birchenough, G. M., Schutte, A., et al. (2014). The Mucus and Mucins of the Goblet Cells and Enterocytes Provide the First Defense Line of the Gastrointestinal Tract and Interact with the Immune System. *Immunol. Rev.* 260, 8–20. doi: 10.1111/imr.12182

Piewngam, P., Zheng, Y., Nguyen, T. H., Dickey, S. W., Joo, H. S., Villaruz, A. E., et al. (2018). Pathogen Elimination by Probiotic *Bacillus via* Signalling Interference. *Nature* 562, 532–537. doi: 10.1038/s41586-018-0616-y

Pradhan, D., Biswasroy, P., Kar, B., Bhuyan, S. K., Ghosh, G., and Rath, G. (2021). Clinical Interventions and Budding Applications of Probiotics in the Treatment and Prevention of Viral Infections. *Arch. Med. Res.* 8, 122–130. doi: 10.1016/j.arcmed.2021.09.008

Rad, A. H., Aghebati-Maleki, L., Kafil, H. S., and Abbasi, A. (2021). Molecular Mechanisms of Postbiotics in Colorectal Cancer Prevention and Treatment. *Crit. Rev. Food Sci. Nutr.* 61, 1787–1803. doi: 10.1080/10408398.2020.1765310

Rice, T. A., Brenner, T. A., Percopo, C. M., Ma, M., Keicher, J. D., Domachowske, J. B., et al. (2016). Signaling *via* Pattern Recognition Receptors NOD2 and TLR2 Contributes to Immunomodulatory Control of Lethal Pneumovirus Infection. *Antiviral Res.* 132, 131–140. doi: 10.1016/j.antiviral.2016.06.002

Salaris, C., Scarpa, M., Elli, M., Bertolini, A., Guglielmetti, S., Pregliasco, F., et al. (2021). *Lacticaseibacillus paracasei* DG Enhances the Lactoferrin Anti-SARS-CoV-2 Response in Caco-2 Cells. *Gut Microbes* 13, 1961970. doi: 10.1080/19490976.2021.1961970

Schmidt, T., Raes, J., and Bork, P. (2018). The Human Gut Microbiome: From Association to Modulation. *Cell* 172, 1198–1215. doi: 10.1016/j.cell.2018.02.044

Sender, R., Fuchs, S., and Milo, R. (2016). Are We Really Vastly Outnumbered? Revisiting the Ratio of Bacterial to Host Cells in Humans. *Cell* 164, 337–340. doi: 10.1016/j.cell.2016.01.013

Shen, J., Zuo, Z. X., and Mao, A. P. (2014). Effect of Probiotics on Inducing Remission and Maintaining Therapy in Ulcerative Colitis, Crohn's Disease, and Pouchitis: Meta-Analysis of Randomized Controlled Trials. *Inflamm. Bowel Dis.* 20, 21–35. doi: 10.1097/01.MIB.0000437495.30052.be

Shida, K., and Nanno, M. (2008). Probiotics and Immunology: Separating the Wheat from the Chaff. *Trends Immunol.* 29, 565–573. doi: 10.1016/j.it.2008.07.011

Song, J. A., Kim, H. J., Hong, S. K., Lee, D. H., Lee, S. W., Song, C. S., et al. (2016). Oral Intake of *Lactobacillus rhamnosus* M21 Enhances the Survival Rate of Mice Lethally Infected with Influenza Virus. *J. Microbiol. Immunol. Infect.* 49, 16–23. doi: 10.1016/j.jmii.2014.07.011

Stavropoulou, E., and Bezirtzoglou, E. (2020). Probiotics in Medicine: A Long Debate. *Front. Immunol.* 11. doi: 10.3389/fimmu.2020.02192

Stefan, K. L., Kim, M. V., Iwasaki, A., and Kasper, D. L. (2020). Commensal Microbiota Modulation of Natural Resistance to Virus Infection. *Cell* 183, 1312–1324.e10. doi: 10.1016/j.cell.2020.10.047

Sugimura, T., Takahashi, H., Jounai, K., Ohshio, K., Kanayama, M., Tazumi, K., et al. (2015). Effects of Oral Intake of Plasmacytoid Dendritic Cells-Stimulative Lactic Acid Bacterial Strain on Pathogenesis of Influenza-Like Illness and Immunological Response to Influenza Virus. *Br. J. Nutr.* 114, 727–733. doi: 10.1017/S0007114515002408

Sundararaman, A., Ray, M., Ravindra, P. V., and Halami, P. M. (2020). Role of Probiotics to Combat Viral Infections with Emphasis on COVID-19. *Appl. Microbiol. Biotechnol.* 104, 8089–8104. doi: 10.1007/s00253-020-10832-4

Tachedjian, G., Aldunate, M., Bradshaw, C. S., and Cone, R. A. (2017). The Role of Lactic Acid Production by Probiotic *Lactobacillus* Species in Vaginal Health. *Res. Microbiol.* 168, 782–792. doi: 10.1016/j.resmic.2017.04.001

Takeda, S., Takeshita, M., Kikuchi, Y., Dashnyam, B., Kawahara, S., Yoshida, H., et al. (2011). Efficacy of Oral Administration of Heat-Killed Probiotics from Mongolian Dairy Products Against Influenza Infection in Mice: Alleviation of

Influenza Infection by Its Immunomodulatory Activity through Intestinal Immunity. *Int. Immunopharmacol.* 11, 1976–1983. doi: 10.1016/j.intimp.2011.08.007

Teame, T., Wang, A., Xie, M., Zhang, Z., Yang, Y., Ding, Q., et al. (2020). Paraprobiotics and Postbiotics of Probiotic *Lactobacilli*, Their Positive Effects on the Host and Action Mechanisms: A Review. *Front. Nutr.* 7. doi: 10.3389/fnut.2020.570344

Tsai, C. Y., Hu, S. Y., Santos, H. M., Catulin, G., Tayo, L. L., and Chuang, K. P. (2021). Probiotic Supplementation Containing *Bacillus velezensis* Enhances Expression of Immune Regulatory Genes against Pigeon Circovirus in Pigeons (*Columba Livia*). *J. Appl. Microbiol.* 130, 1695–1704. doi: 10.1111/jam.14893

Tyssen, D., Wang, Y. Y., Hayward, J. A., Agius, P. A., DeLong, K., Aldunate, M., et al. (2018). Anti-HIV-1 Activity of Lactic Acid in Human Cervicovaginal Fluid. *mSphere* 3, e00055–e00018. doi: 10.1128/mSphere.00055-18

VanderWaal, K., and Deen, J. (2018). Global Trends in Infectious Diseases of Swine. *Proc. Natl. Acad. Sci. U. S. A.* 115, 11495–11500. doi: 10.1073/pnas.1806068115

Vieira, A. T., Galvão, I., Macia, L. M., Sernaglia, E. M., Vinolo, M. A. R., Garcia, C. C., et al. (2017). Dietary Fiber and the Short-Chain Fatty Acid Acetate Promote Resolution of Neutrophilic Inflammation in a Model of Gout in Mice. *J. Leukocyte Biol.* 101, 275–284. doi: 10.1189/jlb.3A1015-453RRR

Villena, J., Chiba, E., Vizoso-Pinto, M. G., Tomosada, Y., Takahashi, T., Ishizuka, T., et al. (2014). Immunobiotic *Lactobacillus rhamnosus* Strains Differentially Modulate Antiviral Immune Response in Porcine Intestinal Epithelial and Antigen Presenting Cells. *BMC Microbiol.* 14, 126. doi: 10.1186/1471-2180-14-126

Wachsman, M. B., Castilla, V., de Ruiz, H. A., de Torres, R. A., Sesma, F., and Coto, C. E. (2003). Enterocin CRL35 Inhibits Late Stages of HSV-1 and HSV-2 Replication *In Vitro*. *Antiviral Res.* 58, 17–24. doi: 10.1016/s0166-3542(02)00099-2

Wang, Z., Chai, W., Burwinkel, M., Twardziok, S., Wrede, P., Palissa, C., et al. (2013). Inhibitory Influence of *Enterococcus faecium* on the Propagation of Swine Influenza A Virus *In Vitro*. *PLoS One* 8, 053043. doi: 10.1371/journal.pone.0053043

Wang, J., Ji, H., Wang, S., Liu, H., Zhang, W., Zhang, D., et al. (2018). Probiotic *Lactobacillus plantarum* Promotes Intestinal Barrier Function by Strengthening the Epithelium and Modulating Gut Microbiota. *Front. Microbiol.* 9. doi: 10.3389/fmicb.2018.01953

Wang, K., Ran, L., Yan, T., Niu, Z., Kan, Z., Zhang, Y., et al. (2019). Anti-TGEV Miller Strain Infection Effect of *Lactobacillus plantarum* Supernatant Based on the JAK-STAT1 Signaling Pathway. *Front. Microbiol.* 10. doi: 10.3389/fmicb.2019.02540

Weiss, G., Rasmussen, S., Zeuthen, L. H., Nielsen, B. N., Jarmer, H., Jespersen, L., et al. (2010). *Lactobacillus acidophilus* Induces Virus Immune Defence Genes in Murine Dendritic Cells by a Toll-Like Receptor-2-Dependent Mechanism. *Immunology* 131, 268–281. doi: 10.1111/j.1365-2567.2010.03301.x

Wieërs, G., Verbelen, V., Van Den Driessche, M., Melnik, E., Vanheule, G., Marot, J. C., et al. (2020). Do Probiotics during in-Hospital Antibiotic Treatment Prevent Colonization of Gut Microbiota with Multi-Drug-Resistant Bacteria? A Randomized Placebo-Controlled Trial Comparing Saccharomyces to a Mixture of *Lactobacillus*, *Bifidobacterium*, and *Saccharomyces*. *Front. Public Health* 8. doi: 10.3389/fpubh.2020.578089

Wong, J. M., de Souza, R., Kendall, C. W., Emam, A., and Jenkins, D. J. (2006). Colonic Health: Fermentation and Short Chain Fatty Acids. *J. Clin. Gastroenterol.* 40, 235–243. doi: 10.1097/00004836-200603000-00015

Xu, H., and Li, H. (2019). Acne, the Skin Microbiome, and Antibiotic Treatment. *Am. J. Clin. Dermatol.* 20, 335–344. doi: 10.1007/s40257-018-00417-3

Zurcher, T., Pavlovic, J., and Staeheli, P. (1992). Mechanism of Human MxA Protein Action: Variants with Changed Antiviral Properties. *EMBO J.* 11, 1657–1661. doi: 10.1002/j.1460-2075.1992.tb05212.x

Conflict of Interest: The authors declare that the research was conducted in the absence of any commercial or financial relationships that could be construed as a potential conflict of interest.

Publisher's Note: All claims expressed in this article are solely those of the authors and do not necessarily represent those of their affiliated organizations, or those of the publisher, the editors and the reviewers. Any product that may be evaluated in this article, or claim that may be made by its manufacturer, is not guaranteed or endorsed by the publisher.

frontiers | Frontiers in Cellular and Infection Microbiology

BRIEF RESEARCH REPORT
published: 13 June 2022
doi: 10.3389/fcimb.2022.879360

Canine Adenovirus 1 Isolation Bioinformatics Analysis of the Fiber

Ben Wang[1], *Minchun Wang*[2], *Hongling Zhang*[1], *Jinfeng Xu*[2], *Jinyu Hou*[2,3] *and Yanzhu Zhu*[2,3]*

[1] Animal Science and Technology College, Jilin Agriculture Science and Technology University, Jilin, China, [2] Institute of Special Animal and Plant Sciences, Chinese Academy of Agricultural Sciences, Changchun, China, [3] College of Veterinary Medicine, Jilin Agricultural University, Changchun, China

Canine adenovirus type 1 (CAdV-1) is a double-stranded DNA virus, which is the causative agent of fox encephalitis. The *Fiber* protein is one of the structural proteins in CAdV-1, which mediates virion binding to the coxsackievirus and adenovirus receptor on host cells. The suspected virus was cultured in the MDCK cells, and it was determined through the cytopathic effects, sequencing and electron microscopy. The informatics analysis of the *Fiber* was done using online bioinformatics servers. The CAdV-1-JL2021 strain was isolated successfully, and were most similar to the CAdV-1 strain circulating in Italy. The occurrence of negative selection and recombination were found in the CAdV-1-JL2021 and CAdV-2-AC_000020.1. Host cell membrane was its subcellular localization. The CAdV-1-JL2021 *Fiber* (ON164651) had 6 glycosylation sites and 107 phosphorylation sites, exerted adhesion receptor-mediated virion attachment to host cell, which was the same as CAdV-2-AC_000020.1 Fiber. The *Fiber* tertiary structure of the CAdV-1-JL2021 and CAdV-2-AC_000020.1 was different, but they had the same coxsackievirus and adenovirus receptor. "VATTSPTLTFAYPLIKNNNH" were predicted to be the potential CAdV-1 B cell linear epitope. The MHC-I binding peptide "KLGVKPTTY" were both presented in the CAdV-1-JL2021 and CAdV-2-AC_000020.1 Fiber and it is useful to design the canine adenovirus vaccine.

Keywords: canine adenovirus 1, phylogenetic tree, bioinformatics analysis, B cell epitope, T cell epitope, *Fiber*

OPEN ACCESS

Edited by:
Zhanbo Zhu, Heilongjiang Bayi Agricultural University, China

Reviewed by:
Yufei Zhang, Huazhong Agricultural University, China
Xijun He, State Key Laboratory of Veterinary Biotechnology, Harbin Veterinary Research Institute, Chinese Academy of Agricultural Sciences, China

***Correspondence:**
Yanzhu Zhu
zyzzu@126.com

Specialty section:
This article was submitted to Clinical Microbiology, a section of the journal Frontiers in Cellular and Infection Microbiology

Received: *19 February 2022*
Accepted: *25 April 2022*
Published: *13 June 2022*

Citation:
Wang B, Wang M, Zhang H, Xu J, Hou J and Zhu Y (2022) Canine Adenovirus 1 Isolation Bioinformatics Analysis of the Fiber. Front. Cell. Infect. Microbiol. 12:879360. doi: 10.3389/fcimb.2022.879360

INTRODUCTION

Canine adenovirus type 1 (CAdV-1) is a double-stranded DNA genome virus belonging to the mastadenovirus genus of the adenoviridae family. This virus is the etiologic agent of fox encephalitis (Balboni et al., 2019). CAdV-1 is transmitted by saliva, feces, urine (Yang et al., 2019). Foxes infected with CAdV-1 present with fever, cough, depression, vomiting, diarrhea, anorexia, convulsions, and the characteristic clinical sign of blue eye (corneal edema) (Sun et al., 2019). The large-scale use of the CAdV-2 live attenuated vaccine has reduced the prevalence of CAdV-1. However, CAdV-1 also circulates in wildlife with high pathogenicity and a broad host range (Verin et al., 2019; Zhu et al., 2020). Surveillance for new genetic variants is necessary to evaluate the potential impacts of CAdV-1 on wildlife species.

The CAdV-1 genome is 32 kb in length and contains 30 open reading frames (Pizzurro et al., 2017). The *Fiber* protein is the main capsid protein. The *Fiber* protein is composed of 3 domains, referred to as the tail, shaft, and knob (Schoehn et al., 2008). During CAdV-1 replication, the *Fiber* protein binds to the receptor, destroys the binding integrity of the receptor, allowing for viral entry

into the host cell, and subsequent dissemination between cells. This cell to cell spread helps the virus minimize time in the extracellular environment, greatly limiting detection by the immune system (Walters et al., 2002). When CAdV-1 is detected and identified, *Fiber* nucleotide sequences are usually selected for homology and similarity analysis in CAdV-1 and CAdV-2 (Balboni et al., 2022).

An immunogenic protein, the *Fiber* protein is an attractive candidate for use in the development of subunit vaccines (De Luca et al., 2020). *Fiber* protein subunit vaccines have been demonstrated to protect fowl against fowl adenovirus serotype 4 (Ruan et al., 2018) and FAdV-8b (Gupta et al., 2017). Limited data have been reported demonstrating efficacy of *Fiber* protein vaccines against CAdV-1. The bioinformatics may have important applications in the newly discovered and emerging viruses prediction (Foroutan et al., 2018). Bioinformatics analysis of the ROP8 protein was conducted during the design process of a vaccine targeting *Toxoplasma gondii* (Foroutan et al., 2018). Bioinformatic analysis of the *Fiber* will be the first step to design the vaccine.

In the present study, a CAdV-1 isolated from a sick fox on a farm was characterized and the resulting *Fiber* sequence data were analyzed using bioinformatics. The resulting data provides a rational and theoretical starting point for the development of CAdV-1 control measures and vaccine development.

MATERIAL AND METHODS

Ethics Statement

This experiment was approved by the ethics committee at the Jilin Agriculture Science and Technology University, and the procedures complied with IACUC guidelines on the animals' care and use for scientific purposes.

Preparation of Liver Tissue

A fox presenting with clinical encephalitis was collected from a farm in Jilin. One part of the liver was stained by hematoxylin and eosin (H&E) (Lin et al., 2018). The other part of the liver was homogenized in 1 mL of sterile phosphate buffer (PBS), and was centrifuged for 10 min at 8000 g/min. The supernatants were collected and filtered through a filter with a 0.22 μ M pore size and stored at - 80°C.

Cytopathic Effect and Virus Morphology

CAdV-1 infection was performed in Madin-Darby Canine Kidney (MDCK) cells (ATCC CCL-34, derived from normal kidney of Canis familiaris). MDCK cells were cultured at 37°C in Dulbecco's modified Eagle's medium (DMEM) containing 10% of fetal bovine solution (FBS) and 1% Penicillin-Streptomycin in a 5% CO_2 incubator. Confluent MDCK cells (70-90%) were washed with PBS (pH 7.2), and inoculated with 100 μL of filtered liver homogenate supernatant at 37°C for 1 h. Nine milliliters of fresh DMEM containing 5% FBS was added, and the plate was incubated at 37°C in 5% CO_2. The cytopathic effect (CPE) was observed and photographed daily. The MDCK infected cells with distinct CPE were further characterized by negative-stain transmission electron microscopy (TEM) to determine morphological characteristics of the infecting virus (Prasad et al., 2020).

Polymerase Chain Reaction

Following infection, DNA was extracted from MDCK cells using the MagicPure® Simple 32 Viral DNA/RNA Kit (EC311-32-11). Amplification of the 508bp CAdV-1 fragment was accomplished using previously published primers (Hu et al., 2001) (Forward primer-HA1:5'-CGCGCTGAACATTACTACCTTGTC-3' and Reverse primer-HA2:5'-CCTAGAGCACTTCGTGTCCG CTT-3'). Reactions were run in a 50 μL sample volume consisting of 1 μL of DNA template, 25 μL of 2×EasyTaq® PCR SuperMix (Transgen Biotech, AS111-01), 1 μL of forward and reverse primers each, and 22 μL of sterile deionized nuclease free water. The thermocycling profile for amplification was as follow: 5 min of denaturation at 95°C followed by 35 cycles of 1 min of denaturation at 95°C, 15 s of annealing at 58°C, and 30 s of extension at 72°C, with a final 5 min of extension at 72°C. Amplicons were resolved using1.0% agarose gel electrophoresis and stained with GelStain (Transgen Biotech, GS101-01) to visualize the product.

PCR amplification using the CAdV-1 *Fiber* primer pair (Fiber-F:5'-ATGAAGCGGACACGAAGTGCT-3'; Fiber-R:5'-TCATTGATTTTCCCCCACATAGGTGAAG-3') yielding a 1063 bp fragment. The target region PCR reactions were performed six times in 50 μL reaction volumes containing 1 μL denatured DNA template, 5 μL of buffer, 2 μL of 25mM MgSO4, 1 μL of each primer (10 pmol/μL), 5 μL of 2 mM dNTPs, 1 μL of KOD plus (TOYOBO, KOD-201, 1.0 U/μL) and 34 μL of sterile deionized water. The thermocycling profile used was as follows: 5 min denaturation at 95°Cfollowed by 30 cycles of 30 s denaturation at 95°C, 30 s annealing at 60°C, and 1 min extension at 72°C, with a final 5 min extension at 72°C. The amplicons were resolved using 1.0% agarose gel electrophoresis and stained with GelStain (Transgen Biotech, GS101-01).

Phylogenetic and Homology Analyses

Electrophoretically resolved amplicons from the PCR reactions were eluted from the gel matrix using the EasyPure® Quick Gel Extraction Kit (TransGen, EG101-01), and cloned into an amplification plasmid using the pMD™18-T Vector Cloning Kit (TaKaRa, 6011). Sequencing of the purified plasmids was performed using Sanger sequencing by the Comate Bioscience Co., Ltd. The sequences were assembled and aligned according to the CAdV-1 reference sequences in GenBank, and were translated into amino acid sequences using BioEdit 7.2.5. The resulting *Fiber* nucleotide sequence (CAdV-1-JL2021 strain) was blasted in the NCBI database and compared to the 14 most similar *Fiber* nucleotide sequence of all CAdV strains. Based on the sequences, a phylogenetic tree was constructed using the MEGA 7.0.20 software with the neighbor-joining method. The reliability of the phylogenetic tree was verified through the bootstrap method with 1,000 replicates.

Selective Pressure and Recombination Analysis

Based on the CAdV-1-JL2021 and CAdV-2-AC_000020.1 Fiber nucleotide sequence, the selective pressure and recombination analysis were conducted through SLAC (Kosakovsky Pond and Frost, 2005) and GARD (Kosakovsky Pond et al., 2006) method in Datamonkey.

Protein Subcellular Localization and Function Prediction

The Protein subcellular localization of CAdV-1-JL2021 *Fiber* and CAdV-2-AC_000020.1 *Fiber* was predicted by Virus-mPLoc in Cell-PLoc 2.0 (Chou and Shen, 2008). The *Fiber* function of the CAdV-1-JL2021 and CAdV-2-AC_000020.1 were predicted by EMBL-EBI (Madeira et al., 2022).

Bioinformatics Analysis of *Fiber* Protein

Physical and Chemical Properties, Phosphorylation, and Glycosylation Sites

Protparam (Walker, 2005) was used to predict the instability coefficient, average water absorption coefficient, relative molecular weight, amino acid composition and isoelectric point of charged amino acids in the *Fiber* protein. The Protscale with Hphob./Kyte & Doolittle (Walker, 2005) was used to predict the hydrophilicity and hydrophobicity of the *Fiber* protein.

The NetPhos 3.1 Server (Blom et al., 1999) (Residues to predict serine-all three, Output format-classical, Generate graphics) was used to predict the potential phosphorylation sites of the *Fiber* protein. The potential glycosylation sites of the *Fiber protein* were predicted using the NetNGlyc 1.0 Server (Gupta and Brunak, 2002) with generate graphics.

Transmembrane Region, Signal Peptide, Secondary and Tertiary Structure Prediction

In the CAdV-1-JL2021 Fiber, CAdV-2-AC_000020.1 *Fiber*, the transmembrane region was predicted using TMHMMServer 2.0 (Krogh et al., 2001) (Extensive, with graphics). SignalP 5.0 Server (Nielsen et al., 2019) (Eukarya, Long output) was used to predict the signal peptide. Potential secondary structure characteristics were predicted using SOPMA (Deléage ALIGNSEC, 2017) (Number of conformational states-4 (Helix, sheet, turn, coil), Similarity threshold-8, Window width-17). The tertiary structure of CAdV-1-JL2021 Fiber, CAdV-2-AC_000020.1 *Fiber* and the Coxsackievirus and adenovirus receptor _XP_038299179 were predicted using Robetta (Nerli and Sgourakis, 2019).

T and B Cell Epitope Prediction

The BCpred method (El-Manzalawy et al., 2008) (Methods: Fixed length epitope prediction- BCPred, Epitope length-20, Specificity-75%, report only non-overlapping epitopes) was used to predict potential B cell epitopes. MHC-I binding peptides were obtained using the IEDB Analysis Resource (Vita et al., 2019) (Sort peptides by-Predicted Score (descend), Output format-XHTML table). The MHC allele selected for the analysis was DLA-8803401, and the length was 14 aa, with the MHC source species being dog. Binding predictions of MHC-II performed using IEDB Analysis Resource as well. The prediction method used was IEDB recommended 2.22. The selected MHC allele was DRB1*01:01.

RESULTS

Virus Isolation and Identification

The CPE was observed in MDCK cells. The typical "grape cluster morphology" of CPE was observed while control monolayers remained intact (**Figures 1A, B**). CAdV-JL2021 caused a series of morphological changes in fox liver, such as cell swelling and necrosis (**Figure 1C**). The cell with CPE were further examined by TEM, PCR, and sequencing. Characteristic adenoviral particles were observed by TEM (**Figure 1D**). A 508 bp fragment of the E3 gene was amplified for primary detection. It indicated that the CAdV-1 strain was first isolated. Next, a 1632 bp (**Figure 1E**) target band consistent with the *Fiber* gene was amplified and submitted to the GeneBank (ON164651).

The Fiber Phylogenetic and Homology Analyses

Three different clusters were identified through the phylogenetic analyses of the *Fiber* gene sequences accessioned in GenBank. The CAdV-1-JL2021 strain belongs to CAdV-1, and apparently has a close relationship with CAdV-1 strain (accession number, KP840546). This present study revealed the unique nature of the new strain (**Figure 2A**).

The protein sequences of the CAdV-1 *Fiber* gene (1632 bp in length, 543 amino acid residues) were compared with CAdV *Fiber* gene sequences available from NCBI (**Figure 2B**). The sequence of the *Fiber* gene was determined and was more similar with isolates from Italy (KP840546), suggesting that the isolated virus was CAdV-1. The virus identified in this study also shared 97.8 to 99.82% identity with other CAdV-1 strains.

The Fiber Selective Pressure Analysis

Negative selective pressure was identified in *375, 281, 292, 170 sites of* CAdV-1-JL2021 Fiber (**Figures 2C–F**). Negative selective pressure was identified in *22 sites of* CAdV-2-AC_000020.1 Fiber (**Figures 2C'–F'**).

The Fiber Recombination Analysis

The evidence of recombination breakpoint was found in the CAdV-1-JL2021 and CAdV-2-AC_000020.1Fiber GARD analysis. The CAdV-1-JL2021 alignment contained 42 potential breakpoints and 1 inferred breakpoint (**Figures 2G–I**). The CAdV-2-AC_000020.1 alignment contained 148 potential breakpoints and 2 inferred breakpoint (**Figures 2G'–I'**).

Fiber Protein Subcellular Localization and Function Prediction

The predicted location of the CAdV-1-JL2021 *Fiber* was host cell membrane (**Figure 2J**). The predicted location of the CAdV-2-AC_000020.1 *Fiber* was host cell membrane and host cytoplasm

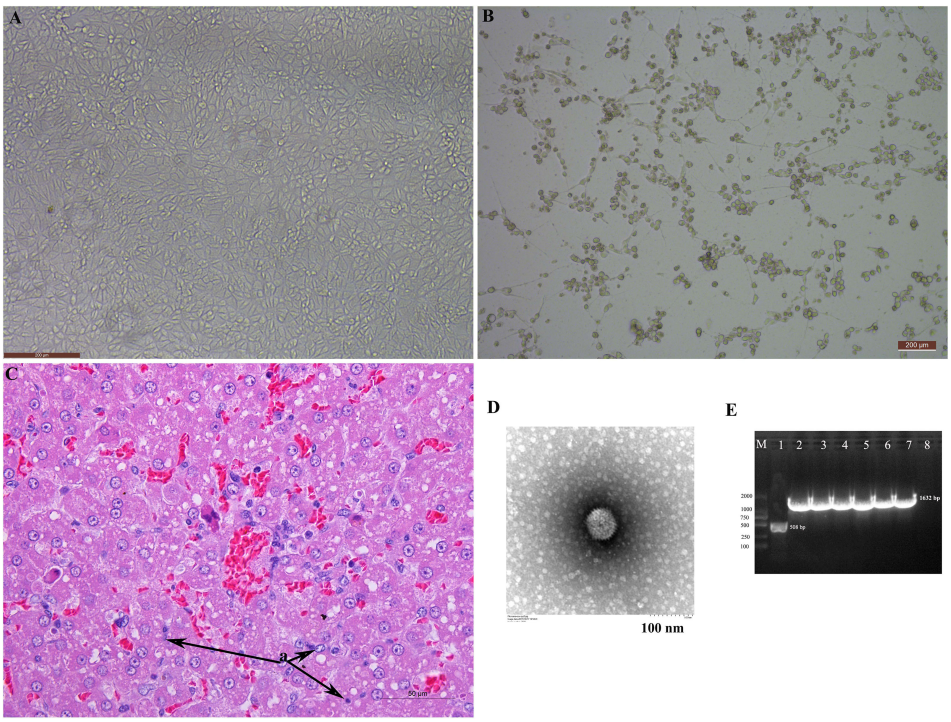

FIGURE 1 | The isolation and identification of the canine adenovirus 1. **(A)** Normal MDCK; **(B)** MDCK with CPE; **(C)** HE staining of liver; **(D)** Electron microscopy observation of the adenovirus particles; **(E)** Amplification of the Fiber gene and identification of adenovirus.

(**Figure 2J'**). CAdV-1-JL2021 and CAdV-2-AC_000020.1*Fiber* exerted adhesion receptor-mediated virion attachment to host cell.

Fiber Prediction of Physical and Chemical Properties

The number of amino acids in the *Fiber* protein was 543, the molecular weight was 56974.49 g/mol, the isoelectric point was 6.26, and the instability coefficient was 39.33. There were 143 amino acids in the hydrophobic region (> 0.5), 168 amino acids in the hydrophilic region (< - 0.5), suggesting that CAdV-1-JL2021 *Fiber* was a hydrophilic protein. (**Figure 3A**). According to the CAdV-2-AC_000020.1 *Fiber*, the average hydrophobicity of the *Fiber* protein is -0.092. There were 129 amino acids in the hydrophobic region (> 0.5), 161 amino acids in the hydrophilic region (< - 0.5), suggesting that CAdV-2-AC_000020.1 *Fiber* was a hydrophilic protein (**Figure 3A'**).

Fiber Prediction of Phosphorylation and Glycosylation Sites

In **Figure 3B**, 6 glycosylation sites (242, 319, 375, 438, 450 and 493) were identified in the *Fiber* protein. It can be seen in **Figure 3C**. CAdV-1-JL2021 *Fiber* had 59 serine phosphorylation sites, 42 potential threonine phosphorylation sites and 6 tyrosine phosphorylation sites. In **Figure 3B'**, 4 glycosylation sites (125, 320, 437, 449) were identified in the *Fiber* protein. It can be seen in **Figure 3C'**, CAdV-2-AC_000020.1 *Fiber* had 42 serine phosphorylation sites, 47 potential threonine phosphorylation sites and 8 tyrosine phosphorylation sites. However, the *Fiber* protein in CAdV-1-JL2021 and CAdV-2-AC_000020.1 were not expected to have either a transmembrane region or signal peptide, as were shown in **Figures 3E, E', F, F'**, respectively.

Prediction on *Fiber* Secondary and Tertiary Structure

The CAdV-1-JL2021 *Fiber* protein α- Helix (Hh), extended chain (EE), β- proportions of angle (TT) and irregular curl (CC) were 0.92%, 34.81%, 6.45% and 57.83% respectively (**Figure 3D**). The CAdV-2-AC_000020.1 *Fiber* protein α-Helix (Hh), extended chain (EE), β- proportions of angle (TT) and irregular curl (CC) were 1.29%, 36.53%, 4.24% and 57.93% respectively (**Figure 3D'**). The *Fiber* tertiary structure of the CAdV-1-JL2021 and CAdV-2-AC_000020.1 was different, but they had the same coxsackievirus and adenovirus receptor (**Figures 3G–I**). Their binding models were also predicted (**Figures 3J, K**).

T and B Cell Epitope Prediction in *Fiber*

11 and 14 of B cell linear epitopes were predicted in the *Fiber* of CAdV-1-JL2021 and CAdV-2-AC_000020.1, respectively (**Figure 4A**). The peptides in the 1, 9, 433, 198, 168, 272, 71 sites of CAdV-1-JL2021 were simultaneously predicted. Importantly, the peptide "VATTSPTLTFAYPLIKNNNH" was both predicted by the IEDB, BCPred and ElliPro. The peptides in

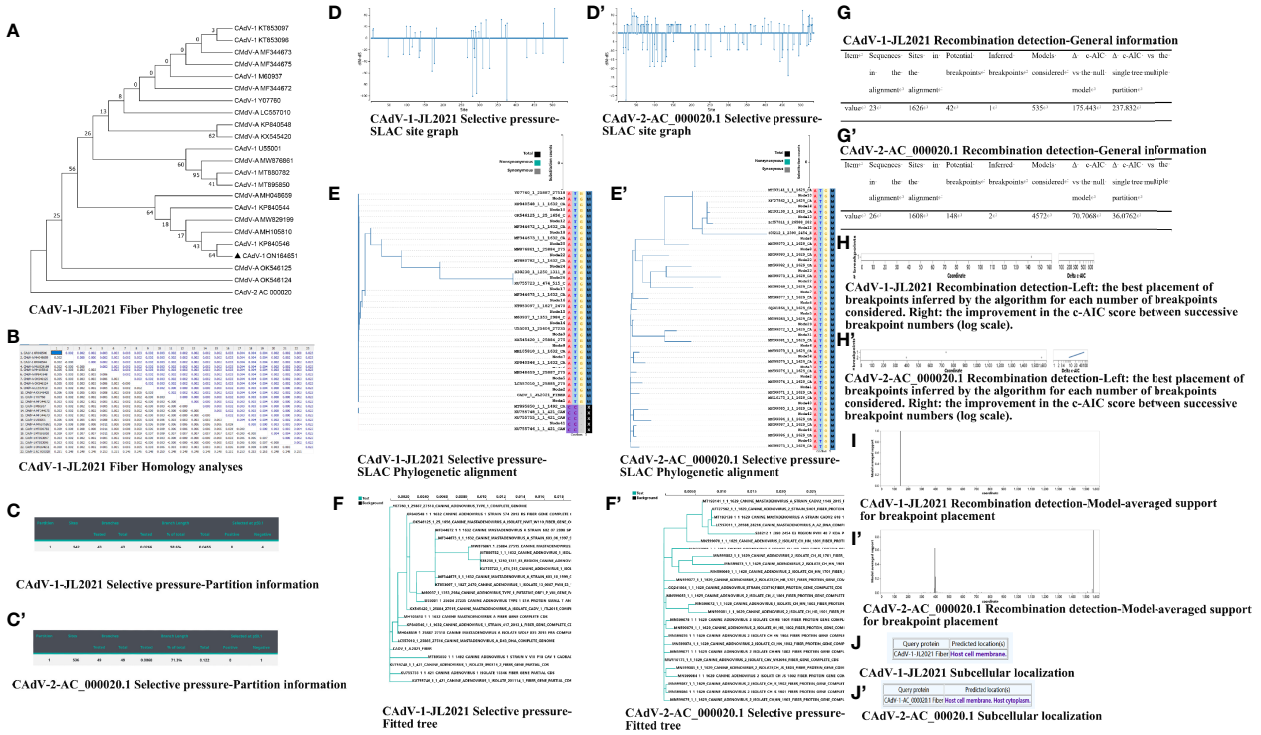

FIGURE 2 | The nucleotide analysis of the Fiber. **(A)** CAdV-1-JL2021 Fiber Phylogenetic tree; **(B)** CAdV-1-JL2021 Fiber Homology analyses; **(C)** CAdV-1-JL2021 Selective pressure-Partition information; **(C')** CAdV-2-AC_000020.1 Selective pressure-Partition information; **(D)** CAdV-1-JL2021 Selective pressure-SLAC site graph; **(D')** CAdV-2-AC_000020.1 Selective pressure-SLAC site graph; **(E)** CAdV-1-JL2021 Selective pressure-SLAC Phylogenetic alignment; **(E')** CAdV-2-AC_000020.1 Selective pressure-SLAC Phylogenetic alignment; **(F)** CAdV-1-JL2021 Selective pressure-Fitted tree; **(F')** CAdV-2-AC_000020.1 Selective pressure-Fitted tree; **(G)** CAdV-1-JL2021 Recombination detection-General information; **(G')** CAdV-2-AC_000020.1 Recombination detection-General information; **(H)** CAdV-1-JL2021 ecombination detection-Left: the best placement of breakpoints inferred by the algorithm for each number of breakpoints considered. Right: the improvement in the c-AIC score between successive breakpoint numbers (log scale). **(H')** CAdV-2-AC_000020.1 Recombination detection-Left: the best placement of breakpoints inferred by the algorithm for each number of breakpoints considered. Right: the improvement in the c-AIC score between successive breakpoint numbers (log scale). **(I)** CAdV-1-JL2021 Recombination detection-Model-averaged support for breakpoint placement; **(I')** CAdV-2-AC_000020.1 Recombination detection-Model-averaged support for breakpoint placement. **(J)** CAdV-1-JL2021 Subcellular localization; **(J')** CAdV-2-AC_00020.1 Subcellular localization.

the 432, 202, 80 sites of CAdV-2-AC_000020.1 were simultaneously predicted. CAdV-1-JL2021 and CAdV-2-AC_000020.1 Fiber did not have the same B cell linear epitopes. CAdV-1-JL2021 and CAdV-2-AC_000020.1 *Fiber* had 3 and 2 discontinuous epitopes, respectively (**Figures 4B–F**).

CAdV-1-JL2021 and CAdV-2-AC_000020.1 *Fiber* had 9 MHC-I binding peptides, respectively. Importantly, the peptide "KLGVKPTTY" were both presented in the CAdV-1-JL2021 and CAdV-2-AC_000020.1 *Fiber* (**Figures 4G, H**). CAdV-1-JL2021 and CAdV-2-AC_000020.1 *Fiber* had 7 MHC-II binding peptides, respectively (**Figures 4I, J**).

DISCUSSION

The size and shape of CAdV particles were similar to those of CAdV-1 and CAdV-2 strains isolated from fox (Choi et al., 2014; Tamukai et al., 2020). However, virus isolation is a very time-consuming diagnostic test, which further necessitates additional molecular tests to classify the etiologic agent as either CAdV-1 or CAdV-2. The haemagglutination and neutralization tests do not provide definitive differentiation between CAdV-1 and CAdV-2 isolated from the digestive tract (Timurkan et al., 2018). However, PCR is a powerful tool for the differentiation of CAdV-1 and CAdV-2 (Balboni et al., 2019; Oleaga et al., 2021). The genomic region encoding the E3 gene and flanking sequences were selected as the target for a pair of primers to diagnose and differentiate the two serotypes of CAdV (Hu et al., 2001). The resulting PCR product produced bands 508 bp of CAdV-1 E3 gene, and 1632 bp of CAdV-1 *Fiber* gene, which will identify the occurrence of CAdV-1 in fox using sequencing and phylogenetic analysis.

Double-stranded DNA viruses tend to have lower mutation rates than RNA genome viruses (Sanjuán and Domingo-Calap, 2016). Nucleotide sequence alignment between the CAdV-1-JL2021 strain and 14 reference strains showed high identities ranging from 97.8 to 99.82%. A phylogenetic tree of 23 *Fiber* nucleatide acid sequences found that the CAdV-1-JL2021 strain was included in the KP840546 strain containing subgroup. The study of this virus strain can provide an alternative strain for the diagnosis and prevention of fox encephalitis.

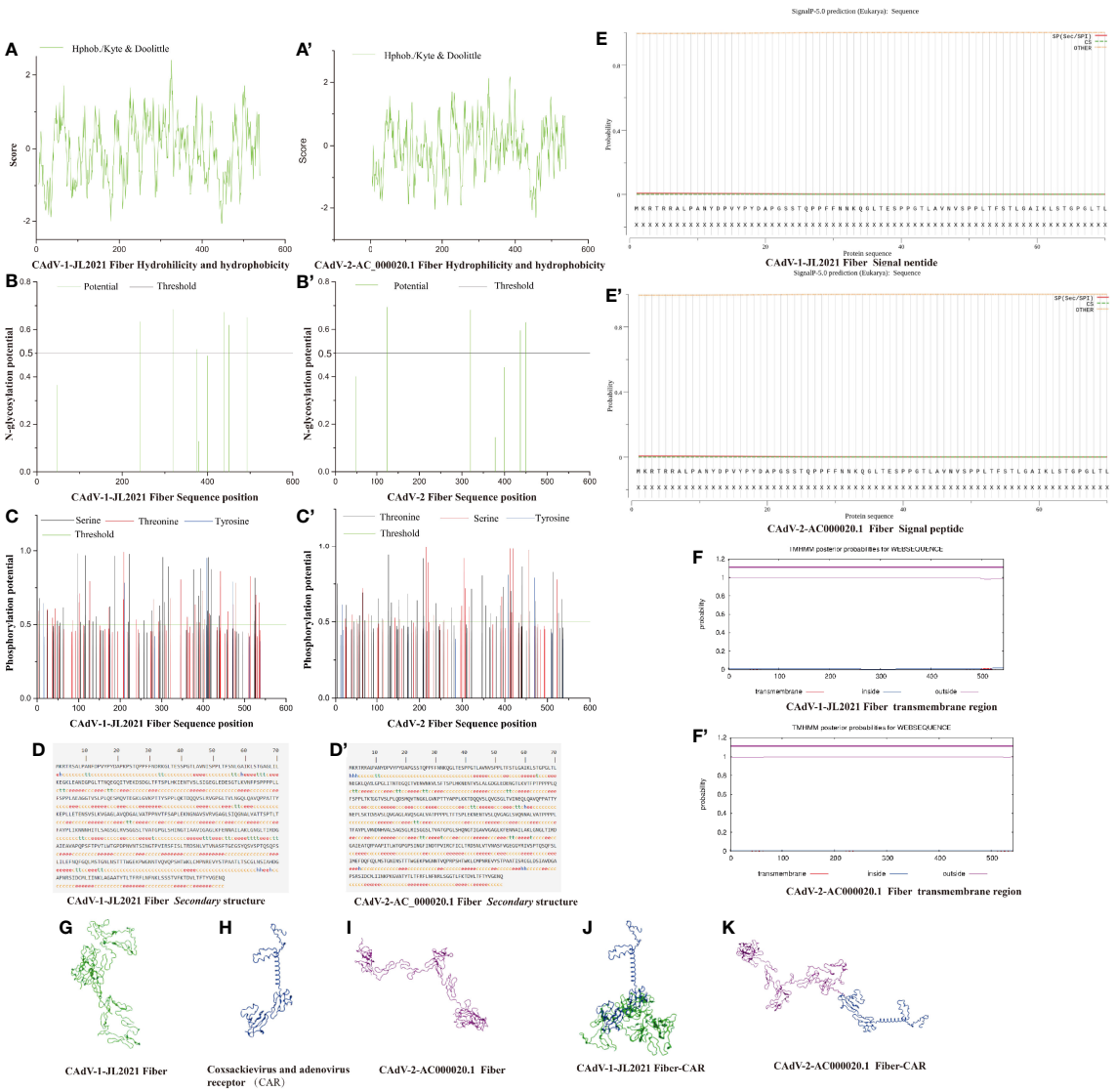

FIGURE 3 | The structure prediction of the Fiber protein. **(A)** CAdV-1 JL2021 Fiber Hydrohilicity and hydeophobicity; **(A')** CAdV-2-AC_000020.1 Fiber Hydrohilicity and hydeophobicity; **(B)** CAdV-1 JL2021 Fiber N-glycosylation potential position; **(B')** CAdV-2-AC_000020.1 Fiber N-glycosylation potential position; **(C)** CAdV-1 JL2021 Fiber Phosphorylation potential position; **(C')** CAdV-2-AC_000020.1 Fiber Phosphorylation potential position; **(D)** CAdV-1 JL2021 Fiber secondary structure; **(D')** CAdV-2-AC_000020.1 Fiber secondary structure; **(E)** CAdV-1 JL2021 Fiber Signal peptide; **(E')** CAdV-2-AC_000020.1 Fiber Signal peptide; **(F)** CAdV-1 JL2021 Fiber transmembrane region; **(F')** CAdV-2-AC_000020.1 Fiber transmembrane region; **(G)** CAdV-1 JL2021 Fiber Three-dimensional structure; **(H)** Coxsackievirus and adenovirus receptor (CAR) Three-dimensional structure; **(I)** CAdV-2-AC_000020.1 Fiber Three-dimensional structure; **(J)** Interaction between CAdV-1 JL2021 Fiber and CAR; **(K)** Interaction between CAdV-2-AC_000020.1 Fiber and CAR.

Selection is an essential component of any evolutionary system and analyzing this fundamental force in evolution can provide relevant insights into the evolutionary development of a population (Haasdijk and Heinerman, 2018). negative selection removed amino-acid changes that reduced fitness, positive selection maintained amino-acid changes that increase virus fitness. Neutral selection was that the fitness was not affected by the amino-acid changes. In this experiment, negative selective pressure was identified in *375, 281, 292, 170 sites of* CAdV-1-JL2021 Fiber and in the 22 sites of CAdV-2-AC_000020.1. The presence of negative selection implies that the sites were functionally important in the virus evolution. *The sites in the* CAdV-1-JL2021 *Fiber* were less than that of CAdV-2-AC_000020.1. *The less negative selection site maybe that* the numbers of nucleotide substitutions (cS 1 cN) observed were insufficient for detecting statistically significant differences between cS and cN. More sequence data should be collected in the future. The negative selection identified in CAdV-1-JL2021 and CAdV-2-AC_000020.1 protein may help the

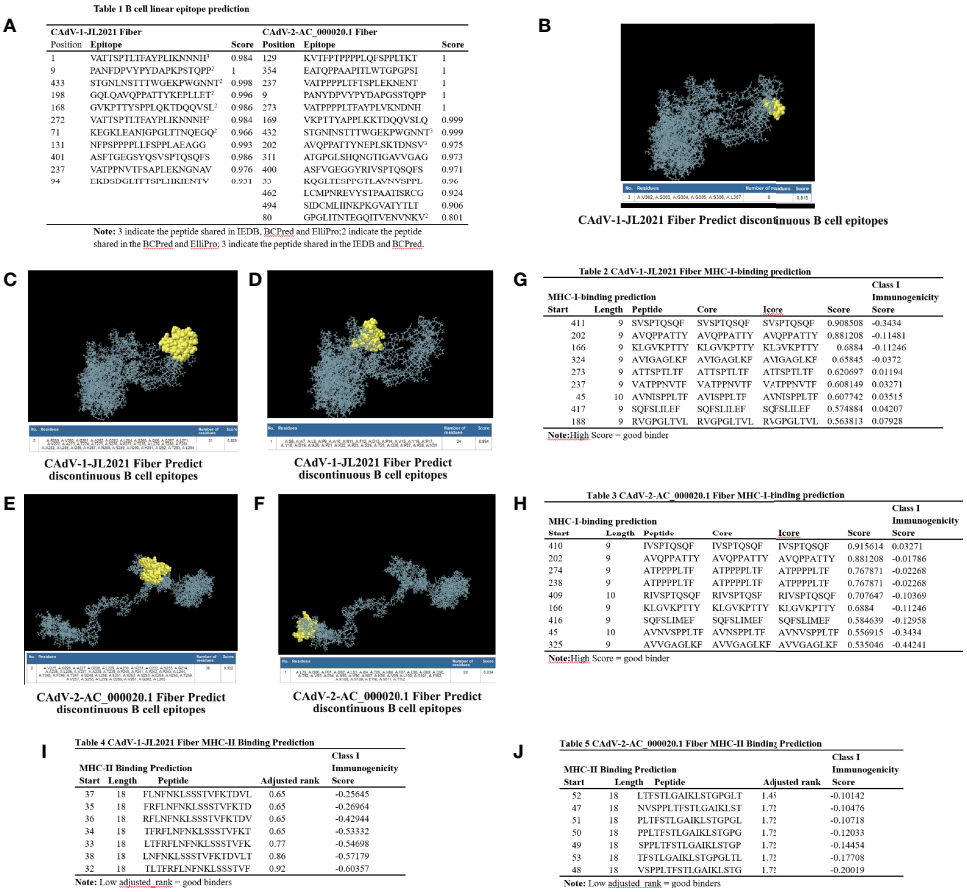

A

Table 1 B cell linear epitope prediction

CAdV-1-JL2021 Fiber			CAdV-2-AC_000020.1 Fiber		
Position	Epitope	Score	Position	Epitope	Score
1	VATTSPTLTFAYPLIKNNNH[1]	0.984	129	KVTTPTPPPPLQFSPPLTKT	1
9	PANFDPVYPYDAPKPSTQPP[2]	1	354	EATQPPAAPITLWTGPGPSI	1
433	STGNLNSTTTWGEKPWGNNT[2]	0.998	237	VATPPPPLTFSPLEKNENT	1
198	GQLQAVQPPATTYKEPLLET[2]	0.996	9	PANYDPVYPYDAPGSSTQPP	1
168	GVKPTTYSPPLQKTDQQVSL[2]	0.986	273	VATPPPPLTFAYPLVKNDNH	1
272	VATTSPTLTFAYPLIKNNNH[2]	0.984	169	VKPTTYAPPLKKTDQQVSLQ	0.999
71	KEGKLEANIGPGLTTNQEGQ[2]	0.966	432	STGNINSTTTWGEKPWGNNT[2]	0.999
131	NFPSPPPPLLFSPPLAEAGG	0.993	202	AVQPPATTYNEPLSKTDNSV[2]	0.975
401	ASFTGEGSYQSVSPTQSQFS	0.986	311	ATGPGLSIHQNGTIGAVVGAG	0.973
237	VATPPNVTFSAPLEKGNAV	0.976	400	ASFVGEGGYRIVSPTQSQFS	0.971
94	EKDSDGLITTSPLIIKIENTV	0.931	33	KQGLTESPTGTLAVNVSPPL	0.96
			462	LCMPNREVYSTPAATISRCG	0.924
			494	SIDCMLIINKPKGVATYTLT	0.906
			80	GPGLITNTEGQITVENVNKV[2]	0.801

Note: 3 indicate the peptide shared in IEDB, BCPred and ElliPro;2 indicate the peptide shared in the BCPred and ElliPro; 3 indicate the peptide shared in the IEDB and BCPred.

B

CAdV-1-JL2021 Fiber Predict discontinuous B cell epitopes

C

CAdV-1-JL2021 Fiber Predict discontinuous B cell epitopes

D

CAdV-1-JL2021 Fiber Predict discontinuous B cell epitopes

E

CAdV-2-AC_000020.1 Fiber Predict discontinuous B cell epitopes

F

CAdV-2-AC_000020.1 Fiber Predict discontinuous B cell epitopes

G

Table 2 CAdV-1-JL2021 Fiber MHC-I-binding prediction

MHC-I-binding prediction						Class I Immunogenicity
Start	Length	Peptide	Core	Icore	Score	Score
411	9	SVSPTQSQF	SVSPTQSQF	SVSPTQSQF	0.908508	-0.3434
202	9	AVQPPATTY	AVQPPATTY	AVQPPATTY	0.881208	-0.11481
166	9	KLGVKPTTY	KLGVKPTTY	KLGVKPTTY	0.6884	-0.11246
324	9	AVIGAGLKF	AVIGAGLKF	AVIGAGLKF	0.65845	-0.0372
273	9	ATTSPTLTF	ATTSPTLTF	ATTSPTLTF	0.620697	0.01194
237	9	VATPPNVTF	VATPPNVTF	VATPPNVTF	0.608149	0.03271
45	10	AVNISPPLTF	AVISPPLTF	AVNISPPLTF	0.607742	0.03515
417	9	SQFSLILEF	SQFSLILEF	SQFSLILEF	0.574884	0.04207
188	9	RVGPGLTVL	RVGPGLTVL	RVGPGLTVL	0.563813	0.07928

Note: High Score = good binder

H

Table 3 CAdV-2-AC_000020.1 Fiber MHC-I-binding prediction

MHC-I-binding prediction						Class I Immunogenicity
Start	Length	Peptide	Core	Icore	Score	Score
410	9	IVSPTQSQF	IVSPTQSQF	IVSPTQSQF	0.915614	0.03271
202	9	AVQPPATTY	AVQPPATTY	AVQPPATTY	0.881208	-0.01786
274	9	ATPPPPLTF	ATPPPPLTF	ATPPPPLTF	0.767871	-0.02268
238	9	ATPPPPLTF	ATPPPPLTF	ATPPPPLTF	0.767871	-0.02268
409	10	RIVSPTQSQF	RIVSPTQSF	RIVSPTQSQF	0.707647	-0.10369
166	9	KLGVKPTTY	KLGVKPTTY	KLGVKPTTY	0.6884	-0.11246
416	9	SQFSLIMEF	SQFSLIMEF	SQFSLIMEF	0.584639	-0.12958
45	10	AVNVSPPLTF	AVNSPPLTF	AVNVSPPLTF	0.556915	-0.3434
325	9	AVVGAGLKF	AVVGAGLKF	AVVGAGLKF	0.535046	-0.44241

Note: High Score = good binder

I

Table 4 CAdV-1-JL2021 Fiber MHC-II Binding Prediction

MHC-II Binding Prediction				Class I Immunogenicity
Start	Length	Peptide	Adjusted rank	Score
37	18	FLNFNKLSSSTVFKTDVL	0.65	-0.25645
35	18	FRFLNFNKLSSSTVFKTD	0.65	-0.26964
36	18	RFLNFNKLSSSTVFKTDV	0.65	-0.42944
34	18	TFRFLNFNKLSSSTVFKT	0.65	-0.53332
33	18	LTFRFLNFNKLSSSTVFK	0.77	-0.54698
38	18	LNFNKLSSSTVFKTDVLT	0.86	-0.57179
32	18	TLTFRFLNFNKLSSSTVF	0.92	-0.60357

Note: Low adjusted rank = good binders

J

Table 5 CAdV-2-AC_000020.1 Fiber MHC-II Binding Prediction

MHC-II Binding Prediction				Class I Immunogenicity
Start	Length	Peptide	Adjusted rank	Score
52	18	LTFSTLGAIKLSTGPGLT	1.45	-0.10142
47	18	NVSPPLTFSTLGAIKLST	1.72	-0.10476
51	18	PLTFSTLGAIKLSTGPGL	1.72	-0.10718
50	18	PPLTFSTLGAIKLSTGPG	1.72	-0.12033
49	18	SPPLTFSTLGAIKLSTGP	1.72	-0.14454
53	18	TFSTLGAIKLSTGPGLTL	1.72	-0.17708
48	18	VSPPLTFSTLGAIKLSTG	1.72	-0.20019

Note: Low adjusted rank = good binders

FIGURE 4 | The epitope analysis of the Fiber protein. **(A)** Table 1 B cell linear epitope prediction; **(B–D)** CAdV-1 JL2021 Fiber discontinuous epitopes; **(E, F)** CAdV-2-AC_000020.1 Fiber discontinuous epitopes; **(G)** Table 2 CAdV-1-JL2021 Fiber MHC-I-binding prediction; **(H)** Table 3 CAdV-2-AC_000020.1 Fiber MHC-I-binding prediction. **(I)** Table 4 CAdV-1-JL2021 Fiber MHC-II Binding Prediction; **(J)** CAdV-2-AC_000020.1 Fiber MHC-II Binding Prediction.

identification of highly conserved regions useful to implement new future diagnostic protocols.

Natural recombination is an important strategy for viruses to adapt to new environmental conditions and hosts. Besides evolving through nucleotide substitution, viruses frequently also evolve by genetic recombination which can occur when related viral variants co-infect the same cells (Varsani et al., 2018). More CAdV genome sequences were added to GenBank, CAdV-1 and CAdV-2 sequences arising from different parts of world. Therefore, it is necessary to find the recombination for genetic variability, and it will be helpful to understand the evolutionary process of the CAdV genome (Eltahir et al., 2011). In our experiment, recombination break-point were observed in the 143 site of CAdV-1-JL2021 *Fiber, and 397, 1558 site of* CAdV-2-AC_000020.1. In the evolution of the CAdV-1 populations, the recombination was not a common event. The genetic diversity of CAdV-1 evolutionary maybe attribute to the recombination. During the infection, the same animal maybe infected by different CAdV genotypes, and this condition will contribute to the CAdV recombination.

The subcellular location of a protein is highly related to its function (Pan et al., 2020). Identifying the location of a given protein is an essential step for investigating its related function. The host cell membrane was the subcellular location of the CAdV-1-JL2021 and CAdV-2-AC_000020.1. But host cytoplasm was also the subcellular location of the CAdV-2-AC_000020.1. It indicates that they may have different function during the virus infection. It predicted that CAdV-1-JL2021 and CAdV-2-AC_000020.1*Fiber* exerted adhesion receptor-mediated virion attachment to host cell. More evidences need to further find the function difference between the CAdV-1 and CAdV-2.

In the process of CAdV infection, the *Fiber* protein interacts with the host cell receptor to adsorb on the host cell. While much of the current literature focuses on analysis of the *Fiber* gene nucleic acid sequence of virus isolates (Schoehn et al., 2008), few have gone so far as to predict the molecular characteristics of the *Fiber* protein. The isoelectric point was predicted to be 6.26. When pH of the environment was 6.26, the net surface charge of CAdV-1-JL2021 *Fiber* protein was 0. At this time, the *Fiber* proteins repeled each other in solution, the force between

molecules was weakened, and *Fiber* precipitation occured readily. Thus, at the isoelectric point, *Fiber* protein was easy to obtain because of its low solubility. When the instability coefficient of the protein was greater than 40, it was considered to be an unstable protein (Dong et al., 2021). The total average hydrophobicity of the hydrophilic protein was less than 0 (Zhou, 2016). The average hydrophobicity of the CAdV-1-JL2021 *Fiber* protein was -0.092, suggesting that it was a hydrophilic protein. Protein dissolution in supernatant was an ideal result of prokaryotic expression, but the specific distribution of protein in supernatant and precipitation still need to be analyzed by SDS-PAGE. In the prokaryotic expression and purification of *Fiber* protein, the corresponding test scheme can be formulated according to its hydrophilic characteristics.

Protein phosphorylation is crucial for multiple biological processes including signal transduction, regulation of cell cycle and gene expression through post-translational modifications (Luo et al., 2019; Mehrpouyan et al., 2021). For example, the N protein phosphorylation impairs porcine reproductive and respiratory syndrome virus growth efficiency in porcine alveolar macrophages (Chen et al., 2019). Thus, it is important to predict protein phosphorylation sites in the *Fiber* protein. It was predicted that CAdV-1-JL2021 *Fiber* protein had 107 phosphorylation sites. The phosphorylation of *Fiber* protein is related to its antigenicity and virulence. Like phosphorylation, glycosylation is also an important post-translational modification, which affects the structure and function of proteins (Macedo-da-Silva et al., 2021). The glycosylation of the Newcastle disease virus (Kosakovsky Pond et al., 2006) resulted in a virus that was able to proliferate faster than that of the vaccine (Schön et al., 2021). The CAdV-1-JL2021 *Fiber* protein has six glycosylation sites, suggesting that it is related to the virus titer and proliferation rate of CAdV-1. The phosphorylation sites and glycosylation sites of CAdV-1-JL2021 *Fiber* protein is the same as that of CAdV-2-AC_000020.1 *Fiber* protein. It indicates that they have the same function.

The secondary structure prediction results showed that the extended chain and irregular curl accounted for the majority of the *Fiber* protein secondary structure. The irregular curl is responsible for a protein's enzymatic activity and protein specific functions (Simm et al., 2021). It was also observed that the CAdV-1-JL2021 and CAdV-2-AC_000020.1 *Fiber* protein contains a large number of antigenic determinants, which is consistent with the prediction results of antigenic determinants. Antigenic determinants can specifically bind to corresponding antibodies or B cells. Since the *Fiber* protein is the main capsid protein on the adenovirus surface, its antigenic determinants can cause strong neutralization reactions. Therefore, predicting the antigenic determinants of *Fiber* protein and the dominant B cell epitopes is helpful to understand the mechanisms of viral neutralization *via* responses to the *Fiber* protein.

The Knob of the adenovirus *Fiber* protein is used for attachment of the virus to a specific receptor on the cell surface. The coxsackievirus and adenovirus receptor (CAR) was both a viral receptor and cell adhesion protein (Readler et al., 2019). CAV-2 had been shown to use CAR as a primary receptor (Soudais et al., 2000). But limited data showed the interaction between Knob of the *Fiber* and the CAR. The CAdV-1 and CAdV-2 fiber–knobs may share a common receptor as evidenced by the ability of the CAdV- 1 knob to inhibit Ad5Luc1-CK2 function (Stoff-Khalili et al., 2005). In our experiment, The *Fiber* in CAdV-1-JL2021 and CAdV-2-AC_000020.1, CAR were predicted. The binding model between *Fiber* and CAR was also predicted. It will be helpful to clarify the interaction between *Fiber* and CAR.

The B cell linear peptide "VATTSPTLTFAYPLIKNNNH" in CAdV-1-JL2021 was predicted by the IEDB, BCPred and ElliPro. It indicates that this peptide had high potential in the epitope vaccine design. The B cell linear peptides "STGNINSTTTWGEKPWGNNT" of CAdV-2-AC_000020.1 were both predicted by the IEDB and BCPred. CAdV-1-JL2021 and CAdV-2-AC_000020.1 *Fiber* did not have the same peptide. It indicates that B cell linear epitope vaccine should be developed in the CAdV-1-JL2021 and CAdV-2-AC_000020.1, respectively. Importantly, the T cell peptide "KLGVKPTTY" were both predicted in the CAdV-1-JL2021 and CAdV-2-AC_000020.1 Fiber. It indicates that T cell epitope vaccine maybe both efficient for the CAdV-1-JL2021 and CAdV-2-AC_000020.1, respectively.

CONCLUSION

In this experiment, the CAdV-1-JL2021 strain was isolated successfully, and were most similar to the CAdV-1 strain circulating in Italy. The occurrence of negative selection and recombination were found in the CAdV-1-JL2021. Host cell membrane was its subcellular localization. The CAdV-1-JL2021 *Fiber* (ON164651) exerted adhesion receptor-mediated virion attachment to host cell, which was the same as CAdV-2-AC_000020.1 Fiber. "VATTSPTLTFAYPLIKNNNH" were predicted to be the potential CAdV-1 B cell linear epitope. The MHC-I binding peptide "KLGVKPTTY" were both predicted in the CAdV-1-JL2021 and CAdV-2-AC_000020.1 *Fiber*, and it is useful to design the canine adenovirus epitope vaccine.

DATA AVAILABILITY STATEMENT

The original contributions presented in the study are included in the article/supplementary files. Further inquiries can be directed to the corresponding author.

ETHICS STATEMENT

This experiment was approved on April 2 in 2021 by Jilin Agriculture Science and Technology College and the procedures complied with IACUCS guidelines on the animals' care and use for scientific purposes.

AUTHOR CONTRIBUTIONS

BW and MW conduct the experiment. HZ, JX, and JH analyze the data and draw the picture. YZ designed and provide the grant for this experiment. YZ also reviews the manuscript. All authors contributed to the article and approved the submitted version.

FUNDING

This work was supported by grants from the Science and Technology department of Jilin Province (20200402045NC) and the Doctoral Start-up Fund Project of the Jilin Agriculture Science and Technology College (20200002).

REFERENCES

Balboni, A., Musto, C., Kaehler, E., Verin, R., Caniglia, R., Fabbri, E., et al. (2019). Genetic Characterization of Canine Adenovirus Type 1 Detected by Real-Time Polymerase Chain Reaction in an Oral Sample of an Italian Wolf (Canis Lupus). *J. Wildl. Dis.* 55, 737–741. doi: 10.7589/2018-08-206

Balboni, A., Terrusi, A., Urbani, L., Troia, R., Stefanelli, S. A. M., Giunti, M., et al. (2022). Canine Circovirus and Canine Adenovirus Type 1 and 2 in Dogs With Parvoviral Enteritis. *Vet. Res. Commun.* 46, 223–232. doi: 10.1007/s11259-021-09850-y

Balboni, A., Tryland, M., Mørk, T., Killengreen, S. T., Fuglei, E., and Battilani, M. (2019). Unique Genetic Features of Canine Adenovirus Type 1 (CAdV-1) Infecting Red Foxes (Vulpes Vulpes) in Northern Norway and Arctic Foxes (Vulpes Lagopus) in Svalbard. *Vet. Res. Commun.* 43, 67–76. doi: 10.1007/s11259-019-09746-y

Blom, N., Gammeltoft, S., and Brunak, S. (1999). Sequence and Structure-Based Prediction of Eukaryotic Protein Phosphorylation Sites. *J. Mol. Biol.* 294, 1351–1362. doi: 10.1006/jmbi.1999.3310

Chen, Y., Yu, Z., Yi, H., Wei, Y., Han, X., Li, Q., et al. (2019). The Phosphorylation of the N Protein Could Affect PRRSV Virulence *In Vivo*. *Vet. Microbiol.* 231, 226–231. doi: 10.1016/j.vetmic.2019.03.018

Choi, J. W., Lee, H. K., Kim, S. H., Kim, Y. H., Lee, K. K., Lee, M. H., et al. (2014). Canine Adenovirus Type 1 in a Fennec Fox (Vulpes Zerda). *J. Zoo Wildl. Med.* 45, 947–950. doi: 10.1638/2013-0286.1

Chou, K. C., and Shen, H. B. (2008). Cell-PLoc: A Package of Web Servers for Predicting Subcellular Localization of Proteins in Various Organisms. *Nat. Protoc.* 3, 153–162. doi: 10.1038/nprot.2007.494

Deléage ALIGNSEC, G. (2017). Viewing Protein Secondary Structure Predictions Within Large Multiple Sequence Alignments. *Bioinformatics* 33, 3991–3992. doi: 10.1093/bioinformatics/btx521

De Luca, C., Schachner, A., Mitra, T., Heidl, S., Liebhart, D., and Hess, M. (2020). Fowl Adenovirus (FAdV) Fiber-Based Vaccine Against Inclusion Body Hepatitis (IBH) Provides Type-Specific Protection Guided by Humoral Immunity and Regulation of B and T Cell Response. *Vet. Res.* 51, 143. doi: 10.1186/s13567-020-00869-8

Dong, D., Wang, X., Deng, T., Ning, Z., Tian, X., Zu, H., et al. (2021). A Novel Dextranase Gene From the Marine Bacterium Bacillus Aquimaris S5 and its Expression and Characteristics. *FEMS Microbiol. Lett.* 368 (3), fnab007. doi: 10.1093/femsle/fnab007

El-Manzalawy, Y., Dobbs, D., and Honavar, V. (2008). Predicting Linear B-Cell Epitopes Using String Kernels. *J. Mol. Recognit.* 21, 243–255. doi: 10.1002/jmr.893

Eltahir, Y. M., Qian, K., Jin, W., and Qin, A. (2011). Analysis of Chicken Anemia Virus Genome: Evidence of Intersubtype Recombination. *Virol. J.* 8, 512–512. doi: 10.1186/1743-422X-8-512

Foroutan, M., Ghaffarifar, F., Sharifi, Z., Dalimi, A., and Pirestani, M. (2018). Bioinformatics Analysis of ROP8 Protein to Improve Vaccine Design Against Toxoplasma Gondii. *Infect. Genet. Evol.* 62, 193–204. doi: 10.1016/j.meegid.2018.04.033

Gupta, A., Ahmed, K. A., Ayalew, L. E., Popowich, S., Kurukulasuriya, S., Goonewardene, K., et al. (2017). Immunogenicity and Protective Efficacy of Virus-Like Particles and Recombinant Fiber Proteins in Broiler-Breeder Vaccination Against Fowl Adenovirus (FAdV)-8b. *Vaccine* 35, 2716–2722. doi: 10.1016/j.vaccine.2017.03.075

Gupta, R., and Brunak, S. (2002). Prediction of Glycosylation Across the Human Proteome and the Correlation to Protein Function. *Pac. Symp. Biocomput.* 2002, 310–322.

Haasdijk, E., and Heinerman, J. (2018). Quantifying Selection Pressure. *Evol. Comput.* 26, 213–235. doi: 10.1162/EVCO_a_00207

Hu, R. L., Huang, G., Qiu, W., Zhong, Z. H., Xia, X. Z., and Yin, Z. (2001). Detection and Differentiation of CAV-1 and CAV-2 by Polymerase Chain Reaction. *Vet. Res. Commun.* 25, 77–84. doi: 10.1023/a:1006417203856

Kosakovsky Pond, S. L., and Frost, S. D. (2005). Not So Different After All: A Comparison of Methods for Detecting Amino Acid Sites Under Selection. *Mol. Biol. Evol.* 22, 1208–1222. doi: 10.1093/molbev/msi105

Kosakovsky Pond, S. L., Posada, D., Gravenor, M. B., Woelk, C. H., and Frost, S. D. (2006). Automated Phylogenetic Detection of Recombination Using a Genetic Algorithm. *Mol. Biol. Evol.* 23, 1891–1901. doi: 10.1093/molbev/msl051

Krogh, A., Larsson, B., von Heijne, G., and Sonnhammer, E. L. (2001). Predicting Transmembrane Protein Topology With a Hidden Markov Model: Application to Complete Genomes. *J. Mol. Biol.* 305, 567–580. doi: 10.1006/jmbi.2000.4315

Lin, Z., Li, Y., Gong, G., Xia, Y., Wang, C., Chen, Y., et al. (2018). Restriction of H1N1 Influenza Virus Infection by Selenium Nanoparticles Loaded With Ribavirin via Resisting Caspase-3 Apoptotic Pathway. *Inter. J. Nanomed.* 13, 5787. doi: 10.2147/IJN.S177658

Luo, F., Wang, M., Liu, Y., Zhao, X.-M., and Li, A. (2019). DeepPhos: Prediction of Protein Phosphorylation Sites With Deep Learning. *Bioinformatics* 35, 2766–2773. doi: 10.1093/bioinformatics/bty1051

Macedo-da-Silva, J., Santiago, V. F., Rosa-Fernandes, L., Marinho, C. R. F., and Palmisano, G. (2021). Protein Glycosylation in Extracellular Vesicles: Structural Characterization and Biological Functions. *Mol. Immunol.* 135, 226–246. doi: 10.1016/j.molimm.2021.04.017

Madeira, F., Pearce, M., Tivey, A. R. N., Basutkar, P., Lee, J., Edbali, O., et al. (2022). Search and Sequence Analysis Tools Services From EMBL-EBI in 2022. *Nucleic Acids Res.* 2022, 1–4. doi: 10.1093/nar/gkac240

Mehrpouyan, S., Menon, U., Tetlow, I. J., and Emes, M. J. (2021). Protein Phosphorylation Regulates Maize Endosperm Starch Synthase IIa Activity and Protein-Protein Interactions. *Plant J.* 105, 1098–1112. doi: 10.1111/tpj.15094

Nerli, S., and Sgourakis, N. G. (2019). CS-ROSETTA. *Methods Enzymol.* 614, 321–362. doi: 10.1016/bs.mie.2018.07.005

Nielsen, H., Tsirigos, K. D., Brunak, S., and von Heijne, G. A. (2019). Brief History of Protein Sorting Prediction. *Protein J.* 38, 200–216. doi: 10.1007/s10930-019-09838-3

Oleaga, A., Balseiro, A., Espí, A., and Royo, L. J. (2021). Wolf (Canis Lupus) as Canine Adenovirus Type 1 (CAdV-1) Sentinel for the Endangered Cantabrian Brown Bear (Ursus Arctos Arctos). *Transbound Emerg. Dis.* 69 (2), 516–523. doi: 10.1111/tbed.14010

Pan, X., Lu, L., and Cai, Y. D. (2020). Predicting Protein Subcellular Location With Network Embedding and Enrichment Features. *Biochim. Biophys. Acta Proteins Proteom.* 1868, 140477. doi: 10.1016/j.bbapap.2020.140477

Pizzurro, F., Marcacci, M., Zaccaria, G., Orsini, M., Cito, F., Rosamilia, A., et al. (2017). Genome Sequence of Canine Adenovirus Type 1 Isolated From a Wolf (Canis Lupus) in Southern Italy. *Genome Announcements* 5, e00225–e00217. doi: 10.1128/genomeA.00225-17

Prasad, S., Potdar, V., Cherian, S., Abraham, P., Basu, A., and Team, I. C. (2020). Transmission Electron Microscopy Imaging of SARS-CoV-2. *Indian J. Med. Res.* 151, 241. doi: 10.4103/ijmr.IJMR_577_20

Readler, J. M., AlKahlout, A. S., Sharma, P., and Excoffon, K. (2019). Isoform Specific Editing of the Coxsackievirus and Adenovirus Receptor. *Virology* 536, 20–26. doi: 10.1016/j.virol.2019.07.018

Ruan, S., Zhao, J., Yin, X., He, Z., and Zhang, G. (2018). A Subunit Vaccine Based on Fiber-2 Protein Provides Full Protection Against Fowl Adenovirus Serotype 4 and Induces Quicker and Stronger Immune Responses Than an Inactivated

Oil-Emulsion Vaccine. *Infect. Genet. Evol.* 61, 145–150. doi: 10.1016/j.meegid.2018.03.031

Sanjuán, R., and Domingo-Calap, P. (2016). Mechanisms of Viral Mutation. *Cell. Mol. Life Sci.* 73, 4433–4448. doi: 10.1007/s00018-016-2299-6

Schoehn, G., El Bakkouri, M., Fabry, C. M., Billet, O., Estrozi, L. F., Le, L., et al. (2008). Three-Dimensional Structure of Canine Adenovirus Serotype 2 Capsid. *J. Virol.* 82, 3192–3203. doi: 10.1128/JVI.02393-07

Schön, K., Lepenies, B., and Goyette-Desjardins, G. (2021). Impact of Protein Glycosylation on the Design of Viral Vaccines. *Adv. Biochem. Eng. Biotechnol.* 175, 319–354. doi: 10.1007/10_2020_132

Simm, D., Hatje, K., Waack, S., and Kollmar, M. (2021). Critical Assessment of Coiled-Coil Predictions Based on Protein Structure Data. *Sci. Rep.* 11, 12439. doi: 10.1038/s41598-021-91886-w

Soudais, C., Boutin, S., Hong, S. S., Chillon, M., Danos, O., Bergelson, J. M., et al. (2000). Canine Adenovirus Type 2 Attachment and Internalization: Coxsackievirus-Adenovirus Receptor, Alternative Receptors, and an RGD-Independent Pathway. *J. Virol.* 74, 10639–10649. doi: 10.1128/jvi.74.22.10639-10649.2000

Stoff-Khalili, M., Rivera, A., Glasgow, J., Le, L., Stoff, A., Everts, M., et al. (2005). A Human Adenoviral Vector With a Chimeric Fiber From Canine Adenovirus Type 1 Results in Novel Expanded Tropism for Cancer Gene Therapy. *Gene Ther.* 12, 1696–1706. doi: 10.1038/sj.gt.3302588

Sun, J., Qin, F. Y., Zhu, Y. Z., Xue, X. H., Wang, Y., Lian, S. Z., et al. (2019). Comparison of Pathogenicity of Canine Adenovirus Type 1 to Arctic Fox and Silver Fox. *Chin. Vet. Sci.* 49, 625–631. doi: 10.16656/j.issn.1673-4696.2019.0094

Tamukai, K., Minami, S., Kurihara, R., Shimoda, H., Mitsui, I., Maeda, K., et al. (2020). Molecular Evidence for Vaccine-Induced Canine Distemper Virus and Canine Adenovirus 2 Coinfection in a Fennec Fox. *J. Vet. Diagn. Invest.* 32, 598–603. doi: 10.1177/1040638720934809

Timurkan, M. O., Aydin, H., and Alkan, F. (2018). Detection and Molecular Characterization of Canine Adenovirus Type 2 (CAV-2) in Dogs With Respiratory Tract Symptoms in Shelters in Turkey. *Vet. Arh.* 88, 467–479. doi: 10.24099/vet.arhiv.0052

Varsani, A., Lefeuvre, P., Roumagnac, P., and Martin, D. (2018). Notes on Recombination and Reassortment in Multipartite/Segmented Viruses. *Curr. Opin. Virol.* 33, 156–166. doi: 10.1016/j.coviro.2018.08.013

Verin, R., Forzan, M., Schulze, C., Rocchigiani, G., Balboni, A., Poli, A., et al. (2019). Multicentric Molecular and Pathologic Study On Canine Adenovirus Type 1 in Red Foxes (Vulpes Vulpes) in Three European Countries. *J. Wildl. Dis.* 55, 935–939. doi: 10.7589/2018-12-295

Vita, R., Mahajan, S., Overton, J. A., Dhanda, S. K., Martini, S., Cantrell, J. R., et al. (2019). The Immune Epitope Database (IEDB): 2018 Update. *Nucleic Acids Res.* 47, D339–d343. doi: 10.1093/nar/gky1006

Walker, J. M. (2005). *The Proteomics Protocols Handbook* (Hatfield, UK: Springer).

Walters, R. W., Freimuth, P., Moninger, T. O., Ganske, I., Zabner, J., and Welsh, M. J. (2002). Adenovirus Fiber Disrupts CAR-Mediated Intercellular Adhesion Allowing Virus Escape. *Cell* 110, 789–799. doi: 10.1016/s0092-8674(02)00912-1

Yang, D.-K., Kim, H.-H., Lee, E.-J., Yoo, J.-Y., Yoon, S.-S., Park, J., et al. (2019). Recharacterization of the Canine Adenovirus Type 1 Vaccine Strain Based on the Biological and Molecular Properties. *jbv* 49, 124–132. doi: 10.4167/jbv.2019.49.3.124

Zhou, S. (2016). *Cloning and Functional Analysis of Fm4CL Family Gene From Fraxinus Mandshurica* (Harbin, China: Northeast Forestry University).

Zhu, Y., Sun, J., Yan, M., Lian, S., Hu, B., Lv, S., et al. (2020). The Biological Characteristics of the Canine Adenovirus Type 1 From Fox and the Transcriptome Analysis of the Infected MDCK Cell. *Cell Biol. Int.* 45 (5), 936–947. doi: 10.1002/cbin.11537

Conflict of Interest: The authors declare that the research was conducted in the absence of any commercial or financial relationships that could be construed as a potential conflict of interest.

Publisher's Note: All claims expressed in this article are solely those of the authors and do not necessarily represent those of their affiliated organizations, or those of the publisher, the editors and the reviewers. Any product that may be evaluated in this article, or claim that may be made by its manufacturer, is not guaranteed or endorsed by the publisher.

frontiers | Frontiers in Cellular and Infection Microbiology

REVIEW
published: 14 June 2022
doi: 10.3389/fcimb.2022.931061

Mechanism of COVID-19 Causing ARDS: Exploring the Possibility of Preventing and Treating SARS-CoV-2

Jiajing Zheng[1†], Jiameng Miao[1†], Rui Guo[2,3†], Jinhe Guo[1], Zheng Fan[4], Xianbin Kong[1], Rui Gao[5*] and Long Yang[2,3*]*

[1] College of Traditional Chinese medicine, Tianjin University of Traditional Chinese Medicine, Tianjin, China, [2] Research Center for Infectious Diseases, Tianjin University of Traditional Chinese Medicine, Tianjin, China, [3] School of Integrative Medicine, Tianjin University of Traditional Chinese Medicine, Tianjin, China, [4] Department of Critical Medicine, The First Affiliated Hospital of Suzhou University, Suzhou, China, [5] Institute of Clinical Pharmacology of Xiyuan Hospital, China Academy of Chinese Medical Sciences, Beijing, China

OPEN ACCESS

Edited by:
Zhanbo Zhu,
Heilongjiang Bayi Agricultural University, China

Reviewed by:
Tong-Qing An,
Harbin Veterinary Research Institute (CAAS), China
Zhiyong Li,
Lanzhou Veterinary Research Institute (CAAS), China

***Correspondence:**
Xianbin Kong
kongxianbinvip@163.com
Rui Gao
ruigao@126.com
Long Yang
long.yang@tjutcm.edu.cn

[†]These authors have contributed equally to this work

Specialty section:
This article was submitted to Clinical Microbiology, a section of the journal Frontiers in Cellular and Infection Microbiology

Received: *28 April 2022*
Accepted: *12 May 2022*
Published: *14 June 2022*

Citation:
Zheng J, Miao J, Guo R, Guo J, Fan Z, Kong X, Gao R and Yang L (2022) Mechanism of COVID-19 Causing ARDS: Exploring the Possibility of Preventing and Treating SARS-CoV-2. Front. Cell. Infect. Microbiol. 12:931061. doi: 10.3389/fcimb.2022.931061

Novel coronavirus pneumonia (COVID-19) is spreading worldwide, causing great harm and stress to humans. Since patients with novel coronavirus (SARS-CoV-2) have a high probability of developing acute respiratory distress syndrome (ARDS) in severe cases, the pathways through which SARS-CoV-2 causes lung injury have become a major concern in the scientific field. In this paper, we investigate the relationship between SARS-CoV-2 and lung injury and explore the possible mechanisms of COVID-19 in ARDS from the perspectives of angiotensin-converting enzyme 2 protein, cytokine storm, activation of the immune response, triggering of Fas/FasL signaling pathway to promote apoptosis, JAK/STAT pathway, NF-κB pathway, type I interferon, vitamin D, and explore the possibility of prevention and treatment of COVID-19. To explore the possibility of SARS-CoV-2, and to provide new ideas to stop the development of ARDS in COVID-19 patients.

Keywords: novel coronavirus, acute respiratory distress syndrome, angiotensin-converting enzyme II protein, cytokine storm, immune response, NF-κB pathway, type I interferon

1 PREFACE

The SARS-CoV-2 was first discovered in China and showed a multi-point outbreak worldwide. For a long time, human life safety and health have been facing a great threat, and the COVID-19 pandemic has caused more than 1 million deaths worldwide. Some data show that the mortality rate of COVID-19 infection is 26%, the ICU admission rate is 47%, and the risk rate of ARDS due to COVID-19 is 3.2 (aOR, 3.20; 95% CI: 1.65-6.18; p=0.001) (Khamis et al., 2021). SARS-CoV-2 has received widespread attention. The World Health Organization (WHO) declared it a global epidemic and tentatively named the coronavirus as 2019 novel coronavirus (2019-nCoV), and pneumonia infected by this virus as "COVID-19", which was officially named by the International Committee on Classification of Viruses as "SARS-CoV-2".

The most common symptom of COVID-19 disease is fever with coughing, sneezing, weakness, and shortness of breath, which can rapidly develop into acute respiratory distress syndrome in severe cases (Zarrilli et al., 2021). Currently, a large number of studies have been made on the pathogenic mechanism of SARS-CoV-2, but the medical community still has a limited

understanding of SARS-CoV-2. Since the SARS-CoV-2 is a highly transmissible and lethal virus and undergoes rapid recombination and mutation in the human body, forming a variety of mutant strains and creating new virulence, this poses a great challenge to humans in the process of antiviral therapy. Understanding the mechanism of lung injury caused by SARS-CoV-2 will best help us find ways to prevent and treat this disease. In this paper, we will discuss the mechanisms of the acute respiratory syndrome caused by SARS-CoV-2 in terms of angiotensin-converting enzyme 2 protein, cytokine storm, activated immune response, triggering Fas/FasL signaling pathway for pro-apoptosis, JAK/STAT pathway, NF-κB pathway, type I interferon, and vitamin D (**Figure 1**).

2 ASSOCIATION OF SARS-COV-2 WITH ACUTE RESPIRATORY DISTRESS SYNDROME

SARS-CoV-2 causes a positive correlation between the incidence and severity of ARDS, and the challenges associated with SARS-CoV-2 and this syndrome are becoming more prominent, for example in terms of their high mortality rate and the lack of effective pharmacological treatment (Meyer et al., 2021). ARDS is characterized histologically by diffuse alveolar damage with increased vascular permeability and reduced compliance, affecting gas exchange and leading to intractable hypoxemia (Batah and Fabro, 2021). Over the last 50 years, researchers have conducted numerous basic and clinical studies on ARDS, but the morbidity and mortality of ARDS remain high and there is a lack of specific drugs for ARDS. Currently, 15-30% of people hospitalized with COVID-19 will go on to develop ARDS (Attaway et al., 2021).

Gibson et al (Gibson et al., 2020) concluded that the prognosis of COVID-19 ARDS appears to be worse than that of ARDS due to other causes, which are pneumonia, pulmonary contusion, toxic substance inhalation, and severe systemic infections. Mortality rates ranged from 26% to 61.5% in patients with COVID-19 ARDS who had been admitted to an intensive care unit, and from 65.7% to 94% in patients receiving mechanical ventilation. Several analyses have shown that COVID-19 ARDS has pathophysiological features similar to those of non-COVID-19 ARDS, namely reduced respiratory compliance, high respiratory mechanics heterogeneity, and hypoxemia. The study suggests that lung-protective ventilation should be implemented in all mechanically ventilated patients with COVID-19 ARDS, and noninvasive ventilation can be performed in mild and moderate patients using dedicated respiratory arrest (Grasselli et al., 2021). Severe COVID-19 produces impairment of ARDS-like hyper inflammation and endothelial dysfunction, ultimately leading to respiratory and multiorgan failure and death. A proportion of surviving patients will have a persistent fibroproliferative response, and interstitial lung disease (ILD) and pulmonary fibrosis will in turn lead to an increased risk of severe disease (Ntatsoulis et al., 2021). This disease is difficult to control in advanced stages, and early treatment is critical for prognosis in controlling and improving symptoms such as pulmonary inflammation, thick airway mucus secretion, elevated levels of pro-inflammatory cytokines, lung injury, and micro thrombosis in patients with ARDS due to SARS-CoV-2 (Quesada-Gomez et al., 2020).

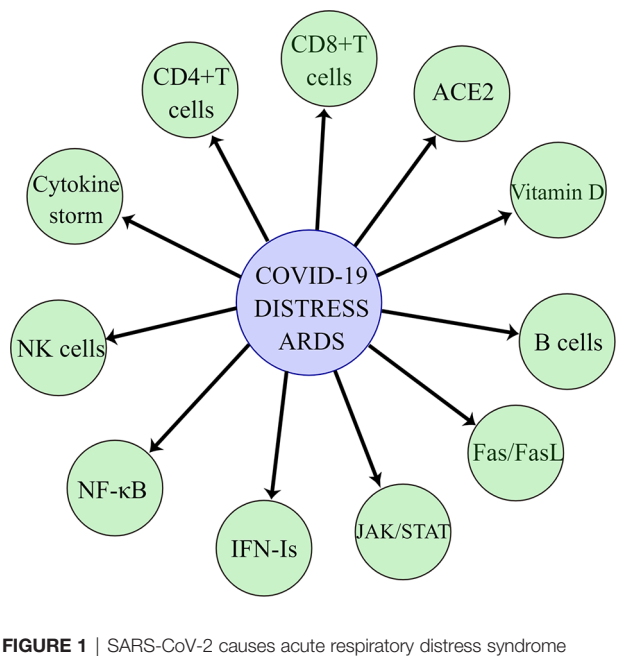

FIGURE 1 | SARS-CoV-2 causes acute respiratory distress syndrome through angiotensin-converting enzyme 2, cytokine storm, immune cells, Fas/FasL pathway, JAK/STAT pathway, NF-κB pathway, type I interferon, and vitamin D.

3 POSSIBLE MECHANISMS OF THE ARDS CAUSED BY SARS-COV-2

3.1 SARS-CoV-2 S Protein Binds to Angiotensin-Converting Enzyme 2 (ACE2) Protein to Cause the ARDS

SARS-CoV-2 S protein in the respiratory tract with respect to alveolar type 2 epithelial cells angiotensin-converting enzyme 2. ACE2 was found to be a major indicator of mortality in COVID-19 patients, and overexpression of ACE2 enhanced viral entry. ACE2 is a transmembrane type I glycoprotein with two functional domains, the N-terminal peptidase domain, and the C-terminal domain, whose physiological role is to control blood pressure and vasoconstriction. SARS-CoV-2 S protein binding to ACE2 protein invades alveolar epithelial cells (Seyed Hosseini et al., 2020), inducing ARDS and leading to death in most patients (Balkhi, 2021). This shows that maintaining normal ACE2 levels in the lung is crucial. The study (Datta et al., 2020) found that ACE2 was expressed at high levels in the epithelial cells of the lung after the death of COVID-19 patients and that targeting the ACE2/Ang 1-7 axis and blocking the S-protein interaction of ACE2 with SARS-CoV-2 to prevent the entry of SARS-CoV-2 into the cells could be used to treat and prevent COVID-19. The study demonstrated (van Eeden et al., 2020a) that ACE2 is the cellular receptor for SARS-

CoV-2 entry into the host and that the high affinity of the receptor-binding domain (RBD) of the SARS-CoV-2 S protein for the ACE2 receptor accelerates the spread of SARS-CoV-2 (Chilamakuri and Agarwal, 2021) (**Figure 2**).

The study has pointed out the key role of ACE2 in acute lung injury through a clinical report of COVID-19 patients, in which ACE, angiotensin II, and angiotensin II type 1a receptor (AT1a) promote the development of the disease and induce pulmonary edema causing impairment of lung function (Verdecchia et al., 2020). It has been shown by mouse models that ACE-deficient mice have a significant improvement in lung function and pulmonary edema, and that recombinant ACE2 prevents mice from suffering acute lung injury. However, other contrary study found the mechanism of ACE2-causing lung injury in experiments with data from acute lung injury models as a decrease in intrapulmonary ACE2 levels, leading to increased vascular permeability, inflammatory cell aggregation, and severe hypoxia causing pulmonary edema (Imai et al., 2005). In conclusion, maintaining normal intrapulmonary ACE2 levels inhibits ARDS, while the mechanisms by which high or low ACE2 levels affect ARDS still need to be further explored and determined (**Figure 2**).

3.2 ARDS due to Cytokine Storm Triggered by SARS-CoV-2 Infection

Recently, a large number of domestic and international experts have pointed out that the severity of COVID-19 is associated with cytokine storm and that the overproduction of pro-inflammatory factors leads to acute respiratory distress syndrome and accelerates the death of patients. Cytokines are produced by a variety of immune cells, including natural killer cells and adaptive T and B lymphocytes (Ragab et al., 2020), which play an important regulatory role in the response to antiviral immunity and inflammation (Tisoncik et al., 2012). Cytokine storm (CS) refers to a series of clinical disorders caused by immune response disorders (Kim et al., 2021), such as inflammatory lung injury and ARDS (Li et al., 2020b),

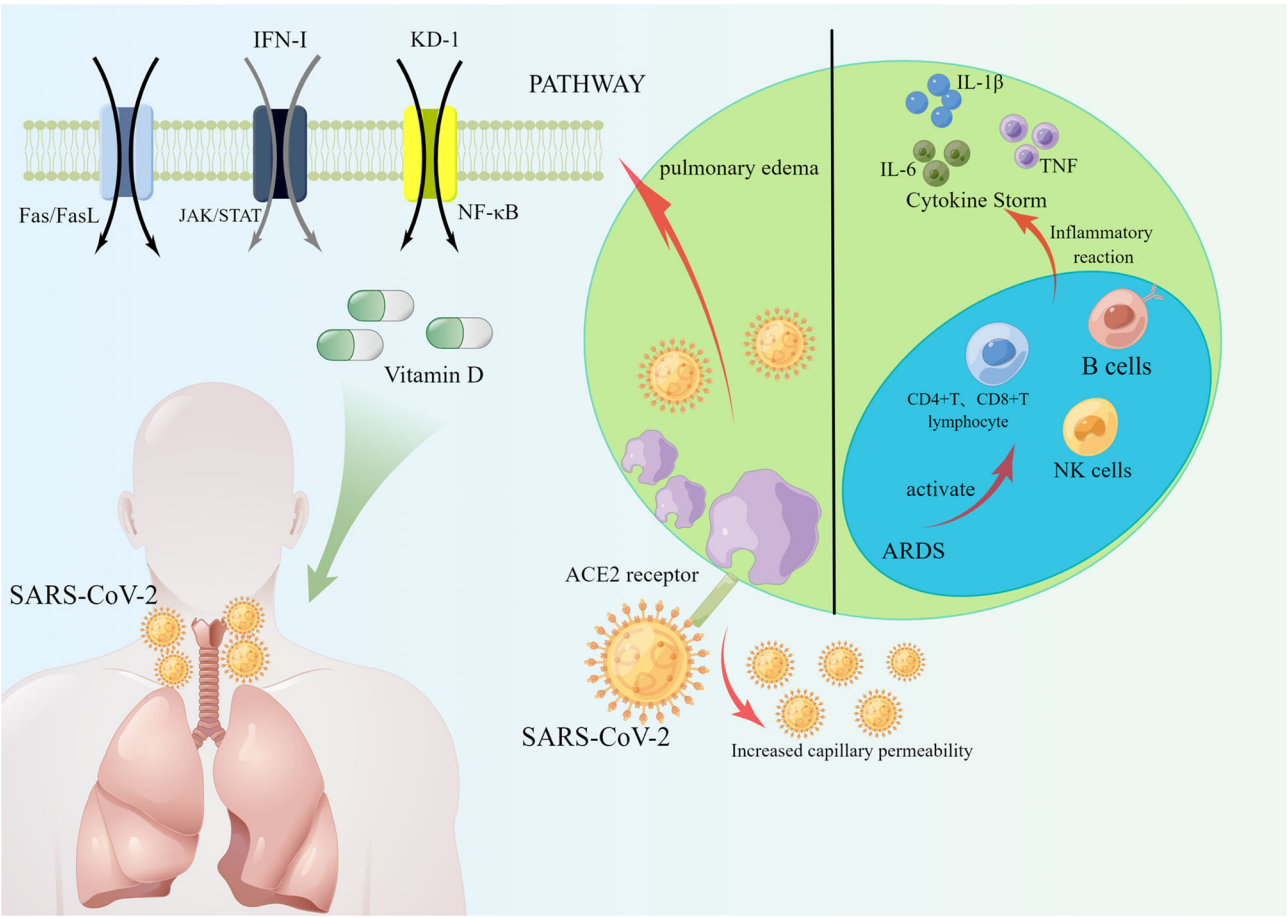

FIGURE 2 | SARS-CoV-2 enters cells through ACE2 receptors, and ACE2 increases capillary permeability, allowing more SARS-CoV-2 to enter cells, which in turn induces the development of ARDS. COVID-19 activated an immune response in which NK cells, CD4+ T lymphocytes, CD8+ T lymphocytes and B cells reacted immunologically in COVID-19 patients, causing the production of cytokines IL-6, IL-1β, TNF, etc. Reducing COVID-19 infection and prevent ARDS through Fas/FasL pathway, JAK/STAT pathway, and NF-κB pathway. Helping patients to prevent and treat COVID-19 by increasing type I interferon and vitamin D.

accompanied by the rapid production of large amounts of cytokines (IL-1β, IL-1RA, IL-7, IL-8, IL-10, IFN-γ, and TNF-α) (**Figure 2**).

It has been clinically found that serum pro-inflammatory factor levels are elevated in COVID-19 patients, and the severity of COVID-19 patients increases (Anka et al., 2021). Due to the abnormal release of pro-inflammatory factors that disrupt the pulmonary microvascular and alveolar epithelial cell barriers, leading to alveolar edema and hypoxia (Ragab et al., 2020; Balkhi, 2021). In clinical applications, it has been found that severe COVID-19 patients presenting with ARDS lead to an increase in pro-inflammatory factors, most notably interleukin 1β (IL-1β), interleukin-6 (IL-6), and TNF (Anka et al., 2021). In an analysis of cytokine-responsive gene sets, one author (Lee et al., 2020) found a significant TNF/IL-1β inflammatory response in lung tissue and that the severity of COVID-19 disease was accompanied by a TNF/IL-1β response.IL-6 is a family of cytokines involved in immune cell differentiation and activation (Sun et al., 2020), and the latest il-6 inhibitor pertuzumab has the potential to treat COVID-19 (Gu et al., 2020) (**Figure 2**).

3.3 SARS-CoV-2 Activates the Immune Response Leading to the ARDS

SARS-CoV-2 infection can activate both innate and adaptive immune responses, and SARS-CoV-2 may lead to too long a delay in the innate immune response as well as an inability to initiate an adaptive immune response for a long time, leading to severe lung disease (Sette and Crotty, 2021).

The innate immune sensing mechanism is the first line of defense against viruses and is an important aspect of viral immunity (Anka et al., 2021). SARS-CoV-2 innate immune responses are initially stimulated by pulmonary epithelial cells, alveolar macrophages, and neutrophils, which then trigger an adaptive immune response involving T and B lymphocytes (Toor et al., 2021). The innate immune response limits viral replication within infected cells, creating an antiviral state in the local tissue environment and initiating an adaptive immune response (Sette and Crotty, 2021). SARS-CoV-2 has four basic components of adaptive immunity: NK cells, B cells, CD4+ T cells, and CD8+ T cells. In COVID-19 patients, total lymphocytes, CD4+ T cells, CD8+ T cells, B cells, and NK cells were found to be decreased (Wang et al., 2020a; Anka et al., 2021), and for data from blood tests at admission, lymphocyte counts were found to be significantly lower in patients with severe disease than in patients with mild disease (0.9×10^9 cells/L [range 0.8–0.9] versus 1.2 [1.0–1.6]; p = 0.011) (Zhou et al., 2020). The possible mechanisms of lung injury caused by these cells will be summarized below (**Figure 1**).

3.3.1 Natural Killer Cells

Natural killer cells are required for the control of viral infections, thus restoring NK cell function has the potential to overcome the immune homeostasis required for COVID-19 infection. NK cells play a crucial role in regulating the immune response, not only by forming part of the innate immune system but also by regulating the adaptive immune response (Schuster et al., 2016; van Eeden et al., 2020b). Recent studies have highlighted that NK cells are regulatory cells that interact with dendritic cells, macrophages, T cells, and endothelial cells (Vivier et al., 2008).NK cells can limit or exacerbate the immune response. The role of NK cells as effectors against transformed and virally infected cells has been demonstrated (Schuster et al., 2016). SARS-CoV-2 infection in alveolar pneumocytes, resident alveolar macrophages, epithelial cells of the alveoli, and damaged lung cells trigger an inflammatory response with the release of cytokines and chemokines. This response further attracts natural killer cells, which enter the alveoli from the bloodstream and exacerbate the inflammatory response. The worsening of excessive inflammation triggers a cytokine storm that eventually progresses to ARDS and even death (Satarker et al., 2021). NKG2A is a receptor expressed on NK cells that induces IFN-γ and TNF-α (André et al., 2018; van Eeden et al., 2020b), and NKG2A expression by NK cells is activated in the peripheral and pulmonary microenvironment of patients with COVID-19 (Hammer et al., 2022). The number of NK cells is reduced in patients with COVID-19, and the function of NK cells is depleted as NKG2A expression increases in patients. Importantly, after treatment and recovery, the number of NK cells in these patients recovered with the decrease in NKG2A expression (Zheng et al., 2020). Chemokines MCP-1 and IP-10 recruit NK cells to inflammatory tissues, yet NK cell cytotoxicity and immune regulation are diminished, leading to an inflammatory response in SARS-CoV-2 infected patients (van Eeden et al., 2020b). This could suggest that the functional depletion of NK cells is associated with infection with SRAS-CoV-2 (**Figure 2**).

3.3.2 CD4+T and CD8+T Lymphocytes

T lymphocytes, CD4+T and CD8+T, play a key role in autoimmune and inflammatory responses (Wang et al., 2020b). Some speculations have been made on the mechanism of lung injury caused by SARS-CoV-2 (Li et al., 2020a). SARS-CoV-2 may act mainly on T lymphocytes, which in turn leads to the deterioration of the patient's condition. It has been shown that T cells undergo immune activation and antiviral immune responses triggered by SARS-CoV-2 and induce infected cell death (Toor et al., 2021). However, the pathogenic synergy between T cell-associated bystander effects and the more pronounced training innate immune effects in adults than in children can lead to abnormal or excessive immune responses in SARS-CoV-2 infected patients, which in turn can lead to tissue damage (Li et al., 2020a; de Candia et al., 2021). T lymphocyte subsets can be divided into CD4+ T cells and CD8+ T cells.19 CD4+T and CD8+ T cells in patients with nCoV are important in clearing infected cells by inducing immune damage SRAS-CoV-2 plays a very important role (Satarker et al., 2021). The study suggested (Zheng et al., 2020) that the functional failure of CD8+ T cells was associated with SRAS-CoV-2 infection. This shows the significance of CD8+ T cells for COVID-19. S protein is an important structural protein in SARS-CoV-2 that mediates the entry of SARS-CoV-2 into host cells (Chilamakuri and Agarwal, 2021). The importance of T lymphocytes in viral clearance and

recovery is also greatly implied by the fact that CD4+ and CD8+ T cells in most recovered patients produce a large number of antiviral immune responses against S proteins (Toor et al., 2021). Another study (Grifoni et al., 2020)also identified circulating SARS-CoV-2 specific CD8+ T cells and CD4+ T cells in COVID-19 recovered patients and also found that CD4+ T cells were positively correlated with the size of anti-SARS-CoV-2 IgG and IgA titers, and anti-acute RBD antibody responses made by COVID-19 patients were positively correlated with the size of specific CD4+ T and CD8+ T cell responses (**Figure 2**).

3.3.3 B Cells

B cells mainly perform humoral immunity of the body and can differentiate into plasma cells upon antigen stimulation, which can further synthesize specific antibodies and play a certain role in immune protection. In response to most viral infections, B cells can bind to viral proteins through their antigen receptors, by secreting effector molecules (IL-2, IL-4, IL-6, IFN-γ, TNF-α) to help contain viral infections (Rodda et al., 2021). Studies have shown that the serum-neutralizing antibody response to SARS-CoV-2 spiking proteins occurs within two weeks after the onset of symptoms, but memory B cells can be rapidly reactivated after secondary infection to help prevent SARS-CoV-2 infection and death (Lee and Oh, 2021). The mechanism of action lies in the fact that B cells can differentiate into plasma cells or form germinal centers through extrafollicular antibody (EF) responses, and in COVID-19 patients, antibodies produced by EF responses effectively neutralize SARS-CoV-2 (Luo and Yin, 2021). Patients recovering from COVID-19 produce specific immunoglobulin (IgG) antibodies that neutralize plasma and memory B cells that persist for at least 3 months. SARS-CoV-2-specific IgG memory B cells increase over time and memory B cell receptors neutralize the virus. Thus COVID-19 patients produce memory cells and display antiviral immunity (Luo and Yin, 2021) (**Figure 2**).

3.4 COVID-19 Triggers Fas/FasL Signaling Pathway Pro-Apoptosis Causing the ARDS

Fas is a tumor necrosis cell surface receptor factor, which has long been considered a death receptor and maintains immune homeostasis by mediating cell apoptosis (Bellesi et al., 2020). The pro-apoptotic role of the Fas/FasL signaling pathway is important in the development of acute lung injury (ALI). The Fas pathway has been studied as a potential contributor to lung inflammation and alveolar epithelial cell apoptosis in patients with ALI. The Fas pathway is activated by activation by FasL binding to Fas on the cell surface, leading to an intracellular cascade response that results in inflammation and apoptosis of Fas-bearing cells. It has been found (Andre et al., 2022) that activated T cells are susceptible to death *via* the Fas/FasL signaling pathway and that sFasL and Fas/CD95 expression correlated positively with T cell apoptosis in the plasma of COVID-19 patients. Selective blockade of Fas was found to attenuate lung injury in animal models, and lung injury could result from Fas activation (Glavan et al., 2011). Another study found that SARS-CoV-2 entered the airway and infected mainly fine bronchial epithelial cells and alveolar epithelial cells, causing local inflammation associated with lung injury (Rendeiro et al., 2021). In contrast, Fas/FasL, an apoptotic mediator, can induce inflammation by releasing pro-inflammatory factors that cause the migration of neutrophils and macrophages to the site of injury (Yu and Fehlings, 2011), and the Fas death receptor is normally expressed on lung epithelial cells. It is hypothesized that COVID-19 infection acts on alveolar epithelial cells to activate the Fas/FasL signaling pathway, which in turn induces abnormal apoptosis and causes acute lung injury (**Figures 1** and **2**).

3.5 COVID-19 Triggers Inflammation Through the JAK/STAT Pathway Causing the ARDS

COVID-19 virus induces activators of message transcription and transcription 1 (STAT1) dysfunction and compensatory hyperactivation of STAT3. The recruitment and subsequent activation of innate immune cells in the infected lung drive the destruction of lung structures, which leads to regional endothelial cell infection and the formation of a hypoxic environment where over-produced PAI-11 binds to TLR4 on macrophages and induces the secretion of pro-inflammatory cytokines and chemokines (Matsuyama et al., 2020). The JAK-STAT signaling pathway refers to the phosphorylation and dimerization of STAT by JAK, followed by its passage through the nuclear membrane translocation to the nucleus to regulate the expression of related genes, which in turn causes a cytokine storm (Zhang et al., 2020a). Some investigators have found in the pathology of SARS-CoV-2 disease that concentrations of pro-inflammatory cytokines and chemokines correlate with disease severity and adverse clinical outcomes, and that levels of pro-inflammatory factors (IL-2, IL-4, IL-6, IL-7, IL-10, TNF-α, and IFN-γ) and chemokines (CCL2, CCL8) are significantly elevated, IL-6 has been shown to activate the JAK-STAT signaling pathway, giving the body an immunomodulatory function, and thus it is hypothesized that the JAK-STAT signaling pathway is a key part of immunity and immunopathology during COVID-19 infection (Luo et al., 2020). The SARS-CoV-2 infection triggers inflammation through the JAK/STAT pathway, leading to lung cells, endothelial cells, macrophages, monocytes, lymphocytes, natural killer cells, and dendritic cells recruitment towards cytokine storm and eventual development of ARDS or even death (Satarker et al., 2021). Today an increasing number of anti-inflammatory drugs are used in the treatment of COVID-19, among which JAK inhibitors, are predicted to be of particular importance in the treatment of SARS-CoV-2 disease (Zhang et al., 2020b) (**Figures 1** and **2**).

3.6 COVID-19 Triggers Inflammation *via* NF-κB Pathway Causing the ARDS

The severity of COVID-19 is related to the activation of the host immune response, especially the inflammatory response, and an excessive inflammatory response will trigger lung injury. Therefore, limiting the dysfunctional inflammatory response is a critical step in anti-SARS-CoV-2 therapy. It was found (Wu et al., 2021) that SARS-CoV-2 infection leads to the development

of an inflammatory response and the release of multiple cytokines by promoting the activation of the NF-κB signaling pathway. The mechanism was experimentally found to be that the nucleocapsid (N) protein in SARS-CoV-2, after binding to viral RNA, undergoes liquid-liquid phase separation (LLPS) to recruit TAK1 and IKK complexes, thus promoting the activation of NF-κB signaling to enhance NF-κB activation. Not only that, but LLPS inhibitors can also attenuate the phase separation of N proteins and limit their regulatory function in NF-κB activation. It has been shown that SARS-CoV-2 ORF3a, M, ORF7a and N proteins are NF-κB activators and that activation is positively correlated with an increase in the amount of viral protein, indicating a dose-dependent activation of NF-κB by SARS-CoV-2 ORF3A, M, ORF7a, and N proteins.SARS-CoV-2 ORF7a protein is the most potent inducer of NF-KB, activating NF-κB signaling and promoting the production of pro-inflammatory cytokines (Su et al., 2021). Recent studies have found that a variety of herbs can inhibit SARS-CoV-2 infection through the NF-κB signaling pathway. Liushen capsule (LS), a traditional Chinese medicine, has anti-inflammatory, antiviral, and immunomodulatory activity properties. Some scholars (Ma et al., 2020) detected the expression of key proteins in the NF-κB/MAPK signaling pathway by protein blotting and found that LS could inhibit SARS-CoV-2 virus infection by downregulating the expression of inflammatory cytokines-induced viruses and regulating the activity of NF-κB/MAPK signaling pathway *in vitro* (**Figure 2**).

Alveolar hypercoagulation and fibrinolytic inhibition are important features in ARDS, and they are closely associated with severe hypoxemia, which is one of the important reasons why ARDS is difficult to cure. Several studies have now found that the NF-KB pathway can be involved in regulating endotoxin (LPS)-induced alveolar hypercoagulation and fibrinolysis inhibition. By targeting the NF-KB signaling pathway, alveolar hypercoagulation and fibrinolytic inflammation in ARDS could be improved. It is further hypothesized that the NF-KB signaling pathway can be targeted to reduce the occurrence of inflammatory response and cytokine release, inhibit SARS-CoV-2 infection, and improve alveolar hypercoagulation and fibrinolytic inhibition in ARDS (Pooladanda et al., 2019; Yang et al., 2021) (**Figure 1**).

3.7 COVID-19 Inhibits IFN-Is Causing the ARDS

Type I interferon (IFN-I) was first discovered in the classical experiments of Isaacs and Lindenman, and IFN-Is were found to have antiviral activity (Schreiber, 2020). The association of IFN-I with lung epithelial barrier function has been demonstrated and some researchers have found that the protective effect of IFN-I can be used in acute lung injury, where the loss of IFN-I signal leads to a significant reduction in barrier function caused by alveolar epithelial type II cell death (Maier et al., 2016). Type I interferons (IFN-Is) secreted by cells are rapidly produced upon viral infection and exhibit their antiviral activity in controlling virus proliferation and dissemination as well as effective antiviral immune responses (King and Sprent, 2021), which, if the immune response is unbalanced, leads to diminished production of IFN-Is and accelerated release of pro-inflammatory cytokines, and eventually, the disease becomes severe (Sa Ribero et al., 2020).SARS-CoV-2 has evolved mechanisms to inhibit IFN-I production to evade the inhibitory effects of IFN-I, by impairing the adaptive immune response and exacerbating inflammatory disease in the late stages of viral infection, ultimately affecting the course and efficiency of disease transmission (King and Sprent, 2021). Currently, in SARS-CoV-2 pneumonia, SARS-CoV-2 is found to cause a delay in IFN-I-mediated defense against viral functions and a large production of cytokines (IFN-α, IFN-β, IL-1, IL-6) (Nilsson-Payant et al., 2021), ultimately maintaining a balance of deleterious host responses.SARS-CoV-2 infection inhibits IFN-I production, impairs the adaptive immune response, and exacerbates inflammatory disease in the late stages of infection. Therefore, clarifying the etiology of SARS-CoV-2 disease is important to investigate the defective responsiveness of IFN-I (King and Sprent, 2021). Hoagland et al. (2021) found reduced viral load and tissue damage by intranasal injection of IFN-I, which reflects that IFN-I can limit viral replication and inflammation. Systemic administration of interferon can lead to some unwanted side effects, but local injection of IFN-I through the respiratory tract has shown excellent recovery in patients with COVID-19, further suggesting that this method may become an effective early intervention in respiratory disease caused by SARS-CoV-2 (**Figures 1** and **2**).

3.8 COVID-19 Causes ARDS Through the Vitamin D Pathway

Vitamin D maintains the balance of blood calcium and blood phosphorus, and for those who are deficient in vitamin D, proper supplementation can enhance our immune system and will bring some help in fighting SARS-CoV-2. Many studies today show that COVID-19 patients who are vitamin D deficient usually have a poor prognosis, while patients with high levels of vitamin D have an even better prognosis. Vitamin D is an immunomodulatory hormone whose active form, 1,25 dihydroxy vitamin D (1,25(OH) D), binds to the vitamin D receptor (VDR) to exert anti-inflammatory and immunomodulatory effects, prevent inflammatory response, and accelerate the healing process in affected areas, and it acts mainly in lung tissue with proven effectiveness against various upper respiratory tract infections (Mohan et al., 2020). One study (Rhodes et al., 2021) found that vitamin D deficiency is also related to the severity of respiratory diseases in children. Vitamin D has also been found by many scientists to affect ACE2 by increasing the ratio of ACE2 to ACE, thereby increasing angiotensin II hydrolysis and decreasing the subsequent inflammatory cytokine response to pathogens and lung injury (Mohan et al., 2020; Xiao et al., 2021). Since ACE2 is the host cell receptor for SARS-CoV-2, vitamin D could attenuate acute lung injury and ARDS by affecting ACE2 (Xiao et al., 2021). However, Ghasemian et al (Ghasemian et al., 2021), focused on the role of vitamin D in patients with COVID-19 and entered a meta-analysis of 23 studies in 11,901 subjects, which found that vitamin D deficiency had no substantial effect on

mortality in patients with COVID-19. However, patients with low vitamin D levels or vitamin D deficiency had a higher risk of developing severe disease (**Figures 1** and **2**).

4 CONCLUSIONS AND CHALLENGES

COVID-19 is a fatal respiratory infectious disease caused by SARS-CoV-2, which can cause the ARDS in severe cases, resulting in lung injury and accelerating the death of patients. In order to reduce the mortality of COVID-19 and gain insight into the study of SARS-CoV-2 causing the ARDS and to develop a broad spectrum of drugs as early as possible, this paper analyzes the possible mechanisms of SARS-CoV-2 causing ARDS in angiotensin-converting enzyme 2, cytokine storm, immune cells, Fas/FasL pathway, JAK/STAT pathway, NF-κB pathway, type I interferon, and vitamin D. Their importance in COVID-19 and the possible mechanisms of lung damage are described. In the future, there are still some areas that need attention and research in the area of SARS-CoV-2 causing the acute respiratory distress syndrome (**Figure 1**).

In terms of ACE2, ACE2 receptor is the key entry point for viral to entry cells, and genetic mutations in ACE2 may affect expression levels as well as protein conformation and stability, which may change the affinity of the SARS-CoV-2 S protein, making individuals more resistant or susceptible to viral infection (Antony and Vijayan, 2021). This latest speculation provides a future understanding of the clinically relevant COVID-19 pathophysiological response brings significant help for the future understanding of COVID-19 clinically relevant pathophysiological response and provides ideas for vaccine development. In terms of cytokine storm, the cytokine storm triggered by COVID-19 exacerbates disease progression and leads to immune disorders, which provides a potential approach to treat COVID-19 by early identification of cytokine storm and anti-inflammatory therapy that reduces cytokine response, ultimately leading to reduced morbidity and mortality. There are a number of anti-cytokine approaches that have been shown to be effective in the treatment of cytokine storm syndrome, such as anti-IL-1, IL-6, and IFN-γ drugs (Nile et al., 2020), but further experiments are needed to determine which drugs are effective in patients with cytokine storm syndrome caused by SARS-CoV-2. In terms of immune response, NK cells control cellular infection and play a key role in maintaining immune homeostasis, and SARS-CoV-2 infection controls NK cell function, thereby disrupting this balance. B cells also play a very important role in maintaining humoral immunity in the body, and the persistence of the immune response is essential to prevent reinfection in patients recovering from COVID-19, and persistent humoral Immunity is mediated by memory B cells and memory B cells can provide protection against re-infection of the body with viruses (Ogega et al., 2021), but there are still many gaps in knowledge and understanding of the immune memory response to SARS-CoV-2. It is hoped that future drug development will be carried out from the perspective of improving NK cell function and exploiting the memory response of B cells. It has been shown that physical inactivity decreases NK cell activity and IFN-γ expression (van Eeden et al., 2020b). This suggests the importance of increased exercise in patients with COVID-19. CD4+ T cells as coordinators of antiviral immune responses can enhance the effector function of CD8+ T cells or directly kill infected cells (Meckiff et al., 2020). CD4+ T cells and CD8+ T cells-mediated immune responses are present throughout the course of COVID-19 disease, but evidence of CD4+ T cells and CD8+ T cells in COVID-19 disease surveillance is still lacking in large samples. It is hoped that the dynamic detection of CD4+ T and CD8+ T cells can be used in the clinic in the future to grasp the patient's disease and eventually eliminate SARS-CoV-2 and prevent the patient from progressing to ARDS (**Figure 2**).

Fas maintains immune homeostasis and the Fas/FasL pathway mediates the formation of ALI. sFasL, Fas/CD95 expression was also found in COVID-19 patients (Glavan et al., 2011). It is hypothesized that COVID-19 infection activates the Fas/FasL signaling pathway, induces abnormal apoptosis, and causes ARDS. COVID-19 infection triggers inflammation through the JAK/STAT pathway, causing a cytokine storm that eventually develops into ARDS. The pro-inflammatory factor IL-6 has been shown to activate the JAK/STAT signaling pathway (Luo et al., 2020), and more experiments are needed to prove whether other pro-inflammatory factors in COVID-19 patients have the same effect. SARS-CoV-2 ORF3a, M, ORF7a and N proteins can promote activation of the NF-κB signaling pathway, with ORF7a being the most potent activator leading to the development of inflammatory responses and cytokine release (Su et al., 2021). the NF-κB pathway can be involved in the regulation of LPS and ameliorate ARDS-induced alveolar hypercoagulation and fibrinolysis inhibition. Although the viral proteins that activate the inflammatory response and their molecular mechanisms are not yet known. However, it can be speculated that by targeting the NF-κB signaling pathway, SARS-CoV-2 infection and inflammatory response can be effectively inhibited and the symptoms of ARDS can be improved. In summary, by inhibiting several aspects of the Fas/FasL signaling pathway, NF-κB signaling pathway, and JAK/STAT pathway, all of them can reduce the infection of COVID-19 to some extent and further prevent the development of ARDS. Future studies can focus on these three pathways as well as other pathways to provide new strategies for the treatment of COVID-19. Increasing type I interferon and vitamin D has a good effect on the prevention and treatment of COVID-19. In the future, intranasal intake of IFN-I may be used as an early treatment to eliminate the virus. For people who lack vitamin D, appropriate vitamin D supplementation can enhance the immune ability and bring some help to fight the virus However, it is still unclear to what extent vitamin D helps patients with COVID-19, and there is a lack of sufficient favorable evidence. (**Figure 2**).

Currently, ARDS remains a state of high morbidity and mortality due to the lack of specific drugs, supportive treatment by mechanical ventilation and non-mechanical ventilation, and long-term sequelae of patients after treatment. Therefore, research on the molecular and physiological

mechanisms of ARDS needs to be further improved to develop specific drugs and find better treatment strategies to reduce the mortality caused by this syndrome.

Nowadays, people all over the world are engaged in the fight against SARS-CoV-2, and the mechanisms of SARS-CoV-2-induced acute respiratory distress syndrome are playing an increasingly important role in understanding the virus, fighting the epidemic, and developing drugs. It is expected that in the future, we will have a deeper understanding of the SARS-CoV-2 and be able to supplement the understanding of the mechanism of acute respiratory distress syndrome with more experimental data and clinical observations, to contribute to the prevention and control of the epidemic as well as to the medical field.

AUTHOR CONTRIBUTIONS

JZ and RGuo: writing and visualization. JM, ZF, and JG: reviewing and editing. XK, RGao, and LY: conceptualization and supervision. All authors contributed to the article and approved the submitted version.

FUNDING

This study was supported by the Scientific research project of Tianjin Education Commission (Grant No. 2021KJ134 to XK); Tianjin Municipal Education Commission Scientific Research Project (Natural Science, Grant No. 2019ZD11 to LY); Scientific and technological innovation project of China Academy of Chinese Medical Sciences (Grant No. C12021A04701 to RG).

ACKNOWLEDGMENTS

We thank all the authors of the original work and reviewers for their time and kindness in reviewing this paper. The figures were drawn by Figdraw (www.figdraw.com).

REFERENCES

André, P., Denis, C., Soulas, C., Bourbon-Caillet, C., Lopez, J., Arnoux, T., et al. (2018). Anti-NKG2A mAb Is a Checkpoint Inhibitor That Promotes Anti-Tumor Immunity by Unleashing Both T and NK Cells. *Cell* 175, 1731–1743.e13. doi: 10.1016/j.cell.2018.10.014

Andre, S., Picard, M., Cezar, R., Roux-Dalvai, F., Alleaume-Butaux, A., Soundaramourty, C., et al. (2022). T Cell Apoptosis Characterizes Severe Covid-19 Disease. *Cell Death Differ* 22, 1–14. doi: 10.1038/s41418-022-00936-x

Anka, A. U., Tahir, M. I., Abubakar, S. D., Alsabbagh, M., Zian, Z., Hamedifar, H., et al. (2021). Coronavirus Disease 2019 (COVID-19): An Overview of the Immunopathology, Serological Diagnosis and Management. *Scand. J. Immunol.* 93, e12998. doi: 10.1111/sji.12998

Antony, P., and Vijayan, R. (2021). Role of SARS-CoV-2 and ACE2 Variations in COVID-19. *BioMed. J.* 44, 235–244. doi: 10.1016/j.bj.2021.04.006

Attaway, A. H., Scheraga, R. G., Bhimraj, A., Biehl, M., and Hatipoğlu, U. (2021). Severe Covid-19 Pneumonia: Pathogenesis and Clinical Management. *BMJ (Clinical Res. ed.)* 372, n436. doi: 10.1136/bmj.n436

Balkhi, M. Y. (2021). Mechanistic Understanding of Innate and Adaptive Immune Responses in SARS-CoV-2 Infection. *Mol. Immunol.* 135, 268–275. doi: 10.1016/j.molimm.2021.04.021

Batah, S. S., and Fabro, A. T. (2021). Pulmonary Pathology of ARDS in COVID-19: A Pathological Review for Clinicians. *Respir. Med.* 176, 106239. doi: 10.1016/j.rmed.2020.106239

Bellesi, S., Metafuni, E., Hohaus, S., Maiolo, E., Marchionni, F., D'innocenzo, S., et al. (2020). Increased CD95 (Fas) and PD-1 Expression in Peripheral Blood T Lymphocytes in COVID-19 Patients. *Br. J. Haematol.* 191, 207–211. doi: 10.1111/bjh.17034

Chilamakuri, R., and Agarwal, S. (2021). COVID-19: Characteristics and Therapeutics. *Cells* 10, 206. doi: 10.3390/cells10020206

Datta, P. K., Liu, F., Fischer, T., Rappaport, J., and Qin, X. (2020). SARS-CoV-2 Pandemic and Research Gaps: Understanding SARS-CoV-2 Interaction With the ACE2 Receptor and Implications for Therapy. *Theranostics* 10, 7448–7464. doi: 10.7150/thno.48076

De Candia, P., Prattichizzo, F., Garavelli, S., and Matarese, G. (2021). T Cells: Warriors of SARS-CoV-2 Infection. *Trends Immunol.* 42, 18–30. doi: 10.1016/j.it.2020.11.002

Ghasemian, R., Shamshirian, A., Heydari, K., Malekan, M., Alizadeh-Navaei, R., Ebrahimzadeh, M. A., et al. (2021). The Role of Vitamin D in the Age of COVID-19: A Systematic Review and Meta-Analysis. *Int. J. Clin. Pract.* 75, e14675. doi: 10.1111/ijcp.14675

Gibson, P. G., Qin, L., and Puah, S. H. (2020). COVID-19 Acute Respiratory Distress Syndrome (ARDS): Clinical Features and Differences From Typical Pre-COVID-19 ARDS. *Med. J. Aust.* 213, 54–56.e1. doi: 10.5694/mja2.50674

Glavan, B. J., Holden, T. D., Goss, C. H., Black, R. A., Neff, M. J., Nathens, A. B., et al. (2011). Genetic Variation in the FAS Gene and Associations With Acute Lung Injury. *Am. J. Respir. Crit. Care Med.* 183, 356–363. doi: 10.1164/rccm.201003-0351OC

Grasselli, G., Cattaneo, E., and Scaravilli, V. (2021). Ventilation of Coronavirus Disease 2019 Patients. *Curr. Opin. In Crit. Care* 27, 6–12. doi: 10.1097/MCC.0000000000000793

Grifoni, A., Weiskopf, D., Ramirez, S. I., Mateus, J., Dan, J. M., Moderbacher, C. R., et al. (2020). Targets of T Cell Responses to SARS-CoV-2 Coronavirus in Humans With COVID-19 Disease and Unexposed Individuals. *Cell* 181, 1489–1501, e1415. doi: 10.1016/j.cell.2020.05.015

Gu, T., Zhao, S., Jin, G., Song, M., Zhi, Y., Zhao, R., et al. (2020). Cytokine Signature Induced by SARS-CoV-2 Spike Protein in a Mouse Model. *Front. In Immunol.* 11, 621441. doi: 10.3389/fimmu.2020.621441

Hammer, Q., Dunst, J., Christ, W., Picarazzi, F., Wendorff, M., Momayyezi, P., et al. (2022). SARS-CoV-2 Nsp13 Encodes for an HLA-E-Stabilizing Peptide That Abrogates Inhibition of NKG2A-Expressing NK Cells. *Cell Rep.* 38, 110503. doi: 10.1016/j.celrep.2022.110503

Hoagland, D. A., Moller, R., Uhl, S. A., Oishi, K., Frere, J., Golynker, I., et al. (2021). Leveraging the Antiviral Type I Interferon System as a First Line of Defense Against SARS-CoV-2 Pathogenicity. *Immunity* 54557–54570.e555. doi: 10.1016/j.immuni.2021.01.017

Imai, Y., Kuba, K., Rao, S., Huan, Y., Guo, F., Guan, B., et al. (2005). Angiotensin-Converting Enzyme 2 Protects From Severe Acute Lung Failure. *Nature* 436, 112–116. doi: 10.1038/nature03712

Khamis, F., Memish, Z., Bahrani, M. A., Dowaiki, S. A., Pandak, N., Bolushi, Z. A., et al. (2021). Prevalence and Predictors of in-Hospital Mortality of Patients Hospitalized With COVID-19 Infection. *J. Infect. Public Health* 14, 759–765. doi: 10.1016/j.jiph.2021.03.016

Kim, J. S., Lee, J. Y., Yang, J. W., Lee, K. H., Effenberger, M., Szpirt, W., et al. (2021). Immunopathogenesis and Treatment of Cytokine Storm in COVID-19. *Theranostics* 11, 316–329. doi: 10.7150/thno.49713

King, C., and Sprent, J. (2021). Dual Nature of Type I Interferons in SARS-CoV-2-Induced Inflammation. *Trends Immunol.* 42, 312–322. doi: 10.1016/j.it.2021.02.003

Lee, E., and Oh, J. E. (2021). Humoral Immunity Against SARS-CoV-2 and the Impact on COVID-19 Pathogenesis. *Mol. Cells* 44, 392–400. doi: 10.14348/molcells.2021.0075

Lee, J. S., Park, S., Jeong, H. W., Ahn, J. Y., Choi, S. J., Lee, H., et al. (2020). Immunophenotyping of COVID-19 and Influenza Highlights the Role of Type I Interferons in Development of Severe COVID-19. *Sci. Immunol.* 5, eabd1554. doi: 10.1126/sciimmunol.abd155

Li, D., Chen, Y., Liu, H., Jia, Y., Li, F., Wang, W., et al. (2020a). Immune Dysfunction Leads to Mortality and Organ Injury in Patients With COVID-19 in China: Insights From ERS-COVID-19 Study. *Signal Transduct Target Ther.* 5, 62. doi: 10.1038/s41392-020-0163-5

Li, M., Guo, W., Dong, Y., Wang, X., Dai, D., Liu, X., et al. (2020b). Elevated Exhaustion Levels of NK and CD8(+) T Cells as Indicators for Progression and Prognosis of COVID-19 Disease. *Front. Immunol.* 11, 580237. doi: 10.3389/fimmu.2020.580237

Luo, W., Li, Y. X., Jiang, L. J., Chen, Q., Wang, T., and Ye, D. W. (2020). Targeting JAK-STAT Signaling to Control Cytokine Release Syndrome in COVID-19. *Trends Pharmacol. Sci.* 41, 531–543. doi: 10.1016/j.tips.2020.06.007

Luo, W., and Yin, Q. (2021). B Cell Response to Vaccination. *Immunol. Invest.* 50, 780–801. doi: 10.1080/08820139.2021.1903033

Maier, B. B., Hladik, A., Lakovits, K., Korosec, A., Martins, R., Kral, J. B., et al. (2016). Type I Interferon Promotes Alveolar Epithelial Type II Cell Survival During Pulmonary Streptococcus Pneumoniae Infection and Sterile Lung Injury in Mice. *Eur. J. Immunol.* 46, 2175–2186. doi: 10.1002/eji.201546201

Ma, Q., Pan, W., Li, R., Liu, B., Li, C., Xie, Y., et al. (2020). Liu Shen Capsule Shows Antiviral and Anti-Inflammatory Abilities Against Novel Coronavirus SARS-CoV-2 *via* Suppression of NF-kappaB Signaling Pathway. *Pharmacol. Res.* 158, 104850. doi: 10.1016/j.phrs.2020.104850

Matsuyama, T., Kubli, S. P., Yoshinaga, S. K., Pfeffer, K., and Mak, T. W. (2020). An Aberrant STAT Pathway Is Central to COVID-19. *Cell Death Differ* 27, 3209–3225. doi: 10.1038/s41418-020-00633-7

Meckiff, B. J., Ramirez-Suastegui, C., Fajardo, V., Chee, S. J., Kusnadi, A., Simon, H., et al. (2020). Imbalance of Regulatory and Cytotoxic SARS-CoV-2-Reactive CD4(+) T Cells in COVID-19. *Cell* 183, 1340–1353.e1316. doi: 10.1016/j.cell.2020.10.001

Meyer, N. J., Gattinoni, L., and Calfee, C. S. (2021). Acute Respiratory Distress Syndrome. *Lancet* 398, 622–637. doi: 10.1016/S0140-6736(21)00439-6

Mohan, M., Cherian, J. J., and Sharma, A. (2020). Exploring Links Between Vitamin D Deficiency and COVID-19. *PLoS Pathog.* 16, e1008874. doi: 10.1371/journal.ppat.1008874

Nile, S. H., Nile, A., Qiu, J., Li, L., Jia, X., and Kai, G. (2020). COVID-19: Pathogenesis, Cytokine Storm and Therapeutic Potential of Interferons. *Cytokine Growth Factor Rev.* 53, 66–70. doi: 10.1016/j.cytogfr.2020.05.002

Nilsson-Payant, B. E., Uhl, S., Grimont, A., Doane, A. S., Cohen, P., Patel, R. S., et al. (2021). The NF-κb Transcriptional Footprint Is Essential for SARS-CoV-2 Replication. *J. Virol.* 95, e0125721. doi: 10.1128/JVI.01257-21

Ntatsoulis, K., Karampitsakos, T., Tsitoura, E., Stylianaki, E.-A., Matralis, A. N., Tzouvelekis, A., et al. (2021). Pulmonary Fibrosis and COVID-19: The Potential of Autotaxin as a Therapeutic Target. *Front. In Immunol.* 12, 687397. doi: 10.3389/fimmu.2021.687397

Ogega, C. O., Skinner, N. E., Blair, P. W., Park, H. S., Littlefield, K., Ganesan, A., et al. (2021). Durable SARS-CoV-2 B Cell Immunity After Mild or Severe Disease. *J. Clin. Invest.* 131, e145516. doi: 10.1172/JCI145516

Pooladanda, V., Thatikonda, S., Bale, S., Pattnaik, B., Sigalapalli, D. K., Bathini, N. B., et al. (2019). Nimbolide Protects Against Endotoxin-Induced Acute Respiratory Distress Syndrome by Inhibiting TNF-Alpha Mediated NF-kappaB and HDAC-3 Nuclear Translocation. *Cell Death Dis.* 10, 81. doi: 10.1038/s41419-018-1247-9

Quesada-Gomez, J. M., Entrenas-Castillo, M., and Bouillon, R. (2020). Vitamin D Receptor Stimulation to Reduce Acute Respiratory Distress Syndrome (ARDS) in Patients With Coronavirus SARS-CoV-2 Infections: Revised Ms SBMB 2020_166. *J. Steroid Biochem. Mol. Biol.* 202, 105719. doi: 10.1016/j.jsbmb.2020.105719

Ragab, D., Salah Eldin, H., Taeimah, M., Khattab, R., and Salem, R. (2020). The COVID-19 Cytokine Storm; What We Know So Far. *Front. In Immunol.* 11, 1446. doi: 10.3389/fimmu.2020.01446

Rendeiro, A. F., Ravichandran, H., Bram, Y., Chandar, V., Kim, J., Meydan, C., et al. (2021). The Spatial Landscape of Lung Pathology During COVID-19 Progression. *Nature* 593, 564–569. doi: 10.1038/s41586-021-03475-6

Rhodes, J. M., Subramanian, S., Laird, E., Griffin, G., and Kenny, R. A. (2021). Perspective: Vitamin D Deficiency and COVID-19 Severity - Plausibly Linked by Latitude, Ethnicity, Impacts on Cytokines, ACE2 and Thrombosis. *J. Internal Med.* 289, 97–115. doi: 10.1111/joim.13149

Rodda, L. B., Netland, J., Shehata, L., Pruner, K. B., Morawski, P. A., Thouvenel, C. D., et al. (2021). Functional SARS-CoV-2-Specific Immune Memory Persists After Mild COVID-19. *Cell* 184, 169–183.e117. doi: 10.1016/j.cell.2020.11.029

Sa Ribero, M., Jouvenet, N., Dreux, M., and Nisole, S. (2020). Interplay Between SARS-CoV-2 and the Type I Interferon Response. *PLoS Pathog.* 16, e1008737. doi: 10.1371/journal.ppat.1008737

Satarker, S., Tom, A. A., Shaji, R. A., Alosious, A., Luvis, M., and Nampoothiri, M. (2021). JAK-STAT Pathway Inhibition and Their Implications in COVID-19 Therapy. *Postgrad Med.* 133, 489–507. doi: 10.1080/00325481.2020.1855921

Schreiber, G. (2020). The Role of Type I Interferons in the Pathogenesis and Treatment of COVID-19. *Front. Immunol.* 11, 595739. doi: 10.3389/fimmu.2020.595739

Schuster, I. S., Coudert, J. D., Andoniou, C. E., and Degli-Esposti, M. A. (2016). "Natural Regulators": NK Cells as Modulators of T Cell Immunity. *Front. Immunol.* 7, 235. doi: 10.3389/fimmu.2016.00235

Sette, A., and Crotty, S. (2021). Adaptive Immunity to SARS-CoV-2 and COVID-19. *Cell* 184, 861–880. doi: 10.1016/j.cell.2021.01.007

Seyed Hosseini, E., Riahi Kashani, N., Nikzad, H., Azadbakht, J., Hassani Bafrani, H., and Haddad Kashani, H. (2020). The Novel Coronavirus Disease-2019 (COVID-19): Mechanism of Action, Detection and Recent Therapeutic Strategies. *Virology* 551, 1–9. doi: 10.1016/j.virol.2020.08.011

Sun, X., Wang, T., Cai, D., Hu, Z., Chen, J., Liao, H., et al. (2020). Cytokine Storm Intervention in the Early Stages of COVID-19 Pneumonia. *Cytokine Growth Factor Rev.* 53, 38–42. doi: 10.1016/j.cytogfr.2020.04.002

Su, C. M., Wang, L., and Yoo, D. (2021). Activation of NF-kappaB and Induction of Proinflammatory Cytokine Expressions Mediated by ORF7a Protein of SARS-CoV-2. *Sci. Rep.* 11, 13464. doi: 10.1038/s41598-021-92941-2

Tisoncik, J. R., Korth, M. J., Simmons, C. P., Farrar, J., Martin, T. R., and Katze, M. G. (2012). Into the Eye of the Cytokine Storm. *Microbiol. Mol. Biol. Rev. MMBR* 76, 16–32. doi: 10.1128/MMBR.05015-11

Toor, S. M., Saleh, R., Sasidharan Nair, V., Taha, R. Z., and Elkord, E. (2021). T-Cell Responses and Therapies Against SARS-CoV-2 Infection. *Immunology* 162, 30–43. doi: 10.1111/imm.13262

Van Eeden, C., Khan, L., Osman, M. S., and Cohen Tervaert, J. W. (2020a). Natural Killer Cell Dysfunction and Its Role in COVID-19. *Int. J. Mol. Sci.* 21, 6351. doi: 10.3390/ijms21176351

Van Eeden, C., Khan, L., Osman, M. S., and Cohen Tervaert, J. W. (2020b). Natural Killer Cell Dysfunction and Its Role in COVID-19. *Int. J. Mol. Sci.* 21, 6351. doi: 10.3390/ijms21176351

Verdecchia, P., Cavallini, C., Spanevello, A., and Angeli, F. (2020). The Pivotal Link Between ACE2 Deficiency and SARS-CoV-2 Infection. *Eur. J. Internal Med.* 76, 14–20. doi: 10.1016/j.ejim.2020.04.037

Vivier, E., Tomasello, E., Baratin, M., Walzer, T., and Ugolini, S. (2008). Functions of Natural Killer Cells. *Nat. Immunol.* 9, 503–510. doi: 10.1038/ni1582

Wang, F., Nie, J., Wang, H., Zhao, Q., Xiong, Y., Deng, L., et al. (2020a). Characteristics of Peripheral Lymphocyte Subset Alteration in COVID-19 Pneumonia. *J. Infect. Dis.* 221, 1762–1769. doi: 10.1093/infdis/jiaa150

Wang, F., Nie, J., Wang, H., Zhao, Q., Xiong, Y., Deng, L., et al. (2020b). Characteristics of Peripheral Lymphocyte Subset Alteration in COVID-19 Pneumonia. *J. Infect. Dis.* 221, 1762–1769. doi: 10.1093/infdis/jiaa150

Wu, Y., Ma, L., Cai, S., Zhuang, Z., Zhao, Z., Jin, S., et al. (2021). RNA-Induced Liquid Phase Separation of SARS-CoV-2 Nucleocapsid Protein Facilitates NF-κb Hyper-Activation and Inflammation. *Signal Transduction Targeted Ther.* 6, 167. doi: 10.1038/s41392-021-00575-7

Xiao, D., Li, X., Su, X., Mu, D., and Qu, Y. (2021). Could SARS-CoV-2-Induced Lung Injury be Attenuated by Vitamin D? *Int. J. Infect. Dis.* 102, 196–202. doi: 10.1016/j.ijid.2020.10.059

Yang, H., Qian, H., Liu, B., Wu, Y., Cheng, Y., Zheng, X., et al. (2021). Triptolide Dose-Dependently Improves LPS-Induced Alveolar Hypercoagulation and Fibrinolysis Inhibition Through NF-kappaB Inactivation in ARDS Mice. *BioMed. Pharmacother.* 139, 111569. doi: 10.1016/j.biopha.2021.111569

Yu, W. R., and Fehlings, M. G. (2011). Fas/FasL-Mediated Apoptosis and Inflammation are Key Features of Acute Human Spinal Cord Injury: Implications for Translational, Clinical Application. *Acta Neuropathol.* 122, 747–761. doi: 10.1007/s00401-011-0882-3

Zarrilli, G., Angerilli, V., Businello, G., Sbaraglia, M., Traverso, G., Fortarezza, F., et al. (2021). The Immunopathological and Histological Landscape of COVID-19-Mediated Lung Injury. *Int. J. Mol. Sci.* 22, 974. doi: 10.3390/ijms22020974

Zhang, X., Zhang, Y., Qiao, W., Zhang, J., and Qi, Z. (2020a). Baricitinib, a Drug With Potential Effect to Prevent SARS-COV-2 From Entering Target Cells and Control Cytokine Storm Induced by COVID-19. *Int. Immunopharmacol.* 86, 106749. doi: 10.1016/j.intimp.2020.106749

Zhang, X., Zhang, Y., Qiao, W., Zhang, J., and Qi, Z. (2020b). Baricitinib, a Drug With Potential Effect to Prevent SARS-COV-2 From Entering Target Cells and Control Cytokine Storm Induced by COVID-19. *Int. Immunopharmacol.* 86, 106749. doi: 10.1016/j.intimp.2020.106749

Zheng, M., Gao, Y., Wang, G., Song, G., Liu, S., Sun, D., et al. (2020). Functional Exhaustion of Antiviral Lymphocytes in COVID-19 Patients. *Cell Mol. Immunol.* 17, 533–535. doi: 10.1038/s41423-020-0402-2

Zhou, R., To, K. K., Wong, Y. C., Liu, L., Zhou, B., Li, X., et al. (2020). Acute SARS-CoV-2 Infection Impairs Dendritic Cell and T Cell Responses. *Immunity* 53864–877.e865. doi: 10.1016/j.immuni.2020.07.026

Conflict of Interest: The authors declare that the research was conducted in the absence of any commercial or financial relationships that could be construed as a potential conflict of interest.

frontiers | Frontiers in Cellular and Infection Microbiology

ORIGINAL RESEARCH
published: 08 July 2022
doi: 10.3389/fcimb.2022.942987

Construction of BHV-1 UL41 Defective Virus Using the CRISPR/Cas9 System and Analysis of Viral Replication Properties

Haiyue Dai, Jianan Wu, Hongshu Yang, Yongli Guo, Haoqing Di, Mingchun Gao and Junwei Wang**

Heilongjiang Provincial Key Laboratory of Zoonosis, Department of Preventive Veterinary Medicine, College of Veterinary Medicine, Northeast Agricultural University, Harbin, China

OPEN ACCESS

Edited by:
Zhanbo Zhu, Heilongjiang Bayi Agricultural University, China

Reviewed by:
Yingyu Chen, Huazhong University of Science and Technology, China
Wang Hongmei, Shandong Normal University, China

***Correspondence:**
Mingchun Gao
gaomingchun@neau.edu.cn
Junwei Wang
jwwang@neau.edu.cn

Specialty section:
This article was submitted to Clinical Microbiology, a section of the journal Frontiers in Cellular and Infection Microbiology

Received: *13 May 2022*
Accepted: *16 June 2022*
Published: *08 July 2022*

Citation:
Dai H, Wu J, Yang H, Guo Y, Di H, Gao M and Wang J (2022) Construction of BHV-1 UL41 Defective Virus Using the CRISPR/Cas9 System and Analysis of Viral Replication Properties. Front. Cell. Infect. Microbiol. 12:942987. doi: 10.3389/fcimb.2022.942987

Bovine herpesvirus type 1 (BHV-1) is a neurotropic herpesvirus that causes infectious rhinotracheitis and vulvovaginitis in cattle. The virion host shutoff protein encoded by the BHV-1 *UL41* gene is highly conserved in the Alphaherpesvirinae subfamily. This protein can degrade viral and host messenger RNA (mRNA) to interrupt host defense and facilitate the rapid proliferation of BHV-1. However, studies on the BHV-1 *UL41* gene are limited, and BHV-1 defective virus construction using the CRISPR/Cas9 system is somewhat challenging. In this study, we rapidly constructed a BHV-1 UL41-deficient strain using the CRISPR/Cas9 system in BL primary bovine-derived cells. BHV-1 UL41-defective mutants were screened by Western blot analysis using specific polyclonal antibodies as the primary antibodies. During the isolation and purification of the defective strain, a mixed virus pool edited by an efficient single-guide RNA (sgRNA) showed a plaque number reduction. Viral growth property assessment showed that BHV-1 UL41 was dispensable for replication, but the UL41-defective strain exhibited early and slowed viral replication. Furthermore, the BHV-1 UL41-deficient strain exhibited enhanced sensitivity to temperature and acidic environments. The BHV-1 UL41-deficient strain regulated viral and host mRNA levels to affect viral replication.

Keywords: BHV-1, UL41, CRISPR/Cas9, defective virus, replications

INTRODUCTION

Bovine herpesvirus type 1 (BHV-1) is a pivotal member of the order Herpesvirales, family Herpesviridae, subfamily Alphaherpesvirinae, and genus *Varicellovirus* (Ackermann and Engels, 2006). BHV-1 has a relatively short reproductive cycle, spreads rapidly in culture, efficiently destroys infected cells, and can quickly establish latent infections not only in ganglia but also in other tissues (Valyi-Nagy et al., 2007). Upon entry into the bovine host, BHV-1 remains latent but infects susceptible animals when it is reactivated (Weidner-Glunde et al., 2020). One characteristic of herpesvirus-infected cells is the rapid shutoff of host macromolecular metabolism at the early stage of infection (Smith et al., 2000). Host protein synthesis also declines very rapidly after infection, and this decline is accompanied by cessation of glycosylation of host proteins. Although some viral

proteins are produced late in infection, they expressed functions early in viral replication (Wentink et al., 1993). The host shutoff protein synthesis occur immediately after infection, and structural proteins release viral DNA from the capsid during nuclear processing.

The *UL41* gene of BHV-1 appears to be non-essential for the multiplication in cell culture under non-selective conditions. This gene encodes the virion host shutoff (VHS) protein, a late tegument protein expressed in BHV-1 infections. The VHS protein has a function similar to that of mRNA-specific ribonuclease (RNase) and can induce host shutoff early in infection (Taddeo and Roizman, 2006). However, VHS does not effectively discriminate between proteins synthesized by viruses and those synthesized by the host in its shutoff process. VHS degrades not only mRNAs from host cells to evade host abrogation but also mRNAs from viruses to facilitate the sequential expression of various classes of viral genes (He et al., 2020). Its unrestrained RNase activity is lethal but can be neutralized *via* formation of a trimeric complex with the tegument proteins VP22 and VP16 at the late stage of infection (Elliott et al., 2018). VP13/14, another viral protein, also plays a vital role in protecting against the degradation of viral transcripts (Shu et al., 2013a; Shu et al., 2013b). The VHS homology protein in varicella-zoster virus, a late protein encoded by open reading frame (ORF) 17, induces delayed shutoff of cellular RNA translation (Desloges et al., 2005). The VHS homology protein of equid herpesvirus type 1 encoded by ORF19 cannot degrade mRNAs or induce the shutoff of cellular and viral protein synthesis (Stokol and Soboll, 2019). The VHS homology protein in Pseudorabies virus (PRV) induces host mRNA degradation and cleaves the internal ribosomal entry site (IRES) sequence containing RNA (Lin et al., 2010; Liu et al., 2016). The VHS homologous protein of DPV influences pol II mRNA degradation, protein synthesis shutoff, and viral replication and spread (He et al., 2021). The VHS homologous protein of BHV-1 degrades the 5′ cap and 3′ untranslated region (UTR) adenylate-uridylate (AU)-rich element (ARE) areas of STAT1 in the antiviral pathway (Ma et al., 2019).

Clustered regularly interspaced short palindromic repeats (CRISPR)/CRISPR-associated protein 9 (Cas9), a revolutionary gene engineering technology, has recently been used to successfully edit various viruses (Borca et al., 2018; Das et al., 2019; Neuhausser et al., 2020; Tang et al., 2021; Van Cleemput et al., 2021). For example, HIV-1 (Das et al., 2019), herpes simplex virus type 1 (Velusamy et al., 2020), Marek's disease virus (Luo et al., 2020), African swine fever virus (Borca et al., 2018), and PRV (Van Cleemput et al., 2021) have been extensively edited with the CRISPR/Cas9 system. The method is straightforward; the only requirement is an effective single-guide RNA (sgRNA) that targets the given gene with a protospacer-adjacent motif (PAM) sequence. The greatest disadvantages of this technique for BHV-1 editing are the plasmid's low transfection efficiency, the unsustainable cell platform (Yang et al., 2019), and the high GC content in the BHV-1 genome. Even though the DNA viral genome can easily be edited, few BHV-1 deficiency mutants have been successfully constructed (Lobanov et al., 2010). To date, the CRISPR/Cas9 system has not been used to efficiently or rapidly construct a defective BHV-1 strain. In this study, we attempted to construct a BHV-1 UL41 strain using the CRISPR/Cas9 system in bovine lung (BL) cells and further explore the replication properties of the deficient strain.

MATERIALS AND METHODS

Cells, Viruses, and Animals

Madin–Darby bovine kidney (MDBK) cells and primary embryonic BL cells were stored at our laboratory and cultured in Dulbecco's modified Eagle's medium (DMEM) with 10% heat-inactivated fetal bovine serum (FBS, Gibco, Life Technologies) and antibiotics (streptomycin, 100 μg/ml; penicillin, 100 IU/ml; and amphotericin B, 0.25 μg/ml). All culture media were maintained in an incubator with 5% CO_2 at 37°C. The BHV-1 strain was obtained from the China Institute of Veterinary Drug Control (Beijing, China). Three New Zealand White rabbits (8 weeks old) were purchased from the Laboratory Animal Center of Harbin Veterinary Research Institute. The animal treatment protocols followed the Chinese Regulations of Laboratory Animals and the Guidelines for the Care of Laboratory Animals. The experiments on rabbits were approved by the Laboratory Animal Ethical Committee of Northeast Agricultural University.

Preparation and Detection of Rabbit Polyclonal Antibodies

An epitope of BHV-1 UL41 was designed and ligated into the pET30a(+) vector. The cloning and expression primers are shown in **Table 1**. Recombinant protein expression was induced with 1 μmol/L isopropyl β-D-1-thiogalactopyranoside (IPTG). The purified recombinant BHV-1 UL41 protein was collected from the gel and used as the immunogen to immunize rabbits. Specifically, after three freeze–thaw cycles, the gelled UL41 protein was injected subcutaneously. Two and four weeks after the first immunization, two more rounds of enhanced immunization were performed. Two weeks after the last

TABLE 1 | Cloning and expression primers used in this study.

Primers	Sequence (5'–3')
UL41-F	CGGCGCTTTCGCTCGCCTCTTA
UL41-R	CGCCTCCTGGGACCGATTT
UL24-F	CAGGTAGATACGCACGACGCGGAGA
UL24-R	TACAAAGACGCGGTCCGCGACTGCG
VP24-F	GCCAACCTGACGTTCCTCTGCG
VP24-R	CACCGTGTTATTTGCGGCTGTTT
30a-UL41-F	CGC*GGATCC*CGCGGCATCCACGGG
30a-UL41-R	CCG*CTCGAG*TTAGAGCCGAGGGTCGGG
30a-UL24-F	GC*GGATTCC*TGCAAAGCCGGCGGCCCGATT
30a-UL24-R	CG*CTCGAG*ATTGCCGCCCGACGCGTCTTTA
30a-VP24-F	GG*GGTACC*GCCCCCTCGCTCACGC
30a-VP24-R	CCC*AAGCTT*ATTAGCGTGCGACGGTGGCGG

immunization, the postimmunization serum containing polyclonal antibodies were collected. The rabbit anti-BHV-1 UL24 and anti-BHV-1 VP24 polyclonal antibodies were prepared in the same manner as the rabbit anti-BHV-1 UL41 polyclonal antibodies.

The sensitivity of the antibodies was detected with ELISA. Antigen (50 ng/well Ni^+ chromatographic affinity-purified recombinant protein) was coated onto the bottom of a 96-well ELISA plate, and 5% skimmed milk was added. The plate was incubated at 37°C for 1 h. The plate was rinsed three times with 1× PBST, and diluted polyclonal antibodies were added to the wells. The samples were incubated at 37°C for another hour and then rinsed three more times. A goat anti-rabbit horseradish peroxidase (HRP)-conjugated secondary antibody (ZB-2301, ZSGB-BIO, Beijing, China) was added, and the plate was incubated for 45 min at 37°C in an incubator. Then, the plate was rinsed, and 3,3′5,5′-tetramethylbenzidine (TMB) solution was used to visualize the HRP. Finally, 2 M H_2SO_4 was used as the stop solution to end the reaction. The results were read at 450 nm with a microplate reader.

The specificity of the polyclonal antibodies was detected by Western blotting. Recombinant proteins were separated by sodium dodecyl sulfate–polyacrylamide gel electrophoresis (SDS-PAGE) and transferred to nitrocellulose (NC) filter membranes (Pall Corporation, USA) with the prepared antibodies as the primary antibodies. A goat anti-rabbit HRP-conjugated antibody was used as the secondary antibody. A GeneGnome XRQ chemiluminescence imaging system (Syngene, UK) was used for image generation. A mouse anti-Flag antibody (M20008XS), mouse anti-Actin monoclonal antibody (M20003XS), and mouse anti-β-tubulin antibody (M20005XS) were purchased from Abmart (Shanghai, China).

Generation of CRISPR/Cas9 sgRNA plasmids

Three sgRNAs targeting the ORF of the UL41 gene were designed using the online CRISPR Design Tool (CRISPR gRNA Design tool - ATUM). The oligo sequences of the three sgRNAs are listed in **Table 2**. Recombinant plasmids were constructed. Briefly, the forward and reverse primers of the oligos $sgRNA_{UL41}1$–3 were annealed, and the oligos were ligated into the *Bbs*I-digested pX330-U6-Chimeric_BB-CBh-hSpCas9 vector. The recombinant plasmids were transformed into DH5α competent cells to amplify the constructs. All constructs were verified by BGI sequencing. Trans2K (BM101) and 15K (BM161) were purchased from TransGen Biotech (Beijing, China).

TABLE 2 | The targeting sgRNA oligo sequences.

Oligos	Sequence (5'–3')
sgRNA-1-F	CACCGATGTGCCAGCTTGGGCGCGT
sgRNA-1-R	AAACACGCGCCCAAGCTGGCACATC
sgRNA-2-F	CACCGCTTGGGCGCGTTGGCCCGCG
sgRNA-2-R	AAACCGCGGGCCAACGCGCCCAAGC
sgRNA-3-F	CACCGTACGCGTAACGCAGTAGCTT
sgRNA-3-R	AAACAAGCTACTGCGTTACGCGTAC

Gene Inactivation By CRISPR/Cas9

BL cells were seeded in six-well plates and transiently transfected 12 h later with CRISPR/Cas9 recombinant plasmids containing sgRNA using a 2× Max transfection reagent (purchased from Harbin Medical University, China). Before transfection, the 2× Max transfection reagent needed to be preheated at 56°C for 5–10 min. The transfection procedure was as follows: dilute 4 μg of DNA to 200 μl with serum-free DMEM; add 8 μl of 2 mg/ml of the Max transfection solution and vortex immediately; let it stand at room temperature for 10 min; and add the mixture to BL cells with 800 μl medium (with serum). Twelve hours post-transfection, the cells were inoculated with BHV-1at an multiplicity of infection (MOI) of 0.01. Forty-eight hours later, the supernatants were purified by plaque formation assay. Several plaques were randomly selected and placed in 48-well cell culture plates. After virus amplification, the cell lysates were analyzed by Western blotting. The supernatants were saved as the primary virus. The viral DNA of the UL41-defective strain was extracted using an AxyPrep Body Fluid Viral DNA/RNA Miniprep Kit (Axygen, USA) according to the manufacturer's instructions. Inactivation-specific genes were confirmed by DNA sequencing.

Effective sgRNA Screening

The resulting virus pools were screened by plaque formation assay and Western blotting. For the plaque formation assay, MDBK cells were seeded the six-well plates and starved for 1 h with serum-free DMEM. Then, serial dilutions (10^{-2}- to 10^{-6}-fold) of BHV-1 were injected with the cells for 2 h. The cells were rinsed three times with PBS, and the empty plates were overlaid with 0.7%–0.8% low-melting-point agarose (Amrosco, USA) mixed with DMEM and 2% FBS. The plates were further incubated at 37°C for 3 days. Then, the plates were stained with 0.5% neutral red and covered with a tinfoil in a 37°C incubator for 30 min. The plaque numbers were calculated in triplicate. Plaques were picked and inoculated into new cell culture plates to expand the viruses. Western blotting was conducted. Briefly, cells were collected, rinsed three times with PBS, and then lysed in RIPA lysis buffer (Beyotime Biotechnology, China) containing a protease inhibitor cocktail (Beyotime). The proteins contained in the cell lysates were separated by SDS-PAGE, and all proteins were transferred to the NC filter membranes. Prepared polyclonal antibodies were used as the primary antibodies to analyze viral protein expression. The defective virus (based on the protein expression levels) that was edited by the most effective sgRNA was selected in this study.

In vitro Growth Property Assessment

Wild-type (WT) BHV-1 or BHV-1 $UL41^-$ was used to infect MDBK cells at an MOI of 0.01. The cells were harvested 6, 12, 24, 36, 48, 60, and 72 h after infection. Serially diluted viruses (10^{-1}- to 10^{-8}-fold) were used to infect the cells at 37°C for 2 h. A PBS rinse was used to remove the excess viral inoculum. Then, 100 μl of 2% FBS DMEM was added to each well, and the cells were further cultured for 3 days. The cytopathic effects were recorded every day, and the tissue culture infective dose

($TCID_{50}$) value was calculated with the Reed–Muench method. The viral titers were recorded as the $TCID_{50}$/ml values at various time points.

Analysis of Viral Environmental Stability

The relative resistance levels of the virus strains to pH and temperature were compared. For acid–base stability analysis, the WT and BHV-1 $UL41^-$ viruses were placed in a pH of 5.0 or 9.0 and then recovered to the normal pH of 7.8. For thermal stability analysis, the virus fluids were incubated at 42°C or 65°C for 30 min and then stored at 4°C for 24 h. The environmental stability was recorded as the viral titers, which were calculated with the Reed–Muench method.

Quantitative Polymerase Chain Reaction Analysis (qPCR)

Total RNA was extracted with TRIzol, and first-strand cDNA was synthesized with NovoScript Plus All-in-one 1st Strand cDNA Synthesis SuperMix (gDNA Purge) according to the manufacturer's instructions. Quantitative PCR (qPCR) was performed on a Real-time PCR Detection System (ABI 7500 qPCR thermal cycler, USA) with a NovoStart SYBR qPCR SuperMix Plus Kit (Novoprotein Scientific). The viral and host mRNA detection primers are shown in **Table 3**. The 20 μl reaction system contained 10 μl of 2× SYBR SuperMix, 6.4 μl of qPCR primers (2.5 μM), 0.4 μl of ROX Reference Dye II, 1 μl of cDNA template, and 2.2 μl of ddH_2O. The reactions were carried out under the following thermal cycling conditions: 95°C for 30 s and 40 cycles of 95°C for 5 s and 60°C for 34 s. A dissociation curve analysis step was also performed. The 18S rRNA was amplified with specific primers to normalize amplification values of the triplicate samples. The comparative $2^{-\Delta CT}$ and $2^{-\Delta\Delta CT}$ methods were used to calculate the relative expression levels.

Statistical Analysis

Graphs were created and relevant statistical tests were performed with GraphPad Prism version 9.0.0 (121) (GraphPad Software, CA, USA) in this work. Statistical analysis was performed by one- or two-way ANOVA methods. Values of $^*p < 0.05$ were considered to indicate statistical significance.

TABLE 3 | Primers used in qPCR detection.

Oligos	Sequence (5'–3')
q-UL34-S	GTGCGTCTTCCAGTTCAA
q-UL34-A	GCCATTAGCCGCAAGATG
q-UL54-S	CTGCGAGACCTGGTGCTG
q-UL54-A	TTCTTGGTGGCGATGAACTTG
q-UL47-S	CGCCGACGACTACGATAG
q-UL47-A	TGCGTCTGTGTCCATAGC
q-ISG15-S	GCAGCCAACCAGTGTCTG
q-ISG15-A	CCTAGCATCTTCACCGTCAG
q-Mx1-S	TCAACCTCCACCGAACTG
q-Mx1-A	TCTTCTTCTGCCTCCTTCTC
q-Viperin-S	TACACCCACGTCCAAGATGG
q-Viperin-A	TACACCCACGTCCAAGATGG
q-OAS-S	TTCGGTCATCTTGCTCTCAG
q-OAS-A	GTCTATCTCAACAGTCACAATCC
18S rRNA-S	TGTGATGCCCTTAGATGTCC
18S rRNA-A	TTATGACCCGCACTTACTGG

RESULTS

Generation of CRISPR/Cas9 sgRNA Plasmids and Construction of BHV-1 $UL41^-$

To investigate the importance of the *UL41* gene for the lytic cycle of BHV-1, we constructed a BHV-1 UL41 defective strain. Using online software, we designed three specific sgRNAs to target the UL41 ORF. The targeting sequences and PAM are shown in **Figure 1A**. The designed three sgRNAs targeted the first 500 bp N-terminal sequence of the *UL41* gene. The $sgRNA_{UL41}1$–3 oligos were inserted into the pX330 vector and the U6-Forward primer was used with specific reverse primer for PCR amplification. The positive recombinant plasmids were identified by PCR (**Figure 1B**). The size of the positive amplification product was approximately 270 bp. To further confirm the insertion of the fragment into the pX330 vector, the restriction endonuclease *Eco*RV was used to digest the constructs, and the recombinant plasmids pX330-$sgRNA_{UL41}1$–3 were identified (**Figure 1C**). The overall size of the pX330 vector and insert was 8,509 bp, and the digestion identification results were as expected. We next tested whether the CRISPR/Cas9 recombinants effectively disrupted the BHV-1 genome by transfecting BL cells. The cells were infected with BHV-1 (MOI=0.01) 12 h post-transfection. BL cells were collected after 48 h of infection, and the cell lysates were analyzed by Western blotting (**Figure 1D**). The Cas9-Flag protein indicated the recombinant plasmids pX330-$sgRNA_{UL41}1$–3 were transfected into the BL cells, and the efficiency of transfection in BL was ideal.

Detection Sensitivity and Specificity of Rabbit Anti-BHV-1 UL41 Antibodies

To screen the recombinant defective mutants by Western blotting, we prepared sensitive and specific antibodies against BHV-1 viral proteins. Specifically, we prepared a rabbit anti-BHV-1 UL41 polyclonal antibody to further detect UL41 expression. Rabbit anti-BHV-1 UL24 and anti-BHV-1 VP24 polyclonal antibodies were prepared as BHV-1 infection-positive controls. The BHV-1 VP24 protein is encoded by the BHV-1 UL26 gene. The ectopic expression of UL41 protein was mainly expressed as an inclusion body with a molecular mass of 52 kDa in the Coomassie blue protein gel (**Figure 2A**), and the purified UL41 protein was prepared as the immunogen to immunize rabbits. The ectopic expression of UL41 protein was expressed with a His-tagged protein in the N-terminus of the insert sequence. **Figure 2B** shows that the ectopic expression of protein was detected with the mouse anti-His monoclonal antibody by Western blotting. Ectopically expressed UL24 showed soluble and inclusion body expression, and it was expressed with a molecular mass of 32 kDa. When the

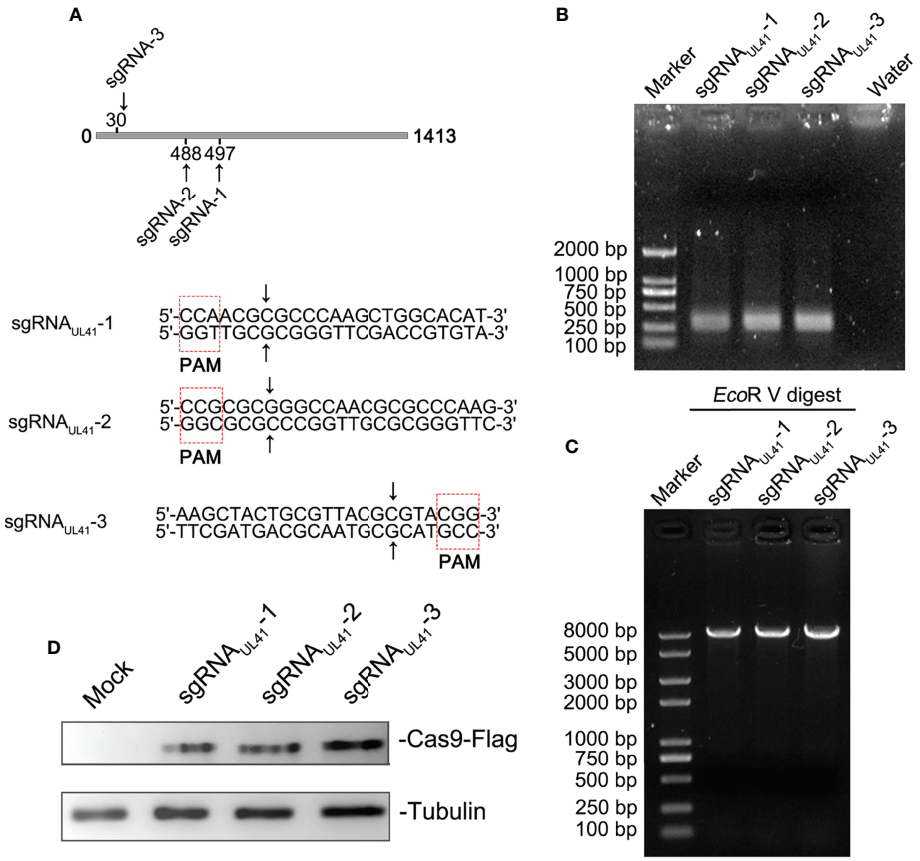

FIGURE 1 | Generation of CRISPR/Cas9 sgRNA plasmids and construction of BHV-1 UL41⁻. **(A)** CRISPR/Cas9 sgRNA-targeted sequences and PAM array. Three sgRNA targeting positions are marked in the UL41 sequence diagram. The CRISPR/Cas9-predicted cleavage sites are indicated by arrows. The red dotted frame areas are the PAM arrays. **(B)** PCR amplification of recombinant plasmids sgRNA$_{UL41}$1–3. The lanes are marked with different recombinant plasmids. Water was used for the negative control lane, and the DNA marker was a 2-kb molecular ladder. The molecular weight of the specific amplified fragment of the positive recombinant plasmids was 300 bp. **(C)** Restriction endonuclease digestion identification of recombinant plasmids. Digestion of the pX330 vector was performed with the *Eco*RV restriction enzyme, and the DNA marker was a 8-kb molecular ladder. **(D)** Analysis of the transfected CRISPR/Cas9 recombinant plasmids. Mock indicates BL cells treated with the transfection agent. Cas9 protein expression was detected with a mouse anti-Flag antibody. The three sgRNA recombinant plasmids are marked above the lane. Tubulin was the internal reference protein.

immunization schedule was finished, serum was collected and used as the polyclonal antibody. The sensitivity of the polyclonal antibody was detected using ELISA, and the P/N value was used to evaluate the serum titer. In our results, P/N=2 was used as the sensitivity criterion, and 1:102,400 was the serum-sensitive dilution of the rabbit anti-BHV-1 UL41 and anti-BHV-1 UL24 polyclonal antibody (**Figure 2C**). The specificity of the polyclonal antibody was detected by Western blotting. As shown in **Figures 2D, E**, the prepared antibodies reacted more strongly with the ectopic expression of proteins than with the vector protein, which indicated well specificity of the rabbit anti-BHV-1 UL41 and anti-BHV-1 UL24 polyclonal antibody. To identify the specificity of the rabbit anti-BHV-1 UL41 polyclonal antibody, the ectopic expression of UL24 and VP24 were used as the irrelevant antigens for detection (**Figure 2F**). The rabbit anti-BHV-1 UL41 polyclonal antibody exhibited good sensitivity and specificity in detection.

Effective sgRNA Screening and Identification of BHV-1 UL41⁻

The supernatants were serially diluted and used to infect MDBK cells to determine the effective sgRNA of BHV-1 UL41. A plaque formation assay was performed to assess the ability of the three groups of sgRNAs to target BHV-1 UL41. The numbers of viral plaques were significantly lower in the supernatants of the groups subjected to editing with sgRNA$_{UL41}$-1 than in those of the other two groups (**Figure 3A**), indicating that the BHV-1 genome was effectively disrupted by sgRNA$_{UL41}$-1. UL41 expression was relatively decreased under sgRNA$_{UL41}$-1 editing after BHV-1 infection for 48 h (**Figure 3B**). Next, we tested whether the DNA breaks induced inactivating indels at the targeted cleavage site. Several plaques were picked and used to inoculate the new MDBK plates. The virus was amplified, and UL41 expression was analyzed. Our results revealed that the A2 strain presented significantly defective UL41

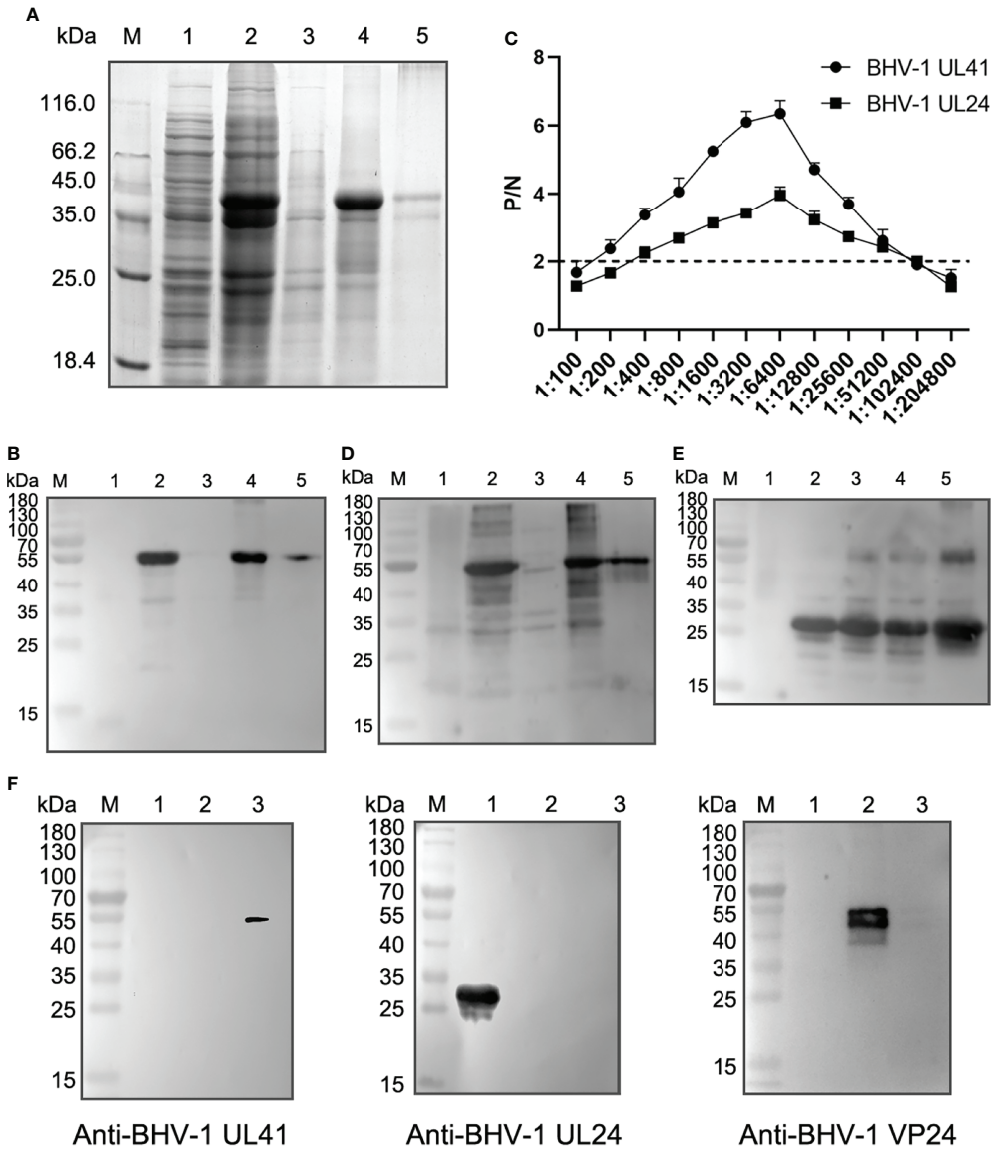

FIGURE 2 | Detection sensitivity and specificity of rabbit anti-BHV-1 UL41 antibodies. **(A)** Expression analysis of rHis-BHV-1 UL41. Lane M: protein molecular ladder; lane 1: negative control of the pET30a(+) vector; lane 2: rHis-BHV-1 UL41 after induction; lane 3: supernatants of rHis-BHV-1 UL41; lane 4: sedimentations of rHis-BHV-1 UL41; lane 5: purified rHis-BHV-1 UL41. **(B)** Western blot analysis of rHis-BHV-1 UL41 expression. Notes of the lanes are the same as panel **(A)**. A mouse anti-His monoclonal antibody was used as the primary antibody. **(C)** ELISA of rabbit anti-rHis-BHV-1 UL41 and rabbit anti-rHis-BHV-1 UL24 polyclonal antibodies. P/N indicates the positive value/negative value ratio. The horizontal axis indicates the serum dilution. The dotted line indicates a P/N value of 2, which was the criterion value. **(D)** Specificity analysis of a rabbit anti-rHis-BHV-1 UL41 polyclonal antibody. Notes of the lanes are the same as panel **(A)**.The prepared rabbit anti-BHV-1 UL41 polyclonal antibody was used as the primary antibody. **(E)** Specificity analysis of a rabbit anti-rHis-BHV-1 UL24 polyclonal antibody. Lane M: protein molecular ladder; lane 1: negative control of the pET30a(+) vector; lane 2: rHis-BHV-1 UL24 after induction; lane 3: supernatants of rHis-BHV-1 UL24; lane 4: sedimentations of rHis-BHV-1 UL24; lane 5: purified rHis-BHV-1 UL24. The prepared rabbit anti-BHV-1 UL24 polyclonal antibody was used as the primary antibody. **(F)** Specificity analysis of the rabbit anti-rHis-BHV-1 polyclonal antibodies. Lane M: protein molecular ladder; lane 1: purified rHis-BHV-1 UL24; lane 2: purified rHis-BHV-1 VP24; lane 3: purified rHis-BHV-1 UL41. The primary antibody on the left is the rabbit anti-rHis-BHV-1 UL41 polyclonal antibody; that in the middle is the rabbit anti-rHis-BHV-1 UL24 polyclonal antibody; and that on the right is the rabbit anti-rHis-BHV-1 VP24 polyclonal antibody.

expression (**Figure 3C**). Thus, the CRISPR/Cas9 system successfully disrupted the BHV-1 genome and induced indels. We further selected a purified A2 isolate for PCR-based sequencing. The UL41 gene of the A2 strain was successfully cloned, and it contained a deletion of "C" at the 497th nucleotide according to sequencing by BGI (**Figure 3D**). Thus, a UL41 gene-inactivated BHV-1 strain was successfully constructed (hereafter named BHV-1 UL41^{-}). The silencing of UL41 protein expression was confirmed by Western blot analysis compared to the expression in the WT strain. The correct

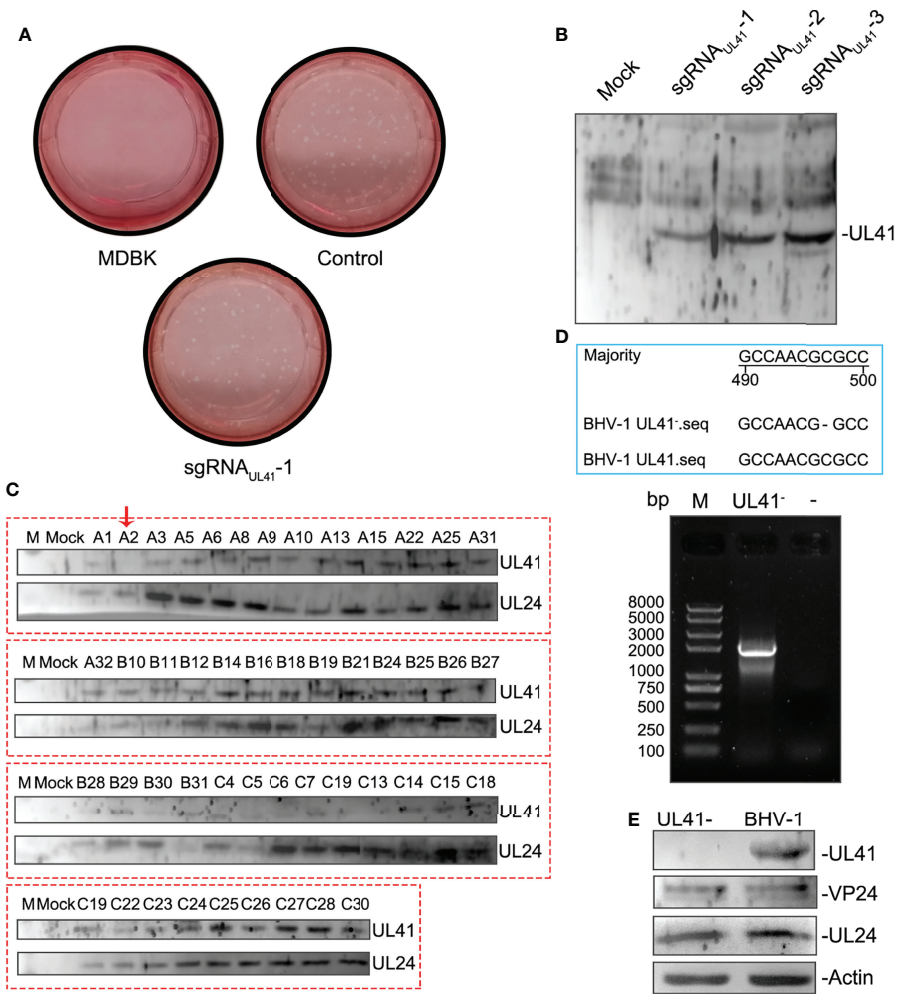

FIGURE 3 | Effective sgRNA screening and identification of BHV-1 UL41^{-}. **(A)** sgRNA$_{UL41}$-1 inhibited BHV-1 plaque formation. BL cells were transfected with 4 μg of sgRNA$_{UL41}$-1, sgRNA$_{UL41}$-2, or sgRNA$_{UL41}$-3. Twelve hours later, the cells were infected with BHV-1 (MOI=0.01), and the supernatants were subjected to a plaque formation assay after 48 h of infection. "Control" indicates the supernatants edited by the plasmids sgRNA$_{UL41}$-2 and sgRNA$_{UL41}$-3 for the plaque formation assay. The plaque numbers were calculated in three independent assays, ** for $p < 0.01$. **(B)** sgRNA$_{UL41}$-1 inhibited BHV-1 UL41 expression. The cell lysates from panel **(A)** were subjected to Western blotting. UL41 expression was detected with the prepared polyclonal antibodies. "Mock" indicates blank BL cells. sgRNA$_{UL41}$-1–3 indicates the cells infected with the sgRNA-Cas9-edited viruses. **(C)** BHV-1 UL41^{-} screening. Plaques from the sgRNA$_{UL41}$-1 group were inoculated into 48-well plates. The cell lysates were collected after virus amplification and analyzed by Western blotting. A2 indicates the UL41-silenced expression virus and is marked with a red arrow. Letters A–C before the numbers indicate the plaques that were amplified from the three sgRNAs (A for sgRNA$_{UL41}$-1, B for sgRNA$_{UL41}$-2, and C for sgRNA$_{UL41}$-3). BHV-1 UL24 and UL41 were detected with the prepared polyclonal antibodies. UL24 was used as the BHV-1 infection reference control. **(D)** Cloning and sequencing analysis of the defective viral UL41 gene. Lane M: Trans 2K Plus II DNA ladder. The blue-line-framed area represents the 490- to 500- nucleotide sequencing results of BHV-1 UL41^{-}; "–" in the BHV-1 UL41^{-} sequence indicates an absent nucleotide. The "–" above the agarose gel chart indicates the water negative control. UL41^{-} indicates the UL41 gene amplification of the deficient virus. **(E)** Western blot analysis of the BHV-1 UL41^{-} strain. "UL41^{-}" indicates the BHV-1 UL41^{-} strain, and BHV-1 indicates the parent strain. UL41, VP24, and UL24 were detected by the prepared polyclonal antibodies. Actin was used as the internal reference control; UL24 and VP24 were used as the BHV-1 infection reference controls.

expression of the UL24 and VP24 proteins in BHV-1 UL41^{-} (**Figure 3E**) indicated that sgRNA$_{UL41}$-1 had good target specificity.

Evaluation of Viral Replication and Environmental Stability

To determine whether UL41 inactivation affected BHV-1 replication, the replication properties of the virus were analyzed. MDBK cells were separately infected with BHV-1 UL41^{-} and the WT strain at an MOI of 0.01. As depicted in **Figure 4A**, the growth property of BHV-1 UL41^{-} resembled that of the WT strain. One-step growth curves indicated that the defective mutant replicated slower than the parent virus from 36 to 60 h and that it replicated earlier than the WT strain. The WT strain did not show replication at 36 h, as shown in **Figure 4A**. Next, we tested the cell tropism of BHV-1 in various research cell

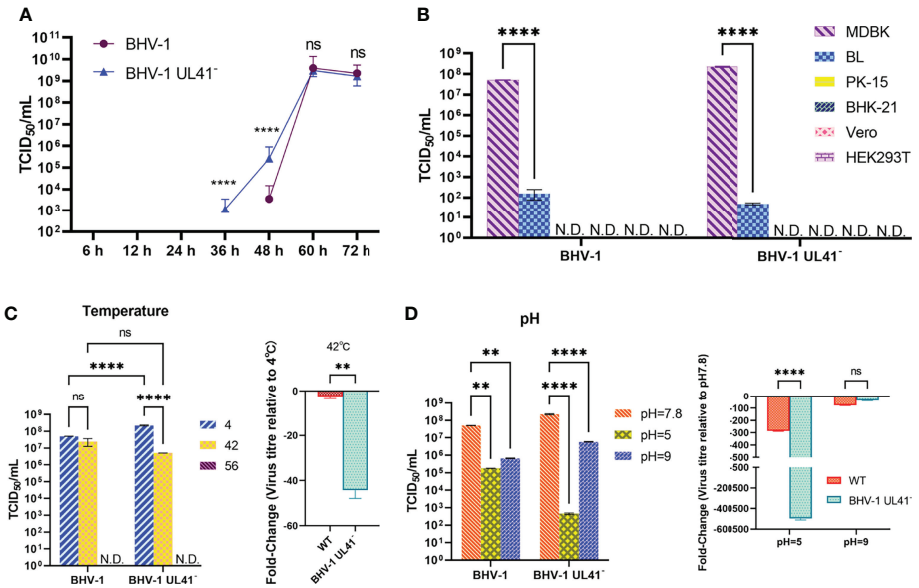

FIGURE 4 | Evaluation of viral replication and environmental stability. **(A)** One-step growth curve of the BHV-1 UL41⁻ and WT viruses. MDBK cells were infected with viruses at an MOI of 0.01, and the viruses were collected after inoculation for 6, 12, 24, 36, 48, 60, and 72 h. The viral titers were recorded as $TCID_{50}$/ml values. The blue triangle indicates the growth curve of BHV-1 UL41⁻, and the purple circle indicates the growth curve of the WT strain. **(B)** Cell tropism analysis of BHV-1 UL41⁻ and the WT strain. MDBK, BL, PK-15, BHK-21, Vero, and HEK293T cells were used to detect the cell tropism of the viruses. N.D. stands for not detected. **(C)** Temperature sensitivity analysis of BHV-1 UL41⁻ and the WT strain. The number 4 indicates that the viruses were collected and stored at 4°C for temperature stability detection. The number 42 indicates that the viruses were kept at 42°C for 30 min and cold at 4°C. The number 56 indicates that the viruses were kept at 56°C for 30 min and cold at 4°C. The data are plotted as the fold change over 4°C. N.D. stands for not detected. **(D)** pH sensitivity analysis of BHV-1 UL41⁻ and the parent strain. pH 7.8 indicates the pH of the initial viral solution; pH 5 indicated that the viruses recovered to pH 7.8 from pH 5; pH 9 indicates that the viruses recovered to pH 7.8 from pH 9; and the data are plotted as the fold change over pH 7.8. The viral titers were detected in three independent experiments and calculated as the mean ± SD. **** for $p < 0.0001$, ** for $p < 0.01$, and ns for no significance.

lines. **Figure 4B** shows that the virus was able to infect the two bovine-derived cell lines, while the MDBK cells presented enhanced adaptability to BHV-1 infection. The viral titer of BHV-1 replication in BL cells was lower (by almost 10^5-fold) than that in MDBK cells. BHV-1 UL41⁻ showed the same cell tropism with the WT strain. To investigate the relative resistance of the defective and WT strains to temperature and pH variations, the viral titers were measured after the environment was changed. The replication of the virus slightly declined with increasing temperature (**Figure 4C**). However, the titer of the defective strain was 40-fold lower than that of the WT strain after the viruses recovered from 42°C exposure. The viruses were inactivated after recovery from 56°C. They replicated relatively stably in the low-temperature environment. BHV-1 UL41⁻ exhibited enhanced sensitivity to the pH 2.0 environment; the viral titer in this strain decreased by 10^5-fold, while the titer in the WT strain decreased by only 200-fold after recovery from the pH 2.0 environment. Both BHV-1 UL41⁻ and the WT strain presented alkaline resistance characteristics after recovery from the pH 9.0 environment (**Figure 4D**). The viral titers of BHV-1 UL41⁻ and the WT strain were 100-fold lower than those under pH 7.8. In our research, BHV-1 UL41⁻ and the WT strain showed different acid–base stabilities in MDBK infections, which also indicated that the viruses could not stably stay in an overly acidic environment. We further tested the stability of BHV-1 UL41⁻ through 10 serial passages in MDBK cells. No reversion mutation was found by sequencing.

The BHV-1 UL41-Deficient Strain Regulates Viral and Host mRNAs

To further investigate whether BHV-1 UL41 regulates viral and host mRNA levels to affect viral replication, MDBK cells were infected with BHV-1 UL41⁻ and the WT strain at an MOI of 1. Samples were collected and then assessed by reverse transcription qPCR. As shown in **Figure 5A**, compared with those in the WT strain, the mRNA levels of the immediate early (IE) gene UL34, the early (E) gene UL54, and the late (L) gene UL47 were changed in the BHV-1 UL41⁻-infected group. The levels of the viral IE and E genes were significantly increased, while those of the viral L gene were significantly decreased. Furthermore, we found that some host genes also exhibited significant changes in BHV-1 UL41⁻ infections (**Figure 5B**). Interferon-stimulated gene 15 (ISG15), Viperin, and oligoadenylate synthetase (OAS) mRNA levels were significantly increased, and Mx1 mRNA levels were significantly decreased. These results showed that stronger regulation of viral and host RNAs occurs following infection with BHV-1 UL41⁻ and indicate that BHV-1 UL41 broadly regulates viral and host mRNAs to affect viral replication.

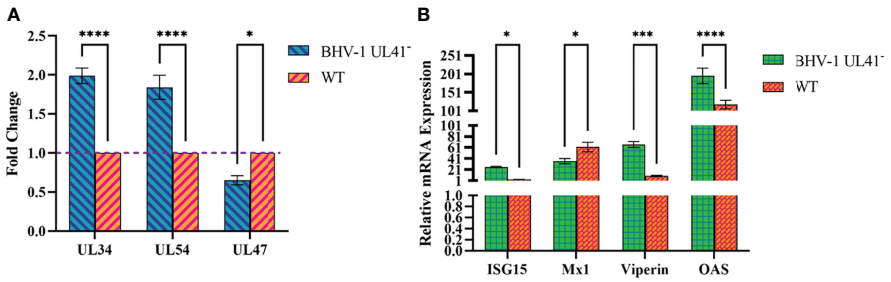

FIGURE 5 | BHV-1 UL41⁻ regulates viral and host mRNAs. **(A)** BHV-1 UL41 regulates viral mRNA. The BHV-1 UL41⁻ and WT strains were used to infect MDBK cells at an MOI of 1, and total RNA was collected at 12 hpi. The mRNA levels of the immediate early gene UL34, the early gene UL54, and the late gene UL47 were analyzed using reverse transcription qPCR and normalized to those of 18S rRNA. The data are plotted as the fold change over the WT strain. **(B)** BHV-1 UL41 regulates host mRNA. The BHV-1 UL41⁻ and WT strains were used to infect MDBK at an MOI of 1, and total RNAs RNA was collected at 8 hpi. The relative gene expression levels were determined with the $2^{-\Delta\Delta CT}$ method. The viral titers were detected in three independent experiments and calculated as the mean ± SD. **** for $p < 0.0001$, *** for $p < 0.001$, and * for $p < 0.05$.

DISCUSSION

Here, we used the BL primary cell line as the construction platform (Osorio and Bionaz, 2017), not only because it could be relatively well transfected with the targeting sgRNA CRISPR/Cas9 system plasmids but also because replication of BHV-1 could be achieved. We found a higher transfection efficiency of BL cells compared to MDBK cells (**Supplementary Figure S1**) and the cells cloud transfected as the normal primary cells with many transfection reagents. We had tried Lipofectamine 3000 and the Max transfection reagent in BL cells, and the transfection efficiency was similar. A specific sgRNA was used to rapidly edit the BHV-1 genome with the CRISPR/Cas9 system. Efficient sgRNAs were screened using polyclonal antibodies that specifically reacted with the expressed target protein expression by Western blotting. We simplified the construction and identification process, and the BHV-1 UL41⁻ strain was effectively screened using specific polyclonal antibodies. Although the CRISPR/Cas9 gene-editing system has some limitations for use in BHV-1 gene inactivation, previous research (Lobanov et al., 2010; Zhang et al., 2011; Sucharita et al., 2021) has revealed that a pivotal step is the discovery of highly transfectable cell lines that can be infected with the virus. The important challenges of CRISPR/Cas9 in genome editing were addressed by Zhang et al. (2014). One of the four issues was the delivery methods, and the efficiency of the delivery methods depends on the types of target cells and tissues. The other three challenges were off-target mutations, PAM dependence, and gRNA production. We selected the most efficient sgRNA for the given coding sequence. The construction method was rapid but had low efficacy. In our research, the UL41 gene was silently expressed in only one strain, so more convenient and highly mutagenic methods need to be studied.

The canonical mutations in a single nucleotide include insertions, substitutions, deletions, and subversions introduced into target genes. The strain under investigation, BHV-1 UL41⁻, appeared to have the single deletion of the nucleotide "C." In this study, we attempted to identify the ORFs that target genes by using anti-UL41, anti-UL24, and anti-VP24 polyclonal antibodies to detect the expression of these genes. These antibodies were prepared in rabbits using the major antigenic domain of each ORF, and they had high sensitivity and specificity for the target proteins. We inactivated the UL41 ORF by introducing frameshift mutations; nucleotide-deletion-induced frameshift mutations are prone to silencing in WT sequences. In the future, to improve the viral reversion problems, large fragment deletions spanning the ORFs can be targeted in gene editing.

The ratio of gene disruption was determined according to the sgRNA efficacy. Although multiple CRISPR sequence online design tools can be utilized, many software programs depend fully on computational analysis, resulting in the design of numerous unclassified sgRNAs (Brazelton et al., 2015). In addition, the BHV-1 genome contains a high GC content, and only three advanced evaluated sgRNAs are available; those with higher scores are more effective. To obtain optimal results, the most effective sgRNA was selected for further study.

The biological characteristics of the BHV-1 UL41-defective strain in viral replication were examined. The BHV-1 UL41⁻ strain showed early viral replication, but it was slower than that of the parent strain. BHV-1 UL41 might shut off host proteins to promote viral replication at the early stage of infection and then interact with other viral proteins to interrupt host and virus shutoff functions. The interaction of UL41 with other proteins needs to be further explored. BHV-1 UL41⁻ was more sensitive to high temperature and acidic environments than the WT strain. Our results reveal that UL41 affects the physical and chemical characteristics of the virus, including the growth curve, temperature sensitivity, and acid–base tolerance. However, the main biological characteristics of the virus are not altered; that is, the virus can still be inactivated at 56°C and is relatively alkaline resistant.

The cell tropism experiment revealed that bovine-derived cells were susceptible to BHV-1 and that the MDBK cells were most suitable for use to evaluate viral replication and proliferation. Although the replication ability of BHV-1 was not as good in BL cells as it was in MDBK cells, BL cells still exhibited greater virus susceptibility than other animal-derived

cells. MDBK cells are ideal for viral replication, but they have a challenging limitation for use in the construction of a gene-editing virus platform: the efficiency of MDBK cell transfection is low, approximately 1.7%–2.4% (Osorio and Bionaz, 2017), and the transfection efficiency of primary cells was higher than that of MDBK (**Supplementary Figure S1**). Therefore, BL cells were used as the platform for construction of the gene-editing virus, and MDBK cells were used as the evaluation model in the subsequent virus biological detection experiments.

BHV-1 UL34, UL54, and UL47 were the representative IE, E, and L genes, respectively (Robinson et al., 2008). ISG15, Mx1, Viperin, and OAS are important immune response molecules induced by interferon and play an important role in host resistance to pathogenic invasion. We selected these genes to investigate the effects of invasion by viruses. The reverse transcription qPCR results showed that BHV-1 UL41^{-} induced viral IE and E gene transcription at a relatively early stage and increased the host mRNA transcript levels. This result indicates that BHV-1 UL41 can inhibit viral IE and E gene transcription and decrease the host mRNA levels to facilitate viral replication.

In the present study, we rapidly knocked out the BHV-1 UL41 gene using the CRISPR/Cas9 gene-editing system. The viral replication levels of BHV-1 UL41^{-} and the WT strain were compared in multiple dimensions. The UL41-defective virus exhibited early but has slow viral replication and increased sensitivity to temperature and the acidity of the environment. The viral and host mRNA levels were regulated in the defective strain compared to the WT strain. Our strategy is pivotal for promoting BHV-1 control and prevention in China. Other viral genes of BHV-1 could also be considered for silencing expression by this method. In addition, efficient viral delivery systems such as lentivirus, adenovirus, or MultiBacMam could also be considered for delivery of CRISPR/Cas9 editing systems in BHV-1 genome editing. Based on the CRISPR/Cas9 gene-editing system, more viral gene functions of the BHV-1 genome could be explored.

DATA AVAILABILITY STATEMENT

The original contributions presented in the study are included in the article/supplementary material. Further inquiries can be directed to the corresponding authors.

ETHICS STATEMENT

The animal study was reviewed and approved by the Laboratory Animal Ethical Committee of Northeast Agricultural University.

AUTHOR CONTRIBUTIONS

HYD wrote the first draft of the manuscript. MG and JWW contributed to the conception and design of the study. YG performed the statistical analysis. JNW organized the database. HQD and HY wrote sections of the manuscript. All authors contributed to manuscript revision, read, and approved the submitted version.

FUNDING

We extend our sincere thanks to all the authors who have devoted themselves to this research. This work was supported by the National Natural Science Foundation of China (32002296) and China Agriculture Research System of MOF and MARA.

ACKNOWLEDGMENTS

This manuscript was edited for English language by American Journal Experts (AJE).

SUPPLEMENTARY MATERIAL

The Supplementary Material for this article can be found online at: https://www.frontiersin.org/articles/10.3389/fcimb.2022.942987/full#supplementary-material

Supplementary Figure 1 | The transfection efficiency of BL cells and MDBK cells. **(A)** Direct fluorescence analysis of the transfection efficiency of BL and MDBK. A plasmid of pcDNA3.1-EGFP transfected into BL and MDBK cells by 2× Max transfection reagent, **(B)** Western blot analysis of the transfection efficiency of BL and MDBK. Recombinant plasmids of pX330-sgRNA$_{UL41}$1-3 were transfected into BL and MDBK cells by Lipofectamine 3000 reagent (Invitrogen, USA). Cas9-Flag indicated the expression of recombinant plasmids, and GAPDH was the internal reference protein.

REFERENCES

Ackermann, M., and Engels, M. (2006). Pro and Contra IBR-Eradication. *Vet. Microbiol.* 113 (3-4), 293–302. doi: 10.1016/j.vetmic.2005.11.043

Borca, M. V., Berggren, K. A., Ramirez-Medina, E., Vuono, E. A., and Gladue, D. P. (2018). CRISPR/Cas Gene Editing of a Large DNA Virus: African Swine Fever Virus. *Bio Protoc.* 8 (16), e2978. doi: 10.21769/BioProtoc.2978

Brazelton, V. J., Zarecor, S., Wright, D. A., Wang, Y., Liu, J., Chen, K., et al. (2015). a Quick Guide to CRISPR sgRNA Design Tools. *GM Crops Food* 6 (4), 266–276. doi: 10.1080/21645698.2015.1137690

Das, A. T., Binda, C. S., and Berkhout, B. (2019). Elimination of Infectious HIV DNA by CRISPR-Cas9. *Curr. Opin. Virol.* 38, 81–88. doi: 10.1016/j.coviro.2019.07.001

Desloges, N., Rahaus, M., and Wolff, M. H. (2005). The Varicella-Zoster Virus-Mediated Delayed Host Shutoff: Open Reading Frame 17 has No Major Function, Whereas Immediate-Early 63 Protein Represses Heterologous Gene Expression. *Microbes Infect.* 7 (15), 1519–1529. doi: 10.1016/j.micinf.2005.05.010

Elliott, G., Pheasant, K., Ebert-Keel, K., Stylianou, J., Franklyn, A., and Jones, J. (2018). Multiple Posttranscriptional Strategies to Regulate the Herpes Simplex Virus 1 Vhs Endoribonuclease. *J. Virol.* 92 (17), e00818–18. doi: 10.1128/JVI.00818-18

He, T., Wang, M., Cheng, A., Yang, Q., Jia, R., Wu, Y., et al. (2021). DPV UL41 Gene Encoding Protein Induces Host Shutoff Activity and Affects Viral Replication. *Vet. Microbiol.* 255, 108979. doi: 10.1016/j.vetmic.2021.108979

He, T., Wang, M., Cheng, A., Yang, Q., Wu, Y., Jia, R., et al. (2020). Host Shutoff Activity of VHS and SOX-Like Proteins: Role in Viral Survival and Immune Evasion. *Virol. J.* 17 (1), 68. doi: 10.1186/s12985-020-01336-8

Lin, H. W., Hsu, W. L., Chang, Y. Y., Jan, M. S., Wong, M. L., and Chang, T. J. (2010). Role of the UL41 Protein of Pseudorabies Virus in Host Shutoff, Pathogenesis and Induction of TNF-Alpha Expression. *J. Vet. Med. Sci.* 72 (9), 1179–1187. doi: 10.1292/jvms.10-0059

Liu, Y. F., Tsai, P. Y., Chulakasian, S., Lin, F. Y., and Hsu, W. L. (2016). The Pseudorabies Virus Vhs Protein Cleaves RNA Containing an IRES Sequence. *FEBS J.* 283 (5), 899–911. doi: 10.1111/febs.13642

Lobanov, V. A., Maher-Sturgess, S. L., Snider, M. G., Lawman, Z., Babiuk, L. A., and van Drunen, L. D. H. S. (2010). A UL47 Gene Deletion Mutant of Bovine Herpesvirus Type 1 Exhibits Impaired Growth in Cell Culture and Lack of Virulence in Cattle. *J. Virol.* 84 (1), 445–458. doi: 10.1128/JVI.01544-09

Luo, J., Teng, M., Zai, X., Tang, N., Zhang, Y., Mandviwala, A., et al. (2020). Efficient Mutagenesis of Marek's Disease Virus-Encoded Micrornas Using a CRISPR/Cas9-Based Gene Editing System. *Viruses* 12 (4), 466. doi: 10.3390/v12040466

Ma, W., Wang, H., and He, H. (2019). Bovine Herpesvirus 1 Tegument Protein UL41 Suppresses Antiviral Innate Immune Response *via* Directly Targeting STAT1. *Vet. Microbiol.* 239, 108494. doi: 10.1016/j.vetmic.2019.108494

Neuhausser, W. M., Oh, H. S., Eggan, P., Angelova, M., Kirchner, R., Eggan, K. C., et al. (2020). Screening Method for CRISPR/Cas9 Inhibition of a Human DNA Virus: Herpes Simplex Virus. *Bio Protoc.* 10 (17), e3748. doi: 10.21769/BioProtoc.3748

Osorio, J. S., and Bionaz, M. (2017). Plasmid Transfection in Bovine Cells: Optimization Using a Realtime Monitoring of Green Fluorescent Protein and Effect on Gene Reporter Assay. *Gene* 626, 200–208. doi: 10.1016/j.gene.2017.05.025

Robinson, K. E., Meers, J., Gravel, J. L., McCarthy, F. M., and Mahony, T. J. (2008). The Essential and non-Essential Genes of Bovine Herpesvirus 1. *J. Gen. Virol.* 89 (Pt 11), 2851–2863. doi: 10.1099/vir.0.2008/002501-0

Shu, M., Taddeo, B., and Roizman, B. (2013a). The Nuclear-Cytoplasmic Shuttling of Virion Host Shutoff RNase is Enabled by Pul47 and an Embedded Nuclear Export Signal and Defines the Sites of Degradation of AU-Rich and Stable Cellular Mrnas. *J. Virol.* 87 (24), 13569–13578. doi: 10.1128/JVI.02603-13

Shu, M., Taddeo, B., Zhang, W., and Roizman, B. (2013b). Selective Degradation of Mrnas by the HSV Host Shutoff RNase is Regulated by the UL47 Tegument Protein. *Proc. Natl. Acad. Sci. U. S. A.* 110 (18), E1669–E1675. doi: 10.1073/pnas.1305475110

Smith, T. J., Ackland-Berglund, C. E., and Leib, D. A. (2000). Herpes Simplex Virus Virion Host Shutoff (Vhs) Activity Alters Periocular Disease in Mice. *J. Virol.* 74 (8), 3598–3604. doi: 10.1128/jvi.74.8.3598-3604.2000

Stokol, T., and Soboll, H. G. (2019). Editorial: Current Research in Equid Herpesvirus Type-1 (EHV-1). *Front. Vet. Sci.* 6. doi: 10.3389/fvets.2019.00492

Sucharita, S., Zhang, K., and van Drunen, L. D. H. S. (2021). VP8, the Major Tegument Protein of Bovine Herpesvirus-1, is Partially Packaged During Early Tegument Formation in a VP22-Dependent Manner. *Viruses* 13 (9), 1854. doi: 10.3390/v13091854

Taddeo, B., and Roizman, B. (2006). The Virion Host Shutoff Protein (UL41) of Herpes Simplex Virus 1 is an Endoribonuclease With a Substrate Specificity Similar to That of RNase A. *J. Virol.* 80 (18), 9341–9345. doi: 10.1128/JVI.01008-06

Tang, N., Zhang, Y., Shen, Z., Yao, Y., and Nair, V. (2021). Application of CRISPR-Cas9 Editing for Virus Engineering and the Development of Recombinant Viral Vaccines. *CRISPR J.* 4 (4), 477–490. doi: 10.1089/crispr.2021.0017

Valyi-Nagy, T., Shukla, D., Engelhard, H. H., Kavouras, J., and Scanlan, P. (2007). ""Latency Strategies of Alphaherpesviruses: Herpes Simplex Virus and Varicella-Zoster Virus Latency in Neurons," in *Latency Strategies of Herpesviruses*. Eds. J. Minarovits, E. Gonczol and T. Valyi-Nagy (Boston, MA: Springer US).

Van Cleemput, J., Koyuncu, O. O., Laval, K., Engel, E. A., and Enquist, L. W. (2021). CRISPR/Cas9-Constructed Pseudorabies Virus Mutants Reveal the Importance of UL13 in Alphaherpesvirus Escape From Genome Silencing. *J. Virol.* 95 (6), e02286–20. doi: 10.1128/JVI.02286-20

Velusamy, T., Gowripalan, A., and Tscharke, D. C. (2020). CRISPR/Cas9-Based Genome Editing of HSV. *Methods Mol. Biol.* 2060, 169–183. doi: 10.1007/978-1-4939-9814-2_9

Weidner-Glunde, M., Kruminis-Kaszkiel, E., and Savanagouder, M. (2020). Herpesviral Latency-Common Themes. *Pathogens* 9 (2), 125. doi: 10.3390/pathogens9020125

Wentink, G. H., van Oirschot, J. T., and Verhoeff, J. (1993). Risk of Infection With Bovine Herpes Virus 1 (BHV1): a Review. *Vet. Q* 15 (1), 30–33. doi: 10.1080/01652176.1993.9694365

Yang, S., Wu, Q., Wei, Y., and Gong, C. (2019). CRISPR-Cas9 Delivery by Artificial Virus (Rrphc). *Methods Mol. Biol.* 1961, 81–91. doi: 10.1007/978-1-4939-9170-9_6

Zhang, M., Fu, S., Deng, M., Xie, Q., Xu, H., Liu, Z., et al. (2011). Attenuation of Bovine Herpesvirus Type 1 by Deletion of its Glycoprotein G and Tk Genes and Protection Against Virulent Viral Challenge. *Vaccine* 29 (48), 8943–8950. doi: 10.1016/j.vaccine.2011.09.050

Zhang, F., Wen, Y., and Guo, X. (2014). CRISPR/Cas9 for Genome Editing: Progress, Implications and Challenges. *Hum. Mol. Genet.* 23 (R1), R40–6. doi: 10.1093/hmg/ddu125

Conflict of Interest: The authors declare that the research was conducted in the absence of any commercial or financial relationships that could be construed as a potential conflict of interest.

Publisher's Note: All claims expressed in this article are solely those of the authors and do not necessarily represent those of their affiliated organizations, or those of the publisher, the editors and the reviewers. Any product that may be evaluated in this article, or claim that may be made by its manufacturer, is not guaranteed or endorsed by the publisher.

frontiers | Frontiers in Cellular and Infection Microbiology

TYPE Original Research
PUBLISHED 18 July 2022
DOI 10.3389/fcimb.2022.967493

OPEN ACCESS

EDITED BY
Zhanbo Zhu,
Heilongjiang Bayi Agricultural University, China

REVIEWED BY
Hongwei Wang,
Nanjing University, China
Zhiyong Li,
Lanzhou Veterinary Research Institute (CAAS), China

*CORRESPONDENCE
Chang Li
lichang78@163.com
Linzhu Ren
renlz@jlu.edu.cn
Ningyi Jin
ningyik@126.com

†These authors have contributed equally to this work

SPECIALTY SECTION
This article was submitted to Clinical Microbiology, a section of the journal Frontiers in Cellular and Infection Microbiology

RECEIVED 13 June 2022
ACCEPTED 28 June 2022
PUBLISHED 18 July 2022

CITATION
Chen J, Xu W, Li L, Yi L, Jiang Y, Hao P, Xu Z, Zou W, Li P, Gao Z, Tian M, Jin N, Ren L and Li C (2022) Immunogenicity and protective potential of chimeric virus-like particles containing SARS-CoV-2 spike and H5N1 matrix 1 proteins. *Front. Cell. Infect. Microbiol.* 12:967493. doi: 10.3389/fcimb.2022.967493

Immunogenicity and protective potential of chimeric virus-like particles containing SARS-CoV-2 spike and H5N1 matrix 1 proteins

Jing Chen[1,2†], Wang Xu[2†], Letian Li[2], Lichao Yi[2], Yuhang Jiang[2], Pengfei Hao[2], Zhiqiang Xu[2], Wancheng Zou[2], Peiheng Li[2], Zihan Gao[2], Mingyao Tian[2], Ningyi Jin[2*], Linzhu Ren[3*] and Chang Li[2*]

[1]College of Veterinary medicine, Key Lab for Zoonoses Research, Ministry of Education, Jilin University, Changchun, China, [2]Research Unit of Key Technologies for Prevention and Control of Virus Zoonoses, Chinese Academy of Medical Sciences, Changchun Veterinary Research Institute, Chinese Academy of Agricultural Sciences, Changchun, China, [3]College of Animal Sciences, Key Lab for Zoonoses Research, Ministry of Education, Jilin University, Changchun, China

Coronavirus Disease 2019 (COVID-19), caused by severe acute respiratory syndrome coronavirus type 2 (SARS-CoV-2), has posed a constant threat to human beings and the world economy for more than two years. Vaccination is the first choice to control and prevent the pandemic. However, an effective SARS-CoV-2 vaccine against the virus infection is still needed. This study designed and prepared four kinds of virus-like particles (VLPs) using an insect expression system. Two constructs encoded wild-type SARS-CoV-2 spike (S) fused with or without H5N1 matrix 1 (M1) (S and SM). The other two constructs contained a codon-optimized spike gene and/or M1 gene (mS and mSM) based on protein expression, stability, and ADE avoidance. The results showed that the VLP-based vaccine could induce high SARS-CoV-2 specific antibodies in mice, including specific IgG, IgG1, and IgG2a. Moreover, the mSM group has the most robust ability to stimulate humoral immunity and cellular immunity than the other VLPs, suggesting the mSM is the best immunogen. Further studies showed that the mSM combined with Al/CpG adjuvant could stimulate animals to produce sustained high-level antibodies and establish an effective protective barrier to protect mice from challenges with mouse-adapted strain. The vaccine based on mSM and Al/CpG adjuvant is a promising candidate vaccine to prevent the COVID-19 pandemic.

KEYWORDS

severe acute respiratory syndrome coronavirus type 2 (SARS-CoV-2), Coronavirus Disease 2019 (COVID-19), virus-like particle (VLP), spike, chimeric

Introduction

Coronavirus can infect many kinds of animals, and it can also cause mild to severe respiratory tract infections in humans. Since it was first reported in China in December 2019, severe acute respiratory syndrome coronavirus type 2 (SARS-CoV-2), as well as two zoonotic highly pathogenic coronaviruses SARS-CoV and Middle East respiratory syndrome coronavirus (MERS-CoV), which appeared in 2002 and 2012 respectively, have made coronavirus infection a new and vital public health problem in the 21st century (Cui et al., 2019).

Significantly, the continuous emergence of the SARS-CoV-2 variants of concern (VOCs), such as Delta, Omicron, and their derivates, have posed a constant threat to human beings and the world economy (Hui et al., 2020; Li et al., 2021a). Although the vaccine is the best choice to prevent virus infection, the main target of current vaccines is viral Spike protein, which may escape the recognition of the vaccine through mutation over time, resulting in the decline of the protection rate of vaccines (Callaway, 2021a; Flanagan et al., 2021; Mccallum et al., 2021; Murano et al., 2021; Pulliam et al., 2022). As reported, mutations in the Spike of variants Kappa and Delta eliminated the recognition of several monoclonal antibodies by changing key antigenic sites, including remodeling the N-terminal domain of the Spike and acquiring an N-linked glycan in the receptor-binding domain (RBD), with a markedly reduced affinity between the Spike and receptor Angiotensin-converting enzyme 2 (ACE2) (Wrapp et al., 2020; Flanagan et al., 2021; Mccallum et al., 2021; Murano et al., 2021; Nabel et al., 2022). These results were similar to the antigenic evolution of the viral Spike in coronavirus 229E, especially in the RBD (Eguia et al., 2021). Furthermore, the currently dominant VOC Omicron harbors more mutations than other variants reported previously, suggesting that SARS-CoV-2 variants further adapt to the human body through continuous mutation, especially in immune-compromised individuals during chronic infection (Callaway, 2021b; Li et al., 2021a; Pulliam et al., 2022). A phylogenetic tree based on the mutations in the S1 subunit of viral Spike showed that the Omicron is far from other variants, indicating that Omicron evolved in parallel with other variants (Kupferschmidt, 2021). These results suggest that the Omicron may escape the vaccine and has enhanced infectivity and/or pathogenicity, proved in the previously reported VOCs. Moreover, although currently available vaccines can induce SARS-CoV-2-specific immune responses, SARS-CoV-2 variants can still bypass the pre-existing immunity and spread to both immature and seroconverted individuals (Horiuchi et al., 2021; Ying et al., 2022), which indicates that virus transmission still occurs in people, even in the vaccinated people and animal reservoirs (Kupferschmidt, 2021). It is one of the reasons why many countries urgently have begun to administrate the third and/or fourth dose of the SARS-CoV-2 vaccine. Therefore, a more efficient single-dose or two-doses SARS-CoV-2 vaccine against the emerging VOCs is still needed.

To date, more than 20 vaccines have been authorized for emergency use, and more than 11,242,252,352 vaccine doses have been administered on 4 April 2022. However, many different platforms of the SARS-CoV-2 vaccine are still under development, based on recombinant vectors, DNA, mRNA, inactivated viruses, attenuated viruses, and protein subunits, etc. (Gao et al., 2020; Smith et al., 2020; Wang et al., 2020a; Zhu et al., 2020; Flanagan et al., 2021; Li et al., 2021b). In addition, evaluation of possible targets and pan-coronavirus antiviral strategies for emerging or re-emerging coronaviruses is also in progress (Li et al., 2021b). Among these strategies, the vaccine based on the virus-like particle (VLP) has attracted more and more attention.

VLP comprises a virus capsid without a virus genome and can be used as multifunctional, safe, and highly immunogenic vaccines (Roy and Noad, 2008; Liu et al., 2011; Lopez-Macias et al., 2011; Matsuda et al., 2020; Won and Lee, 2020; Prates-Syed et al., 2021; Tariq et al., 2021; Kim et al., 2022). Moreover, the repeated antigen pattern on the surface of VLP makes it easier to be recognized by antigen-presenting cells than subunit vaccines to induce more robust and broader humoral and cellular immune responses (Bright et al., 2007; Bright et al., 2008; Song et al., 2010). Therefore, the VLP-based vaccine may be safer than inactivated or attenuated virus vaccine and more immunogenic than subunit or DNA vaccines. Besides, there were reported that Matrix 1 (M1) from avian influenza A H5N1 can promote the efficient assembly of influenza VLP (Bright et al., 2008; Song et al., 2010). Furthermore, a previous study also indicated that the chimeric VLPs containing the SARS-CoV-1 Spike (with a replacement of the TM/CT by the corresponding sequence of influenza virus HA) and the influenza M1 could be highly expressed in the baculovirus insect cell expression system (Liu et al., 2011). Moreover, influenza VLPs expressing the SARS-CoV-2 Spike can induce high levels of humoral immune responses against SARS-CoV-2, whereas neutralizing activities of the antibody were not strong enough to completely inhibit receptor-ligand binding of the SARS-CoV-2 (Chu et al., 2021b). Therefore, in this study, the *Spike* (S) gene of SARS-CoV-2 was optimized, and the chimeric VLPs based on the optimized Spike of SARS-CoV-2 and H5N1 M1 protein were constructed by a baculovirus system. In addition, the immunogenicity and protective effect of the VLP-based vaccine were also verified.

Materials and methods

Plasmid construction

The *spike* (S) gene of SARS-CoV-2 was designed according to the sequence of SARS-CoV-2/Wuhan-Hu-1 (GenBank ID:

MN908947) (Yang et al., 2004) by adding the *Bam*HI and *Xba*I at the 5' and 3' terminal of the gene, respectively. Then, a Syn21 sequence (AACTTAAAAAAAAAAATCAAA) (Liu et al., 2015) was also inserted before the start codon (ATG) of the *spike* gene to enhance transcription. Furthermore, the transmembrane and carboxyl terminus (TM/CT) of S was replaced by the corresponding transmembrane sequence of H5N1 hemagglutinin (HA) (aa 531-568, 38aa, A/Indonesia/5/2005 M1) (Liu et al., 2011). The resulting sequence was named the *S* gene (**Figure 1A**).

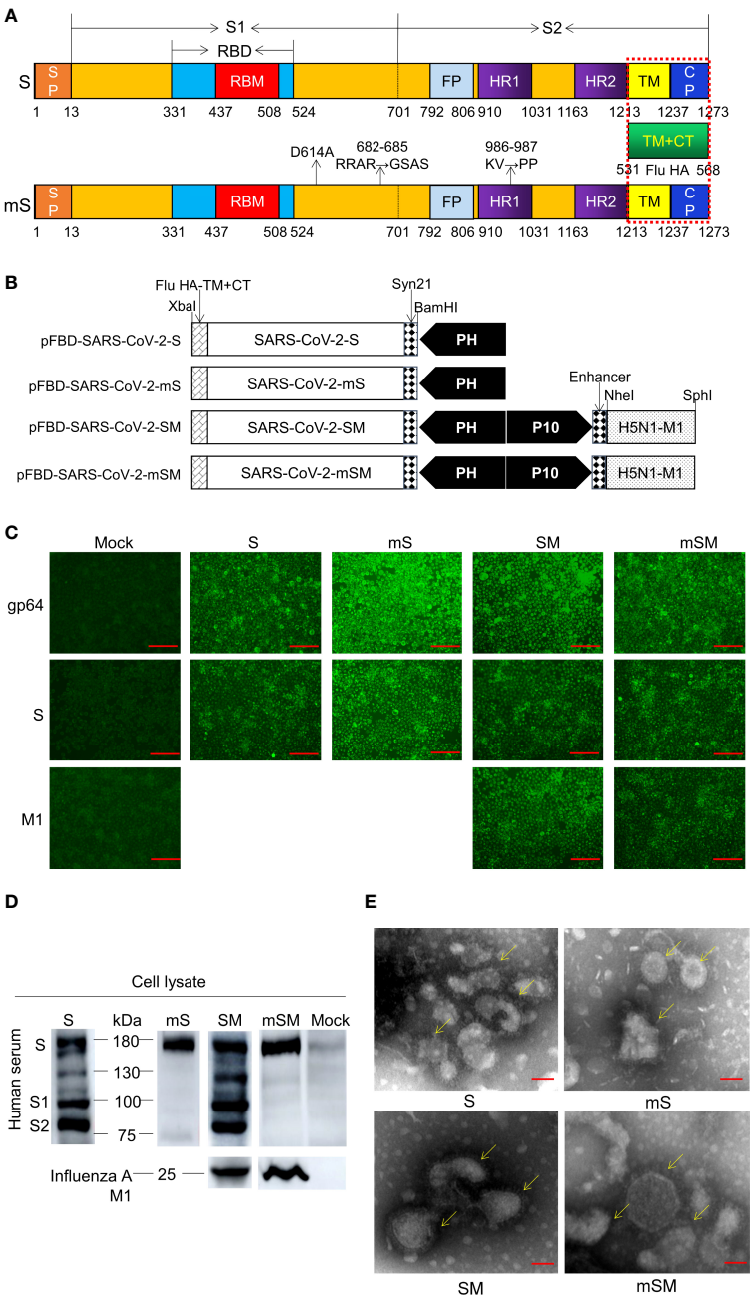

FIGURE 1
Generation of SARS-CoV-2 VLPs. **(A)** Schematic of SARS-CoV-2 S/M1 and its mutation. **(B)** Schematics of the four recombinant bacmid rFBD-SARS-CoV-2. **(C, D)** Expression of exogenous genes by recombinant baculoviruses identified by IFA **(C)** and Western blot **(D)**. The scale bar corresponds to 150 μm. Convalescent serum of COVID-19 patient or Influenza A M1 as the primary antibody, and HRP-labeled Goat Anti-Mouse IgG (H+L) as the secondary antibody. Mock, wild baculoviruses infected cell. Unprocessed original images can be found in Supplemental Figure S6. **(E)** Transmission electron micrograph of negatively stained SARS-CoV-2 VLPs. The scale bar corresponds to 50 nm.

As reported, three sites of the Spike, including D614, RRAR (682-685), and KV986-987, are crucial for the virus infection. The mutation of D614 to A614 may avoid Antibody-dependent enhancement (ADE) (Wang et al., 2016). The mutation of RRAR (682-685) to GSAS can inhibit the recognition and cleavage by furin (Kalnin et al., 2021). Finally, the mutation of KV986-987 to PP986-987 can enhance immunogenicity (Kirchdoerfer et al., 2018; Dagotto et al., 2020; Wrapp et al., 2020). Therefore, these sites were replaced by the corresponding sequence, respectively, and the optimized sequence was designated the *mS* gene (**Figure 1A**). The *S* gene and *mS* gene were synthesized according to the codon usage preference of insect cells and linked downstream of promoter PH of pFastBac™ Dual donor plasmid (Invitrogen, USA) according to the protocol described previously (Xu et al., 2021). The resulting shuttle plasmids were designated as pFBD-SARS-CoV-2-S and pFBD-SARS-CoV-2-mS, respectively (**Figure 1B**).

Moreover, to improve the stability of the VLP (Liu et al., 2011), the expression frame of the H5N1 *M1* gene (A/Indonesia/5/2005 M1, 252aa) was added to the downstream promoter P10 of pFastBac™ Dual donor plasmid (Invitrogen, USA), generating two shuttle plasmids pFBD-SARS-CoV-2-SM and pFBD-SARS-CoV-2-mSM, respectively (**Figure 1B**).

Baculovirus rescue and VLP preparation

To generate recombinant bacmid, the donor plasmids pFBD-SARS-CoV-2-S, pFBD-SARS-CoV-2-mS, pFBD-SARS-CoV-2-SM, and pFBD-SARS-CoV-2-mSM were transformed into Competent DH10Bac™ *E. coli* cells, followed by the antibiotic selection. The positive *E. coli* colonies containing recombinant bacmids rBD-S, rBD-mS, rBD-SM, and rBD-mSM was identified by PCR. In addition, the recombinant bacmids were verified by PCR (**Table 1**).

Recombinant baculovirus was rescued according to the previously described protocol (Xu et al., 2021). Briefly, sf9 cells in a 6-well plate (1×10^6cells/well) were transfected with the recombinant bacmids using Cellfectin® II Reagent (Gibco, USA) according to the manufacturer's instructions and cultured in Grace's medium (Gibco, USA) for 5-7 days at 27°C until apparent cytopathic effect (CPE) appeared. Then, cells and supernatant were collected, centrifuged at 3000 rpm, 4°C for 5 min, and filtered with a 0.22 μm filter. Next, the pellets were resuspended in PBS and evaluated using indirect fluorescence assay (IFA), Western blot, and transmission electron microscopy (TEM). The recombinant baculoviruses were named rBDV-S, rBDV-mS, rBDV-SM, and rBDV-mSM. Afterward, the baculoviruses were blind passaged in Sf9 cells and stored at -80°C. Finally, the viral titer of the third passage was examined according to the protocol described by BacPAK Baculovirus Rapid Titer Kit (Clontech, USA).

To generate VLPs, sf9 cells in a shake flask (1×10^6cells/well) were infected with the third passage recombinant baculoviruses (multiplicity of infection, MOI=1) for 72 h. Medium supernatant was collected and ultracentrifuged through a 20% sucrose cushion at 30,000rpm, 4°C for 2 h. The pellets were resuspended in PBS and further purified using a stepwise sucrose density gradient consisting of 2 mL of 10%, 30%, and 60% sucrose in PBS and centrifuged at 30,000 rpm and 4°C for 2 h. The white circular target protein in 10%-30% was collected and transferred to the centrifuge tube containing 5mL PBS and centrifugated at 30,000 rpm, 4°C for 2 h. The pellets were resuspended in PBS and evaluated using SDS-PAGE and Western blot. At the same time, the target protein was also examined by SARS-CoV-2 (2019-nCoV) Spike ELISA Kit (Sino Biological, China) according to the manufacturer's

TABLE 1 Primers and probes used in this study.

Primers		Sequence (5'-3')	Length (bp)	Gene Name
1	SF	AATGTTCGTGTTCTTGGTCTTGC	3800	S
	pUC/M13R	AGCGGATAACAATTTCACACAGG		
2	M1F	ATGAGCCTGTTGACCGAGGT	750	M1
	M1R	CTACTTGAAACGCTGCATC		
3	mSF	AATGTTCGTGTTCTTGGTCTTGC	3800	mS
	pUC/M13R	AGCGGATAACAATTTCACACAGG		
4	M1F	ATGAGCCTGTTGACCGAGGT	1500	M1
	pUC/M13F	CCCAGTCACGACGTTGTAAAACG		
5	SARS-CoV-2 NF	GGGGAACTTCTCCTGCTAGAAT	99	N
	SARS-CoV-2 NR	CAGACATTTTGCTCTCAAGCTG		
	SARS-CoV-2 NP	5'-FAM-TTGCTGCTGCTTGACAGATT-TAMRA-3'	Probe	
6	SARS-CoV-2 SgEF	CGATCTCTTGTAGATCTGTTCTC	171	E
	SARS-CoV-2 SgER	ATATTGCATTGCAGCAGTACGCACA		
	SARS-CoV-2 SgEP	5'-FAM-ACACTAGCCATCCTTACTGCGCTTGC-TAMRA-3'	Probe	

instructions. The standard curve was drawn according to the mean absorbance of optical density 450 (OD 450), and the concentration of the target antigen was calculated based on the standard curve.

Indirect fluorescence assay

Sf9 cells (5×10^5 cells/well) cultured in a 6-well plate were infected with the recombinant baculoviruses (MOI=1) for 48 h at 27°C. The IFA was performed as described by Xu *et al.* (Xu et al., 2021). Briefly, cells were fixed in 4% paraformaldehyde for 10 min at room temperature and washed three times with PBS for 5 min each. Next, the cells were blocked with 1% skim milk at 37°C for 30 min. After that, the cells were incubated with 500 µL AcMNPV GP64 antibody (1:1000, Sino Biological, China), SARS-CoV-2 (2019-nCoV) Spike RBD Antibody (1:1000, Sino Biological, China), or Influenza A M1 (1:1000, GeneTex, USA) at 37°C for 120 min. Then, the cells were incubated with 500 µL FITC-labeled Goat Anti-Rabbit IgG (H+L) (1:2,000, Beyotime, China) at 37°C for 40 min in the darkroom. Finally, the cells were examined using an Eclipse TE2000-V (Nikon, Japan).

Western Blot

Western blot was performed according to the protocol described by Xu et al. (Xu et al., 2021). Briefly, cell lysate or protein solution was loaded (1:5) and separated *via* 10% SDS-PAGE. Then, the protein was transferred onto the PVDF membrane, blocked with 5% skim milk for 1 h at room temperature, followed by incubating with the convalescent serum of the COVID-19 patient (1:1000) or Influenza A M1 (1:1000, GeneTex, USA) for 2 h at room temperature. After that, the membrane was incubated with HRP-labeled Goat Anti-Rabbit IgG (H+L) or HRP-labeled Goat Anti-Mouse IgG (H+L) (1:3000, Beyotime, China) for 1 h at room temperature. Subsequently, the band was developed using the GEGEGNOME XRQ enhanced chemiluminescence (ECL) (Thermo Fisher SCIENTIFIC, USA).

Transmission electron microscopy

The sample was absorbed on the grid and stained with 1% Phosphotungstic Acid for 1-2 min. Then, TEM was performed to examine the VLPs using a JEM-1200EXII transmission electron microscope (JEOL USA, Peabody, MA, USA).

Animal immunization and challenge

Specific pathogen-free (SPF, 6-8 weeks old) Balb/c mice and C57/BL/6N mice were purchased from Vital River Laboratory (Beijing, China). In addition, Humanized Balb/c mice containing human ACE2 (Balb/c-hACE2) were constructed by Cyagen (Suzhou, China). Mice were housed in SPF stainless steel with a constant atmosphere (22-25°C, 45-50% relative humidity), natural light cycle, and unlimited feeding and drinking. The virus infection experiment was conducted in the BSL-3 laboratory, Changchun Institute of Veterinary Medicine, Chinese Academy of Agricultural Sciences. Mice were monitored three times daily for changes in physical appearance and deaths (if any) and weighed every day during the experiment. In addition, the blood was collected weekly for specific antibody evaluation. At the end of the experiment, mice were anesthetized by carbon dioxide (CO_2), euthanized by cervical dislocation, and lung and other organs were collected for further evaluation.

Firstly, SPF Balb/c mice were randomly divided into five groups (6 mice in each group) and intramuscularly immunized with indicated VLPs and adjuvant (**Table 2**, group A). Then, SARS-CoV-2 specific antibody and T-cell subset distribution were evaluated at the indicated weeks *via* Enzyme-linked immunosorbent assay (ELISA) and Flow cytometry, respectively.

The effects of adjuvant and duration of immune interval on antibody production were evaluated to optimize the immunization strategy. For adjuvant (**Table 2**, group B), C57/BL/6N mice were divided into three groups (8 mice in each group), and intramuscular immunization was carried out on the hind legs with the mSM and candidate adjuvants, or PBS. For immune interval (**Table 2**, group C), C57/BL/6N mice were divided into five groups (6 mice in each group), and intramuscular immunization was carried out with the mSM and candidate adjuvants or PBS for indicated intervals. In addition, SARS-CoV-2 specific antibody was evaluated at the indicated weeks *via* ELISA.

Moreover, humanized Balb/c mice were randomly divided into two groups (6 mice in each group), immunized with the mSM and Al/CpG adjuvant, or PBS, and boosted with the identical inocula at 3 weeks later (**Table 2**, Group D). SARS-CoV-2 specific antibody and neutralization activity of SARS-CoV-2 specific antibodies were determined by the pseudovirus-based neutralization assay at the indicated weeks *via* ELISA. Then, the mice were challenged with SARS-CoV-2/Wuhan-Hu-1 strain (Yan et al., 2022) ($10^{5.5}$ $TCID_{50}$/mL) by nasal drops (0.05 mL) 2 weeks post the boost immunization. The body weight was monitored at an interval of 2 days. Then, mice were euthanized, and viral loads in the lung were examined by real-time PCR on days 3, 5, and 7 post-infection (dpi).

To evaluate the protective efficiency of the candidate vaccine, SPF Balb/c mice were randomly divided into two groups (6 mice in each group), immunized with the mSM and Al/CpG adjuvant, or PBS, and boosted with the identical inocula at 3 weeks later (**Table 2**, group E). Then, the mice were infected with a mouse-adapted SARS-CoV-2/C57MA14 strain (Kindly provided by Prof. Yuwei Gao) (Yan et al., 2022) ($10^{5.5}$ $TCID_{50}$/mL) by nasal drops (0.05 mL) 10 days post the boost immunization. Mice were euthanized, and viral loads in the lung were examined by real-time PCR on 7 dpi.

TABLE 2 Information on immunization Groups.

Group		Vaccine	Dose (μg)	adjuvant	animals	Immunetimes	Interval times (weeks)	Number
A	1	S	100	MF59 (60μl)+CpG (10μg)	Balb/c	2	3	6
	2	SM	100	MF59 (60μl)+CpG (10μg)	Balb/c	2	3	6
	3	mS	100	MF59 (60μl)+CpG (10μg)	Balb/c	2	3	6
	4	mSM	100	MF59 (60μl)+CpG (10μg)	Balb/c	2	3	6
	5	PBS	–	–	Balb/c	2	3	6
B	1	mSM	100	Al (300μl)+CpG (10μg)	C57/BL/6NC57/BL/6N/BL/6N	1	–	8
	2	mSM	100	MF59 (60μl)+CpG (10μg)	C57/BL/6N	1	–	8
	3	PBS	–	–	C57/BL/6N	1	–	8
C	1	mSM	50	MF59 (60μl)+CpG (10μg)	C57/BL/6N	2	2	6
	2	mSM	50	MF59 (60μl)+CpG (10μg)	C57/BL/6N	2	3	6
	3	mSM	50	Al (150μl)+CpG (10μg)	C57/BL/6N	2	4	6
	4	mSM	50	Al (150μl)+CpG (10μg)	C57/BL/6N	2	5	6
	5	PBS	–	–	C57/BL/6N	2	–	6
D	1	mSM	50	Al (150μl)+CpG (10μg)	Babl/c-hACE2	2	3	6
	2	PBS	–	–	Babl/c-hACE2	2	3	6
E	1	mSM	50	Al (150μl)+CpG (10μg)	Balb/c	2	3	6
	2	PBS	–	–	Balb/c	2	3	6

Detection of specific antibodies

SARS-CoV-2 specific antibody was examined using Mouse IgG Antibody Detection Kit for COVID-19 (ELISA) (Darui Technology, China) according to the manufacturer's instruction. The coating antigen used in the kit was RBD protein. Briefly, serum was diluted with PBS (1:100) and added to the ELISA plate (100μL per well) at 37 °C for 40 min. After washing four times with PBS, 100μL HRP-labeled Goat pAb to Ms IgG (Darui Technology, China) or HRP-labeled Goat pAb to Ms IgG1, HRP-labeled Goat pAb to Ms IgG2a (Abcam, Britain) was added into the well and incubated at 37 °C for 20 min, followed by washing six times. Then, substrates A and B (50μL each) were added and reacted at 37 °C for 10 min in the dark. The reaction was stopped by adding 50μL stop buffer, and the absorbance values (optical density, OD) were examined at 450 nm or 630 nm using a microplate reader (TECAN SPARK, Switzerland). The serum of convalescent patients with COVID-19 and the normal person was used as the positive and negative control, respectively. Three replicates were used for each sample. When the OD value of the sample is greater than or equal to 2.1 times that of the negative control, the sample is defined as a positive. If the OD value of negative control is less than 0.1, it is calculated as 0.1.

Neutralizing assay

The neutralization activity of SARS-CoV-2 specific antibodies was determined by the pseudovirus-based neutralization assay. Briefly, mice serum was inactivated at 56°C for 30 min, serially diluted with DMEM (3-fold dilutions), and added to a 96-well plate (50 μL/well). Then, SARS-CoV-2 pseudovirus (Du et al., 2022) was added to the well (100μL/well, MOI=100) and incubated at 37°C for 60 min. After that, Huh7 cells (2×10^5 cells/mL) resuspended in DMEM (containing 10% FBS) were added to the well (100 μL/well) and incubated at 37°C. 48 h later, the cells were detected using One-Lumi™ Firefly Luciferase Reporter Gene Assay Kit (Beyotime, China) according to the manufacturer's instruction and examined using a microplate reader (TECAN SPARK, Switzerland). The mock cell was used as negative control (CC), and SARS-CoV-2 pseudovirus was used as the positive control (VC). The Cut-Off Value is set as Value (sample)≤Value (VC)×0.5. The quality control is set as Value (VC)≥Value (CC)×3.

T-cell subset distribution assay

The splenocytes were isolated from immunized mice at the end of the experiment according to the previously described protocol (Liu et al., 2013; Xu et al., 2021). Briefly, the mouse spleen was homogenized and suspended in Roswell Park Memorial Institute (RPMI) 1640 (Hyclone, Beijing, China) to prepare cell suspension. Then, the splenic lymphocytes were isolated by centrifugation using a mouse lymphocyte isolation solution according to the manufacturer's instructions (Hao Yang Biological Manufacture Co., Ltd., Tian Jin, China). Afterward, lymphocytes were resuspended in RPMI 1640 supplemented with 10% fetal bovine serum and counted.

The splenocytes (10^6 cells) were incubated with 1 mL PE/Cyanine7 anti-mouse CD3ε Antibody, FITC anti-mouse CD4

Antibody, or APC anti-mouse CD8a Antibody (Biolegend, USA) at 4 °C for 30 min, centrifuged at 1500 rpm for 5 min. Next, the pellet was resuspended in PBS and centrifuged at 1500 rpm for 5 min, followed by examination using Flow cytometry (CytoFLEX, Beckman, USA).

Real-time PCR

Total RNA was extracted from the lung of the animals using QIAamp Viral RNA Mini Kit (QIAGEN, Germany) and examined using HiScript II U$^+$ One Step qRT-PCR Probe Kit (Vazyme, China) with indicated primers (**Table 1**).

Statistical analysis

Statistical analysis was performed using GraphPad 8.0 (GraphPad Software, SanDiego, CA) with the one-way analysis of variance (ANOVA; two-tailed, confidence intervals (CI) 95%), as indicated by the p-value. The results were statistically significant at $p<0.05$. At least three independent experiments were evaluated for each separate set of assays. The results are expressed as the mean ± standard deviation (SD).

Results

Generation of SARS-CoV-2 VLPs from the recombinant baculovirus

SARS-CoV-2 S gene was optimized and synthesized (**Figure 1A**), followed by subcloning into shuttle plasmid pFastBac^{TM} Dual according to the protocols described previously (Xu et al., 2021), resulting in four recombinant bacmids, including pFBD-SARS-CoV-2-S, pFBD-SARS-CoV-2-SM, pFBD-SARS-CoV-2-mS, and pFBD-SARS-CoV-2-mSM (**Figure 1B**). Then, the bacmids were identified using PCR (**Supplemental Figure S1**), and the corrected bacmids were transfected into Sf9 cells to rescue recombinant baculoviruses (**Supplemental Figures S2** and **S3**), respectively. The recombinant baculoviruses are designated as rBDV-S, rBDV-SM, rBDV-mS, and rBDV-mSM. Thereafter, the expression of exogenous genes in the Sf9 cells was evaluated by IFA. As shown in **Figure 1C**, the cells infected by recombinant baculoviruses exhibited apparent fluorescence compared with the mock-infected group, suggesting exogenous genes were efficiently expressed in the cells. These results were further confirmed by Western blot. As expected, four kinds of S proteins can be detected in cells infected with the recombinant baculovirus (**Figure 1D**). There were several bands in the wild-type groups, while the optimized S protein (mS) had only one specific band at 180 kDa, indicating the optimized protein is more stable and not easily degraded by protease than the wild-type S. Moreover, the M1 protein of H5N1 can be detected between 22 and 25 kDa (**Figure 1D**), which further proves the successful expression of these proteins.

To prepare VLPs, sf9 cells were infected with recombinant baculoviruses, and the protein was purified by ultracentrifugation with sucrose cushions, followed by transmission electron microscope observation (TEM). As shown in **Figure 1E**, the VLPs showed spherical shapes as typical SARS-CoV-2 virions. Spike structure can be observed around VLP, similar to the characteristic spike structure of intact virus particles, indicating that the recombinant SARS-CoV-2 VLPs were generated successfully. The expression of *mSM* genes was more effective than in the other three groups, suggesting that codon optimization can enhance the expression of exogenous genes in the Sf9 cells.

SARS-CoV-2 VLPs induced effective immune responses in mice

Mice were immunized with the purified VLP or PBS, followed by an evaluation of the immune responses. Animals were monitored daily for adverse effects. No obvious adverse events were observed. Blood was collected at 0, 1, 2, 3, 4, 5, and 6 weeks after the first dose of the immunization, and the boost was conducted three weeks after the first vaccination (**Figure 2A** and **Table 2**, group A).

As shown in **Figure 2B**, levels of SARS-CoV-2 specific antibody increased gradually in the VLP groups after the first dose of the immunization, which was significantly higher than that of the PBS group. The highest titer of specific antibodies in serum reached the peak four weeks post the first immunization in the VLP groups, with the highest level in the mSM group, and then decreased slightly in each group. After the boost immunization, the titers of the mSM and mS groups were higher than those of other groups, up to 1: 102,400 (**Figure 2C**). Compared with the control group, IgG, IgG1, and IgG2a at six weeks post initial immunization in the immunized groups increased to different degrees (**Figures 2D–F**), and the levels of specific IgG2a antibodies were higher than that of IgG1 (**Figures 2E, F**). In addition, the levels of specific IgG2a in the mSM and mS groups were higher than in other infected groups (**Figure 2F**). Three weeks post the boost immunization, the splenocytes were isolated from immunized mice according to a previously described protocol (Liu et al., 2013), followed by an evaluation of the T-cell subset distribution. As shown in **Figure 2G**, the levels of CD3$^+$CD4$^+$T and CD3$^+$CD8$^+$T lymphocytes in the mSM group were highest than in the other groups. These results suggest that the optimized S proteins, especially the mSM protein, had more robust immunogenicity than the wild-type S. Therefore, recombinant baculovirus rBDV-mSM and the optimized mSM were further evaluated in the subsequent studies. Then, the mSM protein in the supernatant was further purified using a stepwise sucrose density gradient and evaluated using SDS-PAGE, Western

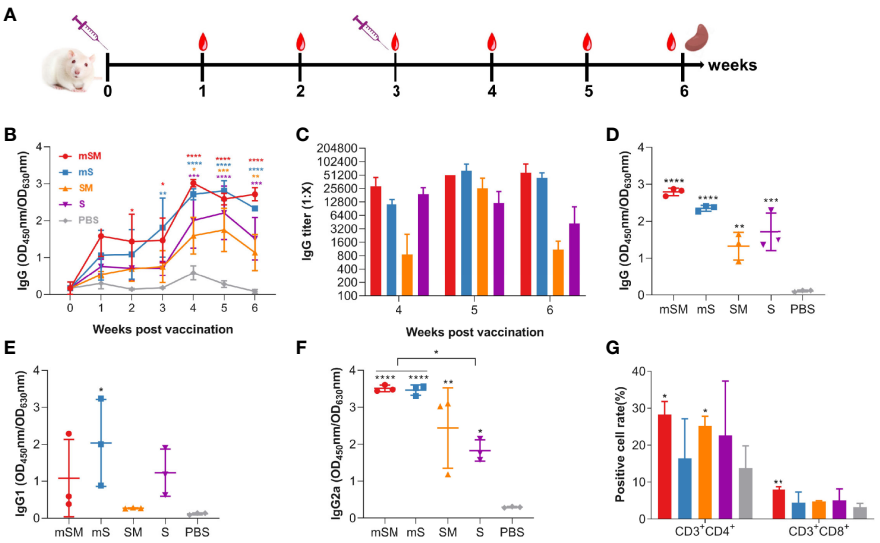

FIGURE 2
Evaluation of the immunogenicity of the VLP. Mice were primed with PBS or SARS-CoV-2 VLPs and boosted three weeks after the prime immunization using the same inocula used for priming. Blood samples were collected from the tail vein of mice at indicated times after the initial vaccination and used to analyze humoral immune responses using an antibody detection kit (The coating antigen used in the kit was RBD protein). Sera collected from the tail vein of pre-immune mice were used as a negative control. *, p< 0.05; **, p< 0.01; ***, p< 0.001; ****, p< 0.0001. The results are expressed as the mean ± standard deviation (SD). **(A)** Schematic diagram of immunization. **(B)** changes of total IgG during the immunization. **(C)** IgG titers at 4, 5, and 6 weeks post initial immunization. **(D-F)** RBD-specific IgG **(D)**, IgG1 **(E)**, and IgG2a **(F)** at six weeks post initial immunization. **(G)** Splenic lymphocyte subtypes.

blot, and ELISA. Figure The purified mSM protein can be efficiently recognized by the convalescent serum of a COVID-19 patient (primary antibody), while the unpurified protein in the supernatant has no obvious band (**Supplemental Figure S4**). The concentration of the purified mSM protein was quantified *via* standard curve (**Supplemental Figure S5**), and it was 0.2 μg/μL.

To optimize the immunization strategy of the mSM group, we evaluated the effects of adjuvant and duration of immune interval on antibody production and compared it with that of the PBS group (**Table 2**, group B-C). As shown in **Figure 3A**, the effect of the Al/CpG adjuvant on antibody production was better than MF59/CpG adjuvant. However, the duration of the immune interval has no significant effect on antibody production (**Figures 3B, C**). Meanwhile, the optimized immunization with mSM and Al/CpG adjuvant can stimulate animals to produce sustained high-level antibodies, which can still be detected after 53 weeks of vaccination (**Figure 3D**). The proportion of positive serum of immunized mice in **Figure 3D** (positive rate) was about 33.33% (**Figure 3E**).

SARS-CoV-2 VLPs induced effective immune responses in humanized mice

To clarify the immunogenicity and protective efficiency of the VLP-based vaccine, humanized ACE2 mice (Balb/c-hACE2) were immunized with the VLP or PBS, followed by an evaluation of the immune responses and virus challenge (**Figure 4A** and **Table 2**, group D). **Figures 4B, C** shows that the optimized vaccinaion with mSM and Al/CpG adjuvant can stimulate humanized mice to produce sustained high-level antibodies at 14, 21, 28, and 35 days post initial vaccination, with the highest titer of about 1:204,800 at 35 days post initial immunization. Furthermore, the titers of neutralizing antibodies reached 1:1,620 on the 35th day of the initial vaccination (**Figure 4D**).

Furthermore, the immunized mice were infected with SARS-CoV-2/Wuhan-Hu-1 14 days post the boost immunization, and animals were monitored at an interval of 2 days for adverse effects. As a result, no apparent adverse events were observed, and the body weights of the vaccine-immunized group were similar to that of the PBS group (**Figure 4E**). Moreover, the viral loads of the vaccine-immunized group were significantly decreased compared with that of the PBS group 3 days post-challenge (**Figure 4F**). These results indicate that the optimized immunization with SARS-CoV-2 VLP (mSM) and Al/CpG adjuvant can induce effective immune responses.

SARS-CoV-2 VLPs can efficiently protect the animal against virus challenge

To further clarify the protective efficiency of the mSM-based vaccine, BABL/c mice were immunized with the VLP or PBS,

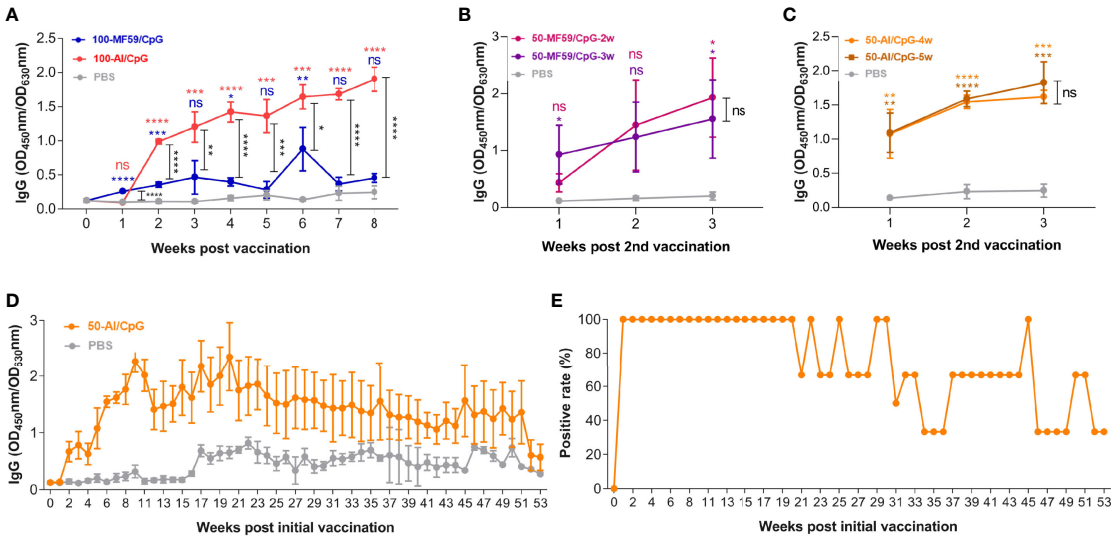

FIGURE 3
Optimization of immunization strategy. **(A)** Adjuvant. **(B, C)** Immune interval duration. **(D)** RBD-specific IgG. **(E)** Proportion of positive serum of immunized mice in Figure3D (positive rate). Differences between vaccine groups are indicated by black asterisks. Differences between vaccine group and PBS are indicated by color asterisks.

followed by an evaluation of the immune responses and challenge with a mouse-adapted SARS-CoV-2 strain (Figure 5A and Table 2, group E). As shown in Figure 5B, the SARS-CoV-2 specific antibody increased gradually in the mSM group, but there was no significant increase in the PBS group. There was a significant difference between the two groups 28 dpi. Furthermore, the body weights of the two groups decreased gradually after being challenged with the virus at 10 days post the boost immunization, but the weight-loss trend of the mSM-immunized mice was significantly lower than that of the control group (Figure 5C). On the fifth day of the virus challenge, one mouse in the PBS group died, while the others survived. At the end of the experiment, the

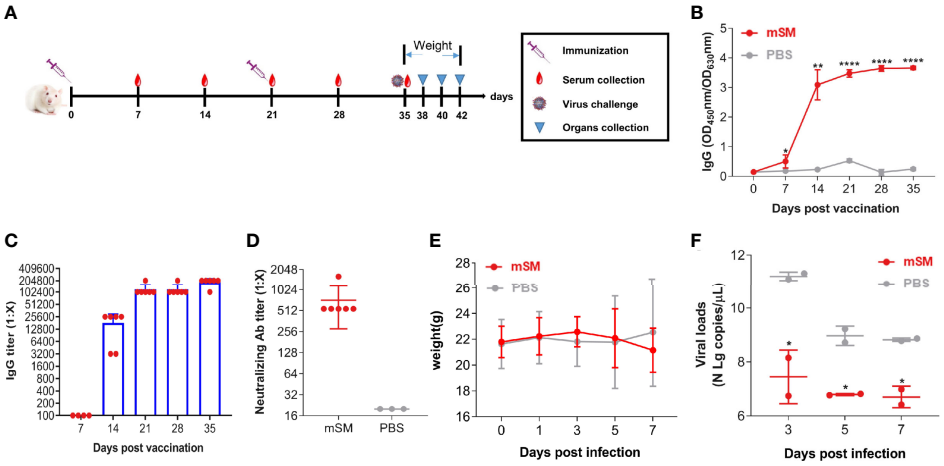

FIGURE 4
Evaluation of the immune effect of the VLP in humanized mice. Humanized mice were primed with PBS or SARS-CoV-2 VLP and boosted three weeks after the prime immunization using the same inocula used for priming. Blood samples were collected from the tail vein of mice at indicated times after the initial vaccination and used to analyze humoral immune responses using an antibody detection kit. Sera collected from the tail vein of pre-immune mice were used as a negative control. *, P< 0.05; **, P< 0.01; ****, P< 0.0001. The results are expressed as the mean ± standard deviation (SD). **(A)** Schematic diagram of immunization. **(B)** RBD-specific IgG. **(C)** IgG titer. **(D)** Neutralizing antibody. **(E)** Bodyweight. **(F)** Virus loads detected by qRT-PCR.

survival rate of the mSM group was 100%, and that of the PBS group was 83.3% (**Figure 5D**). Then, the viral loads were examined on the seventh dpi. As shown in **Figure 5E** and 5F, the copy numbers of viral genomic RNA (N gRNA, **Figure 5E**) and viral subgenomic RNA (sgERNA, **Figure 5F**) in the lung of the mSM group decreased significantly from that of the PBS group. These results indicate that the candidate vaccine based on the mSM VLP and Al/CpG adjuvant can establish an effective protective barrier to protect mice from virus attacks.

Discussion

The Spike of β-coronavirus is the main target of vaccine and therapeutic drug development (Du et al., 2009). Most vaccines of SARS-CoV-2, including subunit vaccines, mRNA vaccines, DNA vaccines, and viral vector vaccines, were constructed based on the Spike or the spike S1 or RBD (RPM) domain (Gao et al., 2020; Smith et al., 2020; Wang et al., 2020a; Zhu et al., 2020; Flanagan et al., 2021; Li et al., 2021b). A previous study indicated that the chimeric VLPs containing the SARS-CoV-1 Spike (with a replacement of the TM/CT by the corresponding sequence of influenza virus HA) and the influenza M1 could be highly expressed in the baculovirus insect cell expression system (Liu et al., 2011). Furthermore, inserting two prolines in the S2 subunit of MERS-CoV and SARS-CoV can effectively stabilize the prefusion conformation of the Spike and improve its stability, which also has been applied to SARS-CoV-2 vaccine development (Kirchdoerfer et al., 2018; Dagotto et al., 2020; Wrapp et al., 2020). Moreover, the mutation in the furin cleavage site (RRAR) between 682-685 in the S1 subunit of the MERS-CoV spike could enhance the homogeneity and stability of the MERS-CoV vaccine (Kirchdoerfer et al., 2018; Dagotto et al., 2020; Wrapp et al., 2020; Kalnin et al., 2021). Moreover, ADE has been reported in several viruses *in vitro* or *in vivo*, such as West Nile fever virus (WNV), Dengue virus (DENV), Ebola virus (EBOV), as well as in coronavirus infections, feline infectious peritonitis virus (FIPV), and SARS-CoV-1 (Negro, 2020). Therefore, although there has no clear evidence that ADE plays a role in the pathogenesis of COVID-19, it is crucial to avoid ADE in vaccine development. Besides, it was reported that a linear epitope (S597-603) of the SARS-CoV-1 spike protein could enhance virus infection *in vitroin vitro* and in non-human primates (Wang et al., 2016). Therefore, due to the above consideration, we constructed a chimeric VLP of SARS-CoV-2 spike protein and H5N1 M1 based on the baculovirus and insect cell expression system. The results showed that the Spike and H5N1 M1 were expressed successfully, and chimeric VLPs could be formed (**Figure 1**). The protocol for preparing a large number of high-purity VLPs is being optimized in our lab.

Notably, the expression of the SARS-CoV-2 Spike and the formation of VLPs are different in different expression systems. SARS-CoV-2 vaccines based on VLPs have been reported (Ghorbani et al., 2020; Biswas et al., 2021; Chu et al., 2021a; Geng et al., 2021; Ward et al., 2021; Boix-Besora et al., 2022; Hemmati et al., 2022; Mohsen et al., 2022), some expressed by mammalian cells or plant cells, while others are based on the RBD. However, only the immunogenicity of most of these VLPs has been studied, and there is no report on the preparation of SARS-CoV-2 VLP by insect baculovirus system. Meanwhile, it

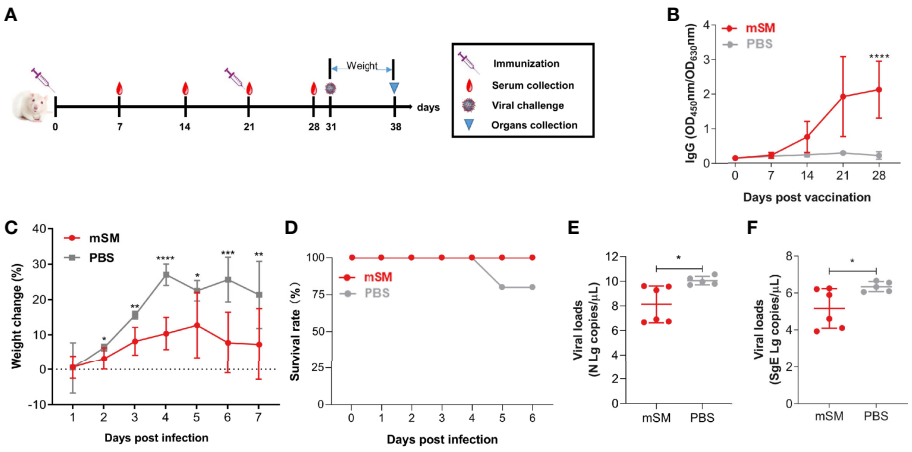

FIGURE 5
The mSM-based vaccine is effective against virus challenges. Mice were primed with PBS or SARS-CoV-2 VLP and boosted three weeks after the prime immunization, followed by virus challenge at 31 days post-prime immunization. Blood samples were collected from the tail vein of mice at indicated times after the initial vaccination and used to analyze humoral immune responses using an antibody detection kit. Sera collected from the tail vein of pre-immune mice were used as a negative control. *, P< 0.05; **, P< 0.01; ***, P< 0.001; ****, P< 0.0001. The results are expressed as the mean ± standard deviation (SD). **(A)** Schematic diagram of immunization and infection. **(B)** RBD-specific IgG. **(C)** Bodyweight. **(D)** Animal survival. **(E, F)** Virus loads detected by qRT-PCR.

was reported that the plant-derived VLP vaccine for COVID-19 was immunogenic, which can be significantly enhanced by adjuvant (Ward et al., 2021), suggesting that the vaccine based on VLPs is promising for the control and prevention of the COVID-19 pandemic. Previous studies also found that optimizing codon usage preference can enhance the expression and formation of VLPs (Wang et al., 2020b; Xu et al., 2021). As reported, three sites of the Spike, including D614, RRAR (682-685), and KV986-987, are crucial for the virus infection. The mutation of D614 to A614 may avoid Antibody-dependent enhancement (ADE) (Wang et al., 2016). The mutation of RRAR (682-685) to GSAS can inhibit the recognition and cleavage of furin (Kalnin et al., 2021). The mutation of KV986-987 to PP986-987 can enhance immunogenicity (Kirchdoerfer et al., 2018; Dagotto et al., 2020; Wrapp et al., 2020). Therefore, these sites were replaced by the corresponding sequence, respectively, and the optimized sequence was designated the *mS* gene (**Figure 1A**). Compared with the unoptimized VLPs, the optimized S protein was more stable and not easily degraded by protease than the wild-type S (Fig1), and it is easier to form VLPs (Fig1). Vaccines based on the codon-optimized VLP can induce higher levels of specific IgG antibodies than the wild-type S. Furthermore, the optimized S protein chimeric with H5N1 M1 (the mSM group) showed better immunogenicity than other groups. It could induce higher levels of specific IgG antibodies and cellular immune responses. Further studies proved that VLPs based on the optimized S protein (the mSM group) can induce immune responses in mice more effectively than wild-type S, provide protection for mice after challenge, reduce virus load and improve survival rate. The viral load in mice decreased obviously, and the survival rate of mice increased obviously.

Moreover, the adjuvant and duration of immune interval of the mSM-VLP-based vaccine were also optimized, followed by evaluation in normal and humanized mice. As expected, the mSM-VLP-based vaccine adjuvanted with Al/CpG can induce high levels of specific IgG antibodies, and the highest titer of neutralizing antibody is 1: 1620. The vaccine can reduce weight loss, significantly reduce the viral load in the lungs of mice, and have an apparent protective effect against virus attack. However, the duration of the immune interval has no significant effect on antibody production (**Figures 3B, C**). Meanwhile, the optimized immunization with mSM and Al/CpG adjuvant can stimulate animals to produce sustained high-level antibodies, lasting at least 53 weeks post the initial vaccination, with a positive rate of about 33.33% (**Figures 3D, E**). These results provide theoretical guidance for designing high-efficiency vaccines, optimizing immunization programs, and developing vaccines against SARS-CoV-2 variants. The construction and research of VLPs for Delta and Omicron variants are in progress.

Conclusion

In conclusion, chimeric VLPs based on the optimized Spike of SARS-CoV-2 and H5N1 M1 protein were constructed using the baculovirus system. The chimeric VLP adjuvanted with Al/CpG can induce effective and sustained immune responses against virus challenges in mice. The present study results provide theoretical guidance for designing high-efficiency vaccines, optimizing immunization programs, and developing vaccines against SARS-CoV-2 variants.

Data availability statement

The original contributions presented in the study are included in the article/**Supplementary Material**. Further inquiries can be directed to the corresponding author.

Ethics statement

The animal study was reviewed and approved by the experimental animal committee of Laboratory Animal Center, Changchun Institute of Veterinary Medicine, Chinese Academy of Agricultural Sciences.

Author contributions

Conceptualization, LR, CL, and NJ; methodology, WX and JC; validation, LL, LY, and YJ; formal analysis, PH and ZX; data curation, WZ and JC; writing—original draft preparation, JC and LR; writing—review and editing, LR and CL; visualization, PL, MT and ZG; supervision, CL and NJ; project administration, CL and NJ; funding acquisition, CL and NJ. All authors have read and agreed to the published version of the manuscript.

Funding

This work was supported by the National Key Research and Development Program of China [No. 2021YFD1801103-6]; the National Natural Science Foundation of China [No. 31972719]; CAMS Innovation Fund for Medical Sciences [2020-12M-5-001]. The funders had no role in study design, data collection and analysis, publishing decisions, or manuscript preparation.

Conflict of interest

The authors declare that the research was conducted in the absence of any commercial or financial relationships that could be construed as a potential conflict of interest.

Publisher's note

All claims expressed in this article are solely those of the authors and do not necessarily represent those of their affiliated organizations, or those of the publisher, the editors and the reviewers. Any product that may be evaluated in this article, or claim that may be made by its manufacturer, is not guaranteed or endorsed by the publisher.

Supplementary material

The Supplementary Material for this article can be found online at: https://www.frontiersin.org/articles/10.3389/fcimb.2022.967493/full#supplementary-material

References

Biswas, A., Mandal, R. S., Chakraborty, S., and Maiti, G. (2021). Tapping the immunological imprints to design chimeric SARS-CoV-2 vaccine for elderly population. *Int. Rev. Immunol.* 1-16. doi: 10.1080/08830185.2021.1925267

Boix-Besora, A., Lorenzo, E., Lavado-Garcia, J., Godia, F., and Cervera, L. (2022). Optimization, production, purification and characterization of HIV-1 gag-based virus-like particles functionalized with SARS-CoV-2. *Vaccines (Basel)* 10, 250. doi: 10.3390/vaccines10020250

Bright, R. A., Carter, D. M., Crevar, C. J., Toapanta, F. R., Steckbeck, J. D., Cole, K. S., et al. (2008). Cross-clade protective immune responses to influenza viruses with H5N1 HA and NA elicited by an influenza virus-like particle. *PLoS One* 3, e1501. doi: 10.1371/journal.pone.0001501

Bright, R. A., Carter, D. M., Daniluk, S., Toapanta, F. R., Ahmad, A., Gavrilov, V., et al. (2007). Influenza virus-like particles elicit broader immune responses than whole virion inactivated influenza virus or recombinant hemagglutinin. *Vaccine* 25, 3871–3878. doi: 10.1016/j.vaccine.2007.01.106

Callaway, E. (2021a). Beyond omicron: what's next for COVID's viral evolution. *Nature* 600, 204–207. doi: 10.1038/d41586-021-03619-8

Callaway, E. (2021b). Omicron likely to weaken COVID vaccine protection. *Nature* 600, 367–368. doi: 10.1038/d41586-021-03672-3

Chu, K. B., Kang, H. J., Yoon, K. W., Lee, H. A., Moon, E. K., Han, B. K., et al. (2021a). Influenza virus-like particle (VLP) vaccines expressing the SARS-CoV-2 s glycoprotein, S1, or S2 domains. *Vaccines (Basel)* 9: 920 doi: 10.3390/vaccines9080920

Chu, K. B., Kang, H. J., Yoon, K. W., Lee, H. A., Moon, E. K., Han, B. K., et al. (2021b). Influenza virus-like particle (VLP) vaccines expressing the SARS-CoV-2 s glycoprotein, S1, or S2 domains. *Vaccines (Basel)* 9, 920. doi: 10.3390/vaccines9080920

Cui, J., Li, F., and Shi, Z. L. (2019). Origin and evolution of pathogenic coronaviruses. *Nat. Rev. Microbiol.* 17, 181–192. doi: 10.1038/s41579-018-0118-9

Dagotto, G., Yu, J., and Barouch, D. H. (2020). Approaches and challenges in SARS-CoV-2 vaccine development. *Cell Host Microbe* 28, 364–370. doi: 10.1016/j.chom.2020.08.002

Du, L., He, Y., Zhou, Y., Liu, S., Zheng, B. J., and Jiang, S. (2009). The spike protein of SARS-CoV–a target for vaccine and therapeutic development. *Nat. Rev. Microbiol.* 7, 226–236. doi: 10.1038/nrmicro2090

Du, S., Xu, W., Wang, Y., Li, L., Hao, P., Tian, M., et al. (2022). The "LLQY" motif on SARS-CoV-2 spike protein affects s incorporation into virus particles. *J. Virol.* 96, e0189721. doi: 10.1128/jvi.01897-21

Eguia, R. T., Crawford, K. H. D., Stevens-Ayers, T., Kelnhofer-Millevolte, L., Greninger, A. L., Englund, J. A., et al. (2021). A human coronavirus evolves antigenically to escape antibody immunity. *PLoS Pathog.* 17, e1009453. doi: 10.1371/journal.ppat.1009453

Flanagan, K. L., Macintyre, C. R., Mcintyre, P. B., and Nelson, M. R. (2021). SARS-CoV-2 vaccines: Where are we now? *J. Allergy Clin. Immunol. Pract.* 9, 3535–3543. doi: 10.1016/j.jaip.2021.07.016

Gao, Q., Bao, L., Mao, H., Wang, L., Xu, K., Yang, M., et al. (2020). Development of an inactivated vaccine candidate for SARS-CoV-2. *Science* 369, 77–81. doi: 10.1126/science.abc1932

Geng, Q., Tai, W., Baxter, V. K., Shi, J., Wan, Y., Zhang, X., et al. (2021). Novel virus-like nanoparticle vaccine effectively protects animal model from SARS-CoV-2 infection. *PLoS Pathog.* 17, e1009897. doi: 10.1371/journal.ppat.1009897

Ghorbani, A., Zare, F., Sazegari, S., Afsharifar, A., Eskandari, M. H., and Pormohammad, A. (2020). Development of a novel platform of virus-like particle (VLP)-based vaccine against COVID-19 by exposing epitopes: an immunoinformatics approach. *N. Microbes N. Infect.* 38, 100786. doi: 10.1016/j.nmni.2020.100786

Hemmati, F., Hemmati-Dinarvand, M., Karimzade, M., Rutkowska, D., Eskandari, M. H., Khanizadeh, S., et al. (2022). Plant-derived VLP: a worthy platform to produce vaccine against SARS-CoV-2. *Biotechnol. Lett.* 44, 45–57. doi: 10.1007/s10529-021-03211-0

Horiuchi, S., Oishi, K., Carrau, L., Frere, J., Moller, R., Panis, M., et al. (2021). Immune memory from SARS-CoV-2 infection in hamsters provides variant-independent protection but still allows virus transmission. *Sci. Immunol.* 6, eabm3131. doi: 10.1126/sciimmunol.abm3131

Hui, D. S., Esam, I. A., Madani, T. A., Ntoumi, F., Kock, R., Dar, O., et al. (2020). The continuing 2019-nCoV epidemic threat of novel coronaviruses to global health - the latest 2019 novel coronavirus outbreak in wuhan, China. *Int. J. Infect. Dis.* 91, 264–266. doi: 10.1016/j.ijid.2020.01.009

Kalnin, K. V., Plitnik, T., Kishko, M., Zhang, J., Zhang, D., Beauvais, A., et al. (2021). Immunogenicity and efficacy of mRNA COVID-19 vaccine MRT5500 in preclinical animal models. *NPJ Vaccines* 6, 61. doi: 10.1038/s41541-021-00324-5

Kim, C., Kim, J. D., and Seo, S. U. (2022). Nanoparticle and virus-like particle vaccine approaches against SARS-CoV-2. *J. Microbiol.* 60, 335–346. doi: 10.1007/s12275-022-1608-z

Kirchdoerfer, R. N., Wang, N., Pallesen, J., Wrapp, D., Turner, H. L., Cottrell, C. A., et al. (2018). Stabilized coronavirus spikes are resistant to conformational changes induced by receptor recognition or proteolysis. *Sci. Rep.* 8, 15701. doi: 10.1038/s41598-018-34171-7

Kupferschmidt, K. (2021). Where did 'weird' omicron come from? *Science* 374, 1179. doi: 10.1126/science.acx9738

Liu, C., Du, S., Li, C., Wang, Y., Wang, M., Li, Y., et al. (2013). Immunogenicity analysis following human immunodeficiency virus recombinant DNA and recombinant vaccinia virus tian tan prime-boost immunization. *Sci. China Life Sci.* 56, 531–540. doi: 10.1007/s11427-013-4484-2

Liu, Y. V., Massare, M. J., Barnard, D. L., Kort, T., Nathan, M., Wang, L., et al. (2011). Chimeric severe acute respiratory syndrome coronavirus (SARS-CoV) s glycoprotein and influenza matrix 1 efficiently form virus-like particles (VLPs) that protect mice against challenge with SARS-CoV. *Vaccine* 29, 6606–6613. doi: 10.1016/j.vaccine.2011.06.111

Liu, Y., Zhang, Y., Yao, L., Hao, H., Fu, X., Yang, Z., et al. (2015). Enhanced production of porcine circovirus type 2 (PCV2) virus-like particles in Sf9 cells by translational enhancers. *Biotechnol. Lett.* 37, 1765–1771. doi: 10.1007/s10529-015-1856-7

Li, X., Zhang, L., Chen, S., Ji, W., Li, C., and Ren, L. (2021a). Recent progress on the mutations of SARS-CoV-2 spike protein and suggestions for prevention and controlling of the pandemic. *Infect. Genet. Evol.* 93, 104971. doi: 10.1016/j.meegid.2021.104971

Li, X., Zhang, L., Chen, S., Ouyang, H., and Ren, L. (2021b). Possible targets of pan-coronavirus antiviral strategies for emerging or re-emerging coronaviruses. *Microorganisms* 9 1479. doi: 10.3390/microorganisms9071479

Lopez-Macias, C., Ferat-Osorio, E., Tenorio-Calvo, A., Isibasi, A., Talavera, J., Arteaga-Ruiz, O., et al. (2011). Safety and immunogenicity of a virus-like particle pandemic influenza a (H1N1) 2009 vaccine in a blinded, randomized, placebo-

controlled trial of adults in Mexico. *Vaccine* 29, 7826–7834. doi: 10.1016/j.vaccine.2011.07.099

Matsuda, T., Tanijima, T., Hirose, A., Masumi-Koizumi, K., Katsuda, T., and Yamaji, H. (2020). Production of influenza virus-like particles using recombinant insect cells. *Biochem. Eng. J.* 163, 107757. doi: 10.1016/j.bej.2020.107757

Mccallum, M., Walls, A. C., Sprouse, K. R., Bowen, J. E., Rosen, L. E., Dang, H. V., et al. (2021). Molecular basis of immune evasion by the delta and kappa SARS-CoV-2 variants. *Science* 374, 1621–1626. doi: 10.1126/science.abl8506

Mohsen, M. O., Balke, I., Zinkhan, S., Zeltina, V., Liu, X., Chang, X., et al. (2022). A scalable and highly immunogenic virus-like particle-based vaccine against SARS-CoV-2. *Allergy* 77, 243–257. doi: 10.1111/all.15080

Murano, K., Guo, Y., and Siomi, H. (2021). The emergence of SARS-CoV-2 variants threatens to decrease the efficacy of neutralizing antibodies and vaccines. *Biochem. Soc. Trans.* 49, 2879–2890. doi: 10.1042/BST20210859

Nabel, K. G., Clark, S. A., Shankar, S., Pan, J., Clark, L. E., Yang, P., et al. (2022). Structural basis for continued antibody evasion by the SARS-CoV-2 receptor binding domain. *Science* 375, eabl6251. doi: 10.1126/science.abl6251

Negro, F. (2020). Is antibody-dependent enhancement playing a role in COVID-19 pathogenesis? *Swiss Med. Wkly* 150, w20249. doi: 10.4414/smw.2020.20249

Prates-Syed, W. A., Chaves, L. C. S., Crema, K. P., Vuitika, L., Lira, A., Cortes, N., et al. (2021). VLP-based COVID-19 vaccines: An adaptable technology against the threat of new variants. *Vaccines (Basel)* 9, 1409. doi: 10.3390/vaccines9121409

Pulliam, J. R. C., Van Schalkwyk, C., Govender, N., Gottberg, A. V., Cohen, C., Groome, M. J., et al. (2022)a. Increased risk of SARS-CoV-2 reinfection associated with emergence of the omicron variant in south Africa. *Science 376:* eabn4947. doi: 10.1126/science.abn4947

Roy, P., and Noad, R. (2008). Virus-like particles as a vaccine delivery system: myths and facts. *Hum. Vaccin* 4, 5–12. doi: 10.4161/hv.4.1.5559

Smith, T. R. F., Patel, A., Ramos, S., Elwood, D., Zhu, X., Yan, J., et al. (2020). Immunogenicity of a DNA vaccine candidate for COVID-19. *Nat. Commun.* 11, 2601. doi: 10.1038/s41467-020-16505-0

Song, H., Wittman, V., Byers, A., Tapia, T., Zhou, B., Warren, W., et al. (2010). *In vitro* stimulation of human influenza-specific CD8+ T cells by dendritic cells pulsed with an influenza virus-like particle (VLP) vaccine. *Vaccine* 28, 5524–5532. doi: 10.1016/j.vaccine.2010.06.044

Tariq, H., Batool, S., Asif, S., Ali, M., and Abbasi, B. H. (2021). Virus-like particles: Revolutionary platforms for developing vaccines against emerging infectious diseases. *Front. Microbiol.* 12, 790121. doi: 10.3389/fmicb.2021.790121

Wang, M., Fu, T., Hao, J., Li, L., Tian, M., Jin, N., et al. (2020b). A recombinant lactobacillus plantarum strain expressing the spike protein of SARS-CoV-2. *Int. J. Biol. Macromol.* 160, 736–740. doi: 10.1016/j.ijbiomac.2020.05.239

Wang, H., Zhang, Y., Huang, B., Deng, W., Quan, Y., Wang, W., et al. (2020a). Development of an inactivated vaccine candidate, BBIBP-CorV, with potent protection against SARS-CoV-2. *Cell* 182, 713–721.e719. doi: 10.1016/j.cell.2020.06.008

Wang, Q., Zhang, L., Kuwahara, K., Li, L., Liu, Z., Li, T., et al. (2016). Immunodominant SARS coronavirus epitopes in humans elicited both enhancing and neutralizing effects on infection in non-human primates. *ACS Infect. Dis.* 2, 361–376. doi: 10.1021/acsinfecdis.6b00006

Ward, B. J., Gobeil, P., Seguin, A., Atkins, J., Boulay, I., Charbonneau, P. Y., et al. (2021). Phase 1 randomized trial of a plant-derived virus-like particle vaccine for COVID-19. *Nat. Med.* 27, 1071–1078. doi: 10.1038/s41591-021-01370-1

Won, J. H., and Lee, H. (2020). The current status of drug repositioning and vaccine developments for the COVID-19 pandemic. *Int. J. Mol. Sci.* 21, 9775. doi: 10.3390/ijms21249775

Wrapp, D., Wang, N., Corbett, K. S., Goldsmith, J. A., Hsieh, C. L., Abiona, O., et al. (2020). Cryo-EM structure of the 2019-nCoV spike in the prefusion conformation. *Science 367:* 1260-1263. doi: 10.1126/science.abb2507

Xu, W., Du, S., Li, T., Wu, S., Jin, N., Ren, L., et al. (2021). Generation and evaluation of recombinant baculovirus coexpressing gp5 and m proteins of porcine reproductive and respiratory syndrome virus type 1. *Viral Immunol.* 34, 697–707. doi: 10.1089/vim.2021.0018

Yang, Z. Y., Kong, W. P., Huang, Y., Roberts, A., Murphy, B. R., Subbarao, K., et al. (2004). A DNA vaccine induces SARS coronavirus neutralization and protective immunity in mice. *Nature* 428, 561–564. doi: 10.1038/nature02463

Yan, F., Li, E., Wang, T., Li, Y., Liu, J., Wang, W., et al. (2022). Characterization of two heterogeneous lethal mouse-adapted SARS-CoV-2 variants recapitulating representative aspects of human COVID-19. *Front. Immunol.* 13, 821664. doi: 10.3389/fimmu.2022.821664

Ying, B., Whitener, B., Vanblargan, L. A., Hassan, A. O., Shrihari, S., Liang, C. Y., et al. (2022). Protective activity of mRNA vaccines against ancestral and variant SARS-CoV-2 strains. *Sci. Transl. Med.* 14, eabm3302. doi: 10.1126/scitranslmed.abm3302

Zhu, F. C., Li, Y. H., Guan, X. H., Hou, L. H., Wang, W. J., Li, J. X., et al. (2020). Safety, tolerability, and immunogenicity of a recombinant adenovirus type-5 vectored COVID-19 vaccine: a dose-escalation, open-label, non-randomised, first-in-human trial. *Lancet* 395, 1845–1854. doi: 10.1016/S0140-6736(20)31208-3

frontiers | Frontiers in Cellular and Infection Microbiology

REVIEW
published: 18 July 2022
doi: 10.3389/fcimb.2022.956417

The Relationship Between Porphyromonas Gingivalis and Rheumatoid Arthritis: A Meta-Analysis

Yilin Li[1,2,3], *Rui Guo*[4,5], *Patrick Kwabena Oduro*[6,7], *Tongke Sun*[1,2,3], *Hao Chen*[1,2,3], *Yating Yi*[1,2,3], *Weiqian Zeng*[1,2,3], *Qilong Wang*[6,7], *Ling Leng*[6,7]*, *Long Yang*[4,5]* and *Jun Zhang*[1,2,3]*

[1] Department of Orthodontics, School and Hospital of Stomatology, Cheeloo College of Medicine, Shandong University, Jinan, China, [2] Shandong Key Laboratory of Oral Tissue Regeneration, Jinan, China, [3] Shandong Engineering Laboratory for Dental Materials and Oral Tissue Regeneration, Jinan, China, [4] Research center for Infectious Diseases, Tianjin University of Traditional Chinese Medicine, Tianjin, China, [5] School of Integrative Medicine, Tianjin University of Traditional Chinese Medicine, Tianjin, China, [6] Institute of Traditional Chinese Medicine, Tianjin University of Traditional Chinese Medicine, Tianjin, China, [7] State Key Laboratory of Component-Based Chinese Medicine, Ministry of Education, Tianjin, China

OPEN ACCESS

Edited by:
Zhanbo Zhu,
Heilongjiang Bayi Agricultural University, China

Reviewed by:
Yonggang Qu,
Shihezi University, China
Mulin Jun Li,
Tianjin Medical University, China

***Correspondence:**
Ling Leng
lengling@tjutcm.edu.cn
Long Yang
Long.yang@tjutcm.edu.cn
Jun Zhang
zhangj@sdu.edu.cn

Specialty section:
This article was submitted to Clinical Microbiology, a section of the journal Frontiers in Cellular and Infection Microbiology

Received: 30 May 2022
Accepted: 23 June 2022
Published: 18 July 2022

Citation:
Li Y, Guo R, Oduro PK, Sun T, Chen H, Yi Y, Zeng W, Wang Q, Leng L, Yang L and Zhang J (2022) The Relationship Between Porphyromonas Gingivalis and Rheumatoid Arthritis: A Meta-Analysis. Front. Cell. Infect. Microbiol. 12:956417. doi: 10.3389/fcimb.2022.956417

Rheumatoid arthritis (RA) is a systematical autoimmune disease, characterized by chronic synovial joint inflammation and hurt. *Porphyromonas gingivalis*(*P. gingivalis*) can cause life-threatening inflammatory immune responses in humans when the host pathogenic clearance machinery is disordered. Some epidemiological studies have reported that *P. gingivalis* exposure would increase the prevalence of RA. However, the results remain inconsistent. Therefore, a meta-analysis was done to systematically analyze the relationship between *P. gingivalis* exposure and the prevalence of rheumatoid arthritis. Database including Cochrane Library, Web of Science, PubMed, and EMBASE were searched for published epidemiological articles assessed the relationship between *P. gingivalis* and RA. Obtained studies were screened based on the predefined inclusion and exclusion criteria. The overall Odds Ratios (ORs) of incorporated articles were pooled by random-effect model with STATA 15.1 software. The literature search returned a total of 2057 studies. After exclusion, 28 articles were included and analyzed. The pooled ORs showed a significant increase in the risk of RA in individuals with *P. gingivalis* exposure (OR = 1.86; 95% CI: 1.43-2.43). Subgroup analysis revealed that pooled ORs from populations located in Europe (OR = 2.17; 95% CI: 1.46-3.22) and North America (OR = 2.50; 95% CI: 1.23-5.08) were significantly higher than that from population in Asia (OR = 1.11; 95% CI: 1.03-1.20). Substantial heterogeneity was observed but did not significantly influence the overall outcome. In conclusion, our results indicated *P. gingivalis* exposure was a risk factor in RA. Prompt diagnosis and management decisions on *P. gingivalis* antimicrobial therapy would prevent rheumatoid arthritis development and progression.

Keywords: porphyromonas gingivalis, rheumatoid arthritis, periodontitis, autoimmune disease, meta-analysis

INTRODUCTION

Rheumatoid arthritis (RA) is a systemic autoimmune disease characterized by the production of anti-citrullinated protein antibodies (ACPA) (Kharlamova et al., 2016; Białowąs et al., 2020) and chronic synovial joint inflammation. If untreated or improperly controlled, this illness can lead to the destruction of cartilage and bone and decrease the quality of the patient's life or even cause disability (Laugisch et al., 2016). RA affects about 1% of the population, with a female/male ratio of 2·5/1 (Bender et al., 2018). The disease can happen at any time in life, but its incidence increases with age, with individuals aged 40–70 years at an increased risk. Although what exactly causes RA remains unclear, several genetic alterations and environmental factors have been identified to contribute to RA pathogenesis (Eriksson et al., 2019).

Chronic periodontitis is the most common inflammatory disease worldwide, affecting 1/3 of the adult population. Both periodontal disease (PD) and RA display systemic markers of inflammation and share an association with HLA-DRB1 alleles and chronic inflammatory pathways (Äyräväinen et al., 2017). PD is much more frequent in RA patients compared with healthy people. Indeed, previous study reports have established a causal relationship between PD and RA (Scher and Abramson, 2013; Kim et al., 2018). Many clinical studies have indicated that patients with RA are more likely to exhibit periodontitis than those without RA (Berthelot and Le Goff, 2010). Individuals with RA also had higher levels of periodontal tissue destruction than the controls. Additionally, patients with periodontitis had a higher prevalence of RA than those without periodontitis.

Moreover, the elevated systemic inflammatory problem in people with PD has been coupled with an increased risk of chronic and potentially grievous diseases (Oluwagbemigun et al., 2019), including heart diseases, enterophthisis, kidney failure, cardiovascular diseases, diabetes, pulmonary diseases, premature infants, and cancers (Kononoff et al., 2020). In PD, the dysregulated immune inflammatory response is associated with the dysbiosis of the oral microbiota (Konig et al., 2015). *Porphyromonas gingivalis*(*P. gingivalis*) is a gram-negative, rod-shaped, obligate anaerobe of the oral cavity. *P. gingivalis* is the causative agent of the chronic inflammatory disease periodontitis. Strikingly, the association between RA and PD is because of the oral pathobiont *P. gingivalis* (Lee et al., 2015).

P. gingivalis and its infection are of clinical concern because of their numerous associations with potentially life-threatening diseases (Fisher et al., 2015). Previous studies report that *P. gingivalis* can induce an inflammatory response since some immunologic and inflammatory reactions are activated in the host, interfering with the bacterium's clearance (Johansson et al., 2016). *P. gingivalis* can invade and penetrate different epithelial cells, and it has a complex mechanism that allows it to alter the cellular defense, notably some of the host's unique genes (Schulz et al., 2019). Some studies have shown the effects of *P. gingivalis*, at diverse levels, on some molecules associated with cellular division. Gingival epithelial cells are the first natural barrier of the host periodontal tissue defense mechanism (Moen et al., 2003; Okada et al., 2011; Mariette et al., 2020; Arévalo-Caro et al., 2022). *P. gingivalis* can adhere to gingival epithelial cells through specific adhesins, triggering various signaling pathways in gingival epithelial cells and causing its internalization in gingival epithelial cells to trigger cell dysfunction (Reichert et al., 2013).

Previous systematic reviews and clinical studies have linked *P. gingivalis* infection to RA (Bello-Gualtero et al., 2016). However, most of these studies were limited by small sample size, geographical location, and the absence of subgroup analysis (Leech and Bartold, 2015). In addition, unfortunately, findings on the link between *P.gingivalis* and RA remain heterogeneous, with some showing a positive correlation and others showing a null correlation between the two (Seror et al., 2015; Janssen et al., 2015). Therefore, current estimates of the risk of RA in *P. gingivalis* exposed individuals are needed to inform decisions on future drug and vaccine development (Ceccarelli et al., 2018). We, therefore, aimed to conduct a meta-analysis of the prevalence of *P. gingivalis* in patients with RA.

MATERIAL AND METHODS

Protocol and Registration

This meta-analysis was designed to investigate the relationship between *P. gingivalis* and RA, with the guidelines provided by the PRISMA statement (Liberati et al., 2009) and the Cochrane Handbook for Systematic Reviews of Interventions Version 5.1.0. Literature from the Cochrane Library, Web of Science, PubMed, and EMBASE were searched by April 14, 2022, with the search strategy of key words including rheumatoid arthritis and *P. gingivalis*. After conducting the literature search, the references of all returned studies were managed and screened.

Eligibility Criteria

The searched articles were screened based the predefined eligible criteria: 1) epidemiological studies including cohort study, case-control study or cross-section study; 2) articles exploring the correlation between *P. gingivalis* and the risk of rheumatoid arthritis. When multiple research articles were available from the same population, the most recent peer-reviewed research article would be selected. On the contrary, articles would be excluded if they are: 1) inappropriate article types, such as comment, letters, review, meta-analysis; 2) results from animal models or *in vitro* experiments; 3) lack of detailed methodology to detect *P. gingivalis* exposure; 4) neither reporting exact odds ratio (OR) or risk ratio (RR), nor supplying enough data to calculate them; 5) articles with paradoxical data describing sample size in paragraphs or tables.

Study Selection

The titles and abstracts from each database were downloaded and imported into the literature management software. Duplicate research articles were removed. Two independent reviewers (Yilin L and Rui G) screened the titles and abstracts in parallel based on the inclusion and exclusion criteria. Then the

full text was retrieved and evaluated in depth. In addition, in scenarios where conflicts about a study could not be resolved after discussing the full-text among the two review authors, a third author (Tongke S) was consulted.

Data Extraction

Two independent authors (Yilin L and Rui G) extracted data from included articles using a pre-piloted standardized data extraction form. The extracted data including author/year of publication, sample location (country), study design, sample size, match for control, biomarker used for determining *P. gingivalis* exposure and the reported or calculated OR and 95%CI.

Quality Assessment

The quality of included articles were assessed by Agency for Healthcare Research and Quality (AHRQ) for cross-sectional studies and Newcastle-Ottawa Scale (NOS) for case-control and cohort studies (detailed items could be found in **Supplementary Materials Table 1** or in this website http://www.ohri.ca/programs/clinical_ epidemiology/oxford.asp). Yilin L and Rui G scored each item separately, and any discrepancies in the scores were resolved through discussion. All included studies were evaluated based on the final quality score, ranging from 0 to 10. Each study was assigned a low, moderate, or high quality based on the scores 0–5, 6–8, and 9–10, respectively.

Statistical Analysis

Stata 15.1 software was used to conduct the meta-analysis. The relationship between *P. gingivalis* and RA was reported as odds ratio (OR) and 95% CI. Heterogeneity across studies was measured by I^2 statistics. The fixed-effect model was used when the I^2 was less than 50%, otherwise the random-effect model was used. Subgroup analysis was conducted to clarify the source of heterogeneity as well as to analyze the diversity among different subgroups. And sensitivity analysis were used to confirm whether the results were robust. Furthermore, Begg's funnel plots and Egger's test were used to examine publication bias across studies.

RESULTS

Study Selection and Flow Diagram

Our literature search identified 2057 studies. After removing duplicates, 901 records were screened for inclusion, among which 156 were proceeded for full-text eligibility and review. 86 studies were excluded based on inclusion and exclusion criteria, leaving 70 eligible studies for further analysis. Finally, after deeply evaluating 42 studies were excluded for insufficient data for OR or RR, yielding a total of 28 eligible studies for the synthesis (**Figure 1**). There were 2 articles reported two different ORs, those were OR calculated before RA treatment and OR after RA treatment (Äyräväinen et al., 2017; Martínez-Rivera et al., 2017). As most of these included articles reported ORs before treatment, in order to minimize the heterogeneity between studies, OR calculated before treatment was chosen in our meta-analysis.

Characteristics of the Studies

Of the 28 studies, 16 were case-control studies, 4 were cohort studies, and 8 were cross-sectional studies, with a total of 4486 RA patients and 2607 controls. The included studies' characteristics were displayed in **Table 1**. Among them, 17 study samples were in Europe, while 5 were in North America, 3 in Asia, and 3 in South America.

Data Synthase

These 28 studies represented 28 independent populations. Results from our meta-analysis showed a significant increase in the risk of rheumatoid arthritis in individuals with *P. gingivalis* exposure, with the overall pooled OR 1.86 (95%CI: 1.43, 2.43, **Figure 2**). There was apparent heterogeneity between these included articles, as the I^2 was 81.6% and the estimate of between-study variance Tau-squared was 0.3015. Therefore, the random-effect model was used. Results from Begg's funnel plot and Egger's tests indicated that there might exist some publish bias (Egger's text p= 0.004) (**Supplementary Figure 1**).

As in Arévalo-Caro's study (Arévalo-Caro et al., 2022), two different ORs were reported because different biomarkers (IgG1 anti-*P. gingivalis* and IgG2 anti-*P. gingivalis*) were used to define *P. gingivalis* exposure. To compare these two different biomarkers on the pooled ORs, the two ORs were calculated separately. The pooled OR showed that *P. gingivalis* exposure defined by IgG1 anti-*P. gingivalis* or IgG2 anti-*P. gingivalis* had limited effect on the final results of the meta-analysis, as the pooled OR were 1.86 vs 1.90 **(Supplementary Figure 2)** in IgG1 anti-*P. gingivalis* and IgG2 anti-*P. gingivalis* respectively. In our pooled data, the OR from IgG1 anti-*P. gingivalis* were mainly chosen.

Subgroup Analysis

To determine the primary sources of heterogeneity, we conducted a subgroup analysis based on study design (case-control, cohort or cross-sectional study), OR's sources (reported by the authors or calculated based on their original data), sample size (RA patients ≥150 or < 150), population locations (countries), the biomarker of *P. gingivalis* (anti-*P. gingivalis*, *P. gingivalis* anti-RgpB or anti-RgpA), the detection methods in evaluation *P. gingivalis* exposure (ELISA, PCR or bacterial culture), the quality (NOS ≥ 8 or < 8) and the population location (continent) (**Figure 3** and **Table 2**). Unfortunately, none of these factors could well explain heterogeneity between studies. Instead, we found that the association might be stronger in Europe and North America than Asia, as the pooled ORs from populations located in Europe (OR = 2.17; 95% CI: 1.46-3.22) and North America (OR = 2.50; 95% CI: 1.23-5.08) were significantly higher than that from population in Asia (OR = 1.11; 95% CI: 1.03-1.20).

Sensitivity Analysis

A sensitivity analysis (**Figure 4**) was performed after excluding one of the 28 included studies to evaluate the impact of an individual study on the overall outcome. The overall sensitivity analyses indicated that our results were robust, omitting anyone

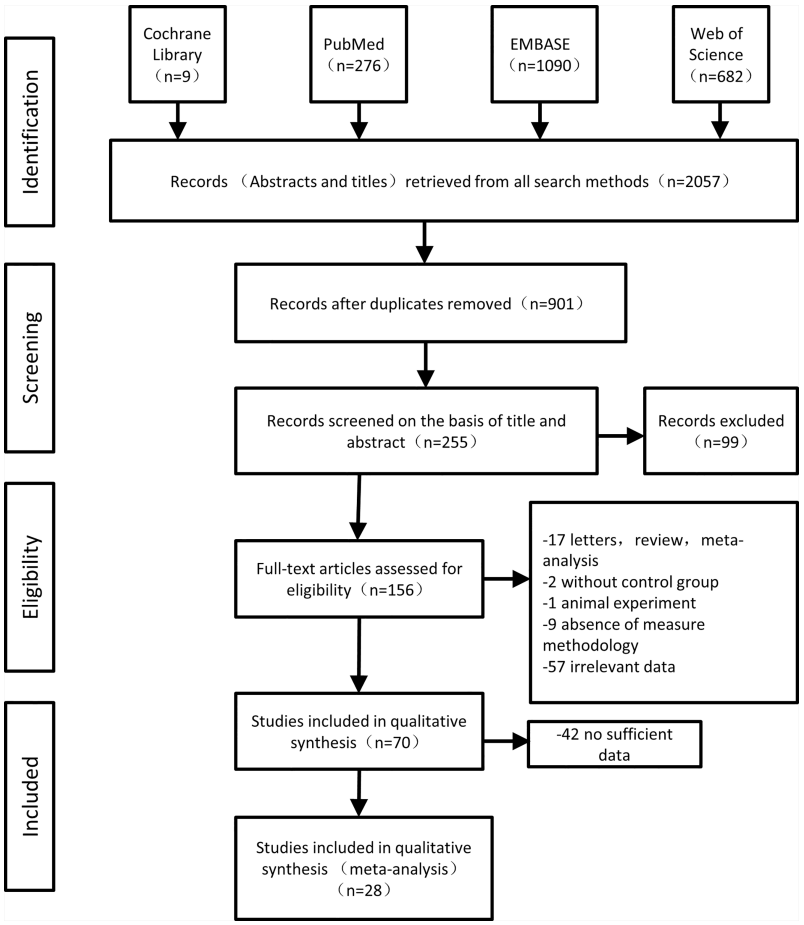

FIGURE 1 | The flow diagram of the selection of the studies.

of the studies would not significantly interfere with the overall measured outcome.

DISCUSSION

The relationship between *P. gingivalis* and RA remains heterogeneous and a subject of concern (Chaparro-Sanabria et al., 2019). Our meta-analysis showed that a patients exposed to *P. gingivalis* would have a higher risk of RA. According to Seror et al.'s study, there was a significant difference between the early RA group and the HC group for the frequency of *P. gingivalis*, which is the same as Goh et al.'s study (Seror et al., 2015; Goh et al., 2016). Contrary to our results, Seror et al.'s and Gon et al.'s studies revealed that they did not detect any association of anti-*P. gingivalis* antibodies with RA or ACPA status (Kharlamova et al., 2017). These results suggest that the association of periodontitis and RA could be linked to bacterial species other than *P. gingivalis* or a mechanism other than citrullination (**Figure 4**). This disparity might be due to various factors, including patient health, sample size, and RA treatment types (Kirchner et al., 2017).

Another study by Schmickler and others showed that patients with RA had worse oral health than healthy controls because of the absolute number of missing teeth and periodontal conditions (Rahajoe et al., 2021). The prevalence of all bacteria investigated in RA and HC groups is similar (Arévalo-Caro et al., 2022). The course of the disease, drug for rheumatism, and restricted motor skills, on the other hand, did not affect periodontal conditions (Janssen et al., 2015), even though there was a statistically significant association between a rheumatoid factor and periodontal condition (Kim et al., 2018). Their studies also reported that within the RA group, higher serum levels of *P. gingivalis* may be a significant marker for the higher burden of the bacteria and invasive periodontal diseases (Martínez-Rivera et al., 2017), which may justify why this bacterium is the only periodontal pathogen correlated with a higher risk of RA (Kononoff et al., 2021).

Also, a comparison between saliva samples of healthy individuals and patients with RA in a recent study indicated a

TABLE 1 | Main characteristics of the studies selected for the systematic review and meta-analysis.

Study	Country	Sample location	Study design	Sample size		Matched	OR (95%CI)	Biomarker	NOS score
				RA	Control				
Arévalo-Caro et al., 2022	Columbia	South America	cross-sectional	50	50	age&sex	0.61 (0.27, 1.36)	anti-*P. gingivalis*	8
Arvikar et al., 2013	USA	North America	cohort study	93	72	age	4.42 (1.81, 10.80)	anti-*P. gingivalis*	6
Äyräväinen et al., 2017	Finland	Europe	cohort study	71	27	age&sex& community	2.29 (0.47, 11.10)	*P. gingivalis*	9
Bello-Gualtero et al., 2016	Columbia	South America	cross-sectional	48	48	age&sex	0.54 (0.24, 1.24)	*P. gingivalis*	8
Bender et al., 2018	Switzerland	Europe	case-control	10	10	age&ethnicity	9.80 (0.44, 219.25)	*P. gingivalis*	8
Ceccarelli et al., 2018	Italy	Europe	case-control	143	57	NA	1.92 (1.01, 3.64)	*P. gingivalis*	6
Fisher et al., 2015	Espana	Europe	case-control	103	309	age&sex	0.66 (0.17, 2.62)	anti-RgpB	8
Janssen et al., 2015	Netherlands	Europe	case-control	86	36	NA	14.60 (0.85, 251.68)	*P. gingivalis*	5
Jasemi et al., 2021	Italy	Europe	case-control	148	148	age&sex	3.08 (1.58, 5.99)	anti-RgpA	8
Johansson et al., 2016	Sweden	Europe	case-control	192	198	age&sex	1.20 (0.75,1.92)	anti-RgpB	9
Kharlamova et al., 2016	Sweden	Europe	case-control	1974	377	age&sex &residential area	2.96 (2.00, 4.37)	anti-RgpB	9
Kim et al., 2018	Korea	Asia	cross-sectional	260	86	age&sex	0.33 (0.04, 2.63)	*P. gingivalis*	7
Kirchner et al., 2017	Germany	Europe	cross-sectional	103	104	age	1.10 (0.64,1.90)	*P. gingivalis*	7
Kononoff et al., 2020	Finland	Europe	case-control	53	82	age	2.55 (1.25, 5.22)	anti-*P. gingivalis*	6
Laugisch et al., 2016	Switzerland	Europe	case-control	52	44	age	2.05 (0.89, 4.73)	*P. gingivalis*	8
Maldonado et al., 2020	Switzerland	Europe	case-control	26	72	NA	1.27 (0.51, 3.14)	*P. gingivalis*	7
Martínez-Rivera et al., 2017	Mexico	North America	cross-sectional	132	10	NA	5.30 (1.80, 6.10)	*P. gingivalis*	6
Mikuls et al., 2009	USA	North America	case-control	78	40	age&sex	3.00 (1.36, 6.60)	anti-*P. gingivalis*	8
Mikuls et al., 2012	USA	North America	cohort study	113	171	NA	1.41 (1.08, 1.85)	anti-*P. gingivalis*	6
Okada et al., 2011	Japan	Asia	case-control	80	38	age&sex &smoking	1.11 (1.03, 1.20)	anti-*P. gingivalis*	8
Rahajoe et al., 2021	Indonesia	Asia	cohort study	70	70	age&sex &smoking &number	1.20 (0.52, 2.74)	*P. gingivalis*	9
Reichert et al., 2013	Germany	Europe	case-control	42	114	age	5.50 (1.50, 19.90)	*P. gingivalis*	8
Rinaudo-Gaujous et al., 2019	France	Europe	case-control	79	27	NA	1001.00 (87.14, 11499.17)	anti-*P. gingivalis*	5
Rodríguez et al., 2021	Columbia	South America	cross-sectional	51	51	age&sex	4.43 (1.86, 10.52)	*P. gingivalis*	8
Scher et al., 2012	USA	North America	case-control	65	18	age&sex &ethnicity	0.73 (0.18, 2.88)	*P. gingivalis*	7
Schmickler et al., 2017	Germany	Europe	cross-sectional	168	168	age&sex &smoking	1.05 (0.68, 1.61)	*P. gingivalis*	7
Schulz et al., 2019	Germany	Europe	case-control	101	100	sex	4.67 (2.07, 10.50)	*P. gingivalis*	7
de Smit et al., 2014	Netherlands	Europe	cross-sectional	95	80	age&sex	0.75 (0.34, 1.63)	*P. gingivalis*	8

NA, not available; not mentioned.

significant relationship between the higher prevalence of *P. gingivalis* and RA (Mikuls et al., 2009; Schmickler et al., 2017). The possible relationship between RA and *P. gingivalis* in different studies has been investigated, and most of these studies have shown a positive relationship between them (Unriza-Puin et al., 2017). A study from the USA reported a positive relationship between *P. gingivalis* and periodontal diseases (Mikuls et al., 2012). Also, it revealed that *P. gingivalis* was the most potent predictor of periodontal diseases among adolescents (Janssen et al., 2015; Manoil et al., 2021). The importance of our findings of a higher correlation rate of *P. gingivalis* in RA compared to healthy tissue is uncertain (Rodriguez et al., 2021). However, this bacterium invades healthy and inflammatory tissue more than other bacteria such as candida (de Smit et al., 2014; Rinaudo-Gaujous et al., 2019). Meanwhile, *P. gingivalis* can intervene in the inflammatory process by inhibiting the host's cellar death and inducing cell proliferation (Arvikar et al., 2013).

It is suggested that anti-*P. gingivalis* antibody levels play a significant role in the pathogenesis of RA (Westra et al., 2021), while distinct similarities are shown in both RA and periodontitis (Papageorgiou et al., 2020). The data suggest that RA and

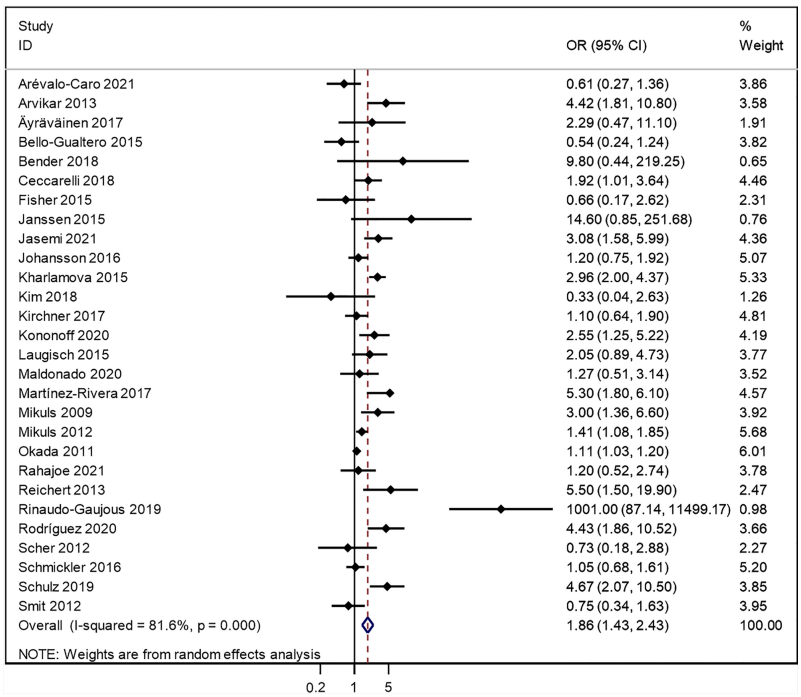

FIGURE 2 | Forest plot for the association between porphyromonas gingivalis (*P. gingivalis*) and rheumatoid arthritis (RA) of dichotomous data.

periodontitis may be linked to the periodontal pathogen *P. gingivalis* (Maldonado et al., 2020). Citrullinated variants of the Fibrin chains are considered target autoantigens in the rheumatoid joint (Perricone et al., 2019). *P. gingivalis* is the only prokaryotic organism that produces PPAD and contributes to the initiation of ACPA generation because of PPAD expression (Quirke et al., 2014). For example, PAD expressed in the joint deaminates synovial fibrin (Valor and de la Torre Ortega, 2012), and these synovial antigens may serve as targets for auto-antibody formation triggered by *P. gingivalis* associated

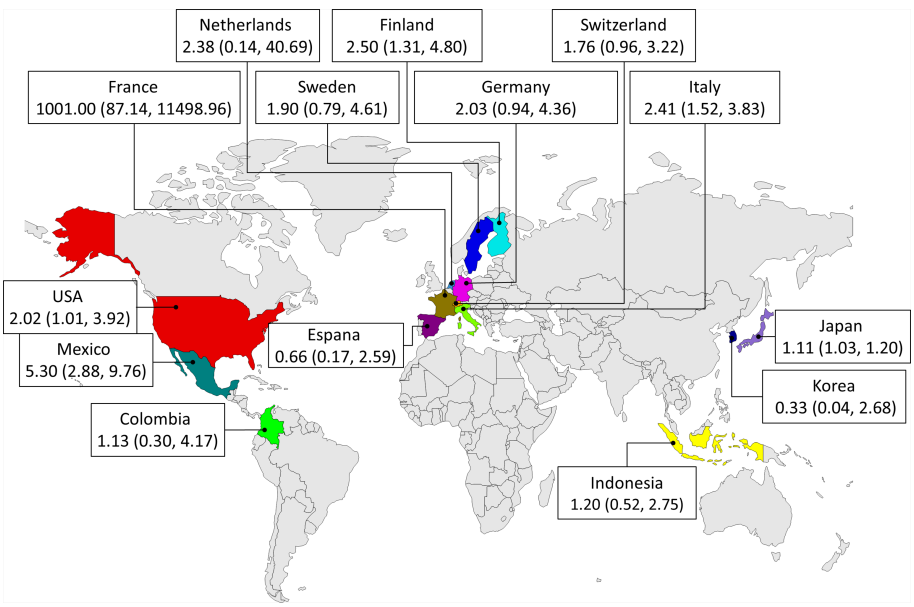

FIGURE 3 | Subgroup analyses of the association between *P. gingivalis* and rheumatoid arthritis in different countries.

TABLE 2 | Results of subgroups analysis.

subgroup analysis types	Subgroups	No. of studies involved	Meta-OR (95% CI)	Heterogeneity between studies (I^2)
Study design	Case-control	16	2.42 (1.60, 3.67)	84.4%
	Cohort	4	1.83 (1.05, 3.19)	52.8%
	Cross-sectional	8	1.22 (0.66, 2.26)	82.8%
Sample size	Cases ≥150	4	1.38 (0.71, 2.68)	82.2%
	Cases < 150	24	1.99 (1.47, 2.70)	81.6%
ORs sources	Reported by authors	8	2.09 (1.36, 3.21)	89.3%
	Calculated based on original data	20	1.82 (1.22, 2.70)	74.5%
Biomarker of *P. gingivalis*	*P. gingivalis*	17	1.76 (1.18, 2.64)	70.7%
	anti-*P.gingivalis*	7	2.14 (1.28, 3.60)	88.9%
	anti-RgpB	3	1.54 (0.69, 3.47)	81.6%
	anti-RgpA	1	3.08 (1.58, 6.00)	/
Detection methods	ELISA	11	2.02 (1.36, 3.01)	88.1%
	PCR	10	1.99 (1.19, 3.32)	79.3%
	Bacterial culture	7	1.23 (0.70, 2.17)	26.7%
Quality	NOS ≥ 8	15	1.61 (1.14, 2.28)	78%
	NOS < 8	13	2.32 (1.44, 3.75)	82%
Sample location (continent)	South America	3	1.13 (0.30, 4.17)	86.5%
	North America	5	2.50 (1.23, 5.08)	81.9%
	Europe	17	2.17 (1.46, 3.22)	75.9%
	Asia	3	1.11 (1.03, 1.20)	0.0%

with periodontitis and epitope spreading (Lee et al., 2015). Because antibody against citrullinated proteins plays a significant role in autoimmunity in RA (Xiao et al., 2020; Jasemi et al., 2021), an assumption is made that individuals predisposed to periodontitis are exposed to citrullinated antigens that become systemic immunogens (Moen et al., 2003). A study shows that antibody responses to *P. gingivalis* may affect ACPA responses, and the data support a role for the oral pathogen *P. gingivalis* in the etiology of RA (Arévalo-Caro et al., 2022).

There are differences between the prevalence rates reported by different studies for *P. gingivalis* that may be associated with the variations of *P. gingivalis* strains used in different studies (Ziebolz et al., 2011; Scher et al., 2012). Two completely different *P. gingivalis* strains differ in several aspects. For instance, the strain *P. gingivalis* ATCC53978 has a recognized capsule as the primary antigen associated with pathogenesis, but the strain *P. gingivalis* ATCC33277 does not have this antigen. Therefore, it leads to inflammation slightly (Sayehmiri et al., 2015). This meta-analysis did not have enough age, gender, smoking, or alcohol consumption data. These variables are essential and may influence the ability of bacteria to invade the immune system during the invasion of

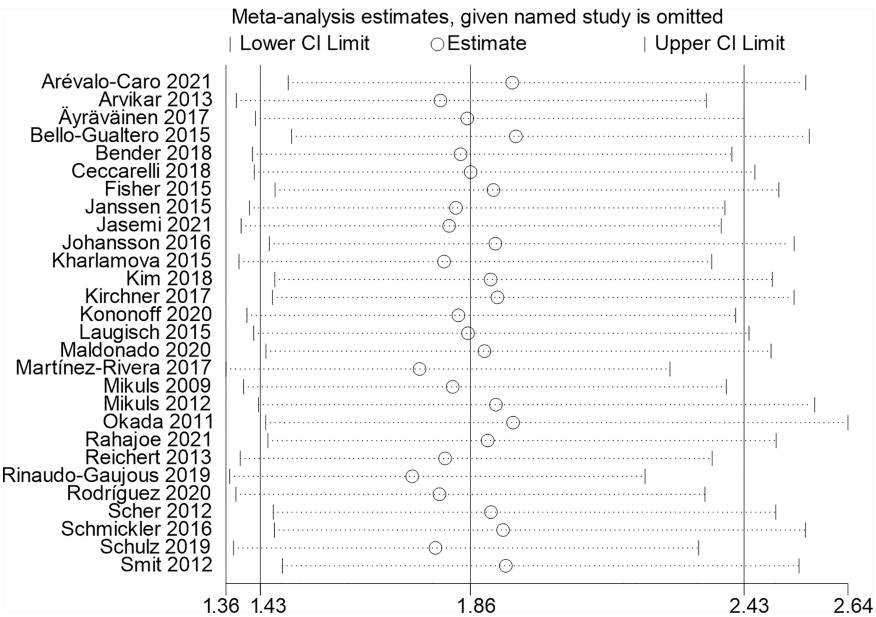

FIGURE 4 | Sensitivity analysis.

tissues and, therefore, potentially influence the inflammatory process.

As we know, sample size and location were critical factors in meta-analysis. Thus in our subgroup analysis, these included studies were distributed to two groups based on sample size (indicated by RA cases ≥150 or < 150), and ORs were pooled respectively. Our results showed that the differences between these two groups were statistically insignificant, as there was an overlap in 95%CI of individual ORs. In addition, we further analyzed pooled ORs in different sample locations in two ways. Firstly, the included studies were distributed to four groups based on their continents. Then the included studies were distributed to fourteen groups based on their countries. Our results showed there exists some regional differences in the relationship between P. gingivalis exposure and RA, as the pooled ORs from populations located in Europe and North America were significantly higher than that located in Asia. Also, pooled ORs from population located in Italy, Finland and Mexico were relatively higher than that in Japan (**Figure 3**). This might be due to the lower prevalence of RA in Japan (Silman and Pearson, 2002). It was a pity that no study reported any information about the relationship between P. gingivalis exposure and RA from population located in China. More studies are warranted to clarify the relationship in Chinese populations. Overall, our results suggested that it should be noted that P. gingivalis was a risk factor in RA development in populations around the world, even though the ORs were different across different areas.

This paper mainly conducted a meta-analysis on different regions, populations, research methods, age, sample size and other factors. The results indicated *P. gingivalis* exposure was a risk factor in RA. Prompt diagnosis and management decisions on *P. gingivalis* antimicrobial therapy would prevent rheumatoid arthritis development and progression. But, factors such as people smoked or not, drank alcohol, congenital hypoplasia, and whether individual has underlying medical conditions were not taken into account. Furthermore, in the included studies, different exposure methods were adopted for different biomarkers. Enzyme-Linked Immunosorbent Assay (ELISA) is generally used for the detection of serum antibodies, (e.g. Arvikar et al., 2013). There were two ways to detect *P. gingivalis*: one was bacterial culture (e.g. Janssen et al., 2015) and the other was Polymerase Chain Reaction (PCR) (e.g. Reichert et al., 2013). Results from subgroup analysis showed that the pooled OR were slightly higher in ELISA or PCR groups compared with Bacterial culture group, suggested that different detection method might influence the association between *P. gingivalis* and RA. This may provide a direction for future research. Meanwhile, a range of biomarkers were involved in the original text, including *P. gingivalis*, anti-*P. gingivalis*, anti-RgpB and anti-RgpA. The impact of different biomarkers was also evaluated in our subgroup analysis. The results showed that the differences were not that obvious. More studies are warranted to compare these difference directly.

As a chronic autoimmune disease, Rheumatoid arthritis is developed due to genetics and environmental risks, and periodontitis is one of the consistently reported risk factors (González-Febles and Sanz, 2021). Most importantly, *P. gingivalis* is one of the commonly found bacterium in periodontitis patients (Jia et al, 2019). It was reported that *P. gingivalis* has a unique ability to produce citrullinate proteins or peptides by proteolytic cleavage at Arg-X peptide bonds by arginine gingipains, followed by citrullination of carboxy-terminal arginines by bacterial PAD (Smolen et al., 2016). Specific citrullinated peptides generated by P. gingivalis could be worked as self-antigen and lead to the breakdown of immune tolerance at the site of gingival inflammation (Muñoz-Atienza et al, 2020). Epitope spreading to other host citrullinated proteins would lead to chronic and destructive inflammation in the joint, which triggers the development of rheumatoid arthritis (Wegner et al, 2010).

In conclusion, our results indicated P. gingivalis exposure was a potential risk factor in RA. More perspective studies and mechanism research are warranted to confirm the causal link between *P. gingivalis* exposure and RA process. Prompt diagnosis and management decisions on *P. gingivalis* antimicrobial therapy would prevent RA development and progression.

AUTHOR CONTRIBUTIONS

JZ and LY conceived the project. YL, RG and LL designed the whole meta-analysis, including article search and exclusion, quality assessment, and analyzed the data. LL, JZ and LY supervised the project, provided the funding, interpreted the results. YL and RG wrote the manuscript with input from all authors. PO helped revise languages. TS, HC, YY and WZ helped with the data analysis. QW reviewed the data, provided advice and funding. All authors contributed to the article and approved the submitted version.

FUNDING

This study was supported by the National Key Research and Development Program of China (2019YFC1708803), the Science and Technology Program of Tianjin, China (21ZYJDJC00070), Innovation Team and Talents Cultivation Program of National Administration of Traditional Chinese Medicine (ZYYCXTD-C-202203) and the Education Committee of Tianjin (2021KJ130).

SUPPLEMENTARY MATERIAL

The Supplementary Material for this article can be found online at: https://www.frontiersin.org/articles/10.3389/fcimb.2022.956417/full#supplementary-material

Supplementary Figure 1 | Publication bias in the risk difference (RD) in dichotomous data, Begg's funnel plot.

Supplementary Figure 2 | Two different ORs were reported for **(A)** IgG1 anti-*P. gingivalis*, **(B)** IgG2 anti-*P. gingivalis* were used to define *P. gingivalis* exposure.

REFERENCES

Arévalo-Caro, C., Romero-Sánchez, C., and Garavito-Rodríguez, E. (2022). Relation Between Anti-Porphyromonas Gingivalis Antibody Titers and HLA-DRB1 Neutral Alleles in Individuals With Rheumatoid Arthritis. *Acta Odontol. Scand.* 80(2), 131–139. doi: 10.1080/00016357.2021.1959053

Arvikar, S. L., Collier, D. S., Fisher, M. C., Unizony, S., Cohen, G. L., McHugh, G., et al. (2013). Clinical Correlations With Porphyromonas Gingivalis Antibody Responses in Patients With Early Rheumatoid Arthritis. *Arthritis. Res. Ther.* 15 (5), R109. doi: 10.1186/ar4289

Äyräväinen, L., Leirisalo-Repo, M., Kuuliala, A., Ahola, K., Koivuniemi, R., Meurman, J. H., et al. (2017). Periodontitis in Early and Chronic Rheumatoid Arthritis: A Prospective Follow-Up Study in Finnish Population. *BMJ Open* 7 (1), e011916. doi: 10.1136/bmjopen-2016-011916

Bello-Gualtero, J. M., Lafaurie, G. I., Hoyos, L. X., Castillo, D. M., De-Avila, J., Munevar, J. C., et al. (2016). Periodontal Disease in Individuals With a Genetic Risk of Developing Arthritis and Early Rheumatoid Arthritis: A Cross-Sectional Study. *J. Periodontol.* 87 (4), 346–356. doi: 10.1902/jop.2015.150455

Bender, P., Egger, A., Westermann, M., Taudte, N., Sculean, A., Potempa, J., et al. (2018). Expression of Human and Porphyromonas Gingivalis Glutaminyl Cyclases in Periodontitis and Rheumatoid Arthritis-A Pilot Study. *Arch. Oral. Biol.* 97, 223–230. doi: 10.1016/j.archoralbio.2018.10.022

Berthelot, J. M., and Le Goff, B. (2010). Rheumatoid Arthritis and Periodontal Disease. *Joint. Bone Spine.* 77 (6), 537–541. doi: 10.1016/j.jbspin.2010.04.015

Białowąs, K., Radwan-Oczko, M., Duś-Ilnicka, I., Korman, L., and Świerkot, J. (2020). Periodontal Disease and Influence of Periodontal Treatment on Disease Activity in Patients With Rheumatoid Arthritis and Spondyloarthritis. *Rheumatol. Int.* 40 (3), 455–463. doi: 10.1007/s00296-019-04460-z

Ceccarelli, F., Orrù, G., Pilloni, A., Bartosiewicz, I., Perricone, C., Martino, E., et al. (2018). Porphyromonas Gingivalis in the Tongue Biofilm is Associated With Clinical Outcome in Rheumatoid Arthritis Patients. *Clin. Exp. Immunol.* 194 (2), 244–252. doi: 10.1111/cei.13184

Chaparro-Sanabria, J. A., Bautista-Molano, W., Bello-Gualtero, J. M., Chila-Moreno, L., Castillo, D. M., Valle-Oñate, R., et al. (2019). Association of Adipokines With Rheumatic Disease Activity Indexes and Periodontal Disease in Patients With Early Rheumatoid Arthritis and Their First-Degree Relatives. *Int. J. Rheumatol. Dis.* 22 (11), 1990–2000. doi: 10.1111/1756-185X.13724

de Smit, M., van de Stadt, L. A., Janssen, K. M., Doornbos-van der Meer, B., Vissink, A., van Winkelhoff, A. J., et al. (2014). Antibodies Against Porphyromonas Gingivalis in Seropositive Arthralgia Patients do Not Predict Development of Rheumatoid Arthritis. *Ann. Rheumatol. Dis.* 73 (6), 1277–1279. doi: 10.1136/annrheumdis-2013-204594

Eriksson, K., Fei, G., Lundmark, A., Benchimol, D., Lee, L., Hu, Y., et al. (2019). Periodontal Health and Oral Microbiota in Patients With Rheumatoid Arthritis. *J. Clin. Med.* 8 (5), 630. doi: 10.3390/jcm8050630

Fisher, B. A., Cartwright, A. J., Quirke, A. M., de Pablo, P., Romaguera, D., Panico, S., et al. (2015). Smoking, Porphyromonas Gingivalis and the Immune Response to Citrullinated Autoantigens Before the Clinical Onset of Rheumatoid Arthritis in a Southern European Nested Case-Control Study. *BMC Musculoskelet. Disord.* 16, 331. doi: 10.1186/s12891-015-0792-y

Goh, C. E., Kopp, J., Papapanou, P. N., Molitor, J. A., and Demmer, R. T. (2016). Association Between Serum Antibodies to Periodontal Bacteria and Rheumatoid Factor in the Third National Health and Nutrition Examination Survey. *Arthritis. Rheumatol.* 68 (10), 2384–2393. doi: 10.1002/art.39724

González-Febles, J., and Sanz, M. (2021). Periodontitis and Rheumatoid Arthritis: What Have We Learned About Their Connection and Their Treatment? *Periodontol.* 87 (1), 181–203. doi: 10.1111/prd.12385

Janssen, K. M., de Smit, M. J., Brouwer, E., de Kok, F. A., Kraan, J., Altenburg, J., et al. (2015). Rheumatoid Arthritis-Associated Autoantibodies in non-Rheumatoid Arthritis Patients With Mucosal Inflammation: A Case-Control Study. *Arthritis. Res. Ther.* 17 (1), 174. doi: 10.1186/s13075-015-0690-6

Jasemi, S., Erre, G. L., Cadoni, M. L., Bo, M., and Sechi, L. A. (2021). Humoral Response to Microbial Biomarkers in Rheumatoid Arthritis Patients. *J. Clin. Med.* 10 (21), 5153. doi: 10.3390/jcm10215153

Jia, L., Han, N., Du, J., Guo, L., Luo, Z., and Liu, Y. (2019). Pathogenesis of Important Virulence Factors of Porphyromonas Gingivalis via Toll-Like Receptors. *Front. Cell. Infect. Microbiol.* 9. doi: 10.3389/fcimb.2019.00262

Johansson, L., Sherina, N., Kharlamova, N., Potempa, B., Larsson, B., Israelsson, L., et al. (2016). Concentration of Antibodies Against Porphyromonas Gingivalis is Increased Before the Onset of Symptoms of Rheumatoid Arthritis. *Arthritis. Res. Ther.* 18 (1), 201. doi: 10.1186/s13075-016-1100-4

Kharlamova, N., Jiang, X., Sherina, N., Potempa, B., Israelsson, L., Quirke, A. M., et al. (2016). Antibodies to Porphyromonas Gingivalis Indicate Interaction Between Oral Infection, Smoking, and Risk Genes in Rheumatoid Arthritis Etiology. *Arthritis. Rheumatol.* 68 (3), 604–613. doi: 10.1002/art.39491

Kharlamova, N., Jiang, X., Sherina, N., Potempa, B., Israelsson, L., Quirke, A. M., et al. (2017). Antibodies to Porphyromonas Gingivalis Indicate Interaction Between Oral Infection, Smoking, and Risk Genes in Rheumatoid Arthritis Etiology. *Arthritis. Rheumatol.* 68 (3), 604–613. doi: 10.1002/art.39491

Kim, J. H., Choi, I. A., Lee, J. Y., Kim, K. H., Kim, S., Koo, K. T., et al. (2018). Periodontal Pathogens and the Association Between Periodontitis and Rheumatoid Arthritis in Korean Adults. *J. Periodontal. Implant. Sci.* 48 (6), 347–359. doi: 10.5051/jpis.2018.48.6.347

Kirchner, A., Jäger, J., Krohn-Grimberghe, B., Patschan, S., Kottmann, T., Schmalz, G., et al. (2017). Active Matrix Metalloproteinase-8 and Periodontal Bacteria Depending on Periodontal Status in Patients With Rheumatoid Arthritis. *J. Periodontal. Res.* 52 (4), 745–754. doi: 10.1111/jre.12443

Konig, M. F., Paracha, A. S., Moni, M., Bingham, C. O.3rd, and Andrade, F. (2015). Defining the Role of Porphyromonas Gingivalis Peptidylarginine Deiminase (PPAD) in Rheumatoid Arthritis Through the Study of PPAD Biology. *Ann. Rheumatol. Dis.* 74 (11), 2054–2061. doi: 10.1136/annrheumdis-2014-205385

Kononoff, A., Elfving, P., Pussinen, P., Hörkkö, S., Kautiainen, H., Arstila, L., et al. (2020). Association of Rheumatoid Arthritis Disease Activity and Antibodies to Periodontal Bacteria With Serum Lipoprotein Profile in Drug Naive Patients. *Ann. Med.* 52 (1-2), 32–42. doi: 10.1080/07853890.2020.1724321

Kononoff, A., Hörkkö, S., Pussinen, P., Kautiainen, H., Elfving, P., Savolainen, E., et al. (2021). Antibodies to Malondialdehyde-Acetaldehyde Modified Low-Density Lipoprotein in Patients With Newly Diagnosed Inflammatory Joint Disease. *Scand. J. Rheumatol.* 50 (2), 113–117. doi: 10.1080/03009742.2020.1795244

Laugisch, O., Wong, A., Sroka, A., Kantyka, T., Koziel, J., Neuhaus, K., et al. (2016). Citrullination in the Periodontium-a Possible Link Between Periodontitis and Rheumatoid Arthritis. *Clin. Oral. Investig.* 20 (4), 675–683. doi: 10.1007/s00784-015-1556-7

Leech, M. T., and Bartold, P. M. (2015). The Association Between Rheumatoid Arthritis and Periodontitis. *Best. Pract. Res. Clin. Rheumatol.* 29 (2), 189–201. doi: 10.1016/j.berh.2015.03.001

Lee, J. Y., Choi, I. A., Kim, J. H., Kim, K. H., Lee, E. Y., Lee, E. B., et al. (2015). Association Between Anti-Porphyromonas Gingivalis or Anti-α-Enolase Antibody and Severity of Periodontitis or Rheumatoid Arthritis (RA) Disease Activity in RA. *BMC Musculoskelet. Disord.* 16 (1), 1–8. doi: 10.1186/s12891-015-0647-6

Liberati, A., Altman, D. G., Tetzlaff, J., Mulrow, C., Gøtzsche, P. C., Ioannidis, J. P., et al. (2009). The PRISMA Statement for Reporting Systematic Reviews and Meta-Analyses of Studies That Evaluate Healthcare Interventions: Explanation and Elaboration. *BMJ.* 339, b2700. doi: 10.1136/bmj.b2700

Maldonado, A., Pirracchio, L., Imber, J. C., Bürgin, W., Möller, B., Sculean, A., et al. (2020). Citrullination in Periodontium is Associated With Porphyromonas Gingivalis. *Arch. Oral. Biol.* 114, 104695. doi: 10.1016/j.archoralbio.2020.104695

Manoil, D., Bostanci, N., Mumcu, G., Inanc, N., Can, M., Direskeneli, H., et al. (2021). Novel and Known Periodontal Pathogens Residing in Gingival Crevicular Fluid are Associated With Rheumatoid Arthritis. *J. Periodontol.* 92 (3), 359–370. doi: 10.1002/JPER.20-0295

Mariette, X., Perrodeau, E., Verner, C., Struillou, X., Picard, N., Schaeverbeke, T., et al. (2020). Role of Good Oral Hygiene on Clinical Evolution of Rheumatoid Arthritis: A Randomized Study Nested in the ESPOIR Cohort. *Rheumatol. (Oxford).* 59 (5), 988–996. doi: 10.1093/rheumatology/kez368

Martínez-Rivera,J.I.,Xibillé-Friedmann,D.X.,González-Christen,J.,delaGarza-Ramos,M. A., Carrillo-Vázquez, S. M., and Montiel-Hernández, J. L. (2017). Salivary Ammonia Levels and Tannerella Forsythia are Associated With Rheumatoid Arthritis: A Cross Sectional Study. *Clin. Exp. Dent. Res.* 3 (3), 107–114. doi: 10.1002/cre2.68

Mikuls, T. R., Payne, J. B., Reinhardt, R. A., Thiele, G. M., Maziarz, E., Cannella, A. C., et al. (2009). Antibody Responses to Porphyromonas Gingivalis (P. Gingivalis) in Subjects With Rheumatoid Arthritis and Periodontitis. *Int. Immunopharmacol.* 9 (1), 38–42. doi: 10.1016/j.intimp.2008.09.008

Mikuls, T. R., Thiele, G. M., Deane, K. D., Payne, J. B., O'Dell, J. R., Yu, F., et al. (2012). Porphyromonas Gingivalis and Disease-Related Autoantibodies in

Individuals at Increased Risk of Rheumatoid Arthritis. *Arthritis. Rheumatol.* 64 (11), 3522–3530. doi: 10.1002/art.34595

Moen, K., Brun, J. G., Madland, T. M., Tynning, T., and Jonsson, R. (2003). Immunoglobulin G and A Antibody Responses to Bacteroides Forsythus and Prevotella Intermedia in Sera and Synovial Fluids of Arthritis Patients. *Clin. Diagn. Lab. Immunol.* 10 (6), 1043–1050. doi: 10.1128/cdli.10.6.1043-1050.2003

Muñoz-Atienza, E., Flak, M. B., Sirr, J., Paramonov, N. A., Aduse-Opoku, J., Pitzalis, C., et al. (2020). The P. Gingivalis Autocitrullinome Is Not a Target for ACPA in Early Rheumatoid Arthritis. *J. Dent. Res.* 99 (4), 456–462. doi: 10.1177/0022034519898144

Okada, M., Kobayashi, T., Ito, S., Yokoyama, T., Komatsu, Y., Abe, A., et al. (2011). Antibody Responses to Periodontopathic Bacteria in Relation to Rheumatoid Arthritis in Japanese Adults. *J. Periodontol.* 82 (10), 1433–1441. doi: 10.1902/jop.2011.110020

Oluwagbemigun, K., Yucel-Lindberg, T., Dietrich, T., Tour, G., Sherina, N., Hansson, M., et al. (2019). A Cross-Sectional Investigation Into the Association Between Porphyromonas Gingivalis and Autoantibodies to Citrullinated Proteins in a German Population. *Ther. Adv. Musculoskelet. Dis.* 11, 1759720X19883152. doi: 10.1177/1759720X19883152

Papageorgiou, S. N., Koletsi, D., Iliadi, A., Peltomaki, T., and Eliades, T. (2020). Treatment Outcome With Orthodontic Aligners and Fixed Appliances: A Systematic Review With Meta-Analyses. *Eur. J. Orthod.* 42 (3), 331–343. doi: 10.1093/ejo/cjz094

Perricone, C., Ceccarelli, F., Saccucci, M., Di Carlo, G., Bogdanos, D. P., Lucchetti, R., et al. (2019). Porphyromonas Gingivalis and Rheumatoid Arthritis. *Curr. Opin. Rheumatol.* 31 (5), 517–524. doi: 10.1097/BOR.0000000000000638

Quirke, A. M., Lugli, E. B., Wegner, N., Hamilton, B. C., Charles, P., Chowdhury, M., et al. (2014). Heightened Immune Response to Autocitrullinated Porphyromonas Gingivalis Peptidylarginine Deiminase: A Potential Mechanism for Breaching Immunologic Tolerance in Rheumatoid Arthritis. *Ann. Rheumatol. Dis.* 73 (1), 263–269. doi: 10.1136/annrheumdis-2012-202726

Rahajoe, P. S., de Smit, M. J., Raveling-Eelsing, E., du Teil Espina, M., Stobernack, T., Lisotto, P., et al. (2021). No Obvious Role for Suspicious Oral Pathogens in Arthritis Development. *Int. J. Environ. Res. Public Health* 18 (18), 9560. doi: 10.3390/ijerph18189560

Reichert, S., Haffner, M., Keyßer, G., Schäfer, C., Stein, J. M., Schaller, H. G., et al. (2013). Detection of Oral Bacterial DNA in Synovial Fluid. *J. Clin. Periodontol.* 40 (6), 591–598. doi: 10.1111/jcpe.12102

Rinaudo-Gaujous, M., Blasco-Baque, V., Miossec, P., Gaudin, P., Farge, P., Roblin, X., et al. (2019). Infliximab Induced a Dissociated Response of Severe Periodontal Biomarkers in Rheumatoid Arthritis Patients. *J. Clin. Med.* 8 (5), 751. doi: 10.3390/jcm8050751

Rodríguez, J., Lafaurie, G. I., Bautista-Molano, W., Chila-Moreno, L., Bello-Gualtero, J. M., and Romero-Sánchez, C. (2021). Adipokines and Periodontal Markers as Risk Indicators of Early Rheumatoid Arthritis: A Cross-Sectional Study. *Clin. Oral. Investig.* 25 (4), 1685–1695. doi: 10.1007/s00784-020-03469-0

Sayehmiri, F., Sayehmiri, K., Asadollahi, K., Soroush, S., Bogdanovic, L., Jalilian, F. A., et al. (2015). The Prevalence Rate of Porphyromonas Gingivalis and its Association With Cancer: A Systematic Review and Meta-Analysis. *Int. J. Immunopathol. Pharmacol.* 28 (2), 160–167. doi: 10.1177/0394632015586144

Scher, J. U., Ubeda, C., Equinda, M., Khanin, R., Buischi, Y., Viale, A., et al. (2012). Periodontal Disease and the Oral Microbiota in New-onset Rheumatoid Arthritis. *Arthritis. Rheum* 64 (10), 3083–3094. doi: 10.1002/art.34539

Scher, J. U., and Abramson, S. B. (2013). Periodontal Disease, Porphyromonas Gingivalis, and Rheumatoid Arthritis: What Triggers Autoimmunity and Clinical Disease? *Arthritis. Res. Ther.* 15 (5), 122. doi: 10.1186/ar4360

Schmickler, J., Rupprecht, A., Patschan, S., Patschan, D., Müller, G. A., Haak, R., et al. (2017). Cross-Sectional Evaluation of Periodontal Status and Microbiologic and Rheumatoid Parameters in a Large Cohort of Patients With Rheumatoid Arthritis. *J. Periodontol.* 88 (4), 368–379. doi: 10.1902/jop.2016.160355

Schulz, S., Pütz, N., Jurianz, E., Schaller, H. G., and Reichert, S. (2019). Are There Any Common Genetic Risk Markers for Rheumatoid Arthritis and Periodontal Diseases? A Case-Control Study. *Mediators. Inflamm.*, (2013). 2907062. doi: 10.1155/2019/2907062

Seror, R., Le Gall-David, S., Bonnaure-Mallet, M., Schaeverbeke, T., Cantagrel, A., Minet, J., et al. (2015). Association of Anti-Porphyromonas Gingivalis Antibody Titers With Nonsmoking Status in Early Rheumatoid Arthritis: Results From the Prospective French Cohort of Patients With Early Rheumatoid Arthritis. *Arthritis Rheumatol.* 67 (7), 1729–1737. doi: 10.1002/art.39118

Silman, A. J., and Pearson, J. E. (2002). Epidemiology and Genetics of Rheumatoid Arthritis. *Arthritis Res.* 4 Suppl 3 (Suppl 3), S265–S272. doi: 10.1186/ar578

Smolen, J. S., Aletaha, D., and McInnes, I. B. (2016). Rheumatoid Arthritis. *Lancet.* 388 (10055), 2023–2038. doi: 10.1016/S0140-6736(16)30173-8

Unriza-Puin, S., Bautista-Molano, W., Lafaurie, G. I., Valle-Oñate, R., Chalem, P., Chila-Moreno, L., et al. (2017). Are Obesity, ACPAs and Periodontitis Conditions That Influence the Risk of Developing Rheumatoid Arthritis in First-Degree Relatives? *Reumatol. Clin.* 36 (4), 799–806. doi: 10.1007/s10067-016-3519-z

Valor, L., and de la Torre Ortega, I. (2012). Should We Use Poor Prognosis Factors to Start Early Treatment in Patients With Rheumatoid Arthritis? *Reumatol. Clin.* 8 (4), 163–167. doi: 10.1016/j.reuma.2011.12.004

Wegner, N., Wait, R., Sroka, A., Eick, S., Nguyen, K. A., Lundberg, K., et al. (2010). Peptidylarginine Deiminase From Porphyromonas Gingivalis Citrullinates Human Fibrinogen and α-Enolase: Implications for Autoimmunity in Rheumatoid Arthritis. *Arthritis Rheumatol.* 62 (9), 2662–2672. doi: 10.1002/art.27552

Westra, J., Brouwer, E., Raveling-Eelsing, E., Arends, S., Eman Abdulle, A., Roozendaal, C., et al. (2021). Arthritis Autoantibodies in Individuals Without Rheumatoid Arthritis: Follow-Up Data From a Dutch Populationbased Cohort (Lifelines). *Rheumatology.* 60 (2), 658–666. doi: 10.1093/rheumatology/keaa219

Xiao, L., Zhang, Q., Peng, Y., Wang, D., and Liu, Y. (2020). The Effect of Periodontal Bacteria Infection on Incidence and Prognosis of Cancer: A Systematic Review and Meta-Analysis. *Medicine* 99 (15), e19698. doi: 10.1097/MD.0000000000019698

Ziebolz, D., Pabel, S. O., Lange, K., Krohn-Grimberghe, B., Hornecker, E., and Mausberg, R. F. (2011). Clinical Periodontal and Microbiologic Parameters in Patients With Rheumatoid Arthritis. *J. Periodontol.* 82 (10), 1424–1432. doi: 10.1902/jop.2011.100481

Conflict of Interest: The authors declare that the research was conducted in the absence of any commercial or financial relationships that could be construed as a potential conflict of interest.

Publisher's Note: All claims expressed in this article are solely those of the authors and do not necessarily represent those of their affiliated organizations, or those of the publisher, the editors and the reviewers. Any product that may be evaluated in this article, or claim that may be made by its manufacturer, is not guaranteed or endorsed by the publisher.

frontiers | Frontiers in Cellular and Infection Microbiology

TYPE Original Research
PUBLISHED 28 July 2022
DOI 10.3389/fcimb.2022.956528

OPEN ACCESS

EDITED BY
Zhanbo Zhu,
Heilongjiang Bayi Agricultural University, China

REVIEWED BY
Tao Wang,
Tianjin University, China
Qiang Dong,
Northwest A and F University, China

*CORRESPONDENCE
Long Yang
long.yang@tjutcm.edu.cn
Yuhong Bian
bianyuhong_2012@163.com

SPECIALTY SECTION
This article was submitted to Clinical Microbiology, a section of the journal Frontiers in Cellular and Infection Microbiology

RECEIVED 30 May 2022
ACCEPTED 04 July 2022
PUBLISHED 28 July 2022

CITATION
Fan Y, Xu C, Xie L, Wang Y, Zhu S, An J, Li Y, Tian Z, Yan Y, Yu S, Liu H, Jia B, Wang Y, Wang L, Yang L and Bian Y (2022) Abnormal bile acid metabolism is an important feature of gut microbiota and fecal metabolites in patients with slow transit constipation.
Front. Cell. Infect. Microbiol. 12:956528. doi: 10.3389/fcimb.2022.956528

Abnormal bile acid metabolism is an important feature of gut microbiota and fecal metabolites in patients with slow transit constipation

Yadong Fan[1], Chen Xu[2], Lulu Xie[3], Ying Wang[1], Shan Zhu[1], Jiren An[4], Yuwei Li[2], Zhikui Tian[1], Yiqi Yan[1], Shuang Yu[1], Haizhao Liu[1], Beitian Jia[1], Yiyang Wang[1], Li Wang[5], Long Yang[1,6]* and Yuhong Bian[1]*

[1]School of Integrative Medicine, Tianjin University of Traditional Chinese Medicine, Tianjin, China, [2]Department of Colorectal Surgery, Tianjin Union Medical Center, Tianjin, China, [3]School of Medicine, Nankai University, Tianjin, China, [4]The First Clinical College, Liaoning University of Traditional Chinese Medicine, Shenyang, China, [5]The Pharmacy Department, Tianjin Second People's Hospital, Tianjin, China, [6]Research Center for Infectious Diseases, Tianjin University of Traditional Chinese Medicine, Tianjin, China

Destructions in the intestinal ecosystem are implicated with changes in slow transit constipation (STC), which is a kind of intractable constipation characterized by colonic motility disorder. In order to deepen the understanding of the structure of the STC gut microbiota and the relationship between the gut microbiota and fecal metabolites, we first used 16S rRNA amplicon sequencing to evaluate the gut microbiota in 30 STC patients and 30 healthy subjects. The α-diversity of the STC group was changed to a certain degree, and the β-diversity was significantly different, which indicated that the composition of the gut microbiota of STC patients was inconsistent with healthy subjects. Among them, Bacteroides, Parabacteroides, Desulfovibrionaceae, and Ruminiclostridium were significantly upregulated, while Subdoligranulum was significantly downregulated. The metabolomics showed that different metabolites between the STC and the control group were involved in the process of bile acids and lipid metabolism, including taurocholate, taurochenodeoxycholate, taurine, deoxycholic acid, cyclohexylsulfamate, cholic acid, chenodeoxycholate, arachidonic acid, and 4-pyridoxic acid. We found that the colon histomorphology of STC patients was significantly disrupted, and TGR5 and FXR were significantly downregulated. The differences in metabolites were related to changes in the abundance of specific bacteria and patients' intestinal dysfunction. Analysis of the fecal genomics and metabolomics enabled separation of the STC from controls based on random forest model prediction [STC *vs*. control (14 gut microbiota and metabolite biomarkers)—Sensitivity: 1, Specificity: 0.877].

This study provided a perspective for the diagnosis and intervention of STC related with abnormal bile acid metabolism.

KEYWORDS

slow transit constipation, bile acid metabolism, 16S rRNA amplicon sequencing, metabolomics, diagnosis and intervention

Introduction

Constipation is a common digestive system symptom with a reported prevalence of 7.0%–20.3% among Chinese adults (Peng et al., 2016; Long et al., 2017b). It is manifested by difficulty in defecation and/or reduced frequency of bowel movements, and dry and hard stools. With the accelerated pace of life, changes in dietary structure, and the influence of social and psychological factors, the prevalence of constipation is on the rise (Chu et al., 2014). It is more symptomatic and common in the elderly and women (Mugie et al., 2011; Vriesman et al., 2020). Slow transit constipation (STC) is the major category of intractable constipation and is characterized by colonic motility disorder (Hanson et al., 2019). The pathogenesis of STC mainly includes dietary structure with insufficient dietary fiber and water intake, lack of intestinal motility, abnormal enteric nervous system, dysfunction of colonic smooth muscle activity, and psychological factors (Rao et al., 2016; Vriesman et al., 2020). Treatments of functional constipation (three different subtypes: constipation with a normal transit, STC, and rectal evacuation disorders) include dietary interventions, educational and behavioral therapy, pharmacological interventions, transanal irrigation, neuromodulation, and imperative surgical interventions (Lacy et al., 2016; Vriesman et al., 2020).

New alternative therapies including fecal microbiota transplantation and acupuncture have been suggested to show the potential to treat functional constipation, but more supported studies are needed (Liu et al., 2016; Ding et al., 2018). The quality of life in patients with STC decreases, causing obvious economic and social burdens (Lacy et al., 2016; Vriesman et al., 2020). Destructions in the intestinal ecosystem are implicated with changes in STC, which suggest the possible roles of microbial disturbances in the development of constipation (Drossman, 2016; Parthasarathy et al., 2016; Ceresola et al., 2018). The structure of the intestinal microbiota is beneficial to the host metabolism, anti-inflammation, immunoregulation, and gastrointestinal motility (Nicholson et al., 2012; Kashyap et al., 2013; Propheter and Hooper, 2015; Si et al., 2018). This association can be explained by the regulation of the intestinal microbiota on the gastrointestinal motility, the osmotic effect of fermentation products, and metabolites, thus resulting in increased gas production (Hooper et al., 2001; Husebye et al., 2001). However, the role of gut microbes in the pathophysiology of STC is not fully understood.

Fecal genomics and metabolomics are useful tools for the quantification of the gut microbiome and related metabolites, which have more possible objective diagnostic potential. Thus, we performed 16S rRNA amplicon sequencing and ultra-high-performance liquid chromatography quadrupole time-of-flight mass spectrometry (UHPLC-Q-TOF-MS)-based metabolomics on fecal samples of patients with STC and healthy subjects to obtain evidence of distinct phenotypes of fecal microorganisms and metabolites. The relationship between different fecal microorganisms, metabolites, and clinical manifestations was explored according to the correlation analysis.

Materials and methods

Study subject recruitment

A total of 30 subjects met the Rome IV criteria for STC and 30 healthy controls were recruited from the outpatient department of Tianjin People's Hospital from April 2020 through December 2020 (Drossman and Hasler, 2016; Rao et al., 2016). All subjects were evaluated by a physician. Inclusion criteria: STC patients confirmed by colonic transit stud with colonic transit time >48 h (Diamant et al., 1999); disease duration ≥ 3 months; age ≥ 18 years; body mass index (BMI): 18.5–25 kg/m^2. Exclusion criteria: congenital megacolon; constipation caused by secondary intervention (e.g., drugs, metabolic disorder, endocrine disorders, or neurological disorders); previous abdominal surgery and perianal surgery; history or current of gastrointestinal diseases (e.g., malignancy and inflammatory bowel disease); infected with enteric pathogens; used prebiotics, probiotics, or proton pump inhibitors within the past month; pregnant or breast-feeding women; long-term smoking and/or alcohol addiction; confirmed to have hepatic, renal, cardiovascular, respiratory or psychiatric disease; suffered from other disease that could affect intestinal transit and the gut microbiota.

The researchers obtained metadata about each participant, including sex, age, gastrointestinal symptoms, dietary supplements, medications, and allergy history. All participants did not take antibiotics, probiotics, and prebiotics in the 3 months before the fecal sample collection. The quality of life of all subjects was evaluated according to the Wexner constipation score standard and the Gastrointestinal Quality of Life Index (GIQLI) (Eypasch et al., 1995; Agachan et al., 1996). All subjects or their families signed informed consents.

Fecal sample collection and preparation

Standardized instructions and kits for collecting stool were provided to subjects, and the feces were collected and frozen in liquid nitrogen for cryopreservation immediately. The feces of the subjects were scored according to the Bristol stool form scale (BSFS) (Chumpitazi et al., 2016).

DNA isolation and 16S rRNA amplicon sequencing

Total genome DNA from fecal samples was extracted using the CTAB/SDS method. DNA concentration and purity were monitored on 1% agarose gels. According to the concentration, DNA was diluted to 1 ng/μl using sterile water for further use. The V3–V4 variable region of 16S rRNA in fecal samples was amplified by PCR using a universal primer designed for the conserved region. According to the characteristics of the amplified 16S region, Illumina Miseq sequencing platform was used to construct a small fragment library and perform paired-end sequencing. Through the splicing and filtering of reads, cluster of operational taxonomic units (OTU) with Greengenes database (http://greengenes.lbl.gov/), species annotation, and abundance analysis, the species composition of the sample was revealed. Sequence analysis was performed by UPARSE software package using the UPARSE-OTU and UPARSE-OUTref algorithms. In-house Perl scripts were used to analyze α-diversity (within samples) and β-diversity (among samples). Sequences with ≥97% similarity were assigned to the same OTU. A representative sequence from each OTU was annotated taxonomic information using the RDP classifier (Wang et al., 2007).

Analysis of species diversity, community structure, and differential microbes

We rarified the out table and drew four curves to evaluate the sequencing data including rarefaction curves, Shannon curves, rank-abundance curves, and species accumulation curves. The differences in α-diversity index between groups were analyzed by seven metrics: Observed Species, Shannon, Simpson, Chao 1, ACE, Coverage, and PD whole tree. Shannon index estimates flora diversity, and Chao1 estimates the species abundance. Principal component analysis (PCA) was applied to reduce the dimension of the original variables using QIIME (Bolyen et al., 2019). QIIME calculates both weighted and unweighted UniFrac distance, which are phylogenetic measures of β-diversity (Caporaso et al., 2010). The unweighted UniFrac distance was used for principal coordinate analysis (PCoA) to get principal coordinates and visualize them from complex, multidimensional data. At the same time, non-metric multi-dimensional scaling (NMDS) was also used to perform rank ordering and PCoA on the OTU data (Rivas et al., 2013). To confirm differences in the abundances of individual taxonomy between the two groups, STAMP software was utilized. Linear discriminant analysis effect size (LEfSe) was used for the quantitative analysis of differential microbes within STC and healthy subject groups (Segata et al., 2011). This method was designed to analyze data in which the number of species is much higher than the number of samples and to provide biological class explanations to establish statistical significance, biological consistency, and effect-size estimation of predicted biomarkers. Finally, PICRUSt software was used to predict the functional gene composition in samples, so as to analyze the functional differences between different samples or groups.

Gut microbiome co-occurrence network analysis

In order to understand the correlations between different genera or species, a co-occurrence network was constructed based on the 16S rRNA data (Wang et al., 2018; Dan et al., 2020). The Spearman's correlation coefficient was used to analyze the bacterial correlations in the STC and C groups according to the relative abundance of each species or genus, respectively. The significant correlations were visualized by Cytoscape version 3.7.1 (http://www.cytoscape.org) (Shannon et al., 2003).

UPLC-Q-TOF-MS-based metabolomics

For fecal metabolomics, the fecal samples were slowly thawed at 4°C. An appropriate amount of samples was added to 800 μl of pre-cooled methanol/acetonitrile/water (2:2:1, v/v) solvent, vortexed to mix, sonicated at low temperature for 30 min, and stood at −20°C for 10 min. Subsequently, the samples were centrifuged at 14,000 g for 20 min at 4°C. The supernatant was dried in a vacuum centrifuge. For UPLC-Q-TOF-MS analysis, 100 μl of acetonitrile/water (1:1, v/v) solvent was used to dissolve the dry substances. The supernatant was taken for analysis, after being vortexed and centrifuged at 14,000

g for 15 min at 4°C. The samples were separated by UHPLC with Agilent 1290 Infinity LC (Agilent Technologies, Santa Clara, CA, USA). The 6600 Triple-TOF mass spectrometer (AB Sciex) was used to collect the first- and second-order spectra of the samples. The metabolite structure identification, data preprocessing, experimental data quality evaluation, and data analysis were performed in turn according to the peak area. Specific chromatography–mass spectrometry analysis conditions were carried out in accordance with the experimental procedures of Shanghai Applied Protein Technology (Shanghai, China).

Based on the fold change (FC) analysis and *t*-test/non-parametric test analysis, the difference analysis of all metabolites detected in the negative ion mode was performed.

After normalizing to total peak intensity, the processed data were analyzed by the R package, where it was subjected to orthogonal partial least-squares discriminant analysis (OPLS-DA) (Worley and Powers, 2013). The sevenfold cross-validation and response permutation testing were used to evaluate the robustness of the model. The variable importance in the projection (VIP) value of each variable in the OPLS-DA model was calculated to indicate its contribution to the classification. Metabolites with the VIP value >1 were further applied to Student's *t*-test at univariate level to measure the significance of each metabolite; *p*-value less than 0.05 was considered as statistically significant. Kyoto Encyclopedia of Genes and Genomes (KEGG) pathway analysis was performed on the screened differential metabolites with VIP (VIP value ≥ 1 and *p*-value < 0.05).

Random forest model prediction of potential diagnostic biomarkers

The receiver operating characteristic (ROC) curve and area under the curve (AUC) index were applied to optimize and verify the identified biomarkers (including gut microbiota and/or metabolites) and determine whether these biomarkers have diagnostic significance for STC (Falony et al., 2016; Liu et al., 2020). Random forest was used to build the diagnostic prediction models using the MetaboAnalyst 5.0 (https://www.metaboanalyst.ca) (Pang et al., 2021). To determine the association between Wexner constipation score, GIQLI, BSFS score, potential diagnostic gut microbiota, and metabolites, a correlation analysis was constructed using Spearman's correlations.

HE staining, immunohistochemistry, quantitative real-time polymerase chain reaction, and Western blot of colon tissues

Tissue samples of the control group were obtained from normal para-cancer colon tissue (more than 3 cm from the tumor) from colon cancer patients undergoing total colon resection. The tissue samples were confirmed to be normal colon tissue by two pathologic examiners. Colon tissues of the STC group were derived from patients who had to undergo surgery. All subjects or their families signed informed consents. All sample collection was performed in the operating room of Tianjin People's Hospital and the samples were immediately stored at −80°C.

Paraffin sections (5 μm thick) of colon tissues from STC patients or healthy subjects were prepared after immersion in 4% paraformaldehyde for 4 h and 70% ethanol. The brief steps of HE staining included dewaxing the sections, impregnating the cytoplasm with eosin, redyeing the nucleus with hematoxylin, and dehydrating and sealing the tablets. The first step of immunohistochemistry was dewaxing and hydration. Permeabilize tissue cells by incubating with 0.1% Triton X-100 in phosphate buffered saline for 15 min on ice. Antigens of Takeda G protein-coupled receptor (TGR5, Lot: ab72608, Abcam, England) and nuclear farnesoid X receptor (FXR, Lot: bs-12867R, Bioss, China) were unmasked by microwaving sections in 10 mmol/L citrate buffer, pH 6.0 for 15 min. After blocking nonspecific proteins and endogenous peroxidase, the primary antibodies (1:200) and fluorescein-conjugated secondary antibody (1:100) were respectively incubated in a dark humidity chamber. Observe the results using a microscope in a dark room. Six to eight different fields were randomly selected from each group, and the number of TGR5- or FXR-positive cells was analyzed and calculated by ImageJ software (National Institutes of Health, United States). The lysate was used to extract the RNA from the colon tissues of two groups [Lot: DP431, Tiangen Biochemical Technology (Beijing) Co., Ltd.], and the RNA purity and concentration were detected by a spectrophotometer. cDNA was synthesized from 1 mg of total RNA using a reverse transcriptase kit [Lot: KR106, Tiangen Biochemical Technology (Beijing) Co., Ltd.]. The relative gene expression levels of *TGR5* and *FXR* were calculated by the $2^{-\triangle\triangle CT}$ method using the qRT-PCR method with *GAPDH* as the internal reference. Primer sequences are outlined in Figure 5B. The extraction of protein of the colon tissues was performed according to the kit instructions, and the protein concentration was determined using BCA assay. The quantified protein was pretreated and separated by SDS-PAGE, and transferred to polyvinylidene difluoride membranes. The membranes were blocked with bull serum albumin for 2 h at room temperature and incubated with rabbit antibodies against TGR5, FXR, or GAPDH (Lot: GB12002, Servicebio, China) (1:2,000) overnight at 4°C. The membranes were washed and further incubated with HRP-conjugated anti-rabbit or anti-mouse secondary antibody (1:10,000 dilution) for 1 h. The protein bands were developed using enhanced chemiluminescence reagent, imaged with a gel imaging system (Tanon, China), and quantified by NIH ImageJ software.

Data analysis

PCoA, Fisher's exact tests, Spearman correlations, and Wilcoxon rank-sum test were used to identify differences and the relations within the clinical characteristics. For normally distributed data, Student's *t*-tests were performed to evaluate the differences in taxonomic abundance, Wilcoxon rank-sum test was performed when data were not normally distributed. p-value < 0.05 was considered statistically significant. The Benjamini–Hochberg method was used to correct p-value as false discovery rate (FDR) (Green and Diggle, 2007).

Results

Clinical characteristics of STC patients and healthy subjects

A total of 30 subjects with a clinical diagnosis of STC (age, 53.2 ± 16.323; sex, male:female, 7:23) and 30 healthy individuals (age, 47.967 ± 13.803; sex, male:female 9:21) were recruited (Table 1). There were no statistical difference in age, gender, and BMI between the two groups.

Alterations of gut microbiota composition and function in STC patients based on the 16S rRNA data

The STC group and the healthy volunteer group displayed 43,697 and 24,730 unique OTUs, respectively. A total of 24,431 OTUs were shared by both groups (Figure 1A). The rarefaction curves, Shannon curves, rank-abundance curves, and species accumulation curves were generated from OTUs, with 97% identity achieved in all samples (Figure S1). This indicated that the testing samples were sufficient and the amount of data were reasonable for the investigation of fecal microbiota. Taking the genus level as an example, there was a difference in the relative abundance of species between the STC group and the healthy group. Bacteroides was significantly increased, while Agathobacter and Subdoligranulum were decreased in the STC group (p-value < 0.05 or 0.01) (Figure 1B). The results of 7 indexes in α-diversity analysis are shown in Table 2 and Figures 1C, D. It is indicated that the α-diversity of gut microbiota in STC patients was richer than healthy subjects, but there were no significant differences except for the Simpson index (p-value = 0.021). The community composition structure and aggregation similarity of two groups were different based on the PCoA and NMDS of their microbiota (Figures 1E, F). The analysis results of LEfSe included cladograms (phylogenetic distribution) (Figure 1G) and histogram of LDA value distribution (LDA>2, Figure 1H). The LEfSe analysis results based on the prediction of KEGG pathway are shown in Figure 1I. The red and green nodes in the branches indicate the functional items and important microbial groups that play vital roles in the healthy or STC group. The differential microflora in the STC group was closely related to carbohydrate metabolism, glycan biosynthesis and metabolism, immune system, energy metabolism, digestive system, metabolic diseases, excretory system, nervous system, transport and catabolism, metabolism of terpenoid and polyketides, and lipid metabolism. There were significant differences in membrane transport (p = 0.037), cell motility (p = 0.047), and digestive system (p = 0.014) between two groups.

Gut microbiota–based prediction of STC

To find and test the potential diagnostic gut microbiota biomarkers, a random forest model was applied based on the differential genus with relative abundance > 0 in at least 95% samples of two groups. With reference to the results of LEfSe analysis of different gut microbiota, we finally selected 14 different bacterial genera or families for performing the multivariate ROC curve based exploratory analysis under the automated important feature identification and performance evaluation (Figure 2A). After comprehensive consideration of the value of the AUC, five potential diagnostic gut microbiota biomarkers (g:Bacteroides, g:Parabacteroides, f:Desulfovibrionaceae, g:Ruminiclostridium 5,

TABLE 1 Study participant demographics and characteristics.

Characteristic	Healthy Subjects	STC Patients	*p*-value
Subjects (*n*)	30	30	–
Age (years)	47.967 ± 13.803	53.2 ± 16.323	0.185 (*t*-test)
Male/Female	9/21	7/23	0.388 (Chi-square test)
Body mass index (kg/m^2)	21.643 ± 1.704	22.076 ± 1.672	0.325(*t*-test)
Disease duration (years)	–	7.325 ± 8.559	–
Bristol Stool Scale	4.233 ± 1.073	2.5 ± 1.306	<0.001(*t*-test)
Wexner	3.767 ± 2.223	18.333 ± 7.439	<0.001(*t*-test)
GIQLI	127.967 ± 17.789	107.767 ± 21.394	<0.001(*t*-test)

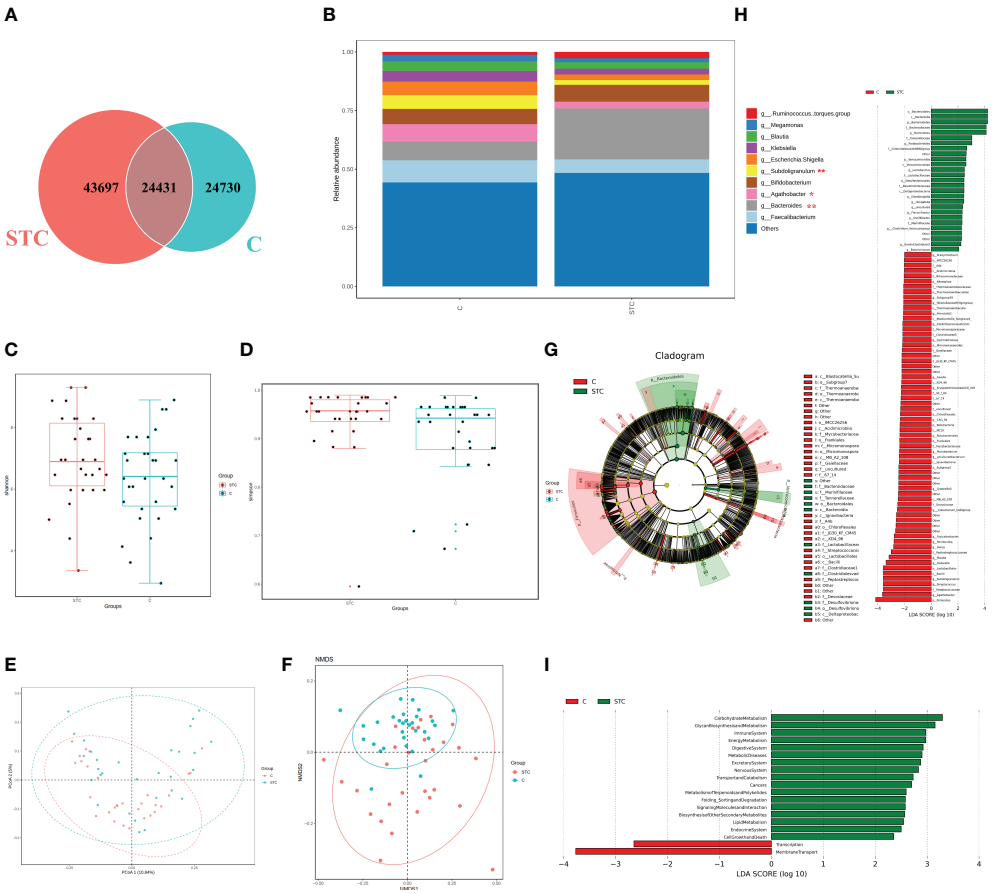

FIGURE 1
The shift of gut microbiome in slow transit constipation (STC) and control C subjects accroding to the 16S rRNA data. **(A)** Venn diagram of the observed OTUs in STC and C. **(B)** The relative abundance of the two groups at the genus level (Top 10). *p-value < 0.05 and ** p-value < 0.01, t-test. **(C, D)** Difference analysis of α-diversity index between the STC and C groups. Boxplot of difference between groups of Shannon index **(C)** with p = 0.094, t-test, and Simpson **(D)** with p = 0.021, Wilcoxon rank-sum test. **(E)** Principal coordinate analysis (PCoA) of the microbiota based on the unweighted UniFrac distance metrics for the STC and C groups. ANOSIM, R = 0.134, p = 0.001. **(F)** The differences between the STC and C groups were observed based on Non-Metric Multi-Dimensional Scaling (NMDS). **(G, H)** Cladograms generated by LEfSe indicating differences in the bacterial taxa between the STC and C groups. Red bars indicate taxa with enrichment in the C group, and green bars indicate taxa with enrichment in the STC group. **(I)** The LEfSe analysis of KEGG pathway (Welch's t-test test).

TABLE 2 α-diversity indices comparing STC patients to healthy subjects.

α-diversity index	Healthy Subjects	STC Patients	p-value
Shannon	6.351 ± 1.466	6.988 ± 1.425	0.094
Simpson	0.907 ± 0.082	0.942 ± 0.072	0.021
Ace	7,978.602 ± 3,979.623	9,247.546 ± 5,687.232	0.622
Goods coverage	0.974 ± 0.015	0.971 ± 0.0180	0.719
Chao1	7,766.749 ± 3,659.184	8,970.217 ± 5,284.232	0.602
Observed species	3,691.433 ± 1,705.291	4,347.967 ± 2,474.777	0.432
PD whole tree	99.107 ± 26.547	107.228 ± 36.495	0.676

Shannon index was tested by t-test, and the others were tested by Wilcoxon rank-sum test.

and g:Subdoligranulum) were screened out and were attempted to be constructed as a diagnostic model with AUC = 0.785 (Figure 2B). The relative abundances of these five bacterial genera in each group are shown in Figure 2C. In addition to g: Subdoligranulum, the other four diagnostic gut microbiota biomarkers were significantly upregulated in the STC group.

The human intestine tract has a complex microbial ecosystem, and the influence of individual groups in different microbial communities on the intestine tract is uneven (Yilmaz et al., 2019). In order to describe the potential relationship between the flora in the gut microbial community, we further constructed a co-occurrence network of five potential diagnostic gut microbiota biomarkers in the control and STC groups based on the significant Spearman correlations (Figure 2D). A different co-occurrence network was displayed between the five potential diagnostic markers. The variation trend relationship between them was visualized. There were 10 edges in total, whose density and colors represented the closeness of the relationship. The size of nodes represented its importance in the five bacterial communities.

Metabolomics analysis revealed aberrant metabolic patterns in STC patients

Based on univariate analysis, differential analysis of all metabolites detected in negative ion mode was performed. The different metabolites with FC > 1.5 or FC < 0.67 and *p*-value < 0.05 were visually displayed in the form of a volcano plot (Figure 3A). There were more downregulated differential metabolites in the STC group than in the control group. The score plot of the OPLS-DA score showed that there was a large

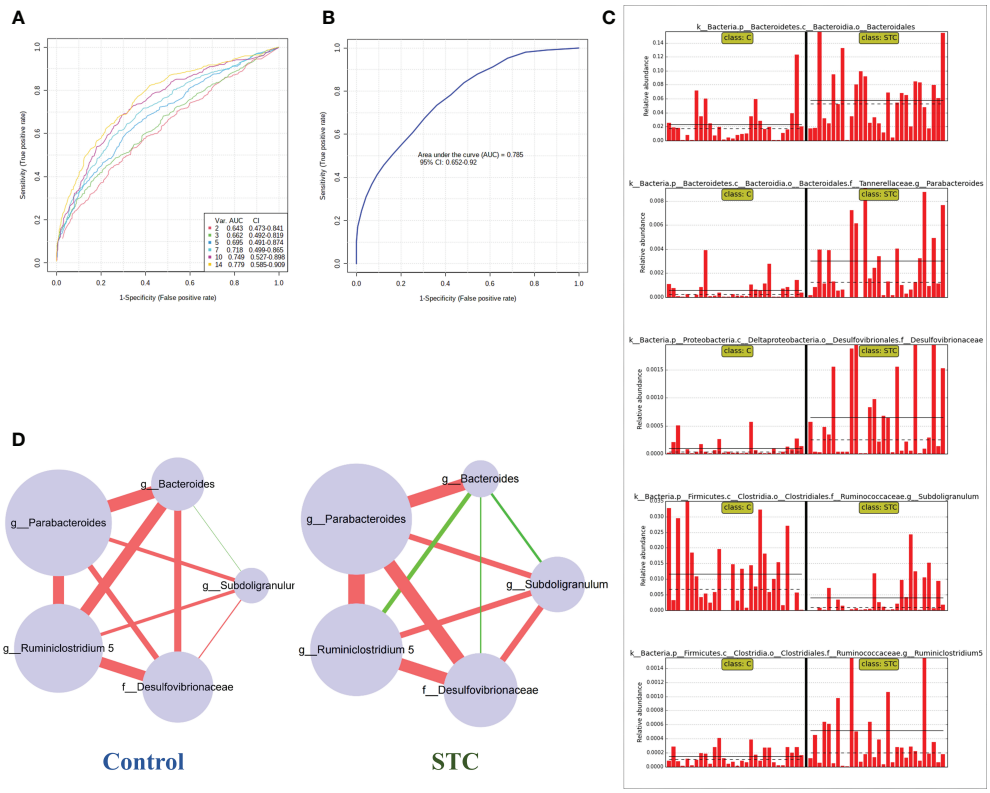

FIGURE 2
Random forest model prediction of potential diagnostic biomarkers of gut microbiota between STC patients and healthy subjects. **(A)** Classification performance of a random forest model using 16S rRNA abundance of 14 different bacterial genera or species. The cross-validation prediction performance of models with increasing number of predictors in order, and sorted by importance. **(B)** ROC curve displaying the classification for STC and C employing five potential diagnostic gut microbiota biomarkers (AUC = 0.785). **(C)** The abundance of 5 potential diagnostic gut microbiota biomarkers in each sample including g:Bacteroides, g:Parabacteroides, f:Desulfovibrionaceae, g: Ruminiclostridium 5, and g:Subdoligranulum. **(D)** Co-occurrence network of five potential diagnostic gut microbiota biomarkers in both the STC group and the control group based on the Spearman correlation algorithms. Each node presents a bacterial genus or species. The node size indicates the relative importance of each genus or species, and the density of the edges represents the Spearman coefficient. Red links stand for positive interactions between nodes, and green links stand for negative interactions.

variation between the two groups (Figure 3B), and this evaluation model was stable with $Q^2 = 0.311$ (Figure 3C). VIP obtained from the OPLS-DA model could be used to measure the influent intensity and explanatory ability of the expression pattern of each metabolite on the classification and discrimination of each group of samples. Generally, metabolites with VIP value ≥ 1 and p-value < 0.05 were considered as differential metabolites to have a significant contribution to model interpretation. The information of the 21 differential metabolites selected is displayed in Table 3.

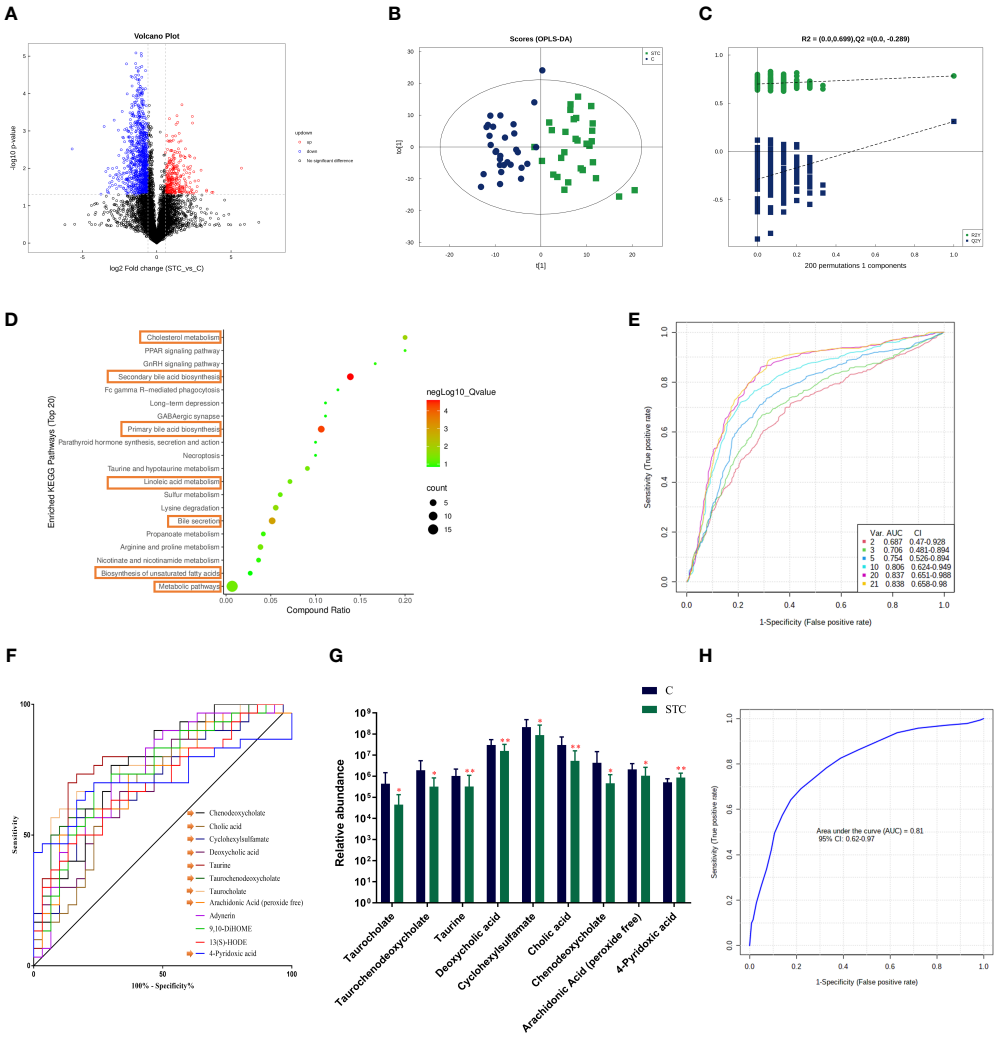

FIGURE 3
The fecal metabolites of STC patients and healthy subjects are significantly different. **(A)** The different metabolites were visualized in the form of volcano plot. The abscissa is the logarithm value of log2 of the fold change, and the ordinate is the logarithm value of –log10 of significance p-value (STC *vs.* C). Metabolites of difference with FC > 1.5, p-value < 0.05 are represented by rose red, while those with FC < 0.67 and p-value < 0.05 are shown in blue. Metabolites that are not significantly different are shown in black. **(B)** The score plot of orthogonal partial least-squares discriminant analysis (OPLS-DA), where t[1] represents principal component 1, t[2] represents principal component 2, and the ellipse represents the 95% confidence interval. The distribution of points reflects the degree of difference between groups and within group. The model evaluation parameter Q^2 obtained by sevenfold cross-validation is 0.311. **(C)** Permutation test of OPLS-DA. The x-coordinate represents the degree of permutation, and the y-coordinate represents the values of R^2 and Q^2. The green dot represents R^2, the blue dot denotes Q^2, and the two dashed lines represent the regression lines of R^2 and Q^2, respectively. **(D)** Top 20 enriched KEGG pathways of 21 screened differential metabolites (VIP value ≥ 1 and p-value < 0.05). **(E)** Classification performance of a random forest model using abundance of 21 differential metabolites based on multivariate ROC curve exploratory analysis. The cross-validation prediction performance of models with inreasing number of predictors in order, and sorted by importance. **(F)** The receiver operating characteristic curve (ROC) of 12 potential diagnostic biomarker metabolites [each area under curve (AUC) ≥ 0.7]. **(G)** The abundance of 9 different metabolites involved in the BA synthesis, metabolism, secretion, and lipid metabolism, which was believed to have diagnostic efficacy. Significance compared with the control group, **P < 0.01 or *P < 0.05 vs. the control group. **(H)** ROC curve displaying the classification for STC and C employing 9 diagnostic biomarker metabolites (AUC = 0.81).

In order to clarify the functional changes related to specific differential metabolites in the stool of STC patients, we performed the KEGG pathway on the 21 screened metabolites (Figure 3D). The results showed that the KEGG pathway was mainly concentrated in secondary bile acid (BA) biosynthesis ($-\log_{10}$ p-value = 6.420), primary BA biosynthesis ($-\log_{10}$ p-value = 5.825), bile secretion ($-\log_{10}$ p-value = 4.266), cholesterol metabolism ($-\log_{10}$ p-value = 3.085), linoleic acid metabolism ($-\log_{10}$ p-value = 2.181), and biosynthesis of unsaturated fatty acids ($-\log_{10}$ p-value = 1.381).

The gut microbiota can modulate intestinal motility through the release of short-chain fatty acids (SCFAs) (Barbara et al., 2005; Martin-Gallausiaux et al., 2021). SCFAs produced by gut bacteria, especially butyrate and propionic acid, have multiple beneficial effects on host health, including the maintenance of mucosal integrity, the prevention of symbiotic expansion of potentially pathogenic bacteria in the gut and the regulation of energy metabolism through the gut–brain axis (Wang et al., 2019; Zhuang et al., 2019). The quantitative comparison analysis (response strength, means ± SD) of propionic acid and isobutyric acid in the feces of healthy subjects was 1,221,545 ± 1,999,220 and 1,563,167± 969,880, while in STC patients, they were reduced to 255,230 ± 550,046 and 1,814,435± 1,329,376 (p-value = 0.013 and 0.406). This indicated that the levels of SCFA changed to some extent, especially the decrease of propionic acid during the occurrence of STC, which was consistent with the previous results (Li et al., 2020; Tian et al., 2021).

We also compared the differences in the content of other secondary BAs or its conjugated BAs. In STC patients, except for lithocholic acid, all of them were reduced to varying degrees compared with healthy subjects, but the statistical differences were not significant (Table 4). Combined with differential metabolites, it was indeed found that primary and secondary BAs were significantly reduced in the feces of STC patients. Based on the above results and the roles of BAs in lipid metabolism (Fiorucci et al., 2021), we selected nine different metabolites that were deeply involved in BA synthesis, metabolism, secretion, and lipid metabolism, and demonstrated their abundance in the two groups (Figure 3G).

Gut metabolite-based prediction of STC

To find the potential diagnostic metabolic biomarkers, the random-forest model was used to evaluate the accuracy of 21

TABLE 3 The information of 21 significantly differential metabolites.

Name	VIP	Fold change	p-value	m/z	RT (s)	Quantitative analysis (Control)	Quantitative analysis (STC)
Thymine	2.004	1.976↑	0.023	125.03524	74.3435	484,330 ± 612,626	956,822 ± 924,101
Taurocholate	1.305	0.101	0.043	514.28179	197.259	439,651 ± 1,041,027	44,580 ± 88,504
Taurochenodeoxycholate	2.909	0.167	0.017	498.28652	145.579	1,912,584 ± 3,520,092	319,093 ± 512,153
Taurine	2.025	0.314	0.007	124.00744	291.676	1,029,081 ± 1,142,722	323,370 ± 770,728
Succinate	3.916	0.199	0.015	117.01962	391.109	3,013,974 ± 5,118,610	598,775 ± 1,387,217
Propionic acid	2.522	0.209	0.013	73.03003	391.176	1,221,545 ± 1,999,220	255,230 ± 550,046
Nervonic acid	1.253	1.878↑	0.027	365.34001	37.606	83,699 ± 61,566	157,186 ± 166,513
Glycyl-L-leucine	1.566	0.597	0.039	187.10837	283.697	687,000 ± 554,262	410,403 ± 456,281
Deoxycholic acid	12.233	0.525	0.008	391.28427	128.334	30,298,350 ± 23,615,390	15,918,241 ± 16,317,735
Cyclohexylsulfamate	26.333	0.417	0.039	178.0543	70.444	212,951,579 ± 270,482,964	88,817,956 ± 175,614,185
Cholic acid	14.581	0.259	0.009	407.27861	218.452	30,438,945 ± 42,352,355	7,880,015 ±16,816,427
Cholesteryl sulfate	1.793	1.643↑	0.009	931.61153	26.4205	285,135 ± 209,642	46,8399 ± 306,055
Chenodeoxycholate	5.894	0.107	0.045	783.57383	128.579	4,318,477 ± 10,292,191	461,818 ± 717,881
Arachidonic acid (peroxide free)	1.986	0.504	0.024	303.23131	38.7865	2,093,885 ± 1,879,405	1,055,170 ± 1,580,409
Adynerin	4.451	0.426	0.002	515.30189	52.427	4,542,108 ± 3,782,549	1,932,674 ± 2,039,784
9,10-DiHOME	2.347	0.436	0.002	313.23647	84.842	1,180,798 ± 1,006,075	514,772 ± 544,196
4-Pyridoxic acid	1.901	1.679↑	0.002	182.04518	44.08	514,197 ± 249,711	863,303 ± 529,983
2-Methylbenzoic acid	2.289	1.652↑	0.016	135.04488	129.02	635,109 ± 518,673	1,049,088 ± 747,583
1-Palmitoyl-2-hydroxy-sn-glycero-3-phosphoethanolamine	2.270	0.558	0.014	452.27705	194.122	4,105,361 ± 3,615,908	2,289,623 ± 1,488,993
1-Methylxanthine	1.211	0.583	0.028	165.04129	109.821	741,523 ± 618,759	432,025 ± 430,157
13(S)-HODE	1.308	0.534	0.015	295.2263	47.747	1,205,164 ± 1,081,968	643,204 ± 569,528

Mass-to-charge ratio (m/z); retention time (RT); quantitative analysis: response strength, means ± SD.

TABLE 4 The information of other secondary BAs or its conjugated Bas.

Name	VIP	Fold change	*p*-value	m/z	RT (s)	Quantitative analysis(Control)	Quantitative analysis (STC)
Glycolithocholic acid	0.196	0.752	0.380	432.30832	166.15	31,903 ± 38,586	23,986 ± 30,246
Lithocholic acid	13.188	1.106↑	0.713	375.28882	72.862	37,217,919 ± 40,433,719	41,149,879 ± 41,811,647
Taurolithocholic acid	0.185	0.727	0.334	482.29091	78.303	166,054 ± 203,462	120,664 ± 154,239
Glycochenodeoxycholate	0.405	0.319	0.017	472.30622	204.659	55,234 ± 83,234	17,642 ± 9,699
Glycodeoxycholic acid	1.079	0.119	0.139	450.31875	205.917	814,328 ± 2,616,266	96,808 ± 183,895
Tauroursodeoxycholic acid	0.338	0.665	0.193	482.29112	142.162	72,381 ± 92,688	48,152 ± 39,440
Taurochenodeoxycholate	0.519	0.427	0.053	500.30143	143.273	124,983 ± 194,069	53,315 ± 42,972

Mass-to-charge ratio (m/z); retention time (RT); quantitative analysis: response strength, means ± SD.

differential metabolite abundances for the classification performance anmong STC patients and healthy subjects (Figure 3E). The AUC and 95% confidence intervals of the top 12 differential metabolites are shown in Figure 3F, which were regarded as potential diagnostic biomarker metabolites. Then, to create a biomarker model, the multivariate ROC curve-based exploratory analysis was performed. It is concluded that the prediction model containing nine differential metabolites [inculding taurocholate, taurochenodeoxycholate, taurine, deoxycholic acid, cyclohexylsulfamate, cholic acid, chenodeoxycholate, arachidonic acid (peroxide free), and 4-pyridoxic acid] deeply involved in BA synthesis, metabolism, secretion, and lipid metabolism showed a high discriminatory power to predict STC status with AUC = 0.81 (Figure 3H).

Changes of morphology and bile acid-related receptor expression in colon tissues of STC patients

In healthy subjects, the epithelium of the colonic mucosa was intact. The glands were abundant and neatly arranged, and there was no obvious cytoplasmic expansion and inflammatory cell infiltration in the interstitium. The epithelium of the mucosal layer of STC patients was damaged or missing, with the number of glands reducing, whose cytoplasm was obviously enlarged. Compared with normal tissues, more inflammatory cells infiltrating were seen in the interstitium (Figure 4A).TGR5 is a cell membrane receptor located on human chromosome 2q35, and its homology is highly conserved in humans and mammals (>80%). TGR5 is highly expressed in immune cells, intestinal tract, and gallbladder (Duboc et al., 2014). FXR is a member of the nuclear receptor superfamily and a ligand-dependent transcription factor. It is mainly expressed in liver, intestine, kidney, and other tissues, which can regulate the metabolism and enterohepatic circulation of BAs (Fiorucci et al., 2010). The results of immunohistochemistry, qRT-PCR and WB experiments showed that compared with healthy controls, the gene and protein expression levels of TGR5 and FXR in the colon tissues of STC patients were significantly reduced (Figures 4B and 5).

Correlation analysis between Wexner constipation score, GIQLI, BSFS score, and diagnostic gut biomarkers

Correlation analysis can help measure the closeness of significant diagnostic gut biomarkers (microbiota and metabolites) to clinical manifestations. The results are shown as heatmap in Figure 6. Red indicated positive correlation, green indicated negative correlation, and white indicated non-significant correlation. The color depth was related to the absolute value of the correlation coefficient. The significance of the correlation was related to the size of the point. The smaller the *p*-value was, the higher the significance was and the larger the point was. Compared with microbiota, Wexner constipation score, GIQLI, and BSFS score were more correlated with diagnostic gut metabolites. Wexner constipation score was negatively correlated with these diagnostic metabolites, while the other two were positively correlated. There was obvious positive correlation among metabolites. On the whole, there was a certain negative correlation between the differential microbiota and the differential metabolites, which provided enlightenment for us to study the regulatory relationship between the two. Comprehensive use of 14 diagnostic gut microbiota and metabolite biomarkers may accurately distinguish STC and healthy population with AUC = 0.877.

Discussion

As shown in the summary of Figure 6, compared to the healthy subjects, the relative abundance of Bacteroides, Parabacteroides, Desulfovibrionaceae, and Ruminiclostridium 5 was increased while Subdoligranulum was decreased significantly in feces of STC patients. STC patients showed increased α-diversity.The β-diversity of the two groups was remarkably different, which displayed alternation of gut

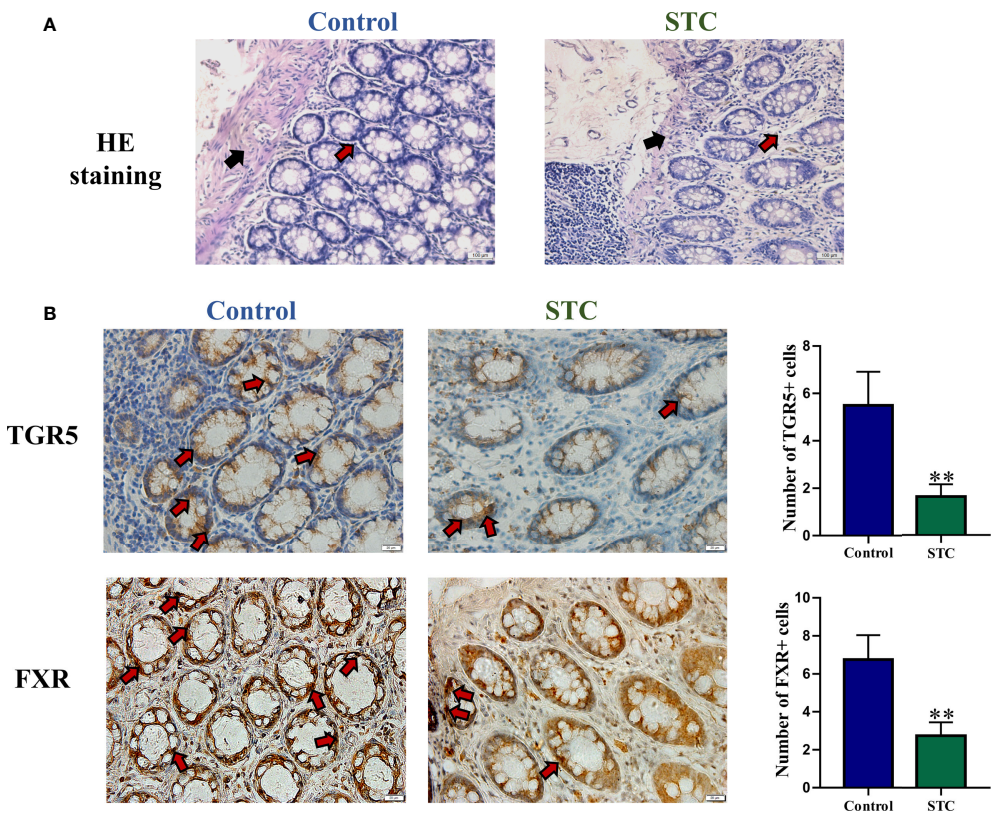

FIGURE 4
The morphology and BA-related receptor expression in colon tissues of STC patients and healthy subjects. **(A)** HE staining of colon tissues. Red arrows indicated inflammatory cell infiltration, and black arrows indicated mucosa layer structure of colon tissues. **(B)** Immunohistochemical staining results of TGR5 and FXR. The number of positive cells was quantitatively analyzed in six random selected fields of the same size using NIH ImageJ software. Significance compared with the control group, $^{**}p < 0.01$ or $^{*}p < 0.05$ *vs*. the control group.

microbiota composition. Furthermore, STC patients displayed a decreased level in metabolites that were associated with BA synthesis, metabolism, secretion, and lipid metabolism. Experimental studies on human colon histology also confirmed this. The random forest prediction model was used to distinguish STC patients from healthy people by using few specific significant diagnostic gut microbiota and metabolites, which had a medium degree of reliability. It provided the possibility of generating a supplementary method for the risk assessment of the intestinal health monitoring model.

STC is a chronic disabling disease characterized by delayed colonic transit without outlet obstruction. It is refractory to drugs and finally treated with colectomy as the disease progresses (Knowles et al., 2017). Gastrointestinal motility is the key to the normal function of the human gastrointestinal tract. Over the years, many studies have been conducted on the mechanism of STC (Mazzone et al., 2020). Although the pathogenesis of STC has been partially elucidated, it is not completely clear. STC has complex pathogenesis, and most studies focus on enteric nerve and muscle diseases, abnormalities of neurotransmitters, interstitial cells of Cajal and enteric glial cell as well as chloride channel dysfunction. In recent years, the correlation between organism flora and diseases has gradually become an important means of disease mechanism research and a new perspective of disease treatment. Under the physiological conditions, the types and proportions of gut microbiota maintain a dynamic balance, which interact with the host to exert essential functions such as immunity, nutrition, immunity, and metabolism (Fiers et al., 2020; Schwabe and Greten, 2020). Studies have found significant differences in the composition of intestinal mucosa and fecal flora between STC patients and healthy controls (Ding et al., 2018; Zhang et al., 2018; Tian et al., 2021). Compared with normal subjects, the structure, abundance, and co-occurrence of gut microbiota were significantly altered in STC patients in our study, which was consistent with the characteristics of microbiota in children with chronic functional constipation (de Meij et al., 2016). The opportunistic pathogen Parabacteroides can induce depressive-like behavior in a mouse model of Crohn's disease, whose relative level can be reduced by dietary synbiotic to ameliorate

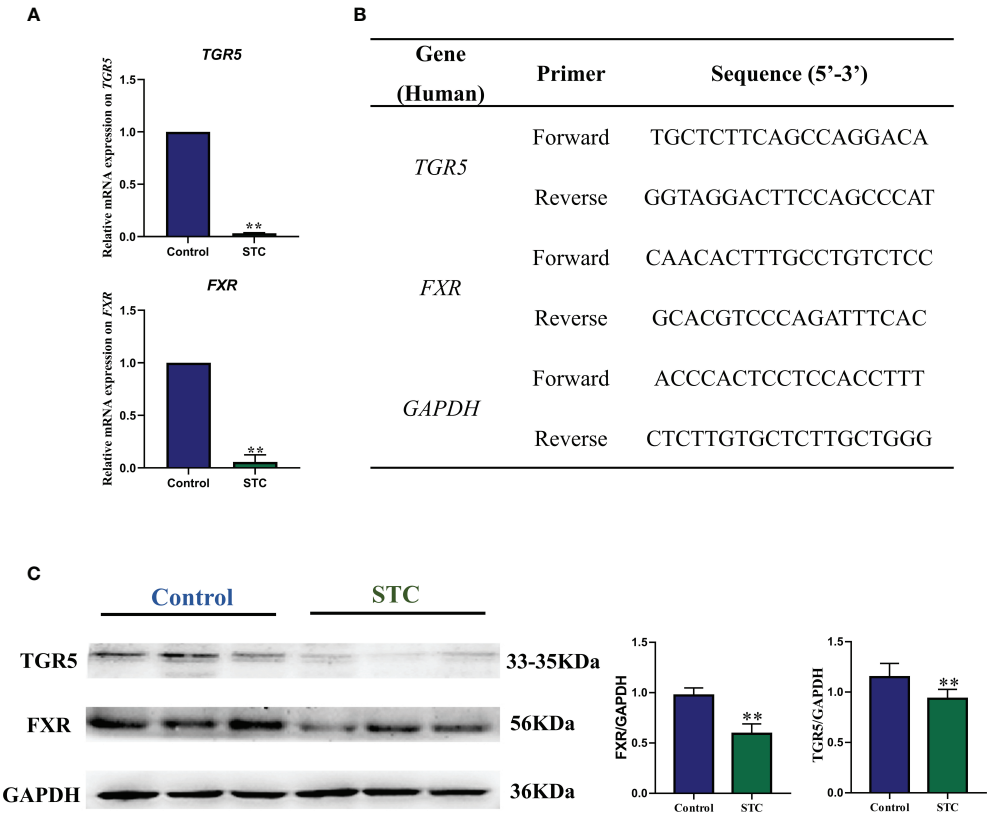

FIGURE 5
The gene and protein expression levels of TGR5 and FXR in colon tissues of STC patients and healthy subjects. **(A)** qRT-PCR results of gene expression of *TGR5* and *FXR*. **(B)** Gene primer sequence. The relative gene expression levels were calculated by the $2^{-\triangle\triangle CT}$ method with *GAPDH* as the internal reference (n = 6). **(C)** Western blotting results of protein expression of TGR5 and FXR. NIH ImageJ software was used to quantify the relative optical density of protein bands. Values are means ± SD (n = 6). The protein expression was detected in the same gel in which GAPDH was used as the internal control. Significance compared with the control group, $^{**}p < 0.01$ or $^{*}p < 0.05$ *vs.* the control group.

constipation (Gomez-Nguyen et al., 2021; Yang et al., 2021). As an important endotoxin producer in patients with constipation, depressed Desulfovibrionaceae bacteria was benificial to promoting intestinal hormone secretion and maintenance of intestinal barrier integrity (Zhuang et al., 2019). It is worth noting that studies have shown that Subdoligranulum is negatively correlated with clinical symptoms and inflammation of inflammatory bowel disease, and may be a potential probiotic for its treatment (Kim et al., 2021; Xia et al., 2021).

Metabolic pathways encoded by the human gut microbiota continuously communicate with the host through a large number of biologically active metabolites (Postler and Ghosh, 2017). BAs have both hydrophilicity and hydrophobicity, which can effectively reduce the surface tension between lipid and water phases to facilitate absorption of fat-soluble vitamins and lipids (Ridlon et al., 2006). Primary BAs are synthesized in hepatocytes using cholesterol as raw material under the catalysis of 17 biochemical enzymes, and excreted into the duodenum with bile. About 95% of BAs pass through the apical sodium-dependent bile acid transporter (ASBT) of intestinal cells in the terminal ileum, which compensate for the lack of BA synthesis ability of hepatocytes. The intestinal symbiotic bacteria convert some BAs (approximately 5%) entering the colon into various intestinal BAs, which are vital hormones regulating host energy balance and cholesterol metabolism through several G-protein-coupled receptors and/or nuclear receptors (Fiorucci and Distrutti, 2015; Wahlstrom et al., 2016). Primary BAs include cholic acid (CA) and chenodeoxycholic acid (CDCA) (Alrefai and Gill, 2007). In the colon, bacterial 7α-dehydroxylase (mainly derived from *Clostridium* spp. Eubacteria and *Clostridium* spp. XIVa) removes 7α-OH groups from CA and CDCA to form deoxycholic acid (DCA) and lithocholic acid (LCA), respectively. CA, CDCA, DCA, and LCA are collectively referred to as free BAs, which are combined with glycine and taurine to produce conjugated BAs (Alrefai and Gill, 2007; Vallim et al., 2013; Appleby and Walters, 2014). In this study, we found that the feces of patients with STC decreased significantly in primary and

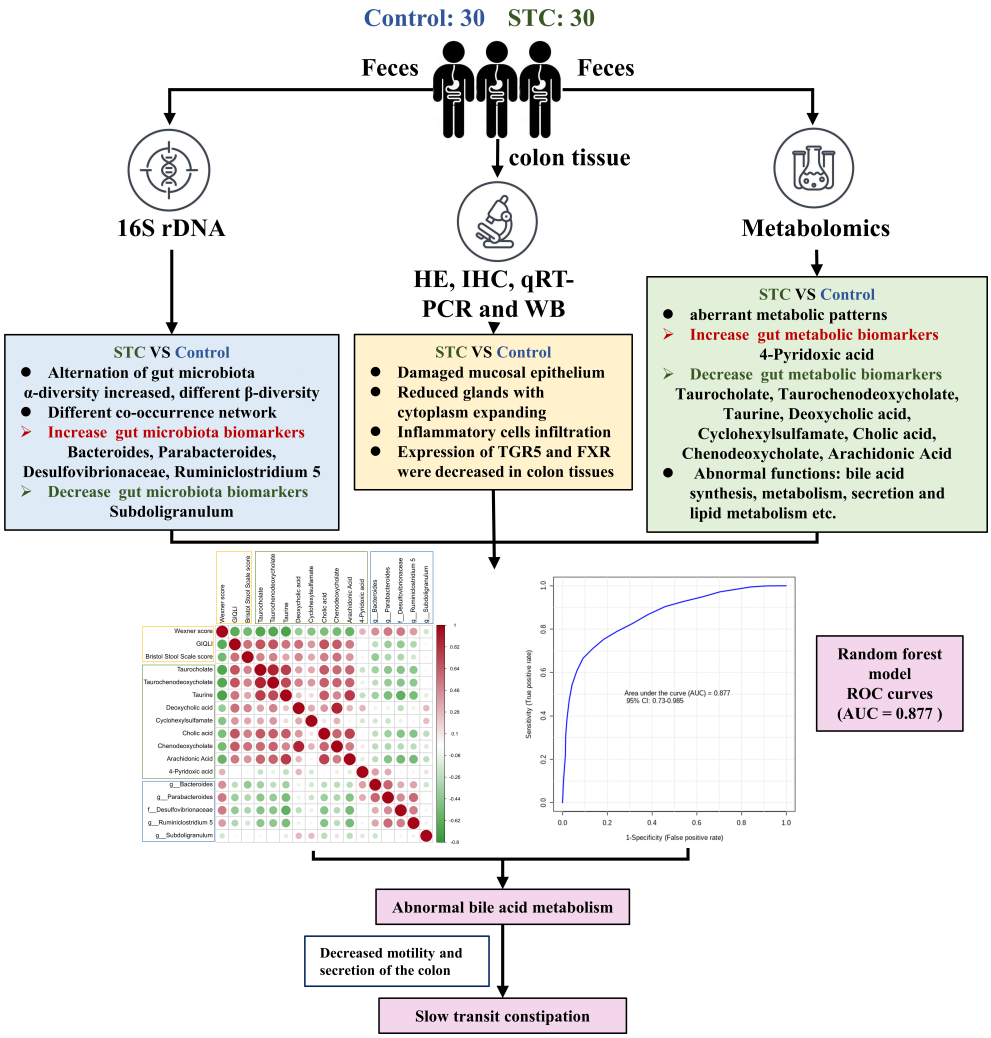

FIGURE 6
The summary of gut microbiota composition and metabolism analysis between STC and healthy subjects. Compared to the healthy subjects, the relative abundance of Bacteroides, Parabacteroides, Desulfovibrionaceae, and Ruminiclostridium 5 were increased while Subdoligranulum was decreased significantly in feces of STC patients. STC patients displayed alternation of gut microbiota composition. STC patients displayed decreased level in metabolites that were associated with BA synthesis, metabolism, secretion, and lipid metabolism. Experimental studies on human colon histology showed decreased expression of TGR5 and FXR in STC patients. Wexner constipation score was negatively correlated with these diagnostic metabolites, while GIQLI and BSFS scores were positively correlated. There was obvious positive correlation among metabolites. There was a certain negative correlation between the differential microbiota and the differential metabolites. Comprehensive use of 14 diagnostic gut microbiota and metabolite biomarkers may accurately distinguish STC and healthy population with AUC = 0.877.

second BAs especially including cholic acid, chenodeoxycholate, taurine, taurocholate, taurochenodeoxycholate, deoxycholic acid, cyclohexylsulfamate, and glycochenodeoxycholate, indicating that the metabolism of BAs in the patient's body was abnormal. BAs can also activate phospholipase 2 by interfering with the cell membrane, causing the cell to release arachidonic acid, promoting the production of reactive oxygen species, and inducing DNA damage (Sanchez, 2018). The reduction of arachidonic acid (peroxide free) is consistent with previous studies. Furthermore, the study of SCFAs as important metabolites in intestinal diseases has received widespread attention. Our study also found a significant reduction in propionic acid during STC, but significant changes in other types of SCFAs were not observed.

The action of BAs in the colon is known as a "physiological laxative". When the reabsorption of BAs in the ileum is insufficient and hepatoenteric circulation is broken, more BAs will be

transported to the colon (Jiang et al., 2015). BAs can activate intracellular adenylate cyclase, increase the permeability of the intestinal mucosa, promote intestinal electrolyte and water secretion, strengthen colonic transmission, and stimulate defecation (Chedid et al., 2018). Clinical studies have indicated that an increase in the total amount of fecal BAs in patients is significantly associated with accelerated colonic transit (Bajor et al., 2015; Dior et al., 2016). Animal studies have shown that BAs directly induce accelerated colonic motility (Traub et al., 2008; Kim et al., 2017). Therefore, supplementation of the proper amount of specific BA analogs or the use of drugs that inhibit the reabsorption of ileal BAs is beneficial to improve the clinical symptoms of patients with constipation, and has become one of the new treatment options for the treatment of STC (Jiang et al., 2015). Elobixibat is a highly selective ASBT inhibitor whose mechanism of action is to reduce the ileum reabsorption of BAs and increase the concentration of BAs entering the colon. Elobixibat resolved constipation in the short term (10 mg/day for 2 weeks) and was well tolerated with short-term and long-term (5 mg/day or 15 mg/day, or maintain the 10 mg/day dose for 1 year) treatments resulting from a randomized, double-blind, placebo-controlled, phase 3 trial and an open-label, single-arm, phase 3 trial (Nakajima et al., 2018). In a double-blind placebo randomized controlled study of oral sodium CDCA (500 mg/day or 1,000 mg/day for 4 days) in the treatment of 36 female patients with constipation-predominant irritable bowel syndrome, it was found that compared with the control group, treatment with sodium CDCA could improve the clinical symptoms including accelerating the transit of the entire colon, increasing the defecation of the patients, and softening the feces to make it easier to excrete from the body (Rao et al., 2010). Evidence supported the use of increasing the concentration of endogenous BAs to treat chronic constipation. However, there are no specific reports of this strategy on the therapeutic effect of STC.

The hepatic BAS synthesis rate is reversibly controlled by a feedback mechanism of FXR mediated in the liver and ileum. The rate of hepatic BA synthesis is reversibly controlled by an FXR-mediated feedback mechanism in the liver and ileum (Galman et al., 2003). The intestinal FXR activity maintained good outflow of BAs back to the portal vein and controled the reuptake of BAs into enterocytes (Stanimirov et al., 2015). After knocking out the *FXR* gene in the intestinal tract of wild mice, there was a significant inflammatory response in the intestinal tract of the mice, and the mRNA expression of inflammatory cytokines increased significantly (Vavassori et al., 2009). A large number of animal studies have confirmed that the activation of intestinal FXR can inhibit the transcriptional activity of NF-κB (Modica et al., 2008; Gadaleta et al., 2011; Miyazaki et al., 2021). The regulation of liver and intestine FXR activity reduced inflammation and epithelial permeability by lowering the levels of proinflammatory mediators in the gut. In addition, intestinal FXR activation induced transcription of genes involved in intestinal protection to prevent bacterial invasion and epithelial damage (Mosińska et al., 2018; Biagioli et al., 2021). Compared to FXR, TGR5 may be activated by hydrophobic BAs (taurine further enhances its potency) to promote permanent signaling transmission. The activation of TGR5 in colonic epithelial cells could suppress cholinergic-induced secretory responses and basal secretory tension (Cozma-Petruţ et al., 2017; Long et al., 2017a). Studies have shown that overactivation of epithelial TGR5 by lipophilic BAs, such as DCA and LCA, promoted colonic motility and led to diarrhea through a 5-HT-mediated pathway. In the mice lacking TGR-5, shortened transit time and increased constipation were reported (Alemi et al., 2013). These results suggested that changes in colonic TGR5 expression could alter small intestinal and colonic transit (Mosińska et al., 2018). Moreover, BA-dependent TGR5 activation significantly inhibited the activation of NF-κB in wild-type mice injected with lipopolysaccharide compared with TGR5-deficient mice (Wang et al., 2011). FXR and TGR5 agonists are promising in controlling inflammation in Crohn's disease and ulcerative colitis (Yoneno et al., 2013; Perino and Schoonjans, 2015; Jia et al., 2018). In our study, we found that the expression of TGR5 and FXR in colon tissues was significantly downregulated. On the one hand, it reflected the result of the significant reduction of BAs in the intestine of STC patients, in turn forming a negative feedback, which inhibits intestinal absorption and increases the rate of liver synthesis; on the other hand, it also explained the significant inflammatory response and decreased motility in colon tissue of STC patients.

Host metabolism is affected not only by the microbial modification of BAs, which leads to changes in the signal pathways through the BA receptors, but also by the changing composition of the microbiota (Wahlstrom et al., 2016). Microbial deconjugation (removal of taurine or glycine conjugates) can prevent the reuptake of BAs through ASBT. BA deconjugation is carried out by Bacteroides with bile salt hydrolase activity (Ridlon et al., 2006). The enterotypes of Bacteroides are resistant to BAs, which grow in the presence of fat and bile (Arumugam et al., 2011; Tan et al., 2019). Studies have shown that Bacteroides coprophilus and Bacteroides thetaiotaomicron can act on the biotransformation of primary BAs, which are released in the intestine when dietary fat is ingested (Staley et al., 2017; Lynch et al., 2019). In our study, FXR in the colon tissues of STC patients was significantly reduced and a previous study also found that FXR deficiency enriched Desulfovibrionaceae (Sheng et al., 2017).

The pathological mechanism of STC is complicated. The amount of clinical samples currently included was not sufficient, and the analysis methods used also had certain limitations, which could not fully reveal the true metabolic state of the host. Future research should focus on targeted and precise quantitative analysis of relevant important differential metabolites and research on the cross-talk pathological mechanism between gut microbiota and the metabolites of the feces, so as to better guide clinical practice.

Conclusion

In summary, the current analysis shows that STC patients exhibited imbalances in the intestinal flora. The α-diversity of the gut microbiota in the STC group was increased. β-diversity was markedly different from healthy subjects. The types of fecal metabolites that specifically changed in STC patients were determined. Further, the possible gut microbiota and metabolites with diagnostic value were screened out, and the interaction analysis was conducted. It may provide clues for a better understanding of STC's intestinal microenvironmental change mechanism, and further experiments are needed to confirm their cross-talk. BAs and lipid metabolism seem to be an important link in the pathogenesis of STC and are, thus, worth further studying. This study provides an in-depth understanding of the relationship between the fecal microbiota, metabolites, and intestinal dysfunction in STC patients, and provides a possible future model for STC diagnosis and interventions targeting specific microbiota related to BA metabolism.

Data availability statement

The datasets presented in this study can be found in online repositories. The names of the repository/repositories and accession number(s) can be found in the article/supplementary material.

Ethics statement

This study was conducted in Tianjin Union Medical Center, Tianjin, China. The samples and clinical data used in this study were obtained with the approval of institutional review boards and under conditions of informed consent (China Clinical Trial Registry, ChiCTR2000033227; Medical ethics approval number: 2021B12). All subjects signed written informed consent upon enrollment and received questionnaires.

Author contributions

YB and LY conceived and designed the project. YF, CX, LX, YW (13th Author), YL, HL, and LW collected samples. YF, CX, YW (4th Author), SZ, JA, and ZT did experiments and analysis. YF, LX, SZ, YL, YY, SY, BJ, and YW (4th Author) carried out data statistics. YF, CX, YL, YW (13th Author), and JA prepared figures. YF, CX, YB, and LY prepared and finished the manuscript. All authors contributed to the article and approved the submitted version.

Funding

This work was supported by the National Key R and D Program of China (2018YFC1706506), the Foundation of Tianjin Municipal Health Commission (No. ZC20097), the Foundation of Tianjin Union Medical Center (No. 2020YJ017, 2017YJZD005), and the National Natural Science Foundation of China (No. 82174374).

Acknowledgments

We greatly thank the patients and healthy volunteers who participated in sample collections.

Conflict of interest

The authors declare that the research was conducted in the absence of any commercial or financial relationships that could be construed as a potential conflict of interest.

Publisher's note

Supplementary material

The Supplementary Material for this article can be found online at: https://www.frontiersin.org/articles/10.3389/fcimb.2022.956528/full#supplementary-material

References

Agachan, F., Chen, T., Pfeifer, J., Reissman, P., and Wexner, S. D. (1996). A constipation scoring system to simplify evaluation and management of constipated patients. *Dis. Colon Rectum* 39 (6), 681–685. doi: 10.1007/BF02056950

Alemi, F., Poole, D., Chiu, J., Schoonjans, K., Cattaruzza, F., Grider, J., et al. (2013). The receptor TGR5 mediates the prokinetic actions of intestinal bile acids and is required for normal defecation in mice. *Gastroenterology* 144 (1), 145–154. doi: 10.1053/j.gastro.2012.09.055

Alrefai, W. A., and Gill, R. K. (2007). Bile acid transporters: Structure, function, regulation and pathophysiological implications. *Pharm. Res.* 24 (10), 1803–1823. doi: 10.1007/s11095-007-9289-1

Appleby, R. N., and Walters, J. R. F. (2014). The role of bile acids in functional GI disorders. *Neurogastroenterol. Motil.* 26 (8), 1057–1069. doi: 10.1111/nmo.12370

Arumugam, M., Raes, J., Pelletier, E., Le Paslier, D., Yamada, T., Mende, D. R., et al. (2011). Enterotypes of the human gut microbiome. *Nature* 473 (7346), 174–180. doi: 10.1038/nature09944

Bajor, A., Tornblom, H., Rudling, M., Ung, K. A., and Simren, M. (2015). Increased colonic bile acid exposure: a relevant factor for symptoms and treatment in IBS. *Gut* 64 (1), 84–92. doi: 10.1136/gutjnl-2013-305965

Barbara, G., Stanghellini, V., Brandi, G., Cremon, C., Di Nardo, G., De Giorgio, R., et al. (2005). Interactions between commensal bacteria and gut sensorimotor function in health and disease. *Am. J. Gastroenterol.* 100 (11), 2560–2568. doi: 10.1111/j.1572-0241.2005.00230.x

Biagioli, M., Marchianò, S., Carino, A., Di Giorgio, C., Santucci, L., Distrutti, E., et al. (2021). Bile acids activated receptors in inflammatory bowel disease. *Cells* 10 (6), 1281. doi: 10.3390/cells10061281

Bolyen, E., Rideout, J. R., Dillon, M. R., Bokulich, N., Abnet, C. C., Al-Ghalith, G. A., et al. (2019). Reproducible, interactive, scalable and extensible microbiome data science using QIIME 2. *Nat. Biotechnol.* 37 (8), 852–857. doi: 10.1038/s41587-019-0209-9

Caporaso, J. G., Kuczynski, J., Stombaugh, J., Bittinger, K., Bushman, F. D., Costello, E. K., et al. (2010). QIIME allows analysis of high-throughput community sequencing data. *Nat. Methods* 7 (5), 335–336. doi: 10.1038/nmeth.f.303

Ceresola, E. R., Ferrarese, R., Preti, A., and Canducci, F. (2018). Targeting patients' microbiota with probiotics and natural fibers in adults and children with constipation. *Eur. Rev. Med. Pharmacol. Sci.* 22 (20), 7045–7057. doi: 10.26355/eurrev_201810_16177

Chedid, V., Vijayvargiya, P., and Camilleri, M. (2018). Elobixibat for the treatment of constipation. *Expert Rev. Gastroenterol. Hepatol.* 12 (10), 951–960. doi: 10.1080/17474124.2018.1522248

Chumpitazi, B. P., Self, M. M., Czyzewski, D. I., Cejka, S., Swank, P. R., and Shulman, R. J. (2016). Bristol Stool form scale reliability and agreement decreases when determining Rome III stool form designations. *Neurogastroenterol Motil.* 28 (3), 443–448. doi: 10.1111/nmo.12738

Chu, H. K., Zhong, L. K., Li, H., Zhang, X. J., Zhang, J. Z., and Hou, X. H. (2014). Epidemiology characteristics of constipation for general population, pediatric population, and elderly population in China. *Gastroenterol. Res. Pract.* 2014, 532734. doi: 10.1155/2014/532734

Cozma-Petruţ, A., Loghin, F., Miere, D., and Dumitraşcu, D. (2017). Diet in irritable bowel syndrome: What to recommend, not what to forbid to patients! *World J. Gastroenterol.* 23 (21), 3771–3783. doi: 10.3748/wjg.v23.i21.3771

Dan, Z., Mao, X. H., Liu, Q. S., Guo, M. C., Zhuang, Y. Y., Liu, Z., et al. (2020). Altered gut microbial profile is associated with abnormal metabolism activity of autism spectrum disorder. *Gut Microbes* 11 (5), 1246–1267. doi: 10.1080/19490976.2020.1747329

de Meij, T. G. J., de Groot, E. F. J., Eck, A., Budding, A. E., Kneepkens, C. M. F., Benninga, M. A., et al. (2016). Characterization of microbiota in children with chronic functional constipation. *PloS One* 11 (10), e0164731. doi: 10.1371/journal.pone.0164731

Diamant, N. E., Kamm, M. A., Wald, A., and Whitehead, W. E. (1999). AGA technical review on anorectal testing techniques. *Gastroenterology* 116 (3), 735–760. doi: 10.1016/S0016-5085(99)70195-2

Ding, C., Fan, W. T., Gu, L. L., Tian, H. L., Ge, X. L., Gong, J. F., et al. (2018). Outcomes and prognostic factors of fecal microbiota transplantation in patients with slow transit constipation: results from a prospective study with long-term follow-up. *Gastroenterol. Rep.* 6 (2), 101–107. doi: 10.1093/gastro/gox036

Dior, M., Delagreverie, H., Duboc, H., Jouet, P., Coffin, B., Brot, L., et al. (2016). Interplay between bile acid metabolism and microbiota in irritable bowel syndrome. *Neurogastroenterol. Motil.* 28 (9), 1330–1340. doi: 10.1111/nmo.12829

Drossman, D. A. (2016). Functional gastrointestinal disorders: History, pathophysiology, clinical features, and Rome IV. *Gastroenterology* 150 (6), 1262–126+. doi: 10.1053/j.gastro.2016.02.032

Drossman, D. A., and Hasler, W. L. (2016). Rome IV-functional GI disorders: Disorders of gut-brain interaction. *Gastroenterology* 150 (6), 1257–1261. doi: 10.1053/j.gastro.2016.03.035

Duboc, H., Tache, Y., and Hofmann, A. F. (2014). The bile acid TGR5 membrane receptor: from basic research to clinical application. *Dig Liver Dis.* 46 (4), 302–312. doi: 10.1016/j.dld.2013.10.021

Eypasch, E., Williams, J. I., Wood-Dauphinee, S., Ure, B. M., Schmulling, C., Neugebauer, E., et al. (1995). Gastrointestinal quality of life index: development, validation and application of a new instrument. *Br. J. Surg.* 82 (2), 216–222. doi: 10.1002/bjs.1800820229

Falony, G., Joossens, M., Vieira-Silva, S., Wang, J., Darzi, Y., Faust, K., et al. (2016). Population-level analysis of gut microbiome variation. *Science* 352 (6285), 560–564. doi: 10.1126/science.aad3503

Fiers, W. D., Leonardi, I., and Iliev, I. D. (2020). From birth and throughout life: Fungal microbiota in nutrition and metabolic health. *Annu. Rev. Nutr.* 40, 323–343. doi: 10.1146/annurev-nutr-013120-043659

Fiorucci, S., Cipriani, S., Baldelli, F., and Mencarelli, A. (2010). Bile acid-activated receptors in the treatment of dyslipidemia and related disorders. *Prog. Lipid Res.* 49 (2), 171–185. doi: 10.1016/j.plipres.2009.11.001

Fiorucci, S., and Distrutti, E. (2015). Bile acid-activated receptors, intestinal microbiota, and the treatment of metabolic disorders. *Trends Mol. Med.* 21 (11), 702–714. doi: 10.1016/j.molmed.2015.09.001

Fiorucci, S., Distrutti, E., Carino, A., Zampella, A., and Biagioli, M. (2021). Bile acids and their receptors in metabolic disorders. *Prog. Lipid Res.* 82, 101094. doi: 10.1016/j.plipres.2021.101094

Gadaleta, R. M., van Erpecum, K. J., Oldenburg, B., Willemsen, E. C. L., Renooij, W., Murzilli, S., et al. (2011). Farnesoid X receptor activation inhibits inflammation and preserves the intestinal barrier in inflammatory bowel disease. *Gut* 60 (4), 463–472. doi: 10.1136/gut.2010.212159

Galman, C., Arvidsson, I., Angelin, B., and Rudling, M. (2003). Monitoring hepatic cholesterol 7alpha-hydroxylase activity by assay of the stable bile acid intermediate 7alpha-hydroxy-4-cholesten-3-one in peripheral blood. *J. Lipid Res.* 44 (4), 859–866. doi: 10.1194/jlr.D200043-JLR200

Gomez-Nguyen, A., Basson, A. R., Dark-Fleury, L., Hsu, K., Osme, A., Menghini, P., et al. (2021). Parabacteroides distasonis induces depressive-like behavior in a mouse model of crohn's disease. *Brain Behav. Immun.* 98, 245–250. doi: 10.1016/j.bbi.2021.08.218

Green, G. H., and Diggle, P. J. (2007). On the operational characteristics of the benjamini and hochberg false discovery rate procedure. *Stat. Appl. Genet. Mol. Biol.* 6, Article27. doi: 10.2202/1544-6115.1302

Hanson, B., Siddique, S. M., Scarlett, Y., Sultan, S., and Assoc, A. G. (2019). American Gastroenterological association institute technical review on the medical management of opioid-induced constipation. *Gastroenterology* 156 (1), 229–22+. doi: 10.1053/j.gastro.2018.08.018

Hooper, L. V., Wong, M. H., Thelin, A., Hansson, L., Falk, P. G., and Gordon, J. I. (2001). Molecular analysis of commensal host-microbial relationships in the intestine. *Science* 291 (5505), 881–884. doi: 10.1126/science.291.5505.881

Husebye, E., Hellstrom, P. M., Sundler, F., Chen, J., and Midtvedt, T. (2001). Influence of microbial species on small intestinal myoelectric activity and transit in germ-free rats. *Am. J. Physiol Gastrointest Liver Physiol.* 280 (3), G368–G380. doi: 10.1152/ajpgi.2001.280.3.G368

Jiang, C., Xu, Q., Wen, X., and Sun, H. (2015). Current developments in pharmacological therapeutics for chronic constipation. *Acta Pharm. Sin. B* 5 (4), 300–309. doi: 10.1016/j.apsb.2015.05.006

Jia, W., Xie, G., and Jia, W. (2018). Bile acid-microbiota crosstalk in gastrointestinal inflammation and carcinogenesis. *Nat. Rev. Gastroenterol. Hepatol.* 15 (2), 111–128. doi: 10.1038/nrgastro.2017.119

Kashyap, P. C., Marcobal, A., Ursell, L. K., Larauche, M., Duboc, H., Earle, K. A., et al. (2013). Complex interactions among diet, gastrointestinal transit, and gut microbiota in humanized mice. *Gastroenterology* 144 (5), 967–977. doi: 10.1053/j.gastro.2013.01.047

Kim, N. H., Park, J. H., Park, J. S., and Joung, Y. H. (2017). The effect of deoxycholic acid on secretion and motility in the rat and Guinea pig Large intestine. *J. Neurogastroenterol. Motil.* 23 (4), 606–615. doi: 10.5056/jnm16201

Kim, E. S., Tarassishin, L., Eisele, C., Barre, A., Nair, N., Rendon, A., et al. (2021). Longitudinal changes in fecal calprotectin levels among pregnant women with and without inflammatory bowel disease and their babies. *Gastroenterology* 160 (4), 1118–111+. doi: 10.1053/j.gastro.2020.11.050

Knowles, C. H., Grossi, U., Horrocks, E. J., Pares, D., Vollebregt, P. F., Chapman, M., et al. (2017). Surgery for constipation: systematic review and clinical guidance: Paper 1: Introduction & methods. *Colorectal Dis.* 19 Suppl 3, 5–16. doi: 10.1111/codi.13774

Lacy, B. E., Mearin, F., Chang, L., Chey, W. D., Lembo, A. J., Simren, M., et al. (2016). Bowel disorders. *Gastroenterology* 150 (6), 1393–139+. doi: 10.1053/j.gastro.2016.02.031

Li, X. R., Liu, C. J., Tang, X. D., Zhang, H. M., Luo, Y. Y., Zhang, L., et al. (2020). Gut microbiota alterations from three-strain yogurt formulation treatments in slow-transit constipation. *Can. J. Infect. Dis. Med. Microbiol.* 2020, 4583973. doi: 10.1155/2020/4583973

Liu, Z. S., Yan, S. Y., Wu, J. N., He, L. Y., Li, N., Dong, G. R., et al. (2016). Acupuncture for chronic severe functional constipation a randomized trial. *Ann. Internal Med.* 165 (11), 761–76+. doi: 10.7326/M15-3118

Liu, X., Zhang, M., Cheng, X., Liu, X., Sun, H., Guo, Z., et al. (2020). LC-MS-Based plasma metabolomics and lipidomics analyses for differential diagnosis of bladder cancer and renal cell carcinoma. *Front. Oncol.* 10. doi: 10.3389/fonc.2020.00717

Long, S., Gahan, C., and Joyce, S. (2017a). Interactions between gut bacteria and bile in health and disease. *Mol. Aspects Med.* 56, 54–65. doi: 10.1016/j.mam.2017.06.002

Long, Y., Huang, Z., Deng, Y., Chu, H., Zheng, X., Yang, J., et al. (2017b). Prevalence and risk factors for functional bowel disorders in south China: a population based study using the Rome III criteria. *Neurogastroenterol. Motil.* 29 (1), e12897. doi: 10.1111/nmo.12897

Lynch, A., Tammireddy, S. R., Doherty, M. K., Whitfield, P. D., and Clarke, D. J. (2019). The glycine lipids of bacteroides thetaiotaomicron are important for fitness during growth *In vivo* and *In vitro*. *Appl. Environ. Microbiol.* 85 (10), e02157–18. doi: 10.1128/AEM.02157-18

Martin-Gallausiaux, C., Marinelli, L., Blottiere, H. M., Larraufie, P., and Lapaque, N. (2021). SCFA: mechanisms and functional importance in the gut. *Proc. Nutr. Soc.* 80 (1), 37–49. doi: 10.1017/S0029665120006916

Mazzone, A., Strege, P. R., Gibbons, S. J., Alcaino, C., Joshi, V., Haak, A. J., et al. (2020). microRNA overexpression in slow transit constipation leads to reduced NaV1.5 current and altered smooth muscle contractility. *Gut* 69 (5), 868–876. doi: 10.1136/gutjnl-2019-318747

Miyazaki, T., Shirakami, Y., Mizutani, T., Maruta, A., Ideta, T., Kubota, M., et al. (2021). Novel FXR agonist nelumal a suppresses colitis and inflammation-related colorectal carcinogenesis. *Sci. Rep.* 11 (1), 492. doi: 10.1038/s41598-020-79916-5

Modica, S., Murzilli, S., Salvatore, L., Schmidt, D. R., and Moschetta, A. (2008). Nuclear bile acid receptor FXR protects against intestinal tumorigenesis. *Cancer Res.* 68 (23), 9589–9594. doi: 10.1158/0008-5472.Can-08-1791

Mosińska, P., Szczepaniak, A., and Fichna, J. (2018). Bile acids and FXR in functional gastrointestinal disorders. *Digest Liver Dis. Off. J. Ital. Soc. Gastroenterol. Ital. Assoc. Study Liver* 50 (8), 795–803. doi: 10.1016/j.dld.2018.05.016

Mugie, S. M., Benninga, M. A., and Di Lorenzo, C. (2011). Epidemiology of constipation in children and adults: A systematic review. *Best Pract. Res. Clin. Gastroenterol.* 25 (1), 3–18. doi: 10.1016/j.bpg.2010.12.010

Nakajima, A., Seki, M., Taniguchi, S., Ohta, A., Gillberg, P. G., Mattsson, J. P., et al. (2018). Safety and efficacy of elobixibat for chronic constipation: results from a randomised, double-blind, placebo-controlled, phase 3 trial and an open-label, single-arm, phase 3 trial. *Lancet Gastroenterol. Hepatol.* 3 (8), 537–547. doi: 10.1016/S2468-1253(18)30123-7

Nicholson, J. K., Holmes, E., Kinross, J., Burcelin, R., Gibson, G., Jia, W., et al. (2012). Host-gut microbiota metabolic interactions. *Science* 336 (6086), 1262–1267. doi: 10.1126/science.1223813

Pang, Z., Chong, J., Zhou, G., de Lima Morais, D. A., Chang, L., Barrette, M., et al. (2021). MetaboAnalyst 5.0: narrowing the gap between raw spectra and functional insights. *Nucleic Acids Res.* 49 (W1), W388–W396. doi: 10.1093/nar/gkab382

Parthasarathy, G., Chen, J., Chen, X. F., Chia, N., O'Connor, H. M., Wolf, P. G., et al. (2016). Relationship between microbiota of the colonic mucosa vs feces and symptoms, colonic transit, and methane production in female patients with chronic constipation. *Gastroenterology* 150 (2), 367–36+. doi: 10.1053/j.gastro.2015.10.005

Peng, W., Liang, H., Sibbritt, D., and Adams, J. (2016). Complementary and alternative medicine use for constipation: a critical review focusing upon prevalence, type, cost, and users' profile, perception and motivations. *Int. J. Clin. Pract.* 70 (9), 712–722. doi: 10.1111/ijcp.12829

Perino, A., and Schoonjans, K. (2015). TGR5 and immunometabolism: Insights from physiology and pharmacology. *Trends Pharmacol. Sci.* 36 (12), 847–857. doi: 10.1016/j.tips.2015.08.002

Postler, T. S., and Ghosh, S. (2017). Understanding the holobiont: How microbial metabolites affect human health and shape the immune system. *Cell Metab.* 26 (1), 110–130. doi: 10.1016/j.cmet.2017.05.008

Propheter, D. C., and Hooper, L. V. (2015). Bacteria come into focus: New tools for visualizing the microbiota. *Cell Host Microbe* 18 (4), 392–394. doi: 10.1016/j.chom.2015.10.004

Rao, S. S. C., Rattanakovit, K., and Patcharatrakul, T. (2016). Diagnosis and management of chronic constipation in adults. *Nat. Rev. Gastroenterol. Hepatol.* 13 (5), 295–305. doi: 10.1038/nrgastro.2016.53

Rao, A. S., Wong, B. S., Camilleri, M., Odunsi-Shiyanbade, S. T., McKinzie, S., Ryks, M., et al. (2010). Chenodeoxycholate in females with irritable bowel syndrome-constipation: A pharmacodynamic and pharmacogenetic analysis. *Gastroenterology* 139 (5), 1549–154+. doi: 10.1053/j.gastro.2010.07.052

Ridlon, J. M., Kang, D. J., and Hylemon, P. B. (2006). Bile salt biotransformations by human intestinal bacteria. *J. Lipid Res.* 47 (2), 241–259. doi: 10.1194/jlr.R500013-JLR200

Rivas, M. N., Burton, O. T., Wise, P., Zhang, Y. Q., Hobson, S. A., Lloret, M. G., et al. (2013). A microbiota signature associated with experimental food allergy promotes allergic sensitization and anaphylaxis. *J. Allergy Clin. Immunol.* 131 (1), 201–212. doi: 10.1016/j.jaci.2012.10.026

Sanchez, B. (2018). Bile acid-microbiota crosstalk in gastrointestinal inflammation and carcinogenesis: a role for bifidobacteria and lactobacilli? *Nat. Rev. Gastroenterol. Hepatol.* 15 (4), 205. doi: 10.1038/nrgastro.2018.23

Schwabe, R. F., and Greten, T. F. (2020). Gut microbiome in HCC - mechanisms, diagnosis and therapy. *J. Hepatol.* 72 (2), 230–238. doi: 10.1016/j.jhep.2019.08.016

Segata, N., Izard, J., Waldron, L., Gevers, D., Miropolsky, L., Garrett, W. S., et al. (2011). Metagenomic biomarker discovery and explanation. *Genome Biol.* 12 (6), R60. doi: 10.1186/gb-2011-12-6-r60

Shannon, P., Markiel, A., Ozier, O., Baliga, N. S., Wang, J. T., Ramage, D., et al. (2003). Cytoscape: a software environment for integrated models of biomolecular interaction networks. *Genome Res.* 13 (11), 2498–2504. doi: 10.1101/gr.1239303

Sheng, L. L., Jena, P. K., Liu, H. X., Kalanetra, K. M., Gonzalez, F. J., French, S. W., et al. (2017). Gender differences in bile acids and microbiota in relationship with gender dissimilarity in steatosis induced by diet and FXR inactivation. *Sci. Rep.* 7 (1), 1748. doi: 10.1038/s41598-017-01576-9

Si, X., Shang, W. T., Zhou, Z. K., Strappe, P., Wang, B., Bird, A., et al. (2018). Gut microbiome-induced shift of acetate to butyrate positively manages dysbiosis in high fat diet. *Mol. Nutr. Food Res.* 62 (3), 1700670. doi: 10.1002/mnfr.201700670

Staley, C., Weingarden, A. R., Khoruts, A., and Sadowsky, M. J. (2017). Interaction of gut microbiota with bile acid metabolism and its influence on disease states. *Appl. Microbiol. Biotechnol.* 101 (1), 47–64. doi: 10.1007/s00253-016-8006-6

Stanimirov, B., Stankov, K., and Mikov, M. (2015). Bile acid signaling through farnesoid X and TGR5 receptors in hepatobiliary and intestinal diseases. *Hepatobil Pancreat Dis. Int. HBPD Int.* 14 (1), 18–33. doi: 10.1016/s1499-3872(14)60307-6

Tan, H., Zhai, Q., and Chen, W. (2019). Investigations of bacteroides spp. towards next-generation probiotics. *Food Res. Int.* 116, 637–644. doi: 10.1016/j.foodres.2018.08.088

Tian, H., Chen, Q., Yang, B., Qin, H., and Li, N. (2021). Analysis of gut microbiome and metabolite characteristics in patients with slow transit constipation. *Dig Dis. Sci.* 66 (9), 3026–3035. doi: 10.1007/s10620-020-06500-2

Traub, R. J., Tang, B., Ji, Y. P., Pandya, S., Yfantis, H., and Sun, Y. (2008). A rat model of chronic postinflammatory visceral pain induced by deoxycholic acid. *Gastroenterology* 135 (6), 2075–2083. doi: 10.1053/j.gastro.2008.08.051

Vallim, T. Q. D., Tarling, E. J., and Edwards, P. A. (2013). Pleiotropic roles of bile acids in metabolism. *Cell Metab.* 17 (5), 657–669. doi: 10.1016/j.cmet.2013.03.013

Vavassori, P., Mencarelli, A., Renga, B., Distrutti, E., and Fiorucci, S. (2009). The bile acid receptor FXR is a modulator of intestinal innate immunity. *J. Immunol.* 183 (10), 6251–6261. doi: 10.4049/jimmunol.0803978

Vriesman, M. H., Koppen, I. J. N., Camilleri, M., Di Lorenzo, C., and Benninga, M. A. (2020). Management of functional constipation in children and adults. *Nat. Rev. Gastroenterol. Hepatol.* 17 (1), 21–39. doi: 10.1038/s41575-019-0222-y

Wahlstrom, A., Sayin, S. I., Marschall, H. U., and Backhed, F. (2016). Intestinal crosstalk between bile acids and microbiota and its impact on host metabolism. *Cell Metab.* 24 (1), 41–50. doi: 10.1016/j.cmet.2016.05.005

Wang, Y., Chen, W., Yu, D., Forman, B., and Huang, W. (2011). The G-protein-coupled bile acid receptor, Gpbar1 (TGR5), negatively regulates hepatic inflammatory response through antagonizing nuclear factor κ light-chain enhancer of activated b cells (NF-κB) in mice. *Hepatol. (Baltimore Md)* 54 (4), 1421–1432. doi: 10.1002/hep.24525

Wang, Q., Garrity, G. M., Tiedje, J. M., and Cole, J. R. (2007). Naive Bayesian classifier for rapid assignment of rRNA sequences into the new bacterial taxonomy. *Appl. Environ. Microbiol.* 73 (16), 5261–5267. doi: 10.1128/Aem.00062-07

Wang, K., Liao, M. F., Zhou, N., Bao, L., Ma, K., Zheng, Z. Y., et al. (2019). Parabacteroides distasonis alleviates obesity and metabolic dysfunctions *via* production of succinate and secondary bile acids. *Cell Rep.* 26 (1), 222–22+. doi: 10.1016/j.celrep.2018.12.028

Wang, J., Zheng, J., Shi, W., Du, N., Xu, X., Zhang, Y., et al. (2018). Dysbiosis of maternal and neonatal microbiota associated with gestational diabetes mellitus. *Gut* 67 (9), 1614–1625. doi: 10.1136/gutjnl-2018-315988

Worley, B., and Powers, R. (2013). Multivariate analysis in metabolomics. *Curr. Metabolomics* 1 (1), 92–107. doi: 10.2174/2213235X11301010092

Xia, Y., Wang, J., Fang, X., Dou, T., Han, L., and Yang, C. (2021). Combined analysis of metagenomic data revealed consistent changes of gut microbiome structure and function in inflammatory bowel disease. *J. Appl. Microbiol.* 131 (6), 308-–31. doi: 10.1111/jam.15154

Yang, Z. D., Ye, S. M., Xu, Z. M., Su, H. H., Tian, X., Han, B., et al. (2021). Dietary synbiotic ameliorates constipation through the modulation of gut microbiota and its metabolic function. *Food Res. Int.* 147, 110569. doi: 10.1016/j.foodres.2021.110569

Yilmaz, B., Juillerat, P., Oyas, O., Ramon, C., Bravo, F. D., Franc, Y., et al. (2019). Microbial network disturbances in relapsing refractory crohn's disease. *Nat. Med.* 25 (2), 323–336. doi: 10.1038/s41591-018-0308-z

Yoneno, K., Hisamatsu, T., Shimamura, K., Kamada, N., Ichikawa, R., Kitazume, M., et al. (2013). TGR5 signalling inhibits the production of pro-inflammatory cytokines by *in vitro* differentiated inflammatory and intestinal macrophages in crohn's disease. *Immunology* 139 (1), 19–29. doi: 10.1111/imm.12045

Zhang, X. Y., Tian, H. L., Gu, L. L., Nie, Y. Z., Ding, C., Ge, X. L., et al. (2018). Long-term follow-up of the effects of fecal microbiota transplantation in combination with soluble dietary fiber as a therapeutic regimen in slow transit constipation. *Sci. China Life Sci.* 61 (7), 779–786. doi: 10.1007/s11427-017-9229-1

Zhuang, M., Shang, W. T., Ma, Q. C., Strappe, P., and Zhou, Z. K. (2019). Abundance of probiotics and butyrate-production microbiome manages constipation *via* short-chain fatty acids production and hormones secretion. *Mol. Nutr. Food Res.* 63 (23), e1801187. doi: 10.1002/mnfr.201801187

frontiers | Frontiers in Cellular and Infection Microbiology

TYPE Original Research
PUBLISHED 02 August 2022
DOI 10.3389/fcimb.2022.957439

OPEN ACCESS

EDITED BY
Zhanbo Zhu,
Heilongjiang Bayi Agricultural University, China

REVIEWED BY
Xiaofan Wang,
University of Arkansas, United States
Feilong Deng,
Foshan University, China

*CORRESPONDENCE
Yongzheng Peng
yzpeng1981@126.com
Xiao-Xuan Zhang
zhangxiaoxuan1988@126.com

SPECIALTY SECTION
This article was submitted to Clinical Microbiology, a section of the journal Frontiers in Cellular and Infection Microbiology

RECEIVED 31 May 2022
ACCEPTED 11 July 2022
PUBLISHED 02 August 2022

CITATION
Lv Q-B, Li S, Zhang Y, Guo R, Wang Y-C, Peng Y and Zhang X-X (2022) A thousand metagenome-assembled genomes of *Akkermansia* reveal phylogroups and geographical and functional variations in the human gut.
Front. Cell. Infect. Microbiol. 12:957439.
doi: 10.3389/fcimb.2022.957439

A thousand metagenome-assembled genomes of *Akkermansia* reveal phylogroups and geographical and functional variations in the human gut

Qing-Bo Lv[1,2], Shenghui Li[2], Yue Zhang[2], Ruochun Guo[2], Yan-Chun Wang[3], Yongzheng Peng[4]* and Xiao-Xuan Zhang[1]*

[1]College of Veterinary Medicine, Qingdao Agricultural University, Qingdao, China, [2]Puensum Genetech Institute, Wuhan, China, [3]College of Animal Science and Technology, Jilin Agricultural University, Changchun, China, [4]Department of Laboratory Medicine, Zhujiang Hospital, Southern Medical University, Guangzhou, China

Akkermansia muciniphila has long been considered to be the only *Akkermansia* species in the human gut and has been extensively studied. The present study revealed the genomic architecture of *Akkermansia* in the human gut by analyzing 1,126 near-complete metagenome-assembled genomes, 84 publicly available genomes, and 1 newly sequenced *Akkermansia glycaniphila* strain from the human gut. We found that 1) the genomes of *Akkermansia* were clustered into four phylogroups with distinct interspecies similarity and different genomic characteristics and 2) *A. glycaniphila* GP37, a strain of *Akkermansia*, was isolated from the human gut, whereas previously, it had only been found in python. Amuc III was present in the Chinese population, and Amuc IV was mainly distributed in Western populations. A large number of gene functions, pathways, and carbohydrate-active enzymes were specifically associated with phylogroups. Our findings based on over a thousand genomes strengthened our previous knowledge and provided new insights into the population structure and ecology of *Akkermansia* in the human gut.

KEYWORDS

***Akkermansia muciniphila*, metagenome-assembled genome, population structure, geographical variation, functional specificity, gut microbiota**

Introduction

Akkermansia is a well-studied genus that has been regarded as a representative of the phylum Verrucomicrobia in the human and animal gut (Derrien et al., 2004; Derrien et al., 2010; Cani et al., 2022). To date, only two species of *Akkermansia*, *A. muciniphila* and *A. glycaniphila* (Derrien et al., 2004; Ouwerkerk et al., 2016), have been isolated and comprehensively described. *Akkermansia muciniphila* is widely present in the intestinal mucosa of human (Ley et al., 2008; Presley et al., 2010; Belzer and de Vos, 2012; Falony et al., 2016), and it can degrade the mucin in epithelial mucosa and produce diverse structural molecules such as short-chain fatty acids (Derrien et al., 2004; Derrien et al., 2010; Hagi and Belzer, 2021). The host range of the *Akkermansia* genus is wide, ranging from mammals (mainly *A. muciniphila*) to non-mammals (e.g., *A. glycaniphila* is isolated from python (Ouwerkerk et al., 2016)) that differed greatly in physiology, dietary structure, and composition of mucinous proteins in the gut (Ley et al., 2008). There is growing evidence showing that *A. muciniphila* is an excellent candidate probiotic. Previous studies have shown a health-promoting effect of *A. muciniphila* (Dao et al., 2016; Derrien et al., 2017; Zhai et al., 2019), owing to the negative correlation of the relative abundance of *A. muciniphila* in gut microbiota with multiple metabolic disorders, such as hyperlipidemia (Yu et al., 2021), severe obesity (Hasani et al., 2021), and type 2 diabetes (Pascale et al., 2019; Zhang et al., 2021). Furthermore, supplementation with *A. muciniphila* in mice exerted a protective effect on colitis induced by dextran sulfate sodium and prevented the age-related decline in the thickness of the colonic mucus layer (Bian et al., 2019; van der Lugt et al., 2019). In clinical trials, oral supplementation of *A. muciniphila* was considered a safe and well-tolerated intervention for weight loss, thus improving insulin sensitivity and reducing insulinemia and plasma total cholesterol (Depommier et al., 2019).

After investigating a large number of full-length 16S sequences in 2011, it had been shown that at least eight species of the *Akkermansia* genus reside in the human digestive tract (van Passel et al., 2011). However, only two strains, *A. muciniphila* ATCC BAA-835 and *A. glycaniphila* Pyt (van Passel et al., 2011; Ouwerkerk et al., 2017), were subjected to a whole-genomic sequencing until 2017. Therefore, we still need to expand our understanding of the distribution of *Akkermansia* in the population to improve their potential applications in biomedicine. In our previous study (Guo et al., 2017), we sequenced and analyzed the draft genomes for 39 A. *muciniphila* strains isolated from China, and the population structure of these species was divided into three phylogroups (Amuc I, II, and III). These phylogroups showed a high genetic diversity in metabolic and functional features. Recently, a large number of metagenome-assembled genomes (MAGs) of the human gut microbiome have been published, and these data provide an opportunity to characterize the genomes of some important bacteria (Pasolli et al., 2019; Almeida et al., 2021). Pasolli et al. characterized the human microbiome from different body parts, ages, and countries through a large number of MAGs (Pasolli et al., 2019). Karcher et al. reported five different *A. muciniphila* candidate species in the human gut using a large-scale population genome analysis of *Akkermansia* (Karcher et al., 2021). These studies have expanded our understanding of genomic variation and species diversity in *A. muciniphila*.

To our knowledge, *A. glycaniphila*, another member of *Akkermansia*, is a strain that has never been isolated in the human gut. *Akkermansia glycaniphila* also appears unable to be assembled in metagenomic data from the human gut microbiome. Here, we isolated an *A. glycaniphila* strain from the gut of a subject and sequenced its whole genome. This does not completely prove that *A. glycaniphila* is endemic in the human gut, but it does expand our understanding of the genus *Akkermansia*. In addition, we also comprehensively analyzed the geographical distribution characteristics of *Akkermansia* based on more than 1,000 published *Akkermansia* genomes. These results reinforce previous findings and provide new insights into *Akkermansia* research.

Methods

Quality control and genome sequencing

We included the MAGs of *Akkermansia* (Supplement Table ST1) from the data made public by two studies (Pasolli et al. (2019) and Kirmiz et al. (2020)). Isolated genomes were downloaded from the National Center of Biotechnology Information (NCBI) database (Supplement Table ST2). The source information of these MAGs and genomes was also collected, such as host, country, etc. Each MAG met the quality standard of completeness of more than 90% and contamination of less than 5%, estimated based on the CheckM lineage (Parks et al., 2015). An *A. glycaniphila* strain (GP37) was isolated from human feces that was primarily isolated as part of a previous study (Guo et al., 2017). Genomes were sequenced using the Illumina HiSeq2500 instrument, and genomic assembly of *A. glycaniphila* GP37 was performed based on the previous pipeline as described previously (Guo et al., 2017).

Gene prediction and functional annotation

To unify the standards, a genome content prediction for all *Akkermansia* genomes was carried out using Prokka (v1.13.3) (Seemann, 2014). The coordinates of genomic features within sequences, including small rRNA (5S, 16S, and 23S rRNA), were identified by using RNAmmer (v1.2) (Lagesen et al., 2007). The protein-coding gene prediction was performed using

Prodigal (Hyatt et al., 2010). 16S rRNA gene sequence similarity was calculated using BLAST+ (v2.9.0). The functional annotation of genes was based on the Kyoto Encyclopedia of Genes and Genomes (KEGG, downloaded in December 2020) (Kanehisa et al., 2021) and CAZy databases (dbCAN2 version, CAZyDB.07312020) (Zhang et al., 2018) using USEARCH (Edgar, 2010) and DIAMOND (Buchfink et al., 2015), respectively, with the parameters e-value <1e−10, identity >70%, and coverage percentage >70%.

Bioinformatic analyses

A phylogenetic tree of the *Akkermansia* strains was constructed based on concatenated protein subsequences by PhyloPhlAn (v.0.99) (Segata et al., 2013) with default parameters. The phylogenetic tree was visualized using iTol (Letunic and Bork, 2016). Pairwise average nucleotide identity (ANI) between two genomes was calculated using FastANI (v1.1) (Jain et al., 2018). Statistical analyses were implemented on the R platform. Heatmap was performed using the "heatmap.2" function, and principal coordinates analysis (PCoA) was performed using the cmdscale function (*vegan* package) and visualized using the *ggplot2* package (Wickham, 2016). The BRIG software was used to visualize genome comparisons (Alikhan et al., 2011).

Results and discussion

Metagenome-assembled genomes and isolated genomes of *Akkermansia*

In order to decipher the population structure and geographical distribution of *Akkermansia*, a total of 1,126 *Akkermansia* MAGs conforming to the "near-complete" standard (completeness > 90% and contamination < 5%) from public data (Pasolli et al., 2019; Kirmiz et al., 2020) were included. Although metagenomic samples were widely collected from multiple human sites, almost all *Akkermansia* MAGs were detected from human fecal samples (Supplement Table ST1). This finding was in line with the previous studies showing that the gut, rather than other body sites, was a major habitat of *Akkermansia* (Geerlings et al., 2018). Similarly, only six non-*Akkermansia* Verrucomicrobia genomes were identified in a recent study reconstructing over 56,000 MAGs from the global human oral metagenomes (Zhu et al., 2021); this result also indicated a very low occurrence of *Akkermansia* in the human oral cavity.

The average completeness and contamination rates of 1,126 *Akkermansia* MAGs were 96.3% and 0.4%, respectively. The genomic data revealed varying genomic sizes ranging from 2.17 to 3.30 Mbp (average 2.73 Mbp, Figure 1A). The MAGs represented five continents and 22 different countries. The majority of the genomes (60.2%, 678/1,126) were from countries in Europe, and the others were from Israel (n = 141), the USA (n = 107), China (n = 97), Canada (n = 53), Kazakhstan (n = 33), Mongolia (n = 10), Fiji (n = 5), and Peru (n = 2) (Figure 1B). In view of the geographical and population spans and the integrity of 1,126 MAGs, we suggested that they effectively represented the characteristics of the human intestinal *Akkermansia* genus and could be used to answer fundamental questions regarding population structure and functional specificity of *Akkermansia*.

To extend the genomic content of *Akkermansia*, we also analyzed 84 isolated genomes from the NCBI database and one newly sequenced *Akkermansia* strain (GP37, an *A. glycaniphila* strain isolated from the human gut). The quality of these genomes was reassessed (Supplement Table ST2). The distribution of genome sizes for the isolated genomes was consistent with that of MAGs (Figure 1B). All of these strains

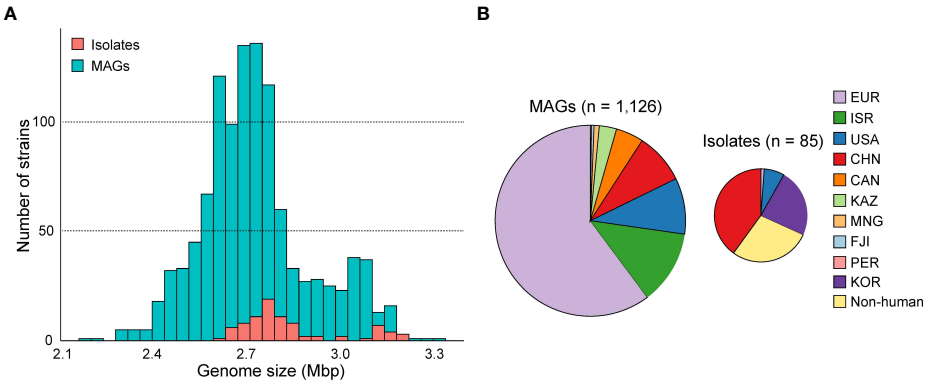

FIGURE 1
The genome size and country distribution of 1,211 strains of *Akkermansia*. **(A)** Distribution of genome size of 1,126 metagenome-assembled genomes (MAGs) and 85 isolated genomes. **(B)** Country distribution of 1,126 MAGs and 85 MAG isolated genomes.

were isolated from the feces, but their hosts were widely distributed, including humans (n = 61), mice (n = 13), chimpanzees (n = 3), and other animals (n = 8). Of the isolated genomes, 96.5% (82/85) were *A. muciniphila*, and the remaining three were *A. glycaniphila*.

Population structure of *Akkermansia*

The phylogenetic relationship of all 1,211 *Akkermansia* genomes was analyzed based on PhyloPhlAn, a method for improving the phylogenetic and taxonomic placement of microbes (Segata et al., 2013). We identified seven distinct phylogroups of *Akkermansia* (Figure 2A), including three *A. muciniphila* phylogroups (Amuc I, II, and III) reported by Guo et al. (2017) and a phylogroup of *A. glycaniphila*. The three *A. muciniphila* phylogroups accounted for 94% of all genomes, of which 945 were Amuc I, 181 were Amuc II, and 6 were Amuc III.

The clustering result of ANI on whole-genome data was identical to the phylogenetic analysis (Figure S1). The three known *A. muciniphila* phylogroups (Amuc I, II, and III) had average between-phylogroup ANIs ranging from 85% to 91% (Figure 2B), and the average 16S rRNA gene similarity was from 98.9% to 99.9% (Figure 2C). This finding suggested that these phylogroups were distinct subspecies, which was consistent with a previous study (Guo et al., 2017). In addition, the new phylogroup (containing 69 genomes) has an average ANI of 82%–84% with the three Amuc phylogroups I to III, and the average 16S rRNA gene similarity was 98.1%–98.5%. Therefore, this new phylogroup was defined as *A. muciniphila* subsp. IV (Amuc IV) according to the criterion for other *A. muciniphila* phylogroups (Guo et al., 2017; Kirmiz et al., 2020). *Akkermansia*

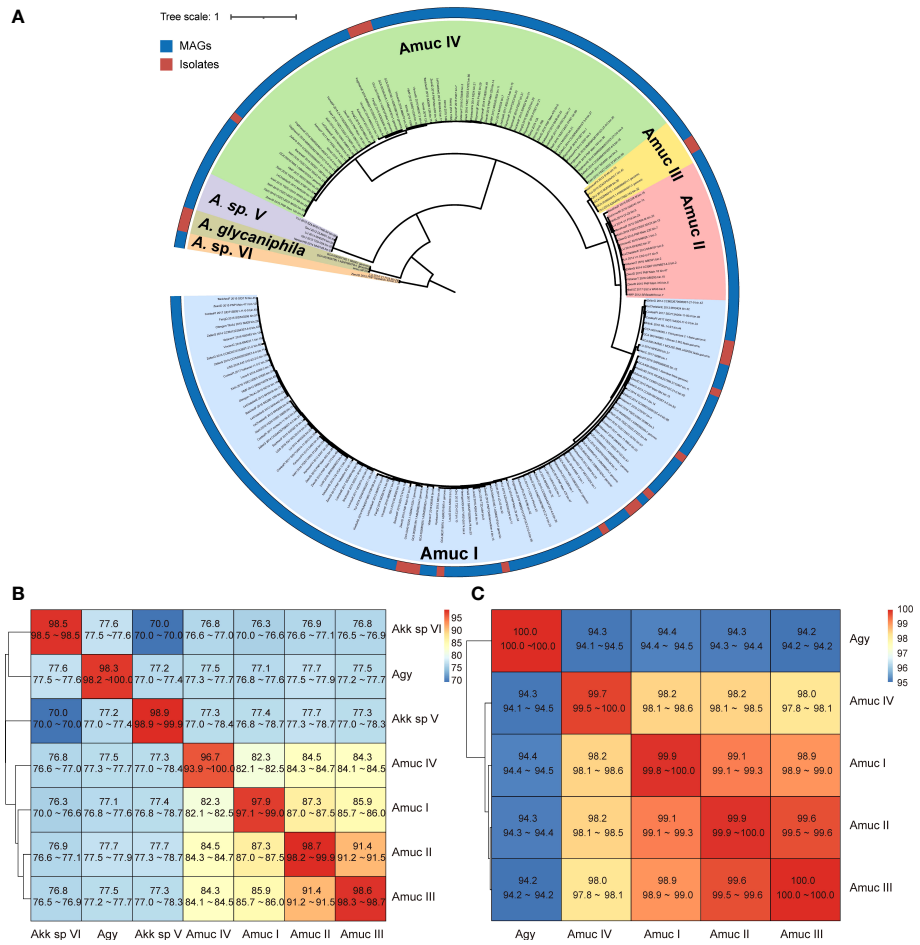

FIGURE 2
Phylogenetic analysis of *Akkermansia* genomes. **(A)** Phylogenetic tree of 1,126 MAG and 85 isolated genomes. Filling colors in the phylogenetic tree represent different species or phylogroups. The outer circle represents the original strains from MAGs and isolated genomes. For better visualization, only 10% of the strains of Amuc I and Amuc II were used, without changing the overall structure of the tree. **(B, C)** Heatmaps show the pairwise ANI among seven *Akkermansia* species and phylogroups **(B)** and the 16S sequence similarity among five *Akkermansia muciniphila* phylogroups and *Akkermansia glycaniphila* **(C)**.

glycaniphila and the two remaining new phylogroups showed a remarkable difference with regard to between-phylogroup ANI (<80%) and 16S rRNA gene similarity (<90%), suggesting that they were different species. These two branches were named as *Akkermansia* sp. V (containing five genomes) and *Akkermansia* sp. VI (containing two genomes). However, due to the small number of genomes and the lack of culture evidence, they cannot yet be defined as potential new species.

There were significant differences in some genomic characteristics for the seven *Akkermansia* phylogroups. The strains of *A. glycaniphila* and *Akkermansia* sp. V had the largest genome size (average 3.08 and 3.10 Mbp, respectively; Figure 3), and the strains of *Akkermansia* sp. VI had the smallest genomes (average 2.39 Mbp). Among *A. muciniphila* subspecies, the genome sizes of Amuc II were the largest (average 2.99 Mbp), while Amuc I was the smallest (average 2.66 Mbp). The distribution of the number of proteins was consistent with that of genome sizes (Figure S2). The G+C content of *Akkermansia* sp. VI was extremely higher than the others (average 64.8%; Figure 3), while that of *Akkermansia* sp. V was remarkably lower (average 52.0%). Amuc II and III had a higher GC content (58.1% and 58.4%, respectively) compared with other *A. muciniphila* phylogroups, and Amuc I had the lowest GC content (55.7%). The representative genomes of Amuc I, II, III, and IV showed differences in several different genomic regions (Figure S3). Diversified genomic characteristics of the *Akkermansia* phylogroups suggested different evolution history and functional habits.

Belzer et al. (Belzer and de Vos, 2012) divided the *Akkermansia* phylogenetic tree into five clades according to the full-length 16S rRNA sequences. Among them, four clades contained human-associated sequences and one clade had a high diversity without human-derived sequences. In this study, we included the *Akkermansia* genomes from diverse transcontinental populations and found that the average similarity of 16S rRNA sequences between *A. muciniphila* and *A. glycaniphila* was 94.3%, and among Amuc I–IV phylogroups, it was >98%. This result indicated a relatively conservative 16S rRNA sequence in *Akkermansia* genomes, suggesting that more potential *Akkermansia* species or phylogroups are still undiscovered, especially in non-human animals. A recent study (Xing et al., 2019) constructed a phylogenetic tree based on 710 single-copy core genes shared by 23 *Akkermansia* genomes and divided *A. muciniphila* into four subspecies. The result was consistent with our findings showing that the genome of an *Akkermansia* strain (*Akkermansia* sp. KLE1797 from the NCBI database) belonged to a distinct phylogroup (in our study, Amuc IV). Amuc IV was also found by Kirmiz et al. based on 35 high-quality MAGs reconstructed from the feces of American children (Kirmiz et al., 2020). A comprehensive genomic diversity study reported that *Akkermansia* in the human gut can be divided into five candidate species (Karcher et al., 2021), of which the Amuc IV phylogroup was considered to contain two candidate species in this study. This is roughly the same as our findings.

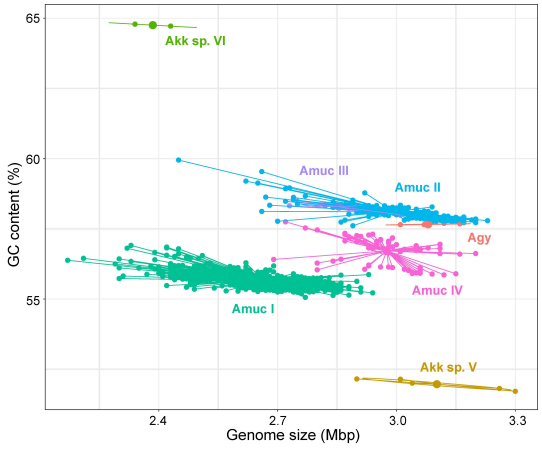

FIGURE 3
Scatter plot of the genome size and GC content of seven *Akkermansia* species and phylogroups.

Global distribution of *Akkermansia* phylogroups

The 1,211 *Akkermansia* genomes with wide distribution in 22 countries allowed us to investigate the biogeographical features of phylogroups. Also, to compare the differences between Western and non-Western populations, we define four Asian countries (China, Kazakhstan, Mongolia, and Israel) as non-Western and the rest as Western. We found that the two most dominant phylogroups, Amuc I and II, were extensively distributed globally (Figures 4A, B). Members of Amuc I and II were observed in trans-continental, trans-oceanic, cross-lifestyle populations and even appeared across-host considering that all non-human *A. muciniphila* isolates were placed in these two phylogroups. Amuc II, especially, had a higher intra-phylogroup genetic diversity in the Western populations compared to that of non-Western populations (Figure 4C). On the other hand, the geographic bias of Amuc III and IV was more prominent (Figure 4A; Figure S4). Moreover, 83.3% (five out of six) of the Amuc III genomes were from the gut microbiotas in a Chinese population and only one genome was from a European population. Conversely, all 69 genomes of Amuc IV were from Europe, the USA, Canada, and Israel, rather than from China or other countries. Moreover, the distributional modes of *Akkermansia* sp. V, *Akkermansia* sp. VI, and *A. glycaniphila* were still hard to accurately estimate due to the few numbers of genomes; however, all these species showed trans-continental distribution (Figure S4).

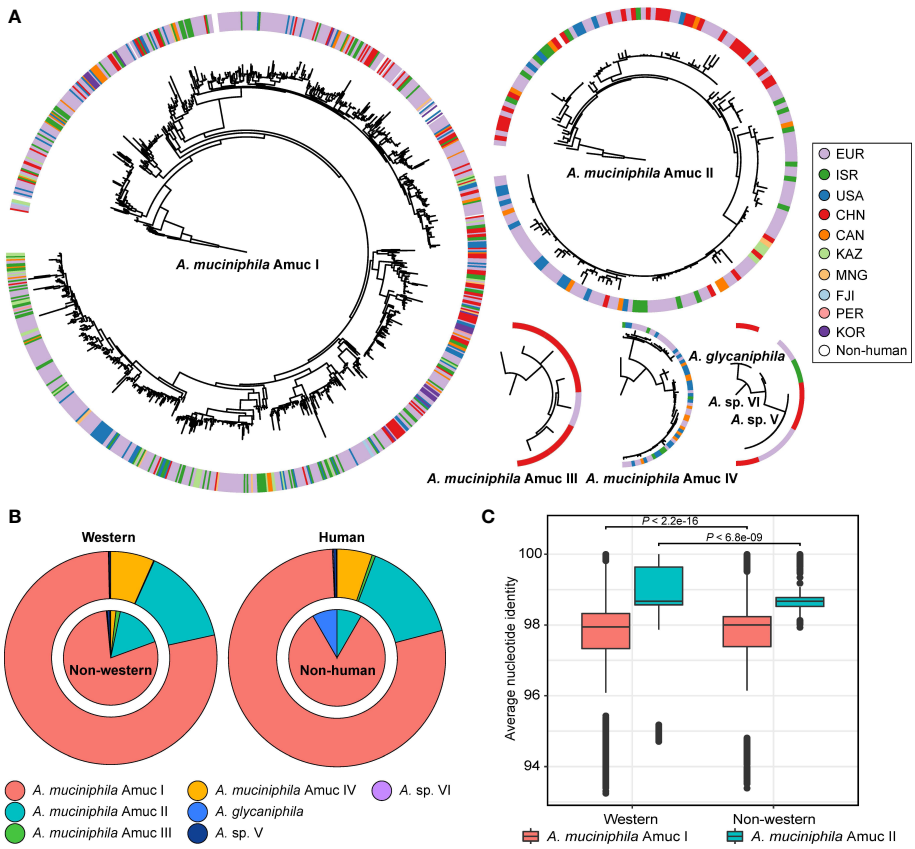

FIGURE 4
Geographic and host source of seven *Akkermansia* species and phylogroups. **(A)** Phylogenetic characteristics of *Akkermansia* species and phylogroups, with circles representing the national origin of each strain. **(B)** The distribution of *Akkermansia* species and phylogroups in Western and non-Western populations (left panel) and human and non-human hosts (right panel). **(C)** Boxplot shows the intra-phylogroup ANI comparisons between Western and non-Western strains.

In recent years, the geographic deviation among different subspecies has been described in several gut bacteria such as *Prevotella copri* (Tett et al., 2019) and *Eubacterium rectale* (Karcher et al., 2020). These findings suggested that not only the geographical factor but also other unknown factors (e.g., diet difference between populations (Cheng et al., 2021; Díez-Sainz et al., 2022), or movement of individuals) are probably the forces for speciation of the gut bacteria. Similarly, except for Amuc III, Amuc I, II, and IV were observed in the gut microbiota of American children in the study of Kirmiz et al. (2020).

Functional characteristics of *Akkermansia* phylogroups

It is possible that each *Akkermansia* phylogroup has a unique functional profile. To test this notion, we annotated all genomes using the KEGG database (Kanehisa et al., 2021) and identified a total of 1,740 KEGG orthologs (KOs). PCoA analysis based on the KO profiles revealed a clear separation among three major phylogroups (Amuc I, II, and IV; adonis $R^2 > 0.25$, $q < 0.001$ in pairwise comparison) (Figure 5A), while the functions of Amuc III strains were relatively close to Amuc II but were still significantly different (adonis $R^2 = 0.058$, $q = 0.001$). Likewise, the functions of *A. glycaniphila* and *Akkermansia* sp. V genomes were close to that of Amuc IV. We then compared the presence of KOs for three representative phylogroups (Amuc I, II, and IV) to identify the phylogroup-specific functions for them. In terms of pan-genome (KOs that occurred in at least one strain), the three phylogroups shared 1,141 functions, while 186, 66, and 55 functions especially occurred in Amuc I, II, and IV, respectively (Figure 5B). The Amuc I-specific functions were involved in the pathways of transporters (14 KOs), prokaryotic defense system (14 KOs), transcription factors (9 KOs), etc. (Supplement Table ST3), while the Amuc II-specific functions

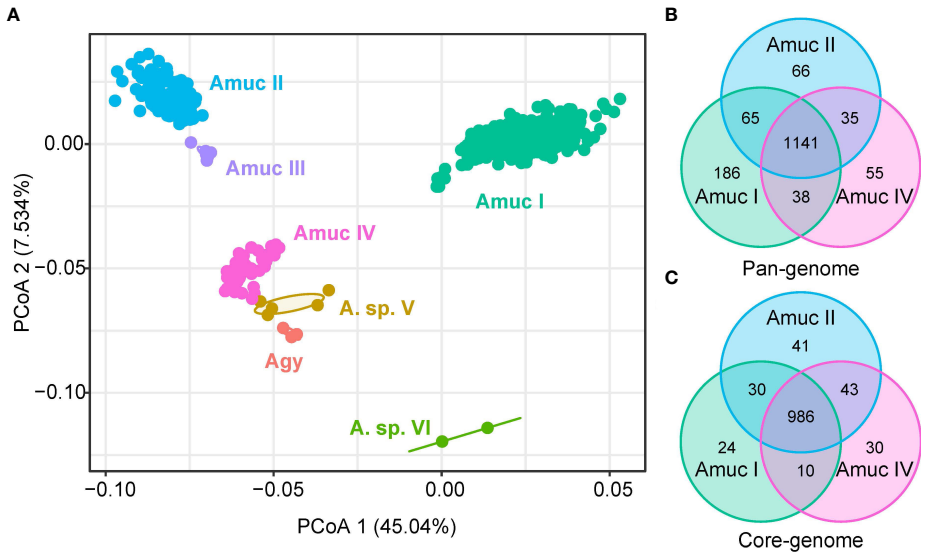

FIGURE 5
Comparison of KEGG functions among *Akkermansia* species and phylogroups. **(A)** PCoA analysis on the KO profiles of 1,211 strains. **(B, C)** Venn diagram shows the overlap of KOs in the pan-genome **(B)** and core-genome **(C)** of Amuc I, Amuc II, and Amuc IV.

were related to transporters (6 KOs) and ABC transporters (6 KOs), peptidases and inhibitors (4 KOs), and others. The Amuc IV-specific functions were involved in pathways of transporters (6 KOs), two-component systems (4 KOs), peptidases and inhibitors (3 KOs), and others. In terms of core-genome (KOs that occurred in >90% of the strains), the three phylogroups shared 986 core functions, while 24, 41, and 30 functions especially occurred in Amuc I, II, and IV, respectively (Figure 5C). In terms of transport pathways, Amuc I-specific KOs mainly involve iron complex transporters, for example, K02016 and K02015. These substrate-binding proteins are usually involved in the transmembrane transport of iron, while Amuc IV-specific KOs participate in organic acid transporters, such as K08191. This is a hexuronate transporter, involved in the carbohydrate metabolic pathway of bacteria. These metabolic pathways are highly diverse in different species of bacteria (Rodionova et al., 2012). Therefore, the functions of these specific codes may suggest differences in energy utilization among different *Akkermansia* phylogroups. In other words, these phylogroup-specific functions were involved in multiple metabolism and transport pathways and potentially associated with the specific adaption mechanism for different *Akkermansia* phylogroups (Supplement Table ST3). In addition, functional differences between groups may be examples of the adaptive evolution of *Akkermansia*. For example, some subspecies lack the ability to make vitamin B_{12} (Karcher et al., 2021), which allows them to interact better with other species in the gut.

In order to further investigate the ability of carbohydrate formation and decomposition of *Akkermansia* species, the genomes were screened for carbohydrate-active enzymes (CAZymes) (Zhang et al., 2018). Notably, a remarkable separation was observed on the CAZyme profiles among members of Amuc I and II–IV (adonis $R^2 = 0.56$, $q < 0.001$; Figure 6A), while the strains of Amuc II, III, and IV were relatively closer. Compared to Amuc II–IV, strains of Amuc I had a fewer number of carbohydrate-active enzymes ($p < 0.001$; Figure 6B) and especially glycosyltransferase (GT) and glycoside hydrolase (GH) proteins ($p < 0.001$; Figure 6C). GT proteins are mostly related to protein glycosylation, cell wall polysaccharide synthesis, or synthesizing exopolysaccharides in the context of biofilm formation (Lairson et al., 2008). This may represent the adaptability of the strains of Amuc II–IV phylogroups to the synthesis of exopolysaccharides or other structural carbohydrates. Moreover, 13 CAZymes were specifically encoded in the pan-genome of Amuc I, while 6 CAZymes were specifically encoded in the genomes of Amuc II–IV members. Interestingly, glycosyl transferase family 61 (GT61, occurred in 98.6% of Amuc IV strains but none in others) and glycoside hydrolase family 130 (GH130, occurred in 78.3% of Amuc IV strains but none in others) were specifically encoded by Amuc IV (Figure 6D; Supplement Table ST4). The GT61 family involved in the synthesis of cell wall xylans is often reported in plant cells (Cenci et al., 2018). These MAGs mainly encode two enzymes (SVE69682.1 and SVE78114.1) of the GT61 family. Interestingly, this family is uncommon in prokaryotes, and as a result, it may indicate that

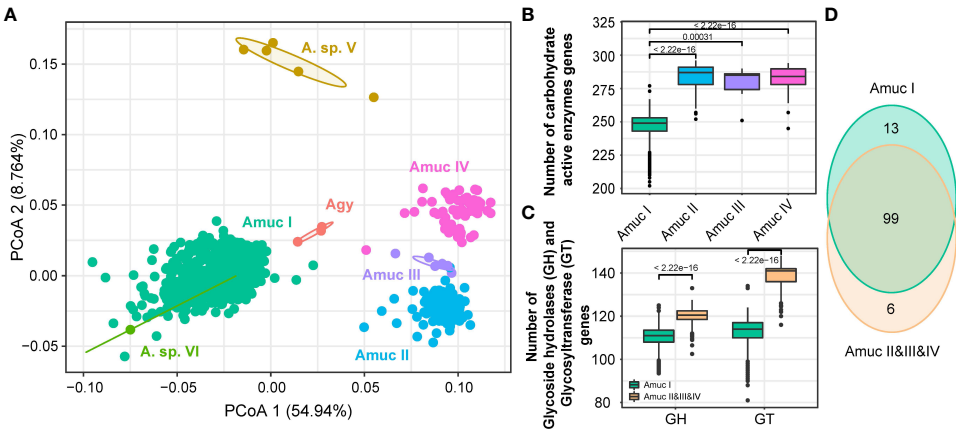

FIGURE 6
Comparison of CAZy functions among *Akkermansia* species and phylogroups. **(A)** PCoA analysis on the CAZymes families of 1,211 strains. **(B, C)** Boxplot showed the content comparison of CAZy enzyme-related genes annotated by the four phylogroups **(B)** and glycosyltransferase (GT) gene content between Amuc I and Amuc II–IV **(C)**; significance was calculated using the rank-sum test. **(D)** Venn diagram shows the overlap of CAZyme families between Amuc I and Amuc II–IV.

the cell wall composition of Amuc IV members is different from that of other phylogroups. The isolation of this type of strain in future studies will help us further understand the role of these enzymes. Similarly, GH130 might potentially provide the ability of mannose hydrolysis for Amuc IV members (Saburi, 2016), and this phenomenon may be correlated to the geographical distribution differences of the Amuc IV phylogroup. In brief, the difference in functional profiles among *Akkermansia* phylogroups may have relativity to their ability for utilizing complex carbohydrates.

In addition, we were concerned about the gene copy number of mucin-degrading GHs in each phylogroup. A total of eight mucin degradation-related GH families were annotated in all genomes (Figure 7). *Akkermansia* sp. VI has the least copy number compared to the other groups, and GH89 and GH95 were absent in these genomes. Compared with Amuc I, Amuc II, III, IV, *Akkermansia* sp. V, and Agy had higher gene copies in GH2, GH20, GH29, and GH95, most notably *Akkermansia* sp. V, which had relatively higher copy numbers on multiple mucin-associated GH. This difference may indicate the carbohydrate preference of each phylogroup strain. *Akkermansia* can degrade mucin into acetic acid and propionic acid, from which it can obtain energy (Kim et al., 2021). The diversity of mucin-related enzymes in *Akkermansia* may indicate that different groups metabolize mucin in different ways. However, we can provide

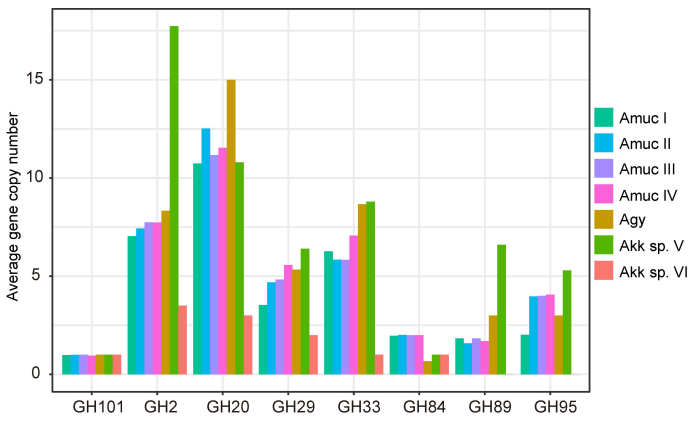

FIGURE 7
Average number of gene copies in each phylogroup of the eight mucin-degrading GH families.

only limited genomic evidence. In future studies, we need to obtain more culturable strains to test this hypothesis.

Assembly of the genome of *Akkermansia glycaniphila* strain from human

GP37 is a strain of *A. glycaniphila* isolated and cultured from human feces. The genome assembly of this strain was assembled by whole-genome sequencing. Its genome size is 3.01 Mbp and has 2,554 genes, its GC content is 57.65%, its completeness is 94.56%, and its contamination rate is zero (Supplement Table ST2). The genome of GP37 contains 13 contigs and the N50 length is 663,974bp, which means that GP37 is a high-quality genome assembly. ANI is commonly used to describe the consistency between the genomes of strains and species. GP37 had greater than 98% ANI with other *A. glycaniphila* genomes (GCF_900097105.1_WK001 and GCF_001683795.1_ASM168379v1), suggesting that they are highly similar strains (Figure S5). In addition, GP37 encodes 270 predictive CAZymes, including 106 glycosyl transferases and 118 glycosyl hydrolases, indicating its role in energy metabolism.

Conclusions

This study characterized the phylogeographic population structure and functional specificity of *Akkermansia* based on 1,126 near-complete MAGs and 85 isolated genomes. The *Akkermansia* genomes were placed into two previously isolated species (*A. muciniphila* and *A. glycaniphila*), and the *A. muciniphila* members were further divided into three previously described phylogroups (Amuc I, II, III, and IV). These species and phylogroups revealed a significant geographical distribution bias; especially, Amuc III was present in the Chinese population and Amuc IV was mainly distributed in Western populations. Functional analyses showed notable specificity in different *Akkermansia* species and phylogroups that were involved in some metabolism and transport pathways and in carbohydrate-active enzymes. In conclusion, our results showed that the *Akkermansia* members in the human gut had high genomic diversity and functional specificity and diverse geographical distribution characteristics.

Data availability statement

The datasets presented in this study can be found in online repositories. The names of the repository/repositories and accession number(s) can be found below: https://www.ncbi.nlm.nih.gov/bioproject/PRJNA662466.

Ethics statement

The studies involving human participants were reviewed and approved by the Ethics Committee of Zhujiang Hospital of Southern Medical University (2014-JYYXB-009). The patients/participants provided their written informed consent to participate in this study. Written informed consent was obtained from the individual(s) for the publication of any potentially identifiable images or data included in this article.

Author contributions

X-XZ, YP, Q-BL, and SL conducted the study. Q-BL, SL, and YZ performed the bioinformatic analyses. X-XZ, Y-CW, YP, Q-BL, and SL wrote and edited the manuscript. All authors read and approved the final manuscript.

Funding

This work was supported by the Research Foundation for Distinguished Scholars of Qingdao Agricultural University (665-1120044).

Conflict of interest

The authors declare that the research was conducted in the absence of any commercial or financial relationships that could be construed as a potential conflict of interest.

Publisher's note

Supplementary material

The Supplementary Material for this article can be found online at: https://www.frontiersin.org/articles/10.3389/fcimb.2022.957439/full#supplementary-material

References

Alikhan, N.-F., Petty, N. K., Ben Zakour, N. L., and Beatson, S. A. (2011). BLAST ring image generator (BRIG): simple prokaryote genome comparisons. *BMC Genomics* 12, 402. doi: 10.1186/1471-2164-12-402

Almeida, A., Nayfach, S., Boland, M., Strozzi, F., Beracochea, M., Shi, Z. J., et al. (2021). A unified catalog of 204,938 reference genomes from the human gut microbiome. *Nat. Biotechnol.* 39, 105–114. doi: 10.1038/s41587-020-0603-3

Belzer, C., and de Vos, W. M. (2012). Microbes inside–from diversity to function: the case of akkermansia. *Isme J.* 6, 1449–1458. doi: 10.1038/ismej.2012.6

Bian, X., Wu, W., Yang, L., Lv, L., Wang, Q., Li, Y., et al. (2019). Et al: Administration of akkermansia muciniphila ameliorates dextran sulfate sodium-induced ulcerative colitis in mice. *Front. Microbiol.* 10, 2259. doi: 10.3389/fmicb.2019.02259

Buchfink, B., Xie, C., and Huson, D. H. (2015). Fast and sensitive protein alignment using DIAMOND. *Nat. Methods* 12, 59–60. doi: 10.1038/nmeth.3176

Cani, P. D., Depommier, C., Derrien, M., Everard, A., and de Vos, W. M. (2022). Akkermansia muciniphila: paradigm for next-generation beneficial microorganisms. *Nat. Rev. Gastroenterol. Hepatol*. doi: 10.1038/s41575-022-00631-9

Cenci, A., Chantret, N., and Rouard, M. (2018). Glycosyltransferase family 61 in liliopsida (Monocot): The story of a gene family expansion. *Front. Plant Sci.* 9, 1843. doi: 10.3389/fpls.2018.01843

Cheng, T., Li, C., Shen, L., Wang, S., Li, X., Fu, C., et al. (2021). The intestinal effect of atorvastatin: Akkermansia muciniphila and barrier function. *Front. Microbiol.* 12, 797062. doi: 10.3389/fmicb.2021.797062

Dao, M. C., Everard, A., Aron-Wisnewsky, J., Sokolovska, N., Prifti, E., Verger, E. O., et al. (2016). Akkermansia muciniphila and improved metabolic health during a dietary intervention in obesity: relationship with gut microbiome richness and ecology. *Gut* 65, 426–436. doi: 10.1136/gutjnl-2014-308778

Depommier, C., Everard, A., Druart, C., Plovier, H., Van Hul, M., Vieira-Silva, S., et al. (2019). Supplementation with akkermansia muciniphila in overweight and obese human volunteers: a proof-of-concept exploratory study. *Nat. Med.* 25, 1096–1103. doi: 10.1038/s41591-019-0495-2

Derrien, M., Belzer, C., and de Vos, W. M. (2017). Akkermansia muciniphila and its role in regulating host functions. *Microb. Pathog.* 106, 171–181. doi: 10.1016/j.micpath.2016.02.005

Derrien, M., van Passel, M. W., van de Bovenkamp, J. H., Schipper, R. G., de Vos, W. M., and Dekker, J. (2010). Mucin-bacterial interactions in the human oral cavity and digestive tract. *Gut Microbes* 1, 254–268. doi: 10.4161/gmic.1.4.12778

Derrien, M., Vaughan, E. E., Plugge, C. M., and de Vos, W. M. (2004). Akkermansia muciniphila gen. nov., sp. nov., a human intestinal mucin-degrading bacterium. *Int. J. Syst. Evol. Microbiol.* 54, 1469–1476. doi: 10.1099/ijs.0.02873-0

Díez-Sainz, E., Milagro, F. I., Riezu-Boj, J. I., and Lorente-Cebrián, S. (2022). Effects of gut microbiota-derived extracellular vesicles on obesity and diabetes and their potential modulation through diet. *J. Physiol. Biochem.* 78, 485–499. doi: 10.1007/s13105-021-00837-6

Edgar, R. C. (2010). Search and clustering orders of magnitude faster than BLAST. *Bioinformatics* 26, 2460–2461. doi: 10.1093/bioinformatics/btq461

Falony, G., Joossens, M., Vieira-Silva, S., Wang, J., Darzi, Y., Faust, K., et al. (2016). Population-level analysis of gut microbiome variation. *Science* 352, 560–564. doi: 10.1126/science.aad3503

Geerlings, S. Y., Kostopoulos, I., de Vos, W. M., and Belzer, C. (2018). Akkermansia muciniphila in the human gastrointestinal tract: When, where, and how? *Microorganisms* 6, 75. doi: 10.3390/microorganisms6030075

Guo, X., Li, S., Zhang, J., Wu, F., Li, X., Wu, D., et al. (2017). Genome sequencing of 39 akkermansia muciniphila isolates reveals its population structure, genomic and functional diverisity, and global distribution in mammalian gut microbiotas. *BMC Genomics* 18, 800. doi: 10.1186/s12864-017-4195-3

Hagi, T., and Belzer, C. (2021). The interaction of akkermansia muciniphila with host-derived substances, bacteria and diets. *Appl. Microbiol. Biotechnol.* 105, 4833–4841. doi: 10.1007/s00253-021-11362-3

Hasani, A., Ebrahimzadeh, S., Hemmati, F., Khabbaz, A., Hasani, A., and Gholizadeh, P. (2021). The role of akkermansia muciniphila in obesity, diabetes and atherosclerosis. *J. Med. Microbiol.* 70(10):001435. doi: 10.1099/jmm.0.001435

Hyatt, D., Chen, G. L., Locascio, P. F., Land, M. L., Larimer, F. W., and Hauser, L. J. (2010). Prodigal: prokaryotic gene recognition and translation initiation site identification. *BMC Bioinf.* 11, 119. doi: 10.1186/1471-2105-11-119

Jain, C., Rodriguez, R. L., Phillippy, A. M., Konstantinidis, K. T., and Aluru, S. (2018). High throughput ANI analysis of 90K prokaryotic genomes reveals clear species boundaries. *Nat. Commun.* 9, 5114. doi: 10.1038/s41467-018-07641-9

Kanehisa, M., Furumichi, M., Sato, Y., Ishiguro-Watanabe, M., and Tanabe, M. (2021). KEGG: integrating viruses and cellular organisms. *Nucleic Acids Res.* 49, D545–d551. doi: 10.1093/nar/gkaa970

Karcher, N., Nigro, E., Punčochář, M., Blanco-Míguez, A., Ciciani, M., Manghi, P., et al. (2021). Genomic diversity and ecology of human-associated akkermansia species in the gut microbiome revealed by extensive metagenomic assembly. *Genome Biol.* 22, 209. doi: 10.1186/s13059-021-02427-7

Karcher, N., Pasolli, E., Asnicar, F., Huang, K. D., Tett, A., Manara, S., et al. (2020). Analysis of 1321 eubacterium rectale genomes from metagenomes uncovers complex phylogeographic population structure and subspecies functional adaptations. *Genome Biol.* 21, 138. doi: 10.1186/s13059-020-02042-y

Kim, S., Shin, Y. C., Kim, T. Y., Kim, Y., Lee, Y. S., Lee, S. H., et al. (2021). Mucin degrader akkermansia muciniphila accelerates intestinal stem cell-mediated epithelial development. *Gut Microbes* 13, 1–20. doi: 10.1080/19490976.2021.1892441

Kirmiz, N., Galindo, K., Cross, K. L., Luna, E., Rhoades, N., Podar, M., et al. (2020). Comparative genomics guides elucidation of vitamin B(12) biosynthesis in novel human-associated akkermansia strains. *Appl. Environ. Microbiol.* 86(3): e02117–19. doi: 10.1128/AEM.02117-19

Lagesen, K., Hallin, P., Rødland, E. A., Staerfeldt, H. H., Rognes, T., and Ussery, D. W. (2007). RNAmmer: consistent and rapid annotation of ribosomal RNA genes. *Nucleic Acids Res.* 35, 3100–3108. doi: 10.1093/nar/gkm160

Lairson, L. L., Henrissat, B., Davies, G. J., and Withers, S. G. (2008). Glycosyltransferases: structures, functions, and mechanisms. *Annu. Rev. Biochem.* 77, 521–555. doi: 10.1146/annurev.biochem.76.061005.092322

Letunic, I., and Bork, P. (2016). Interactive tree of life (iTOL) v3: an online tool for the display and annotation of phylogenetic and other trees. *Nucleic Acids Res.* 44, W242–W245. doi: 10.1093/nar/gkw290

Ley, R. E., Hamady, M., Lozupone, C., Turnbaugh, P. J., Ramey, R. R., Bircher, J. S., et al. (2008). Evolution of mammals and their gut microbes. *Science* 320, 1647–1651. doi: 10.1126/science.1155725

Ley, R. E., Lozupone, C. A., Hamady, M., Knight, R., and Gordon, J. I. (2008). Worlds within worlds: evolution of the vertebrate gut microbiota. *Nat. Rev. Microbiol.* 6, 776–788. doi: 10.1038/nrmicro1978

Ouwerkerk, J. P., Aalvink, S., Belzer, C., and de Vos, W. M. (2016). Akkermansia glycaniphila sp. nov., an anaerobic mucin-degrading bacterium isolated from reticulated python faeces. *Int. J. Syst. Evol. Microbiol.* 66, 4614–4620. doi: 10.1099/ijsem.0.001399

Ouwerkerk, J. P., Koehorst, J. J., Schaap, P. J., Ritari, J., Paulin, L., Belzer, C., et al. (2017). Complete genome sequence of akkermansia glycaniphila strain PytT, a mucin-degrading specialist of the reticulated Python gut. *Genome Announc.* 5(1): e01098–16. doi: 10.1128/genomeA.01098-16

Parks, D. H., Imelfort, M., Skennerton, C. T., Hugenholtz, P., and Tyson, G. W. (2015). CheckM: assessing the quality of microbial genomes recovered from isolates, single cells, and metagenomes. *Genome Res.* 25, 1043–1055. doi: 10.1101/gr.186072.114

Pascale, A., Marchesi, N., Govoni, S., Coppola, A., and Gazzaruso, C. (2019). The role of gut microbiota in obesity, diabetes mellitus, and effect of metformin: new insights into old diseases. *Curr. Opin. Pharmacol.* 49, 1–5. doi: 10.1016/j.coph.2019.03.011

Pasolli, E., Asnicar, F., Manara, S., Zolfo, M., Karcher, N., Armanini, F., et al. (2019). Extensive unexplored human microbiome diversity revealed by over 150,000 genomes from metagenomes spanning age, geography, and lifestyle. *Cell* 176, 649–662.e620. doi: 10.1016/j.cell.2019.01.001

Presley, L. L., Wei, B., Braun, J., and Borneman, J. (2010). Bacteria associated with immunoregulatory cells in mice. *Appl. Environ. Microbiol.* 76, 936–941. doi: 10.1128/AEM.01561-09

Rodionova, I. A., Scott, D. A., Grishin, N. V., Osterman, A. L., and Rodionov, D. A. (2012). Tagaturonate-fructuronate epimerase UxaE, a novel enzyme in the hexuronate catabolic network in thermotoga maritima. *Environ. Microbiol.* 14, 2920–2934. doi: 10.1111/j.1462-2920.2012.02856.x

Saburi, W. (2016). Functions, structures, and applications of cellobiose 2-epimerase and glycoside hydrolase family 130 mannoside phosphorylases. *Biosci. Biotechnol. Biochem.* 80, 1294–1305. doi: 10.1080/09168451.2016.1166934

Seemann, T. (2014). Prokka: rapid prokaryotic genome annotation. *Bioinformatics* 30, 2068–2069. doi: 10.1093/bioinformatics/btu153

Segata, N., Börnigen, D., Morgan, X. C., and Huttenhower, C. (2013). PhyloPhlAn is a new method for improved phylogenetic and taxonomic placement of microbes. *Nat. Commun.* 4, 2304. doi: 10.1038/ncomms3304

Tett, A., Huang, K. D., Asnicar, F., Fehlner-Peach, H., Pasolli, E., Karcher, N., et al. (2019). The prevotella copri complex comprises four distinct clades underrepresented in westernized populations. *Cell Host Microbe* 26, 666–679.e667. doi: 10.1016/j.chom.2019.08.018

van der Lugt, B., van Beek, A. A., Aalvink, S., Meijer, B., Sovran, B., Vermeij, W. P., et al. (2019). Akkermansia muciniphila ameliorates the age-related decline in colonic mucus thickness and attenuates immune activation in accelerated aging Ercc1 (-/Δ7) mice. *Immun. Ageing I A* 16, 6–6. doi: 10.1186/s12979-019-0145-z

van Passel, M. W., Kant, R., Zoetendal, E. G., Plugge, C. M., Derrien, M., Malfatti, S. A., et al. (2011). The genome of akkermansia muciniphila, a dedicated intestinal mucin degrader, and its use in exploring intestinal metagenomes. *PloS One* 6, e16876. doi: 10.1371/journal.pone.0016876

Wickham, H. (2016). *ggplot2: Elegant Graphics for Data Analysis.* (Cham: Springer), 189–201

Xing, J., Li, X., Sun, Y., Zhao, J., Miao, S., Xiong, Q., et al. (2019). Comparative genomic and functional analysis of akkermansia muciniphila and closely related species. *Genes Genomics* 41, 1253–1264. doi: 10.1007/s13258-019-00855-1

Yu, Y., Lu, J., Sun, L., Lyu, X., Chang, X. Y., Mi, X., et al. (2021). Akkermansia muciniphila: A potential novel mechanism of nuciferine to improve hyperlipidemia. *BioMed. Pharmacother.* 133, 111014. doi: 10.1016/j.biopha.2020.111014

Zhai, Q., Feng, S., Arjan, N., and Chen, W. (2019). A next generation probiotic, akkermansia muciniphila. *Crit. Rev. Food Sci. Nutr.* 59, 3227–3236. doi: 10.1080/10408398.2018.1517725

Zhang, J., Ni, Y., Qian, L., Fang, Q., Zheng, T., Zhang, M., et al. (2021). Decreased abundance of akkermansia muciniphila leads to the impairment of insulin secretion and glucose homeostasis in lean type 2 diabetes. *Adv. Sci. (Weinh)* 8, e2100536. doi: 10.1002/advs.202100536

Zhang, H., Yohe, T., Huang, L., Entwistle, S., Wu, P., Yang, Z., et al. (2018). dbCAN2: a meta server for automated carbohydrate-active enzyme annotation. *Nucleic Acids Res.* 46, W95–w101. doi: 10.1093/nar/gky418

Zhu, J., Tian, L., Chen, P., Han, M., Song, L., Tong, X., et al. (2021). Over 50,000 metagenomically assembled draft genomes for the human oral microbiome reveal new taxa. *Genomics Proteomics Bioinf.* doi: 10.1016/j.gpb.2021.05.001

frontiers | Frontiers in Cellular and Infection Microbiology

TYPE Original Research
PUBLISHED 14 September 2022
DOI 10.3389/fcimb.2022.988355

OPEN ACCESS

EDITED BY
Fangfeng Yuan,
University of Illinois at Urbana-Champaign, United States

REVIEWED BY
Tao Lin,
InnovHope, United States
Yuekun Lang,
Albert Einstein College of Medicine, United States
Jiexiong Xie,
Janssen Research and Development, Belgium

*CORRESPONDENCE
Yanhua Li
007206@yzu.edu.cn

†These authors have contributed equally to this work

SPECIALTY SECTION
This article was submitted to Clinical Microbiology, a section of the journal Frontiers in Cellular and Infection Microbiology

RECEIVED 07 July 2022
ACCEPTED 22 August 2022
PUBLISHED 14 September 2022

CITATION
Ding J, Yang J, Jiang D, Zhou Y, Li C and Li Y (2022) Development of a highly sensitive Gaussia luciferase immunoprecipitation assay for the detection of antibodies against African swine fever virus.
Front. Cell. Infect. Microbiol. 12:988355.
doi: 10.3389/fcimb.2022.988355

Development of a highly sensitive Gaussia luciferase immunoprecipitation assay for the detection of antibodies against African swine fever virus

Jingjing Ding[1†], Jifei Yang[2†], Daoyuan Jiang[1], Yanyang Zhou[1], Chenxi Li[1,3,4] and Yanhua Li[1,3,4*]

[1]College of Veterinary Medicine, Yangzhou University, Yangzhou, China, [2]African Swine Fever Regional Laboratory of China (Lanzhou), State Key Laboratory of Veterinary Etiological Biology, Lanzhou Veterinary Research Institute, Chinese Academy of Agricultural Sciences, Lanzhou, China, [3]Comparative Medicine Research Institute, Yangzhou University, Yangzhou, China, [4]Jiangsu Co-Innovation Center for Prevention and Control of Important Animal Infectious Diseases and Zoonoses, Yangzhou, China

In recent years, African swine fever (ASF) has caused a devastating blow to the swine industry globally. Since no effective vaccine is available, strict biosafety measures and rapid diagnosis are the most effective strategies for ASF control. ASFV p30 is one of the most antigenic viral proteins that have been widely used in the field for serological diagnosis of ASF infection. In this study, we developed a luciferase immunoprecipitation system (LIPS) assay for the detection of ASFV antibodies in pig serum using Gaussia luciferase (GLuc)-tagged p30 as a diagnostic antigen. The optimal GLuc-p30 input of 10^7 luminance units (LU) and optimal serum dilution factor of 1/100 were set to achieve the highest P/N ratio. Based on 87 ASFV-positive and negative pig sera, the cutoff value of the S/N ratio could be set between 2.298 and 30.59 to achieve 100% sensitivity and 100% specificity. Moreover, the diagnostic sensitivity of this LIPS is comparable to that of a commercial enzyme-linked immunosorbent assay (ELISA) and the specificity of LIPS is even superior to the tested ELISA. In conclusion, we have established a LIPS assay for ASFV antibody detection, which could be a potential method for ASFV diagnosis in laboratories and farms.

KEYWORDS

African swine fever virus, luciferase immunoprecipitation system, gaussia luciferase, p30, p54, Serological diagnosis

Introduction

African swine fever (ASF) is an acute, hemorrhagic, and highly contagious swine disease caused by the African swine fever virus (ASFV) which is the only arthropod-borne DNA virus in the *Asfarviridae* family. It was first diagnosed in Kenya in 1909 and reported as a swine disease with clinical symptoms indistinguishable from those of classical swine fever (CSF) in 1921 (Cwynar et al., 2019). On August 3, 2018, ASF emerged in the Liaoning province of China and gradually spread in this largest pig-producing and pork-consuming country in the world (Zhou et al., 2018). It is listed as one of the notifiable diseases by the World Organization for Animal Health (OIE) and is also recognized as a class I animal epidemic disease in China (Blome et al., 2020). The ASFV genome is about 170-190 kb in length and encodes more than 150 open reading frames (ORFs). ASFV can be classified according to their virulence into high pathogenicity, medium virulence, low virulence, and asymptomatic infection strains. The highly pathogenic viral infection caused almost 100% morbidity and mortality (Wang et al., 2021). Due to its high morbidity and mortality, ASF causes devastating losses to the swine industry and has important socio-economic significance.

Lacking effective vaccines and antiviral treatments, ASF control attaches great importance to efficient diagnosis methods of ASFV (Wu et al., 2020). ASFV-specific antibodies appear soon after infection and can persist in convalescent animals for months to years (Gallardo et al., 2019). Recently, the low virulent strains of genotype II ASFV and genotype I ASFV have been identified in domestic swine herds in China (Sun et al., 2021; Sun et al., 2021). In comparison with the prevalent high virulent strains, the low virulent variants cause mild and delayed clinical symptoms but can shed viruses *via* the oral and rectal routes (Sun et al., 2021). Diagnosis methods targeting viral antigens or DNA do not always guarantee the identification of infected animals with chronic or inapparent forms of the disease. Under this circumstance, the serological diagnosis would be more informative and important (Kazakova et al., 2017). The OIE recommended serological diagnostic methods for ASFV include indirect fluorescent antibody (IFA) test, indirect enzyme-linked immunosorbent assays (ELISA), immunoblotting test, or immunoperoxidase staining (https://www.woah.org/fileadmin/Home/eng/Health_standards/tahm/3.08.01_ASF.pdf). Although IFA shows great sensitivity, it is only suitable to be used as a confirmatory test due to its complicated procedure and time-consuming (Wu et al., 2020). Many commercialized ELISA tests have been widely used for ASFV serological diagnosis, but their sensitivity is not comparable to IFA. Currently, it is urgent to develop rapid, high-throughput, cost-effective, and easy-to-implement serological methods.

To date, several ASFV proteins have been explored as diagnostic targets for the development of ELISA assays, including p72, p54, p30, CD2v, and p35 (Perez-Filgueira et al., 2006; Gimenez-Lirola et al., 2016; Lv et al., 2021; Cao et al., 2021; Shi et al., 2021; Yu et al., 2021; Yuan et al., 2021; Zhao et al., 2022; Wang et al., 2022; Carmina et al., 2022). ASFV p30 is a phosphorylated structural protein encoded by the early gene *CP204L*. It is distributed in the inner membrane of viral particles with a size of 22.4 kDa (Afonso et al., 1992). Serological studies of ASFV by radioimmunoprecipitation showed that the virus-specific antibodies detected in sera during the early stage of viral infection (3 to 6 days after infection) were mainly specific to the p30 (Kazakova et al., 2017). Furthermore, p30 demonstrates a high degree of antigenic conservation among virus strains in different geographic locations, and it induced the production of antibodies in all naturally infected and experimentally infected pigs (Oviedo et al., 1997). Given these characteristics, p30 is an ideal diagnostic target for the early detection of ASFV infection. ASFV p54 encoded by the gene *E183L* was identified as a highly antigenic protein during infection (Cubillos et al., 2013). So, p54 is another attractive candidate for ASF detection.

The luciferase immunoprecipitation system (LIPS) is a liquid phase immunoassay that uses a luciferase-tagged antigen to capture antigen-specific antibodies (Burbelo et al., 2005). The luciferase-tagged antigens used for LIPS assay are usually produced in mammalian cells, allowing them to go through necessary post-translational modifications as well as proper folding and exposure of the antigenic epitopes. Due to the low natural background of bioluminescence, soluble crude cell lysates of the luciferase-tagged recombinant proteins can be extracted from transfected cells and used without purification (Haljasmagi et al., 2020). As a liquid-phase immunoassay, the antigens in their native conformation enable LIPS to detect antibodies against linear and conformational epitopes. When being mixed with the tested samples, the luciferase-tagged antigen will form immunocomplex with antigen-specific antibodies, which can be captured by Protein A/G conjugated beads. The activity of luciferase-tagged antigen captured by the beads is correlated with specific antibody responses. LIPS assays have been widely used for antibody detection in autoimmune and infectious diseases (Burbelo et al., 2015; Shabani Azim et al., 2016). Studies showed that the detection sensitivity of LIPS is higher than ELISA for profiling human norovirus antibodies (Tin et al., 2017). In this study, we established a *Gaussia luciferase* (GLuc) immunoprecipitation assay for the serological detection of ASFV infection based on the immunogenic viral protein p30. Based on the ROC curve analysis, when the cutoff value of S/N (sample/negative) is set as >2.298 and ≤30.59, this LIPS assay can perfectly identify ASFV infection. In addition, no cross-reactivity to other common swine pathogens was observed in our hands. Therefore, this newly developed LIPS for the rapid and easy detection of ASFV antibodies could serve as another promising assay for ASF diagnosis and ASFV antibody surveillance.

Materials and methods

Cells, antibodies, and reagents

HEK-293T cells from American Type Culture Collection (ATCC; Manassas, VA, USA) were maintained in Dulbecco's modified Eagle's medium (DMEM; Hyclone, Logan, UT, USA) supplemented with 10% fetal bovine serum (FBS; Sigma-Aldrich, St Louis, MO, USA) and 1% penicillin-streptomycin (Thermo Fisher Scientific Waltham, MA). Coelenterazine h (Maokang Biotechnology, Shanghai, China) was used for the gaussia luciferase assay. Mouse monoclonal antibody against FLAG-tag (MBL, Nagoya, Japan), HRP-conjugated goat anti-mouse IgG (Sangon Biotech, Shanghai, China), and GAPDH monoclonal antibody (Bioworld Technology, Nanjing, China) were used in Western blot analysis. Alexa Fluor® 488-conjugated goat anti-mouse IgG antibody (Jackson ImmunoResearch, West Grove, PA, USA) was used as the secondary antibody in the immunofluorescence assay.

Pig serum samples

Thirty-seven ASFV-positive serum samples were provided by the African Swine Fever Regional Laboratory of China (Lanzhou), Lanzhou Veterinary Research Institute, Chinese Academy of Agricultural Sciences. Forty pig serum samples collected before the ASF outbreak in China were used and considered as negative samples. All serum samples were inactivated at 60°C for 30 min before use. Serum samples collected from pigs infected with a specific pathogen were used to evaluate the diagnostic specificity of the GLuc-p30-based LIPS assay, including 5 porcine reproductive and respiratory syndrome virus-positive (Li et al., 2022), 2 classical swine fever virus-positive provided by Dr. Qin Wang from China Institute of Veterinary Drugs Control, 5 Senecavirus A-positive serum provided by Dr. Zuzhang Wei from Guangxi University, and 3 porcine delta coronavirus-positive and 2 porcine epidemic diarrhea virus-positive provided by Dr. Yongning Zhang from China Agriculture University.

Construction of plasmids expressing ASFV p30 and p54 fused with gaussia luciferase

The coding regions of *CP204L* (p30) and *E183L* (p54) from ASFV isolate Pig/HLJ/2018 (Genbank accession No. MK333180.1) were codon-optimized according to human codon usage, synthesized by Genscript (Nanjing, China), and cloned into pcDNA3.1(+)-P2A-eGFP vector, respectively. These two plasmids were digested with restriction enzymes *EcoR* V and *Xho* I, and the codon-optimized p30 and p54 genes were gel-purified and cloned into the pCAGGS-GLuc-FLAG vector using T4 DNA ligase (Vazyme Biochem, Nanjing, China). Finally, the plasmids for the expression of the fusion proteins, GLuc-p30 and GLuc-p54, were designated as pCAGGS-GLuc-p30 and pCAGGS-GLuc-p54 (Figure 2A). The correct insertion of p30 and p54 coding sequences was verified *via* DNA sequencing by Genscript (Nanjing, China).

The expression of GLuc-p30 and GLuc-p54 in HEK-293T cells

The plasmids containing the codon-optimized ASFV p30 and p54 were transfected into HEK-293T cells to express the fusion proteins, GLuc-p30 and GLuc-p54. Briefly, HEK-293T cells at 80% confluency in the 6-well tissue culture plate were DNA transfected with 2μg plasmid per well using Lipofactemin 2000 (Thermo Fisher Scientific Waltham, MA) according to the manufacturer's instructions. At 24, 48, and 72 hours post-transfection (hpt), culture supernatants were harvested, whereas cell lysates were harvested with IP lysis buffer (Biosharp, Hefei, China) supplemented with a protease inhibitor cocktail (Roche). Both culture supernatants and cell lysates were clarified by centrifugation at 12,000×g at 4°C for 10 min and then stored at -80°C. The expression of the fusion proteins was confirmed by gaussia luciferase assay, Western blot analysis, and immunofluorescence assay using a monoclonal antibody against the FLAG tag.

Western blot analysis

Cell lysates and culture supernatants harvested at 48 hpt were mixed with 5X sample loading buffer (Beyotime Biotech, Shanghai, China) and boiled at 95°C for 5 min. Denatured proteins were separated by sodium dodecyl sulfate-polyacrylamide gel electrophoresis (SDS-PAGE) in 12% Tris-glycine gels and transferred to a nitrocellulose membrane. The membrane was blocked with 5% skim milk in phosphate-buffered saline (PBS) at 4°C overnight and then incubated with the anti-FLAG antibody diluted at 1:10000 at room temperature (RT) for 1 h. After five washes with PBS-0.05% Tween 20 (PBST), the membrane was incubated with a goat anti-mouse horseradish peroxidase (HRP)-conjugated secondary antibody diluted at 1:5000 at RT for 1 h. After five washes in PBST, the targeted proteins were visualized with the ECL chemiluminescence substrate (Vazyme Biotech, Nanjing, China) using a Tanon 5200 Multi Imaging system (Tanon, Shanghai, China). In addition, glyceraldehyde-3-phosphate dehydrogenase (GAPDH) was detected as a loading control using a rabbit polyclonal antibody (HuaBio, Hangzhou, China).

Indirect immunofluorescence assay (IFA)

HEK-293T cells transfected with indicated plasmids in a six-well plate were fixed 48 hours post-transfection (hpt) with 4% (w/v) paraformaldehyde (PFA) in PBS for 20 min and then permeabilized with 0.1% (v/v) Triton X-100 for 10 min at RT. The cell monolayers were blocked with 1% bovine serum albumin (BSA) diluted in PBS for 30 min at RT. The mouse anti-FLAG antibody (MBL, Nagoya, Japan) diluted at 1:1000 was added to each well and incubated for 1 h at 37°C. After five washes with PBS, the cell monolayers were incubated with a goat anti-mouse IgG antibody conjugated with Alexa Fluor 488 at RT for 1 h. Following five washes with PBS, 4'6'-diamidino-2-phenylindole (DAPI) (Solarbio, Beijing, China) was added to stain the cell nucleus. The cell monolayers were observed under an inverted epifluorescence microscope IX73 (Olympus LS, Japan).

Gaussia luciferase assay

The gaussia luciferase assay was performed with coelenterazine h substrate (Maokang Biochem, Shanghai, China) as described previously (Zhou et al., 2022). The substrate was prepared by diluting coelenterazine h stock to 20 μM with PBS supplemented with 5 mM NaCl, pH 7.2, and incubated at RT in the dark for 30 min. To measure the gaussia activity, mix 50 μL of 20 μM coelenterazine h with 20 μL sample in a white plate and acquire photon counts for 10 sec using a SuPerMax 3000FL (Flash Spectrum Biological Technology, Shanghai, China) plate reader.

A GLuc-p30-based LIPS assay for ASFV antibody detection

As shown in Figure 1, pig serum samples at an appropriate dilution were mixed with an indicated amount of GLuc-p30 protein and incubated on a rotator at 4°C overnight. To capture the antigen and antibody complex, added 5 μL of Protein A MagBeads (GenScript, Nanjing, China) to each reaction and incubated at RT for 1 h. After being washed five times with PBST, the magnetic beads were collected with a Magnetic Separator Stand 96-I (BEAVER biomedical, Suzhou, China) and transferred to a white 96-well plate for the gaussia luciferase assay.

LIPS assay optimization

To get the optimum conditions of LIPS assay for ASFV antibody detection, one known ASFV-positive serum and one known ASFV-negative serum were used to check the signal-to-noise ratio that was calculated as P/N. The parameters tested with the highest P/N were chosen to set up the protocol for the LIPS assay. Initially, we optimized the input of GLuc-p30. Four different doses were tested, including 10^8, 10^7, 10^6, and 10^5 luminance units per reaction, and pig serum samples were diluted at 1:100. Next, the optimal dilution of serum samples for the LIPS assay was confirmed. A panel of serum dilutions was tested, including 1/50, 1/100, 1/200, 1/400, 1/800, 1/1600, and 1/3200, and the input of GLuc-p30 was 10^7 luminance units per reaction.

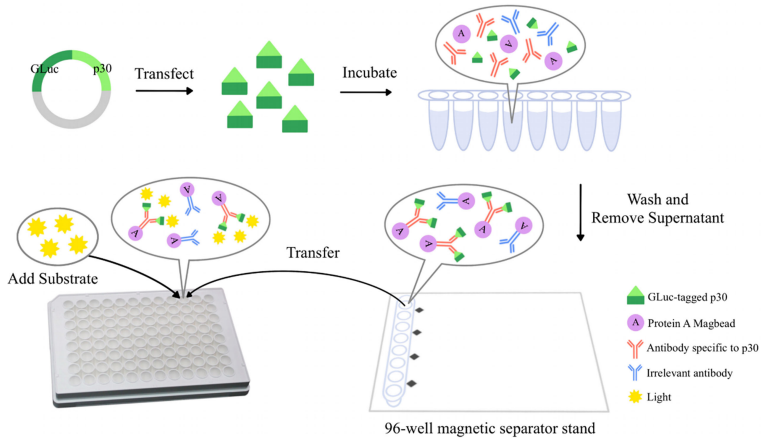

FIGURE 1
The schematic diagram of a GLuc immunoprecipitation assay for the detection of ASFV antibodies. The GLuc-p30 transiently expressed in HEK-293T cells is naturally secreted into the culture supernatant with the help of the GLuc secretory signal peptide. GLuc-p30 in culture supernatant is used directly for the GLuc immunoprecipitation assay without purification. Pig serum samples at appropriate dilution are mixed with GLuc-p30 and protein A Magbeads (Genscript, Nanjing, China) and then incubated in a rotator at 4 °C overnight. Magbeads are collected with a 96-well magnetic separator stand and washed extensively with PBST to remove the non-specific binding of GLuc-p30. Finally, the Magbeads are mixed with the substrate of GLuc to measure the luciferase activity of GLuc-p30 captured by p30-specific antibodies in the serum.

Determination of cutoff value for the LIPS assay

A total of 37 ASFV-positive and 40 ASFV-negative pig serum samples were utilized to determine the cutoff value for the LIPS assay. Serum samples were diluted at 1:100, and 10^7 luminance units of GLuc-p30 were used per reaction. We determined the optimal cutoff value with the receiver operating characteristic (ROC) curve using the GraphPad Prism version 9.1.1 (GraphPad Software, San Diego, CA, USA). In addition, the cutoff value was also calculated as the mean+2SD.

The diagnostic specificity of the LIPS assay

The diagnostic specificity of the GLuc-p30-based LIPS assay was evaluated with 17 pig serum samples collected from pigs infected with a specific pathogen as described in Pig serum samples.

Indirect ELISA for ASFV antibody detection

A commercial indirect ELISA kit (Yisen-Bio, Beijing, China) using p30 as a diagnostic antigen was used to detect ASFV antibodies in serum samples according to the manufacturer's instructions.

Results

The expression of GLuc-p30 and GLuc-p54 in HEK-293T cells

To generate recombinant proteins for the LIPS assay, two eukaryotic plasmids were constructed for the expression of GLuc-p30 and GLuc-p54, as illustrated in Figure 2A. These plasmids were transfected into HEK-293T cells to prepare the fusion proteins. As shown in Figure 2B, the expression of the fusion proteins was confirmed by IFA using anti-FLAG mAb at 48 hpt. Western blot analysis also detected the fusion proteins in cell lysates but not in the culture supernatants (Figure 2C). Since GLuc is a naturally secreted

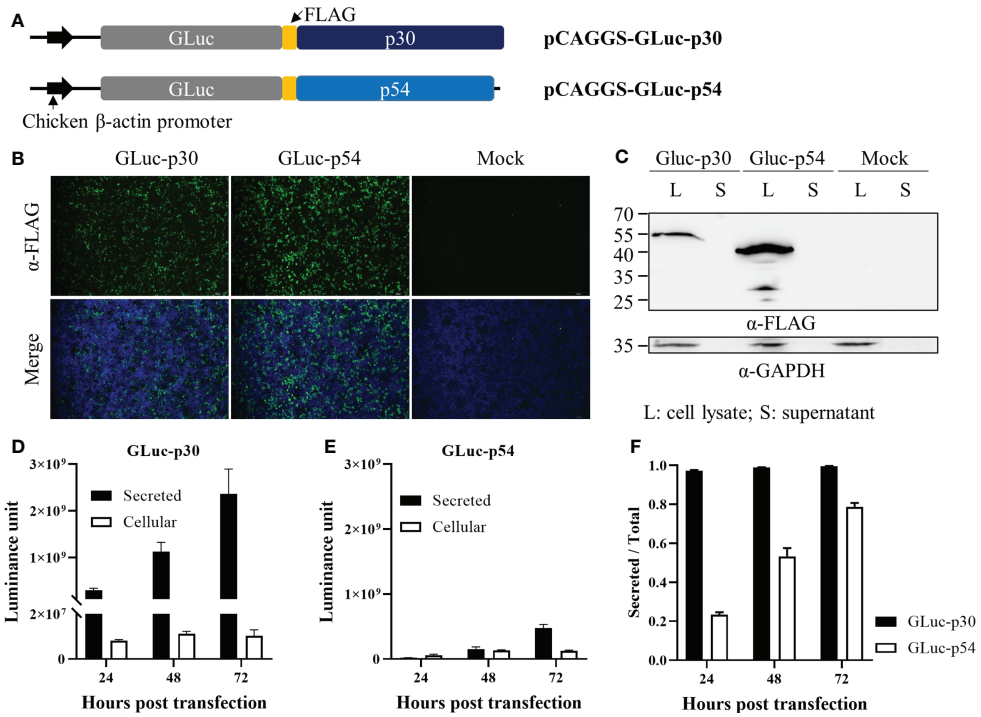

FIGURE 2
The expression of ASFV p30 and p54 as fusion proteins in HEK-293T cells. **(A)** A schematic representation of the plasmids expressing the fusion proteins, GLuc-p30 and GLuc-p54. HEK-293T cells were transfected with pCAGGS-GLuc-p30, pCAGGS-GLuc-p54, or pCAGGS vector. At 24, 48, and 72 hpt, culture supernatants were harvested, while cells were lysed with IP lysis buffer or fixed with 4% paraformaldehyde. The expression of GLuc-p30 and GLuc-p54 at 48 hpt was evaluated by IFA using an antibody against the FLAG tag **(B)** and western blot analysis using antibodies against the FLAG tag and GAPDH **(C)**. Luciferase assay was performed to measure GLuc-p30 **(D)** and GLuc-p54 **(E)** in cell lysates and supernatants at 24, 48, and 72 hpt. **(F)** The ratio of secreted GLuc-p30 and GLuc-p54. The data **(E, F)** represent the means ± SD (standard deviation) of triplicate.

protein, we also checked whether the fusion proteins could be secreted into the culture supernatant. The expression dynamics of the fusion proteins in culture supernatants and cell lysates at 24, 48, and 72 hpt were evaluated by gaussia luciferase assay. The expression levels of GLuc-p30 and GLuc-p54 increased gradually in culture supernatants from 24 hpt to 72 hpt, and GLuc-p30 exhibited much higher expression levels in culture supernatants (Figures 2D, E). As shown in Figure 2F, more than 97.3% of GLuc-p30 was secreted into culture supernatants at all time points, while the distribution of GLuc-p54 in culture supernatant increased gradually from 23.4% to 78.7%. Based on the expression level and distribution of the fusion proteins, the culture supernatant containing GLuc-p30 without purification was chosen as the antigen for the development of LIPS assay against ASFV.

The establishment and optimization of the GLuc-p30-based LIPS assay for ASFV antibody detection

Initially, we established the GLuc-p30-based LIPS assay using an anti-FLAG mAb, as shown in Figure 1. In comparison with the mock control, the anti-FLAG mAb was able to pull down GLuc-p30 efficiently as indicated by a ~10000-fold increase of luminance signal (Figure 3A).

To find the optimal detection conditions for the LIPS assay, we mainly optimized the input of GLuc-p30 and serum dilution factor. For this optimization, an ASFV-positive and an ASFV-negative pig serum were used, and the P/N ratio was used as the criteria to evaluate the signal-to-noise ratio. As shown in Figure 3B, with the decrease of GLuc-p30 input, the relative luciferase activities for both positive and negative sample detection were decreased. However, among the tested doses, 10^7 luminance units of GLuc-p30 per reaction reached the highest P/N ratio of 112 (Figure 3C). Therefore, the optimal input of GLuc-p30 is 10^7 luminance units.

Next, seven serum dilutions (1/50 ~ 1/3200) were tested to find the optimal serum dilution factor. In this experiment, 10^7 luminance units of GLuc-p30 and the positive and negative serum samples mentioned above were used. As shown in Figures 3D, E, the optimal serum dilution factor is 1/100, which gives the highest P/N ratio of 109.93. In line with the results in Figure 2B, the luciferase activities of negative serum detections remained consistently low at all dilutions. In addition, we also compared the limit of detection between our LIPS assay and an ASFV p30-based indirect ELISA kit. Both methods were

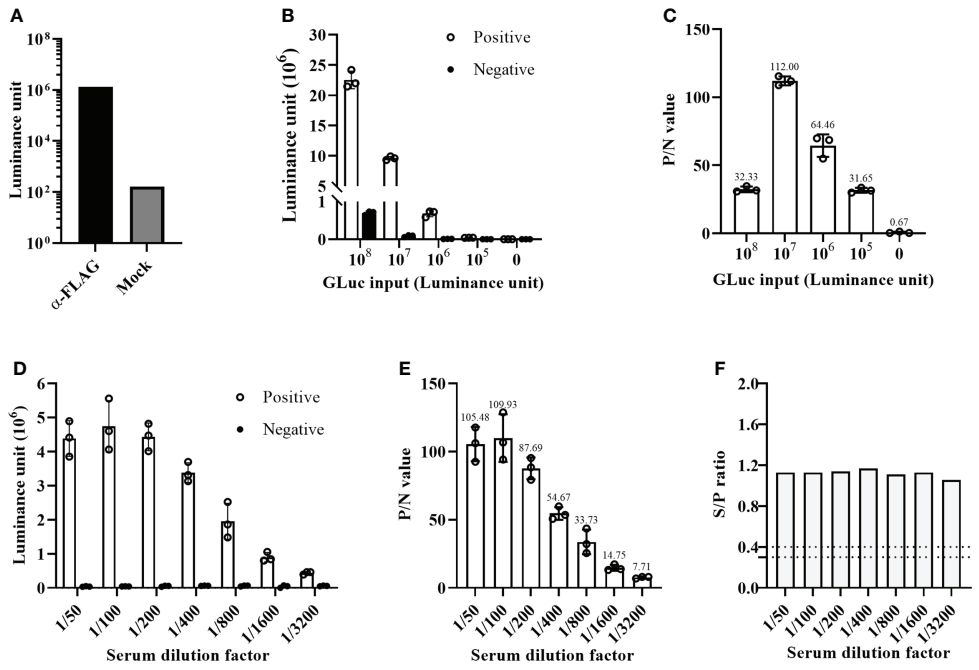

FIGURE 3
Optimization of the GLuc-p30-based LIPS assay. **(A)** The GLuc-p30-based LIPS recognized a mAb against the FLAG tag. **(B)** Optimization of GLuc-p30 input. Four different doses of GLuc-p30 were tested using an ASFV-positive serum and an ASFV-negative serum. The P/N ratios of the positive serum and the negative serum were calculated **(C)**. **(D)** Optimization of the serum dilution factor. Seven dilution factors were tested using 10^7 LU per reaction. P/N ratios of the positive serum to the negative serum were calculated **(E)**. **(F)** The limit of detection of a p30-based indirect ELISA was evaluated with the same positive and negative serum. The S/P ratios were calculated for different serum dilutions. The data represent the means ± SD of triplicate.

able to detect ASFV antibodies from 1/50 to 1/3200 dilutions of the positive serum. However, as the dilution factor increased, the gradual reduction of the P/N ratio was observed in our LIPS assay but not for the S/N ratio in the indirect ELISA (Figures 3E, F), suggesting that the GLuc-p30-based LIPS assay could be used for ASFV antibody detection and quantification.

The cutoff value and diagnostic specificity of the GLuc-p30-based LIPS assay

A total of 77 pig serum samples were used to determine the cutoff value of the GLuc-p30-based LIPS assay, including 37 positive sera and 40 negative sera which were collected from ASFV-infected or non-infected pigs. Firstly, these serum samples have been verified by a commercial indirect ELISA for ASFV antibody detection (Figure 4A) according to the manufacturer's instructions. As expected, this indirect ELISA was able to identify positive and negative samples. Based on the ROC curve generated with all of the S/N ratios, the cutoff values could be set >2.298 and ≤30.59 to reach 100% sensitivity and 100% specificity for this LIPS assay (Figures 4B, C).

Subsequently, to check the cross-activity against other common swine pathogens, we evaluated the diagnostic specificity of the GLuc-p30-based LIPS assay using 17 sera collected from pigs infected with one specific swine pathogen as described in the section of Materials and methods. The S/N ratios of all serum samples were below the cutoff value, suggesting that this LIPS assay exhibited excellent diagnostic specificity (Figure 4D). The ASFV infection status of these samples was also tested with a commercial indirect ELISA. Except for one PRRSV-positive serum, all samples were determined to be ASFV-negative (Figure 4E), indicating that this indirect ELISA exhibited cross-activity with other pathogens. This PRRSV-positive serum was confirmed as ASFV-negative by IFA (data not shown).

Discussion

Due to the lack of an efficient ASF vaccine, early diagnosis and strict application of biosecurity measures to recognize infection, remove infected animals, and restrict animal movement are crucial for ASF control. Accurate and simple serological methods for antibody detection in body fluid or sera

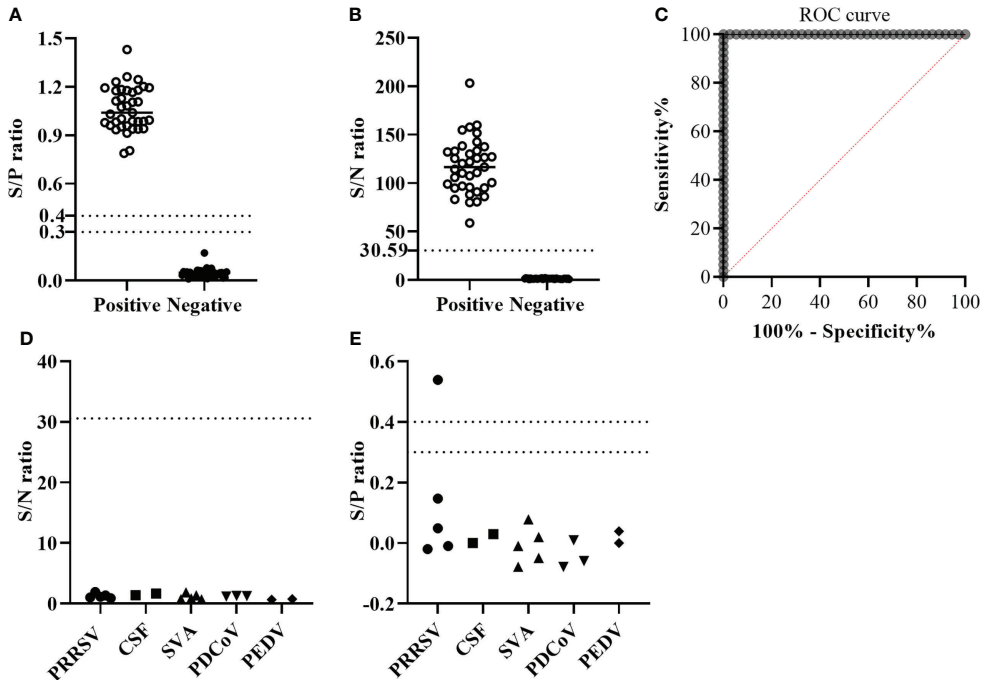

FIGURE 4
The performance of GLuc-p30-based LIPS with field serum samples. **(A)** S/P ratios were determined by a p30-based indirect ELISA to confirm the ASFV infection status of 37 ASFV-positive sera and 40 ASFV-negative sera. The cutoff value of the S/P ratio is between 0.3 and 0.4. **(B)** S/N ratios were obtained by the GLuc-p30-based LIPS assay of 37 ASFV-positive sera and 40 ASFV-negative sera. **(C)** The cutoff value of the LIPS assay was determined by ROC analysis. The diagnostic specificities of LIPS **(D)** and ELISA **(E)** were evaluated with 17 pig serum samples collected from pigs infected with specific swine pathogens, including PRRSV, CSFV, SVA, PDCoV, and PEDV.

would be more informative and beneficial to curb the development of epidemics. Due to its advantages as compared to other serological assays such as ELISA or protein microarray, the LIPS assay has already been widely used for measuring humoral immune responses in autoimmune and infectious diseases (Burbelo et al., 2015). In this study, we established a GLuc immunoprecipitation assay for the serological detection of ASFV infection based on the immunogenic viral protein p30. The GLuc-tagged p30 antigen was transiently expressed in HEK-293T cells and efficiently secreted in the cell culture supernatant (Figure 2), which was directly used for LIPS assay development. The optimal GLuc-p30 input and serum dilution factor for this LIPS were 10^7 LU and 1/100 dilution (Figure 3). This GLuc-p30-based LIPS can perfectly distinguish the known positive and negative pig sera, indicated by the 100% sensitivity and 100% specificity (Figure 4C). Moreover, in comparison with a well-validated indirect ELISA for ASFV antibody detection (Figure 4E), our LIPS assay demonstrated better diagnostic specificity (Figure 4D).

Various luciferase genes have been used as the reporter gene in LIPS assays, including Renilla *luciferase* (Berguido et al., 2021; Hachim et al., 2022), NanoLuciferase (Honda et al., 2021), and GLuc (Honda et al., 2021). GLuc from the marine copepod *Gaussia princeps* is naturally secreted from mammalian cells in an active form and can be released efficiently into the conditioned medium of mammalian cells (Tannous, 2009). In addition, GLuc is over 1,000 times more sensitive than the commonly used firefly luciferase and *Renilla* luciferase. Because of its small size, unique thermal stability, and genetically encoded secretion system, GLuc could further simplify the preparation of luciferase-tagged antigens. Studies on bioluminescence kinetics showed obvious positive cooperativity of *Gaussia* luciferase with coelenterazine at different coelenterazine concentrations (Larionova et al., 2018). In this study, we fused the GLuc gene with the codon-optimized ASFV CP204L gene or E183L gene to express GLuc-p30 and GLuc-p54 proteins. As expected, GLuc-p30 was efficiently expressed and secreted (more than 97%) into the culture supernatant. Nevertheless, the expression level of GLuc-p54 was much lower. In addition, the low secreted percentage of GLuc-p54 may be due to the transmembrane domain of p54. So we developed the LIPS assay only with GLuc-p30 protein. Since p54 is also an immunogenic ASFV protein and has been used for ELISA development, we will continue to optimize the expression and secreted level of GLuc-p54 for LIPS assay development in our future study. Compared to the luciferase-tagged antigens utilizing other luciferase genes (non-secreted), the preparation of GLuc-tagged antigens can be easier and less time-consuming.

Recently, another research group established an MP-LIPS assay for the detection of ASFV antibodies using a similar strategy (Liu et al., 2021). They also chose ASFV p30 as the target antigen and purified firefly luciferase tagged p30 from *Escherichia coli* for LIPS assay, which is more complicated and time-consuming than our preparation of GLuc-p30 in the eukaryotic expression system. The optimal P/N ratio (about 100) of this LIPS is very similar to our results (Figure 3). However, the sensitivity and specificity of this LIPS assay are much lower than those of our GLuc-p30-based LIPS, although less serum samples were tested in this study. ASFV p30 is usually expressed in *Escherichia coli* as inclusion bodies and can be purified when denatured. However, only a small part of denatured protein can be refolded to its native confirmation. Therefore, we believe that the native conformation of the luciferase-tagged p30 used for LIPS is essential for the recognition of various antibodies against this antigen in samples. Since this MP-LIPS is semi-automated and can be finished in 30 min, we will further optimize our GLuc-p30-based LIPS assay with a fully automated system to decrease the detection time in the future.

The performance of the GLuc-p30-based LIPS assay was compared with a commercial indirect ELISA kit using p30 as the diagnostic antigen. Using a panel of known positive and negative serum samples confirmed with this ELISA kit, our LIPS assay can correctly identify samples with ASFV antibodies. Our LIPS exhibited no cross-reactivity to other common swine pathogens, while the ELISA recognized a sample with PRRSV infection as ASFV-positive. Consequently, the diagnostic sensitivity of this LIPS is comparable to that of this commercial indirect ELISA, while the specificity of LIPS is even superior to the ELISA. In addition to serum, oral fluid is another sample used for the diagnosis of infectious diseases in the population because its collection requires little labor and is stress-free for animals. Since ASFV antibodies could be detected in oral fluids, oral fluids could be a suitable diagnostic specimen for ASFV surveillance (Olsen et al., 2013). We will test whether our LIPS assay can be used with pig oral fluids.

In conclusion, we have established a GLuc-p30-based LIPS assay that is a cheap, easy-to-implement and highly adaptable method for large-scale screening of ASFV antibodies. Because of its similar diagnostic sensitivity and superior diagnostic specificity to the commercial indirect ELISA, this LIPS could be a potential method for ASFV diagnosis in laboratories and farms.

Data availability statement

The datasets presented in this study can be found in online repositories. The names of the repository/repositories and accession number(s) can be found in the article/supplementary material.

Author contributions

YL: conceptualization, supervision, founding acquisition. YL and JD wrote the original draft. JD, JY, and DJ: investigation. JD

and DJ: methodology, formal analysis, and data curation. JD, JY, and YL reviewed and edited the manuscript. JY contributed to the resources. All authors contributed to the article and approved the submitted version.

Funding

This project was supported by the Key Research and Development Plan (Modern Agriculture) of Jiangsu Province (Grant No. BE2020398), Jiangsu Co-innovation Center for Prevention and Control of Important Animal Infectious Diseases and Zoonoses, and the Priority Academic Program Development of Jiangsu Higher Education Institutions (PAPD). JD is supported by the Postgraduate Research & Practice Innovation Program of Jiangsu Province (Grant No. KYCX22_3551). YL is supported by the Scientific Research Foundation of Yangzhou University and the "LvYangJinfeng Program" of Yangzhou City.

Acknowledgments

We thank Dr. Adolfo García-Sastre from Icahn School of Medicine at Mount Sinai, New York for kindly sharing the pCAGGS vector.

Conflict of interest

The authors declare that the research was conducted in the absence of any commercial or financial relationships that could be construed as a potential conflict of interest.

Publisher's note

References

Afonso, C., Alcaraz, C., Brun, A., Sussman, M., Onisk, D., Escribano, J., et al. (1992). Characterization of p30, a highly antigenic membrane and secreted protein of African swine fever virus. *Virology* 189 (1), 368–373. doi: 10.1016/0042-6822(92)90718-5

Berguido, F. J., Burbelo, P. D., Bortolami, A., Bonfante, F., Wernike, K., Hoffmann, D., et al. (2021). Serological detection of SARS-CoV-2 antibodies in naturally-infected mink and other experimentally-infected animals. *Viruses* 13 (8), 1649. doi: 10.3390/v13081649

Blome, S., Franzke, K., and Beer, M. (2020). African Swine fever - a review of current knowledge. *Virus Res.* 287, 198099. doi: 10.1016/j.virusres.2020.198099

Burbelo, P. D., Goldman, R., and Mattson, T. L. (2005). A simplified immunoprecipitation method for quantitatively measuring antibody responses in clinical sera samples by using mammalian-produced renilla luciferase-antigen fusion proteins. *BMC Biotechnol.* 5, 22. doi: 10.1186/1472-6750-5-22

Burbelo, P. D., Lebovitz, E. E., and Notkins, A. L. (2015). Luciferase immunoprecipitation systems for measuring antibodies in autoimmune and infectious diseases. *Transl. Res.* 165 (2), 325–335. doi: 10.1016/j.trsl.2014.08.006

Cao, Y., Han, D., Zhang, Y., Zhang, K., Du, N., Tong, W., et al. (2021). Identification of one novel epitope targeting p54 protein of African swine fever virus using monoclonal antibody and development of a capable ELISA. *Res. Vet. Sci.* 141, 19–25. doi: 10.1016/j.rvsc.2021.10.008

Carmina, G., Nieto, R., and Arias, M. (2022). African Swine fever virus (ASFV) indirect ELISA test based on the use of the soluble cytoplasmic semi- purified antigen (ASFV CP-Ag). *Methods Mol. Biol.* 2503, 133–145. doi: 10.1007/978-1-0716-2333-6_9

Cubillos, C., Gomez-Sebastian, S., Moreno, N., Nunez, M. C., Mulumba-Mfumu, L. K., Quembo, C. J., et al. (2013). African Swine fever virus serodiagnosis: a general review with a focus on the analyses of African serum samples. *Virus Res.* 173 (1), 159–167. doi: 10.1016/j.virusres.2012.10.021

Cwynar, P., Stojkov, J., and Wlazlak, K. (2019). African Swine fever status in Europe. *Viruses* 11(4), 310. doi: 10.3390/v11040310

Gallardo, C., Fernandez-Pinero, J., and Arias, M. (2019). African Swine fever (ASF) diagnosis, an essential tool in the epidemiological investigation. *Virus Res.* 271, 197676. doi: 10.1016/j.virusres.2019.197676

Gimenez-Lirola, L. G., Mur, L., Rivera, B., Mogler, M., Sun, Y., Lizano, S., et al. (2016). Detection of African swine fever virus antibodies in serum and oral fluid specimens using a recombinant protein 30 (p30) dual matrix indirect ELISA. *PLoS One* 11 (9), e0161230. doi: 10.1371/journal.pone.0161230

Hachim, A., Gu, H., Kavian, O., Mori, M., Kwan, M. Y. W., Chan, W. H., et al. (2022). SARS-CoV-2 accessory proteins reveal distinct serological signatures in children. *Nat. Commun.* 13 (1), 2951. doi: 10.1038/s41467-022-30699-5

Haljasmagi, L., Remm, A., Rumm, A. P., Krassohhina, E., Sein, H., Tamm, A., et al. (2020). LIPS method for the detection of SARS-CoV-2 antibodies to spike and nucleocapsid proteins. *Eur. J. Immunol.* 50 (8), 1234–1236. doi: 10.1002/eji.202048715

Honda, T., Gomi, S., Yamane, D., Yasui, F., Yamamoto, T., Munakata, T., et al. (2021). Development and characterization of a highly sensitive NanoLuciferase-based immunoprecipitation system for the detection of anti-influenza virus HA antibodies. *mSphere* 6 (3), e01342-20. doi: 10.1128/mSphere.01342-20

Kazakova, A. S., Imatdinov, I. R., Dubrovskaya, O. A., Imatdinov, A. R., Sidlik, M. V., Balyshev, V. M., et al. (2017). Recombinant protein p30 for serological diagnosis of African swine fever by immunoblotting assay. *Transbound Emerg. Dis.* 64 (5), 1479–1492. doi: 10.1111/tbed.12539

Larionova, M. D., Markova, S. V., and Vysotski, E. S. (2018). Bioluminescent and structural features of native folded gaussia luciferase. *J. Photochem. Photobiol. B* 183, 309–317. doi: 10.1016/j.jphotobiol.2018.04.050

Li, Y., Ren, C., Li, C., Xiao, Y., and Zhou, Y. A. (2022). Recombinant porcine reproductive and respiratory syndrome virus stably expressing a gaussia luciferase for antiviral drug screening assay and luciferase-based neutralization assay. *Front. Microbiol.* 13, 907281. doi: 10.3389/fmicb.2022.907281

Liu, H., He, P., Meng, F., Jiang, M., Xiong, J., Li, J., et al. (2021). A semiautomated luciferase immunoprecipitation assay for rapid and easy detection of African swine fever virus antibody. *J. Clin. Microbiol.* 59 (10), e0099021. doi: 10.1128/JCM.00990-21

Lv, C., Zhao, Y., Jiang, L., Zhao, L., Wu, C., Hui, X., et al. (2021). Development of a dual ELISA for the detection of CD2v-unexpressed lower-virulence mutational ASFV. *Life (Basel)* 11 (11), 1214. doi: 10.3390/life11111214

Olsen, C., Wang, C., Christopher-Hennings, J., Doolittle, K., Harmon, K. M., Abate, S., et al. (2013). Probability of detecting porcine reproductive and respiratory syndrome virus infection using pen-based swine oral fluid specimens as a function of within-pen prevalence. *J. Vet. Diagn. Invest.* 25 (3), 328–335. doi: 10.1177/1040638713481471

Oviedo, J. M., Rodríguez, F., Gómezpuertas, P., Brun, A., Gómez, N., Alonso, C., et al. (1997). High level expression of the major antigenic African swine fever virus proteins p54 and p30 in baculovirus and their potential use as diagnostic reagents. *J. Virol Methods* 64 (1), 27–35. doi: 10.1016/S0166-0934(96)02140-4

Perez-Filgueira, D. M., Gonzalez-Camacho, F., Gallardo, C., Resino-Talavan, P., Blanco, E., Gomez-Casado, E., et al. (2006). Optimization and validation of recombinant serological tests for African swine fever diagnosis based on detection of the p30 protein produced in trichoplusia ni larvae. *J. Clin. Microbiol.* 44 (9), 3114–3121. doi: 10.1128/JCM.00406-06

Shabani Azim, F., Zare Bavani, M., and Nikmanesh, B. (2016). Luciferase immunoprecipitation system assay, a rapid, simple, quantitative, and highly sensitive antibody detection for parasitic diseases. *Iranian J. Parasitol.* 11 (3), 426–428.

Shi, L., Tian, Z., Yang, J., Gao, S., Du, J., Zhao, Y., et al. (2021). [Comparison of the antigenicity of African swine fever virus p35 protein as diagnostic antigen]. *Sheng Wu Gong Cheng Xue Bao* 37 (1), 187–195. doi: 10.13345/j.cjb.200359

Sun, E., Huang, L., Zhang, X., Zhang, J., Shen, D., Zhang, Z., et al. (2021). Genotype I African swine fever viruses emerged in domestic pigs in China and caused chronic infection. *Emerg. Microbes Infect.* 10 (1), 2183–2193. doi: 10.1080/22221751.2021.1999779

Sun, E., Zhang, Z., Wang, Z., He, X., Zhang, X., Wang, L., et al. (2021). Emergence and prevalence of naturally occurring lower virulent African swine fever viruses in domestic pigs in China in 2020. *Sci. China Life Sci.* 64 (5), 752–765. doi: 10.1007/s11427-021-1904-4

Tannous, B. A. (2009). Gaussia luciferase reporter assay for monitoring biological processes in culture and in vivo. *Nat. Protoc.* 4 (4), 582–591. doi: 10.1038/nprot.2009.28

Tin, C. M., Yuan, L., Dexter, R. J., Parra, G. I., Bui, T., Green, K. Y., et al. (2017). A luciferase immunoprecipitation system (LIPS) assay for profiling human norovirus antibodies. *J. Virol. Methods* 248, 116–129. doi: 10.1016/j.jviromet.2017.06.017

Wang, C., Qiu, S., Xiao, Y., Yu, H., Li, H., Wu, S., et al. (2022). Development of a blocking ELISA kit for detection of ASFV antibody based on a monoclonal antibody against full length p72. *J. AOAC Int* qsac050. doi: 10.1093/jaoacint/qsac050

Wang, F., Zhang, H., Hou, L., Yang, C., and Wen, Y. (2021). Advance of African swine fever virus in recent years. *Res. Vet. Sci.* 136, 535–539. doi: 10.1016/j.rvsc.2021.04.004

Wu, K., Liu, J., Wang, L., Fan, S., Li, Z., Li, Y., et al. (2020). Current state of global African swine fever vaccine development under the prevalence and transmission of ASF in China. *Vaccines (Basel)* 8 (3), 531. doi: 10.3390/vaccines8030531

Wu, P., Lowe, A. D., Rodriguez, Y. Y., Murgia, M. V., Dodd, K. A., Rowland, R. R., et al. (2020). Antigenic regions of African swine fever virus phosphoprotein P30. *Transbound Emerg. Dis* 67, 1942–1953. doi: 10.1111/tbed.13533

Yuan, F., Petrovan, V., Gimenez-Lirola, L. G., Zimmerman, J. J., Rowland, R. R. R., and Fang, Y. (2021). Development of a blocking enzyme-linked immunosorbent assay for detection of antibodies against African swine fever virus. *Pathogens* 10 (6), 760. doi: 10.3390/pathogens10060760

Yu, X., Zhu, X., Chen, X., Li, D., Xu, Q., Yao, L., et al. (2021). Establishment of a blocking ELISA detection method for against African swine fever virus p30 antibody. *Front. Vet. Sci.* 8, 781373. doi: 10.3389/fvets.2021.781373

Zhao, H., Ren, J., Wu, S., Guo, H., Du, Y., Wan, B., et al. (2022). HRP-conjugated-nanobody-based cELISA for rapid and sensitive clinical detection of ASFV antibodies. *Appl. Microbiol. Biotechnol.* 106 (11), 4269–4285. doi: 10.1007/s00253-022-11981-4

Zhou, X., Li, N., Luo, Y., Liu, Y., Miao, F., Chen, T., et al. (2018). Emergence of African swine fever in China, 2018. *Transbound Emerg. Dis.* 65 (6), 1482–1484. doi: 10.1111/tbed.12989

Zhou, Y., Li, C., Ren, C., Hu, J., Song, C., Wang, X., et al. (2022). One-step assembly of a porcine epidemic diarrhea virus infectious cDNA clone by homologous recombination in yeast: Rapid manipulation of viral genome with CRISPR/Cas9 gene-editing technology. *Front. Microbiol.* 13, 787739. doi: 10.3389/fmicb.2022.787739

Advantages of publishing in Frontiers

OPEN ACCESS
Articles are free to read for greatest visibility and readership

FAST PUBLICATION
Around 90 days from submission to decision

HIGH QUALITY PEER-REVIEW
Rigorous, collaborative, and constructive peer-review

TRANSPARENT PEER-REVIEW
Editors and reviewers acknowledged by name on published articles

Frontiers
Avenue du Tribunal-Fédéral 34
1005 Lausanne | Switzerland

Visit us: www.frontiersin.org
Contact us: frontiersin.org/about/contact

REPRODUCIBILITY OF RESEARCH
Support open data and methods to enhance research reproducibility

DIGITAL PUBLISHING
Articles designed for optimal readership across devices

FOLLOW US
@frontiersin

IMPACT METRICS
Advanced article metrics track visibility across digital media

EXTENSIVE PROMOTION
Marketing and promotion of impactful research

LOOP RESEARCH NETWORK
Our network increases your article's readership